The role of hypoxic signaling in evasive tumor resistance against anti-angiogenic therapy

Inaugural Dissertation
submitted to the
Faculty of Medicine
in fulfillment of the requirements
for the PhD-Degree
of the Faculties of Veterinary Medicine and Medicine
of the Justus Liebig University Giessen

by
Omelyan Trompak
of
Mukachevo, Ukraine

Giessen 2019

From the Institute of Neuropathology
(Director: Prof. Dr. med. Till Acker)
of the Faculty of Medicine of the Justus Liebig University Giessen

In memory of my teacher, mentor, and dear friend ***Alexander Fedorchuk*** *(1958-2018), a man who was always there for everyone in need, who introduced me to cancer biology and instilled in me a deep interest in mechanisms of tumor metastasis.*

Table of content

1. Summary

Rapidly growing tumors depend on supply of oxygen and nutrients and avascular neoplastic lesions do not grow larger than 1-2 mm in diameter. At a very early stage of tumor growth, a phenotypic shift occurs, referred to as “angiogenic switch”, during which hypoxia induces secretion of angiogenic factors by tumor cells driving the formation of new vessels, which is a critical milestone in tumor progression. Realization of this key feature of tumor biology led Judah Folkman in the 1970s to propose a novel therapeutic approach – anti-angiogenic therapy, the rationale for which was based on blocking the growth of tumor vessels. At that time, it was believed that since tumor cells were not the primary target, no resistance mechanisms would be encountered. Yet, after the first clinical trials, it became obvious that tumors could indeed adapt to the therapy. One of the resistance mechanisms, which is the primary focus of the current thesis, is characterized by increased invasion and metastasis, preventing wider application of anti-angiogenic agents for the treatment of various carcinomas.

Epithelial-to-mesenchymal transition (EMT), a process characterized by specific changes in epithelial cells leading to weakening of cell-to-cell contacts and increased motility, has been shown to regulate tumor cell migration and metastatic dissemination. Since hypoxia is a well characterized trigger of EMT, we hypothesized that enhanced tumor hypoxia generated by anti-angiogenic therapy could be the driver of this form of resistance. To explore this hypothesis, several *in vivo* models of treatment with anti-angiogenic drugs (sunitinib, sorafenib, or bevacizumab) were established, which revealed increased metastasis following therapy. Next, using human lung and breast cancer lines re-isolated from tumors of animals receiving antiangiogenic therapy with sunitinib, we could show that these cells acquire a stable EMT-phenotype with invasive and metastatic traits. Importantly, the cells isolated from tumors of animals receiving anti-angiogenic therapy were more responsive to hypoxia, showing increased levels of hypoxia inducible factor 2 alpha (HIF2α). We could further show that prolonged exposure to intermittent hypoxia is sufficient to induce an EMT phenotype in tumor cells. Moreover, loss of function experiments identified HIF2α as a factor required for maintenance and acquisition of the EMT phenotype. Finally, we identified DNA demethylation mediated by the Ten-Eleven Translocation 1 (TET1) methylcytosine dioxygenase as a mechanism by which intermittent hypoxia upregulates HIF2α expression.

Taken together, our findings provide insight into the mechanisms underlying evasive resistance of tumors to anti-angiogenic therapy. In particular, we show that intermittent hypoxia induces a feed-forward loop involving HIF2α and TET1 which leads to epigenetic reprogramming of tumor cells promoting enhanced tumor response to hypoxia and increased invasion and metastasis. This work may contribute to a more rational approach to anti-angiogenic therapy, specifically combining anti-angiogenic and HIF2α-targeting approaches, which could potentially decrease the risk of tumor metastasis, and thus improve the clinical outcome of anti-angiogenic treatment.

2. Zusammenfassung

Schnell wachsende Tumore sind auf die Versorgung mit Sauerstoff sowie Nährstoffen angewiesen, so dass avaskuläre Tumore nicht größer als 1-2mm in Durchmesser werden können. In dieser Phase des Tumorwachstums findet eine angiogene Umstellung statt, bei der Hypoxie die Sekretion von angiogene Faktoren induziert, welche die Bildung neuer Blutgefäße fördern. Dies stellt einen essentiellen Schritt in der Tumorprogression dar und führte zur Entwicklung von anti-angiogenen Therapien in der Tumorbehandlung. Bei diesen von Judah Folkmann entdeckten Therapien sollte eine Gefäßbildung in Tumoren blockiert werden. Da bei einem solchen Therapiekonzept die Tumorzellen nicht direkt angegriffen werden, erwartete man, dass keine Resistenzbildung stattfinden würde. Dennoch wurde in ersten klinischen Studien schnell klar, dass sich Tumore der Therapie anpassen konnten. Einer dieser Resistenzmechanismen, der den Hauptfokus dieser Dissertation darstellt, zeichnet sich durch verstärkte Invasion und Metastasenbildung aus, was die Anwendung anti-angiogener Therapien bei vielen Karzinomen erschwert.

Die epitheliale-mechenchymale Transition (EMT) ist ein Prozess, der durch spezifische Veränderungen des Phänotyps der Epithelzellen, einer Schwächung der Zell-Zell-Kontakte und erhöhter Motilität gekennzeichnet ist. Zudem ist er auch an der Regulation der Tumorzellmigration und des Metastasenausbreitung beteiligt. Ein bekannter Auslöser der EMT ist Hypoxie. Unsere Hypothese war es daher, dass die durch anti-angiogene Therapie verstärkte Hypoxie, den Auslöser dieser Form der Resistenz darstellt. Um diese Hypothese zu überprüfen, wurden mehrere *in vivo* Studien mit anti-angiogenen Substanzen (Sunitinib, Sorafenib oder Bevacizumab) durchgeführt, in denen wir eine verstärkte Metastasenbildung nach anti-angiogener Therapie nachweisen konnten. Als nächstes wurden humane Lungen- sowie Brustkrebszelllinien aus Tumoren von Mäuse isoliert, die mit anti-angiogenetischen Therapien behandelt wurden. Wir konnten zeigen, dass diese einen stabilen Phänotyp angenommen hatten, der sich durch erhöhten EMT und Invasivität auszeichnete. Zusätzlich zeigten diese Zellen keine Anzeichen der klassischen Resistenzbildung, zeichneten sich aber stattdessen durch eine verstärkte Hypoxieantwort aus (mit höherer Expression vom Hypoxie-induzierten Faktor 2α, HIF2α). Weiterhin konnten wir in einem *in vitro* Modell zeigen, dass eine prolongierte Inkubation der Tumorzellen unter einer intermittierenden Hypoxie (IH) ausreichend war, um den EMT-Phänotypen auszulösen. Des Weiteren konnten wir zeigen mit Hilfe von funktionellen genetischen Experimenten, dass HIF2α essentiell für die Entstehung, sowie für den Erhalt dieses Phänotyps war. Abschließend

identifizierten wir eine, von TET1-methylcytosin-dioxygenase vermittelte DNA-Demethylierung als einen entscheidenden Faktor für die durch intermittierende Hypoxie ausgelöste, verstärkte Expression von HIF2α.

Zusammenfassend zeigt diese Arbeit einen grundliegenden Mechanismus bezüglich der Resistenzentwicklung von Tumoren gegenüber anti-angiogener Therapien. Wir konnten zeigen, dass intermittierende Hypoxie über einen Mechanismus der positiven Rückkopplung, der sowohl HIF2α als auch TET1 beinhaltet zu einer verstärkte Hypoxieantwort mit erhöhter Metastasenbildung führt. Diese Arbeit könnte zu neuen Ansätzen in der Anwendung anti-angiogener Therapien führen. Durch Kombination von HIF2 und TET1-Inhibtioren könnte das Risiko der Metastasenbidung durch anti-angiogenen Therapien effektiv verringert werden, was die Wirksamkeit der Behandlung verbessern könnte.

3. Introduction

3.1. Tumor therapy: a historical perspective

It is widely held that the advent of modern chemotherapy was brought about with the discovery of antileukemic potential of the antifolate aminopterin by Sidney Farber in 1948 (DeVita and Chu, 2008). Farber's pioneering work was the first to approach cancer treatment based on some (even if very limited) knowledge of tumor biology: learning from the failed previous attempts to treat patients with teropterin and diopterin, both conjugates of folic acid, whose application led to an "acceleration phenomenon", i.e. increased tumor growth, Farber suggested an opposite approach – using antifolates as means of treatment. In that first trial, Farber's aminopterin produced only few short-lived remissions, but it was a true breakthrough, as at the time all cases of childhood leukemias were invariably and rapidly fatal (Farber *et al*., 1948).

Since then, much effort has been invested in screening for tumor-targeting drugs reviving Ehrlich's concept of a "magic bullet" (Strebhardt and Ullrich, 2008). The progress made in the following years is best exemplified by the 5-year survival rate of childhood leukemia patients, which currently stands around 90% (depending on the specific type; Bonaventure *et al*., 2017).

Another major success story in antitumor drug discovery was the development of the small molecule inhibitor imatinib (Kantarjian *et al*., 2012). This kinase inhibitor targeting the Bcr-Abl oncogene is truly approaching Ehrlich's criteria of a "magic bullet". Since its approval for medical use in 2001, the eight-year survival rate of patients with chronic myeloid leukemia (CML) increased to 87%, compared to less than 15% in the 1980s. This unprecedented success was made possible by standing on the shoulders of giants, as it required careful study of the biology of CML and its driver oncogene, namely – the discovery of the Philadelphia chromosome by Nowell P. and Hungerford D., isolation of the Bcr-Abl oncogene, and chemical synthesis and modification of a suitable inhibitor by Novartis labs (Kantarjian *et al*., 2012; Nowell and Hungerford, 1961).

These two examples – aminopterin and imatinib, their discoveries standing more than 50 years apart, represent major triumphs in treating leukemias – "liquid cancers". Alas, the situation is very different with solid tumors. Comprising a much larger group of heterogeneous types, solid malignancies proved to be much more challenging to cure.

Among the most commonly used treatment modalities for solid tumors, chemotherapy is a latecomer. Following the early success of antifolates and the first combination chemotherapy trials, Li demonstrated the possibility of a cure by successfully treating a choriocarcinoma (Li *et al*., 1958). These studies were followed by wider trials of new classes of drugs, like the non-specific alkylating chemotherapeutic agents (e.g. cisplatin), antimetabolites (e.g. 5-fluorouracil), kinase inhibitors and other groups of antineoplastic agents (Baines and Ley, 1962; Kantarjian *et al*., 2012; Rosenberg *et al*., 1969). Adjuvant and neoadjuvant approaches in cancer chemotherapy were employed as supportive treatment in combination with surgery and/or radiation. These developments, combined with earlier tumor diagnosis, improved surgical and radiation treatments resulted in considerably improved survival rates according to NIH statistics (examples for most common tumors are presented in **Table 3.1.**; modified from Manrow R., 2010).

As we can see from the table, some of the tumor types are very well managed, e.g. prostate and breast cancers, while survival is still quite low with other tumors, like colorectal or lung cancer. One common thread uniting the difficult to treat malignancies is the problem of metastatic tumor dissemination. Neither radical surgery, nor sophisticatedly radiotherapy, chemotherapy and the latest developments of targeted tumor therapy can ensure the complete removal of all tumor cells from a patient or their dissemination to other organs to form metastases, which was shown in a number of studies to be the leading cause of deaths of cancer patients (Klein, 2009).

Table 3.1. Five-year survival rates of patients with common tumor types in 1976 and 2006

	5-year survival rates, in %	
Cancer type	**1976**	**2006**
Childhood cancers (combined)	62	81
Breast cancer	75	90
Prostate cancer	69	100
Lung cancer	13	16
Colorectal cancer	51	67
Bladder cancer	74	81

The significance of tumor dissemination is highlighted by the fact that metastasis is one of the key criteria used in the TNM classification of tumors, as patients with manifest distant metastases have a much worse prognosis. **Fig. 3.1.** represents Kaplan-Meyer survival plots

for patients with various tumor types segregated according to their metastasis status. Even in the case of relatively well treatable cancers, like breast carcinomas, patients with distant metastases (M1 in the TNM) have a median survival more than three-fold lower than M0 patients (37 months in M1 vs 130 months in M0; Gao *et al*., 2013; Grossman *et al*., 2016).

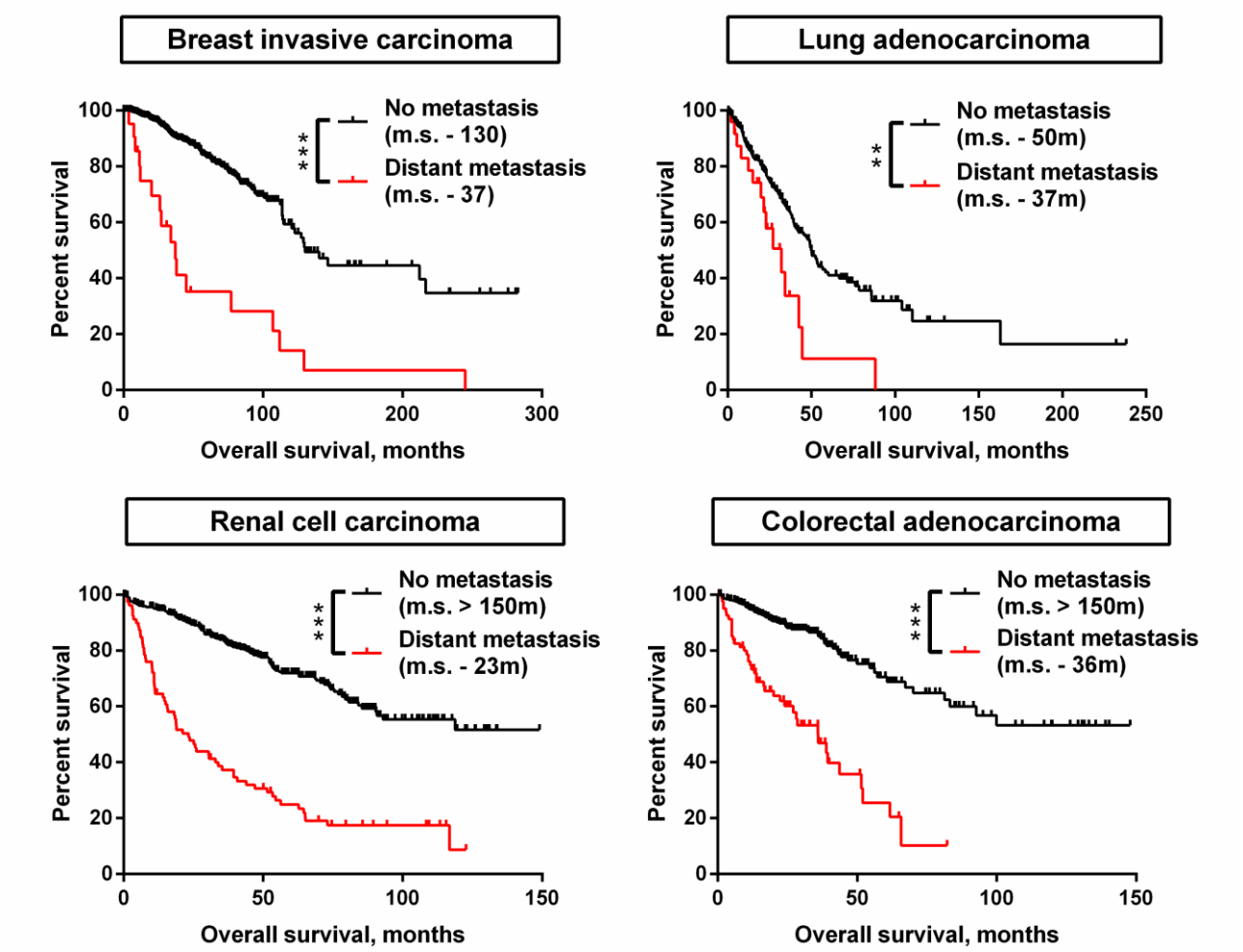

Fig. 3.1. Patients with manifest distant metastases show a significantly reduced overall survival. Kaplan-Meyer analysis of patient survival showed that in different tumor types, patients harboring distant metastases (M1 stage according to the TNM classification) have a significantly worse overall survival in comparison to M0 patients (clinical data derived from TCGA, m.s. – median survival in months (m) after diagnosis).

The problem of tumor metastasis is further complicated by the fact that some treatments can even stimulate tumor dissemination. For instance, surgery (Tohme *et al*., 2017) or even some newly developed chemotherapeutic approaches can provoke metastasis (Bluemn *et al*., 2017; Montgomery *et al*., 2008). One such novel treatment modality was the focus of this thesis – anti-angiogenic therapy. Previous reports have shown that resistance to anti-

angiogenesis involves a group of mechanisms united under the term “evasive resistance”, which denotes increased migration, invasion, and metastasis following anti-angiogenic therapy (Bergers and Hanahan, 2008; Depner *et al*., 2016; Ebos *et al*., 2009a; Jahangiri *et al*., 2017).

Therefore, a better understanding of the mechanisms leading to evasive resistance is required to prevent metastasis and improve the outcomes of anti-angiogenic therapy. The next chapters will provide an overview of metastasis, evasive resistance, and the role of the tumor microenvironment in tumor resistance to anti-angiogenic therapy.

3.2. Tumor angiogenesis and metastasis: two interconnected hallmarks of cancer

Tumor angiogenesis and metastasis were recognized as two of the ten hallmarks of cancer (Hanahan and Weinberg, 2011). Despite constituting two distinct processes, formation of new vessels (or remodeling of existing vasculature) and metastatic dissemination of tumors are inherently interconnected: ingrowing tumor vessels, required to meet the ever-increasing demands for nutrients and oxygen, also serve as ports of access for metastasizing cells (Gupta *et al*., 2007; Nguyen *et al*., 2009). On the other hand, metastasized tumors often incorporate pre-existing blood vessels or induce the formation of new vessels in the stroma to ensure further growth of the new lesions (Lu et al., 2012; Pàez-Ribes et al., 2009a). Both steps represent major developments on the journey of tumor progression from localized avascular clumps of renegade cells to highly aggressive, vascularized, and metastatic lesions, rapidly bringing the patient’s demise (Döme *et al*., 2007; Folkman, 1972).

3.2.1. The many varieties of tumor angiogenesis

“Ὁκόσοισι κρυπτοὶ καρκίνοι γίνονται, μὴ θεραπεύειν βέλτιον: θεραπευόμενοι γὰρ ἀπόλλυνται ταχέως, μὴ θεραπευόμενοι δὲ, πουλὺν χρόνον διατελέουσιν.”

Αφορισμοί, Ιατρική του Ιπποκράτη

“It is better not to apply any treatment in cases of occult cancer; for, if treated, the patients die quickly; but if not treated, they hold out for a long time.”

Aphorisms, Corpus Hippoctaticum, 4th century BC

Angiogenesis is arguably one of the oldest characteristics attributed to cancer. In fact, it is believed that the name cancer (from the Greek "*καρκίνος"* [karkinos], meaning crab) was given to the disease by Hippocrates (460-375 BC) for the resemblance of tumor vessels to the limbs of a crab (Faguet, 2015; Sudhakar, 2010). Despite the many centuries that passed since those first observations of tumor vessels, the recognition of tumor angiogenesis as one of the principal hallmarks of cancer came relatively recently. In some early experiments, tumor cells were transplanted into the anterior chamber of the eye which was believed to be an immune privileged site. It was shown that tumor cells suspended in the anterior chamber would not undergo vigorous proliferation as was expected. However, upon attachment to the corneal limbus, tumor spheroids would induce formation of new blood vessels and start to proliferate rapidly (Greene, 1941).

By now, it is well established that growth of tumors heavily depends on the adequate supply of oxygen and nutrients which is primarily achieved by angiogenesis (Hanahan and Weinberg, 2000). As is the case for many other physiological processes that cancer cells adapt to their needs, formation of new blood vessels in the tumor shares many similarities with physiological angiogenesis. During embryogenesis, *de novo* vessel formation (the process of vasculogenesis) is triggered by the secretion of pro-angiogenic factors that stimulate and direct angioblasts to form blood vessels (Drake *et al*., 2000; Poole *et al*., 2001). In the adult body this capability is limited to the formation of new vessels from the pre-existing vasculature (angiogenesis) and is normally restricted to wound repair and the female reproductive system (Gale *et al*., 2002; Okuno *et al*., 2011). Tumors exploit the same mechanisms to form their own vascular supply, yet due to the excessive and irregular amounts of angiogenic stimuli they produce, tumor angiogenesis takes on a much more aberrant nature (thus the notion of tumors as "never healing wounds", Lu *et al*., 2012a; Zhang *et al*., 2010).

As a result of their immature state, tumor vessels are characterized by abnormal structure and function: irregular shape (due to constantly changing gradients of angiogenic factors), profound leakiness (in part due to the absence of the basement membrane), poor organization into arterioles and venules (presence of arterio-venous shunts), constantly changing blood flow, etc. (Scharpfenecker, 2005; Vermeulen *et al*., 2001). The abnormal state of tumor angiogenesis reflects the aberrant signaling fueling this process and the resulting lack of vessel maturation. In contrast, in normal tissues growth of new vessels is achieved by rigorously controlled tipping of the balance from anti-angiogenic to pro-

angiogenic factors (Nissen *et al*., 1998). Many anti-angiogenic factors are generated from cleaved derivatives of ECM components (e.g. angiostatin and endostatin), while pro-angiogenic factors are typically secreted by stromal cells (Bergers and Benjamin, 2003; O'Reilly *et al*., 1997).

Tumor cells secrete a plethora of pro-angiogenic factors, among them – vascular endothelial growth factors (VEGFs), platelet derived growth factors (PDGFs), fibroblast growth factors (FGFs), placental growth factor (PlGF), etc. It is widely acknowledged that the transition from the slow avascular phase of growth to exponential growth following vascularization represents a milestone stage in tumor development. This transition phase, referred to as "angiogenic switch", is primarily triggered by hypoxia, which drives the expression of many pro-angiogenic factors (Bergers and Benjamin, 2003; Folkman, 1972; Hu *et al*., 2003).

Many families of angiogenic factors have been described until now, among which VEGFs and angiopoietins (ANGPT, **Fig. 3.2.**) are believed to play a central role (Ahmad *et al*., 2001; Kim *et al*., 2004; Weis and Cheresh, 2011; Zhang *et al*., 2010).

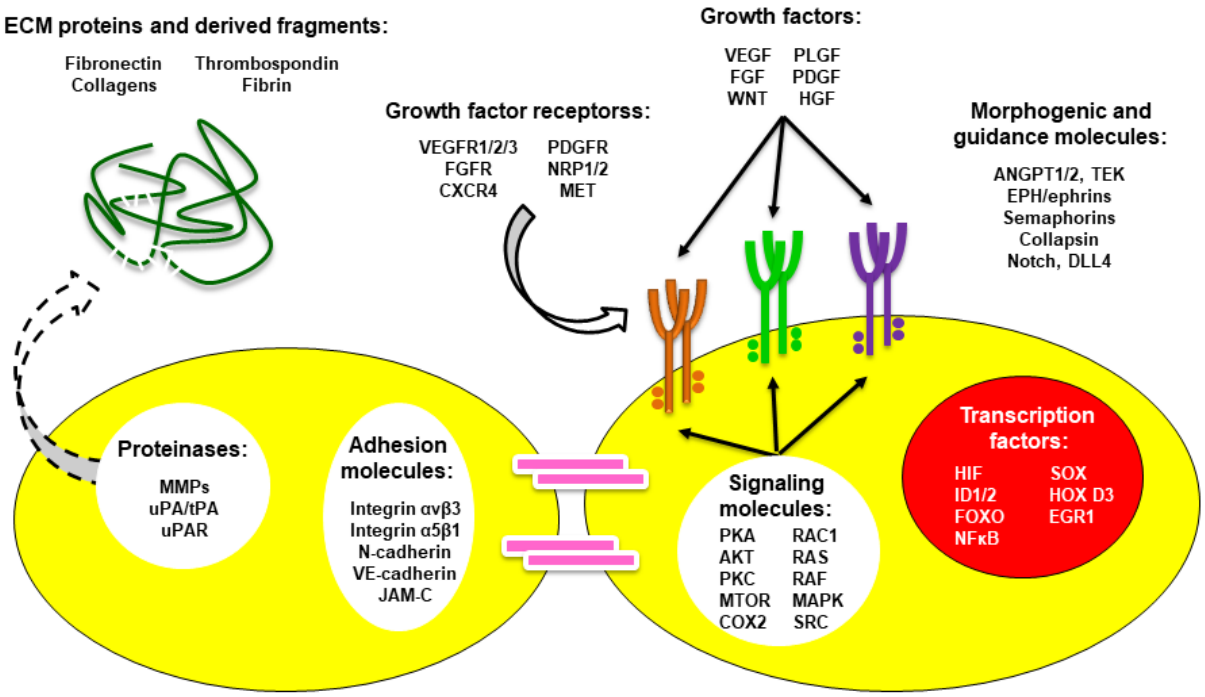

Fig. 3.2. Major players in the regulation of tumor angiogenesis. Multiple classes of proteins are involved in tumor angiogenesis: various ligands, like VEGFs, PDGFs, FGFs, bind to respective receptor tyrosine kinases (e.g. VERGFRs, c-MET, PDGFRs, etc.) and alter intracellular signaling cascades regulating endothelial cell survival and proliferation (e.g. MAPKs). Other protein families, like adhesion molecules and secreted proteases, modify the ECM and influence endotheliocyte migration aided by guidance molecules, e.g. semaphorins, ephrins, and other growth factors (modified from Jayson *et al*., 2016)**.**

The VEGF family of ligands contains five members that can stimulate tumor angiogenesis and lymphangiogenesis: VEGFA, VEGFB, VEGFC, VEGFD, and PlGF. Several isoforms of VEGFA have been described as the result of alternative splicing, with VEGF-A165 eliciting the strongest effect (Bates *et al*., 2002; Lee *et al*., 2007; Nowak *et al*., 2008). VEGFs bind to one of the three cognate receptor tyrosine kinases:

1) VEGFR1 has the highest affinity, but weak kinase activity;
2) VEGFR2 is the main receptor triggering angiogenesis; it has a weaker affinity than VEGFR1, but a higher kinase activity;
3) VEGFR3 is primarily involved in lymphangiogenesis.

Ligand-receptor binding typically results in MAPK activation and endothelial cell survival and proliferation (Gerber *et al*., 1997; Sakurai *et al*., 2005).

Another group of ligands that stimulate vessel growth and remodeling are the angiopoietins. Among the four ANGPT ligands present in the human genome, ANGPT1 and ANGPT2 were shown to have opposing but nonetheless vital roles in tumor angiogenesis. ANGPT1 binding to the Tie2 receptor tyrosine kinase is a part of the survival signaling in endothelial cells and results in vessel stabilization and maturation, enhanced attachment of pericytes, and a quiescent state of vessels. On the contrary, ANGPT2 binding to Tie2 results in vessel destabilization, decreased binding of pericytes, and, in case adequate concentrations of VEGFs are present, leads to vessel remodeling or endothelial cell sprouting (Fagiani *et al*., 2011; Stratmann *et al*., 2001).

Several distinct types of tumor angiogenesis have been described until now, including endothelial sprouting, vessel co-option, vasculogenic mimicry, postnatal angiogenesis, etc. (Frentzas *et al*., 2016; Kim *et al*., 2000; Williamson *et al*., 2016). Among all the types of tumor vessel formation, endothelial sprouting is the best described mechanism present in the majority of tumors. Endothelial sprouting begins with vessel dilation and induced leakiness, which in part is mediated by the tumor-secreted VEGF (the old name of VEGF is VPF – vascular permeability factor). Next, ECM-degrading proteases (primarily matrix metalloproteases, MMPs) remodel the stroma surrounding the vessel and alter the basement membrane. Pericyte attachment decreases in response to ANGPT2 and the freed endothelial cells become activated in the presence of VEGFs and ANGPT2. Due to the weakened basement membrane and increased concentration of multiple pro-angiogenic factors endotheliocytes begin to migrate and divide along the growth factor gradient, with a tip-cell leading the way. Appearance of the basement membrane along the growing vessel

sprout serves as the platform for pericytes from the mother vessel to migrate, divide, and stimulate vessel maturation, completing the process of new vessel formation (Jeong *et al*., 2017; Kim *et al*., 2000).

Another type of vessel acquisition in tumors is the so-called vessel co-option. This type of tumor vascularization can be described as the process of acquisition of vessels from the surrounding stroma: as opposed to stimulating growth of new vessels, tumors grow along the vessels in the tissue until they completely replace the normal surrounding stroma (Coelho *et al*., 2015). This process is not passive in nature, but involves extensive vessel remodeling (e.g. by vessel fusion resulting in much widened vessels with high pressure, often resulting in intratumoral hemorrhages). Vessel co-option is often observed in tumor metastasis, which typically arise when cancer cells start growing alongside vessels in distant organs (Frentzas *et al*., 2016). Interestingly, melanomas are also believed to be highly dependent on vessel co-option, whereby the tumor cells infiltrate and appropriate the rich vascular bed of the connective tissue stroma. Additionally, these tumors, despite having comparatively small volumes, are known to be highly metastatic, reflecting the tight connection between tumor vascularization and metastasis (Bentolila *et al*., 2016).

3.2.2. The multistep process of metastasis

“The best work in the pathology of cancer is now done by those… who are studying the nature of the seed. They are like scientific botanists; and he who turns over the records of cases of cancer is only a ploughman, but his observation of the properties of the soil may also be useful.”

S. Paget, The Lancet, 1889

At present, metastasis and not the primary tumor growth remains the leading cause of deaths of patients with cancer (Talmadge and Fidler, 2010). Metastatic dissemination of tumors is believed to constitute one of the milestone stages in tumor progression, yet it does not necessarily happen late in tumor development. Currently, there are two complementary models of metastasis: 1) late stage dissemination – observed in advanced, larger in size, tumors; 2) parallel progression model – according to this model even very small lesions are

capable of shedding metastatic cells. To date, evidence exists in support of both models, which may reflect certain characteristics of particular tumor types (Klein, 2009).

In general, metastasis may serve as the best example of a Darwinian microevolutionary process, which is inherent to tumors: genetic instability is generating new clones that go through a rigorous selection in the harsh tumor microenvironment, followed by a second selection for their ability to adapt to the foreign microenvironment in distant locations after seeding (Cunningham *et al*., 2015; Yamamoto *et al*., 2015). In reality, the situation is even more complex, as tumors were shown to be capable of self-seeding, through which highly invasive and malignant clones can be re-introduced into the primary tumor (Kim *et al*., 2009). This complex scheme of clonal expansion and diversification contributes to tumor relapses following resection and acquisition of chemo- and radioresistance (Dong *et al*., 1994; Su *et al*., 2012).

Fig. 3.3 represents the five basic steps characteristic of metastatic dissemination of tumors (Friedl and Alexander, 2011; Minn *et al*., 2005; Nguyen *et al*., 2009; Wang *et al*., 2005):

1) Migration and invasion of tumor cells into the surrounding stroma – the initial step to metastasis at which cancer cells actively degrade the extracellular matrix, reorganize their cytoskeleton and migrate as single cells or in groups (Friedl *et al*., 2004; Stichel *et al*., 2017). In carcinomas, this stage is usually accompanied by epithelial-mesenchymal transition (EMT).

2) Intravasation of tumor cells into blood vessels and migration to distant sites – achieved by entry of tumor cells into the tortuous and leaky tumor vessels. Translocation into distant organs was long believed to be passive, yet further research indicated a more complex picture: for example, it was shown that tumor cells become protected from immune destruction in the bloodstream by clustering with platelets (Im *et al*., 2004);

3) Extravasation of tumor cells at distant sites – in case of site specific metastasis this stage if often referred to as homing (e.g. almost exclusive metastasis of uveal melanoma cells to the liver; Eskelin *et al*., 2003). This capability of tumor cells to exit specific sites in a body and survive represents their adaptation to the microenvironment, which is the result of rigorous clonal selection in the primary tumor and often – adaptation of the “soil” to foster the “seed” (which is the basis of the pre-metastatic niche concept; Kaplan *et al*., 2006);

4) Mesenchymal-epithelial transition and formation of micrometastases – reversal of the EMT and renewed proliferation of tumor cells leading to the formation of clinically

undetectable lesions comprising several dozens to hundreds of cells (Yao *et al*., 2011). At this stage, tumor cells can enter a dormant state, delaying the further progression to macrometastasis. Nowadays, tumor dormancy is believed to be a dynamic process whereby tumor cells actively resist immune destruction at the new hostile microenvironment (Malladi *et al*., 2016).

5) Progression to macrometastases – final step in the colonization of distant sites by tumors typically accompanied by active recruitment of immune cells that support the tumor growth and angiogenesis. It can result in the metastatic cascade where metastases seed further metastases (Pantel and Brakenhoff, 2004).

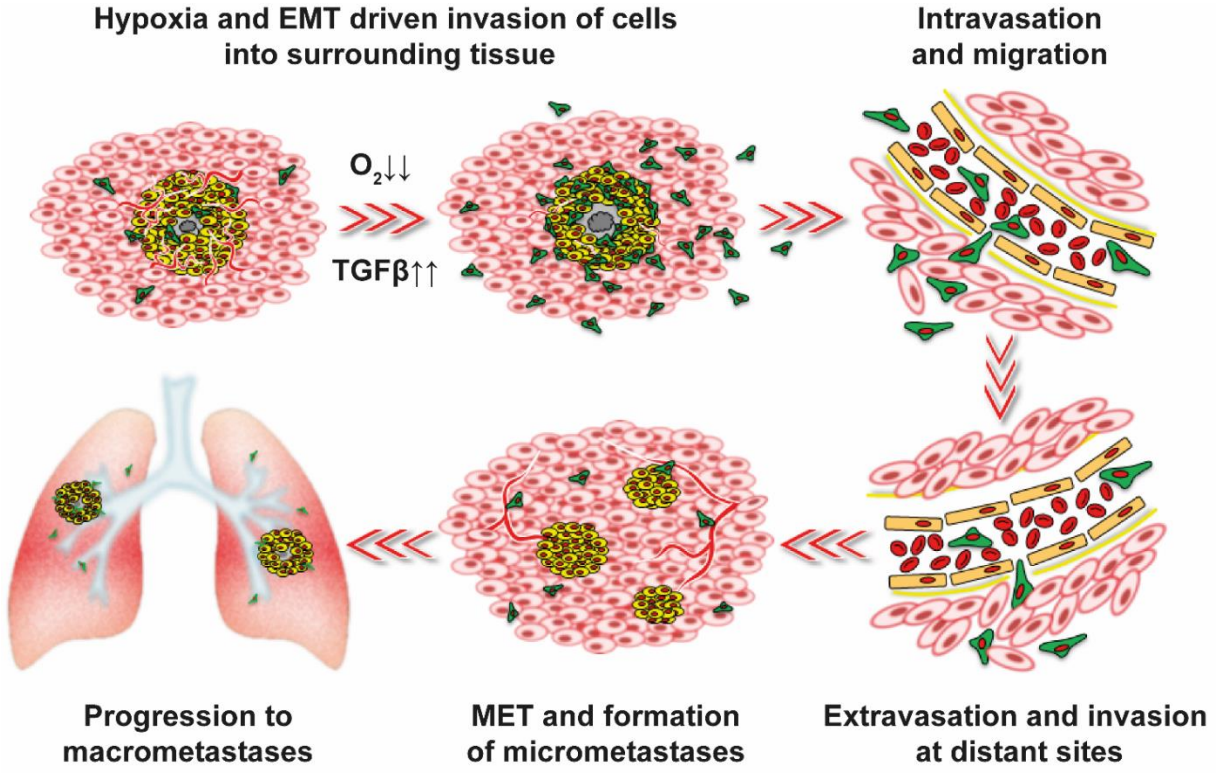

Fig. 3.3. Scheme representing the multistage process of metastasis. The process of tumor dissemination can be roughly subdivided in five different stages. It begins with tumor cell migration and invasion into the surrounding stroma, followed by intravasation and transportation to distant locations in the body. Afterwards, tumor cells exit the vessels and are challenged to survive in the new and foreign microenvironment. In case they succeed, micrometastases are formed which in turn may progress to clinically relevant macrometastases (modified from Nguyen *et al*., 2009).

Despite the overwhelming complexity of metastasis and the availability of genetic and phenotypic profiling data of metastatic cells, mechanisms of metastasis initiation and tumor

cell migration remain largely unresolved. Nonetheless, it is widely accepted that EMT plays a significant role is the initial steps of metastasis (Voulgari and Pintzas, 2009).

3.2.2.1. Epithelial to mesenchymal transition as the first step to metastasis

"It is not birth, marriage or death which is the most important time in your life, but Gastrulation."

Lewis Wolpert, 1989

The multistep process of metastasis in carcinomas is usually initiated after the tumor cells undergo EMT – a process that plays a significant role in embryogenesis (in gastrulation during formation of the mesoderm, neural crest, the heart, etc.) and in wound healing (Arnoux *et al*., 2008; Nakaya *et al*., 2008; Yan *et al*., 2010). EMT is characterized by the loss of polarity and cell-to-cell contacts between epithelial cells, and enhanced migration. Carcinoma cells hijack this highly important developmental program leading to migration and invasion of tumor cells through the extracellular matrix (Craene and Berx, 2013).

Fig. 3.4. represents the major phenotypic and molecular changes in cells undergoing EMT. Specifically, during the transition cells show a switch in expression of multiple markers. For example, expression of epithelial cadherin (E-cadherin), the classical marker for EMT, as well as other epithelial markers, as T-cadherin or ZO-1, is significantly downregulated. On the contrary, mesenchymal markers, such as N-cadherin, vimentin, and α5β1 integrin, become upregulated (Lombaerts *et al*., 2006; Mendez *et al*., 2010; Qian *et al*., 2014). This results in loss of adherence and tight junctions and liberation of cells from their local constrains (but avoiding anoikis). Additionally, due to active reorganization of the actin cytoskeleton and formation of lamellipodia and filopodia cells acquire a spindle-cell shaped morphology that facilitates migration (Holle *et al*., 2017; Schoumacher *et al*., 2010).

Besides the phenotypical change cells undergoing EMT acquire the ability to actively remodel the extracellular matrix. Specifically, this is achieved by secretion of matrix metalloproteinases (MMPs), which not only degrade the ECM, but also release growth factors embedded in the ECM, further promoting tumor growth and metastasis (e.g. TFGβ, VEGF, etc.; Hofmann *et al*., 2003; Pellikainen *et al*., 2004; Xu *et al*., 2005).

EMT was shown to be governed by a range of transcription factors, referred to as EMT regulators. These master regulators comprise several families of transcription factors that drive the phenotypic changes, enhanced invasion, and metastasis: Snail family of zinc-finger proteins (comprises two members – Snail and Slug); Zeb family of transcriptional repressors (consists of two members – Zeb1 and Zeb2); and Twist1/2 transcription factors (Hofmann *et al*., 2003; Pellikainen, 2004; Xu *et al*., 2005).

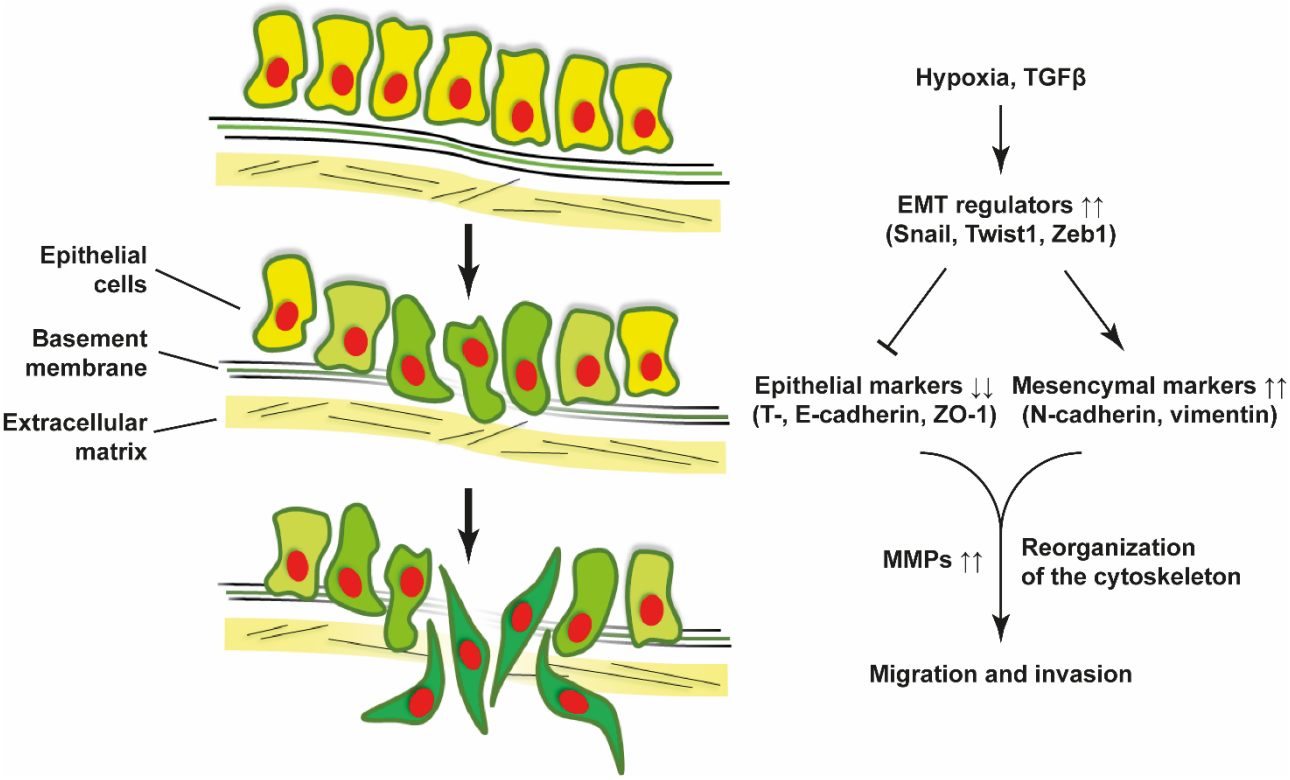

Fig. 3.4. Epithelial-to-mesenchymal transition (EMT) and the main molecular changes in the cell phenotype accompanying it. The process of EMT is characterized by loss of cell-to-cell contacts between epithelial cells, and increased cell migration and invasion into the surrounding tissues, which is believed to constitute the initial steps of tumor metastasis. Hypoxia and TGFβ are both potent triggers of EMT via EMT regulators, initiating complex changes in the molecular phenotype of cells, e.g. downregulation of epithelial markers and increased expression of mesenchymal markers. These changes lead to the remodeling of the cellular cytoskeleton facilitating migration and induce destruction of the ECM by tumor cells by secreted MMPs (modified from Gavert and Ben-Ze'ev, 2008).

All EMT regulators are believed to act primarily as transcriptional repressors (through binding to E-boxes in gene enhancers). In particular, all of them were shown to directly repress E-cadherin. Such a redundancy in regulation of E-cadherin is due to its importance for driving EMT: after the *ECAD* gene is repressed (either transcriptionally by the EMT-

regulators, or via epigenetic mechanisms), E-cadherin-bound β-catenin is released, whereupon it translocates to the nucleus and after binding with the TCF/LEF1 and other co-factors further stimulates EMT, cell survival, proliferation, and stem cell characteristics (Bolos *et al*., 2016; Craene and Berx, 2013; Vandewalle *et al*., 2005).

Multiple factors are known to induce epithelial-to-mesenchymal transition, including hypoxia, TGFβ, epigenetic regulators, certain RTK ligands (e.g. FGF2, HGF, IGF1, etc.), proinflammatory cytokines (e.g. IL-6 or IL-8), various cytokines provided by tumor associated fibroblasts/macrophages, etc. (Fernando *et al*., 2011; Ogunwobi *et al*., 2013). In the next sections, TGFβ, hypoxia and epigenetic factors will be discussed in more details as the most prominent stimuli of EMT.

3.2.2.1.1. TGFβ-induced EMT and metastasis

Transforming growth factor β (TGFβ) can drive EMT in tumor cells via several distinct molecular pathways. These can be subclassified into SMAD-dependent and SMAD-independent (non-canonical) signaling cascades. The SMAD-dependent activation of EMT in tumors is primarily mediated by TGFβ1-3 ligands, which upon binding to the TGFβR2 receptor, induce its heteromerization with the TGFβR1 receptor. Heteromerization of the two types of receptors leads to activation of the C-terminal kinase domain of TGFβR1 and phosphorylation of SMAD2/3. Phosphorylated SMAD2/3 proceed to form a complex with the common SMAD – SMAD4. The full SMAD complex is then translocated to the nucleus, where upon binding with other transcription factors it can repress or induce gene expression. It was shown that the SMAD complex can interact with Snail or Zeb1 and further stimulate the transcription of these EMT regulators, thus forming a feed-forward loop resulting in further potentiation of EMT (Horbelt *et al*., 2012; Peinado *et al*., 2003; Schmierer and Hill, 2007).

Complementing the classical TGFβ pathway, several non-SMAD related signaling cascades leading to EMT have been described. For example, TGFβ was shown to activate AKT through PI3K, resulting in induction of mTORC1/2, increased motility, and metastasis. Another example of non-canonical TGFβ regulation of EMT involves the activation of GTPases, like RHO, RAC, and CDC42, that actively regulate cytoskeletal reorganization, formation of lamellipodia and filopodia (Nakaya et al., 2008; Xu et al., 2009).

3.2.2.1.2. The role of hypoxia in EMT, invasion, and metastasis

"Probably chronic intermittent oxygen deficiency plays a greater role in the formation of cancer in the body than does the chronic administration of respiratory poisons."

O. Warburg, Science, 1956

Hypoxia is a physiological condition characterized by inadequate supply of oxygen (oxygen levels of 1-3% are typically considered hypoxic, depending on the tissue). Many tumors were shown to exhibit signs of hypoxia and ischemia (lack of oxygen and nutrients) as the result of their rapid growth and aberrant vasculature. Moreover, hypoxia has been correlated with a poor prognosis in the clinics (Dekervel *et al*., 2014; Henze and Acker, 2010; Höckel and Vaupel, 2001; Jubb *et al*., 2010).

The cellular response to hypoxia is primarily mediated by HIFs, which are heterodimeric transcription factors consisting of two parts – one alpha and one beta subunit. Three HIFα and one common HIFβ/ARNT subunits are known, of which HIF1α and HIF2α were shown to play a significant role in tumor progression and metastasis. HIFα subunits are oxygen sensitive and their stability is primarily regulated on the posttranslational level. HIFβ, by contrast, is ubiquitously expressed and not dependent upon oxygen concentrations (Hu *et al*., 2003; Koh *et al*., 2011).

Fig. 3.5. illustrates the mechanism of oxygen dependent regulation of the hypoxic response: under normoxic conditions HIF1α and HIF2α are hydroxylated by prolyl hydroxylases (PHDs) at specific proline residues (P402/P564 and P405/P531, respectively) within their oxygen-dependent degradation domains. PHD1-3 serve as the primary cellular oxygen sensors because their enzymatic activity depends upon the availability of oxygen, iron, ascorbate, and oxoglutarate. Next, a ubiquitin ligase complex containing the von Hippel-Lindau protein (pVHL) ubiquitinates the hydroxylated alpha subunits, targeting them for proteasomal degradation. In contrast, under hypoxic conditions PHDs fail to hydroxylate HIF1/2α. This results in stabilization of the alpha subunits, their translocation into the nucleus, and formation of a functional transcription factor following heterodimerization with HIFβ (Filatova *et al*., 2016; Henze *et al*., 2014; Maxwell *et al*., 1999; Minamishima *et al*., 2009).

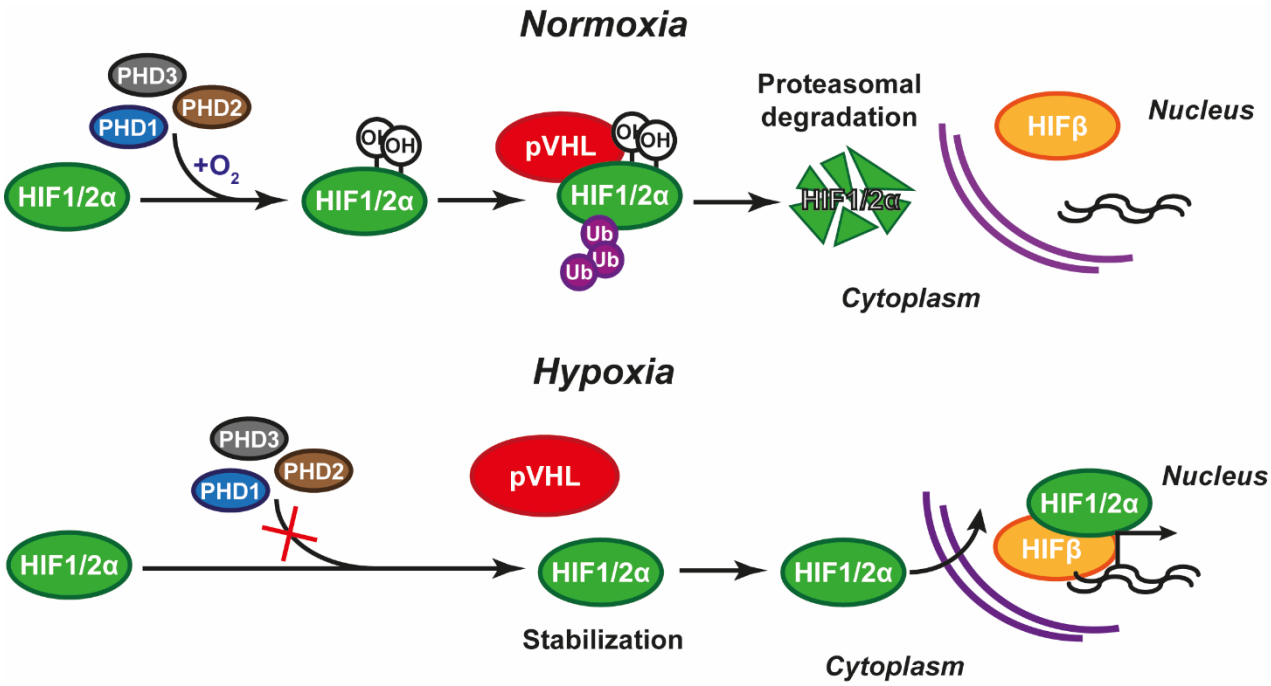

Fig. 3.5. Oxygen-dependent regulation of hypoxia signaling. In the presence of oxygen (i.e. under normoxia) the HIF1/2α subunits become hydroxylated at their oxygen-dependent degradation domains by prolyl hydroxylases (PHD1-3). Hydroxylated HIFs are then ubiquitinated by a ubiquitin ligase complex containing pVHL and targeted for proteasomal degradation. By contrast, under hypoxic conditions the lack of oxygen prevents PHDs from hydroxylating HIFs leading to their increased stability. This results in the translocation of HIF1/2α to the nucleus and formation of an active transcription factor though heterodimerization with the HIFβ subunit (modified from Martínez-Sáez *et al*., 2017).

HIF1/2 regulate transcription by binding to hypoxia response elements (with a consensus sequence of A/GCGTG) in gene promoters, or in enhancers that are distant from promoters (especially in the case of HIF2; Dengler *et al*., 2014). Most hallmarks of cancer are known to be affected by hypoxia:

1) invasion and metastasis – HIFs can stimulate EMT via induction of EMT regulators, like Snail, Slug, Twist1, and Zeb1; in addition, hypoxia strongly increases secretion of ECM modifying enzymes, like MMPs, cathepsin S, uPA and others(Araos *et al*., 2018; Raval *et al*., 2005; Semenza, 2012);

2) angiogenesis – HIF1/2α expression strongly correlates with vascularization of tumors, as HIFs (especially HIF2) increase transcription of VEGFs, PDGFβ, ANGPT2, etc. (Hirota and Semenza, 2006; Otrock *et al*., 2009; Raval *et al*., 2005; Uniacke *et al*., 2012);

3) metabolic reprogramming – HIF1α was shown to strongly activate the expression of genes facilitating glycolysis, like *GLUT1/3*, *PGK1*, *LDHA*. Hypoxia was also shown to affect autophagy and fatty acid oxidation (Arreola *et al*., 2014; Semenza, 2010);

4) cell proliferation and survival – depending on the context, hypoxia can either stimulate (primarily HIF2) or inhibit (HIF1) Myc activity; HIF2 was also shown to inhibit TP53 (Gordan *et al*., 2007; Kim *et al*., 2007; Qin *et al*., 2014);

5) modulation of the immune response – hypoxia is associated with increased presence of tumor associated macrophages (TAMs), regulatory T-cells, myeloid-derived suppressor cells, and other cells which can stimulate tumor growth by providing growth stimulating cytokines and angiogenesis factors. In addition, HIF1 drives the expression of the immune checkpoint inhibitor PD-L1, IL-6, and other immunosuppressive cytokines (Facciabene *et al*., 2011; Fang *et al*., 2018; Noman *et al*., 2014).

Investigations into tumor angiogenesis revealed a complex picture wherein different regions in a single tumor could experience significant changes in blood perfusion (Benjaminsen *et al*., 2004; Wu *et al*., 2009a). As expected, tissue oxygen tension was also shown to strongly fluctuate between different tumor areas, creating in some parts the pathophysiological condition of intermittent (cycling) hypoxia (Thews *et al*., 2004). As opposed to prolonged chronic hypoxia (e.g. in perinecrotic areas), much less information is available on the role of intermittent hypoxia in tumor progression and metastasis. In several recent studies, it was shown that despite the very short half-life of HIFα subunits in normoxia (estimated at approx. 5 min), in human neuroblastoma, glioblastoma multiforme (GBM), and breast cancer lines (NB1691, U87, and MCF10, respectively) intermittent hypoxia induced high expression of hypoxia response genes, in some cases even to a greater extent than chronic hypoxia (Bhaskara *et al*., 2012; Chou *et al*., 2012; Verduzco *et al*., 2015).

In addition, exposure of mice transplanted with melanoma or lung carcinomas to regimens of intermittent hypoxia (*in vivo* models mimicking obstructive sleep apnea) lead to enhanced tumor growth, vascularization, and metastasis in the lung (Almendros *et al*., 2013). In a recent publication, Chen *et al*. showed that *in vitro* exposure of cells to intermittent hypoxia promotes lung metastasis of a syngenic mouse mammary tumor line (Chen *et al*., 2018). Nonetheless, the exact mechanisms and contribution of intermittent hypoxia to EMT and tumor metastasis still remain elusive.

3.2.2.1.3. Epigenetic regulation of EMT

"…We observed substantial hypomethylation in several specific genomic regions of four of five human cancers, compared with adjacent normal cells from the same patients. A metastasis from one patient showed an even greater degree of hypomethylation than the primary tumor… This study clearly shows that such DNA alterations exist in at least some human cancers."

A. Feinberg and B. Vogelstein, Nature, 1983

Recent developments in next generation sequencing and methylation analysis have significantly broadened the scope of epigenetic studies, in particularly in the field of cancer biology. Nowadays, epigenetic regulation is also reported to play a major role in EMT and tumor metastasis (Baxter *et al*., 2014; Feinberg and Tycko, 2004).

Epigenetic regulation of gene activity comprises all the mechanisms that lead to changes of cellular phenotype without altering its genotype, i.e. primary DNA sequence. Three main classes of epigenetic mechanisms have been described until now – DNA methylation, genomic imprinting, and histone modification, all of which are significantly deregulated during cancer development and progression (Dawson and Kouzarides, 2012; Sharma *et al*., 2009).

Modification of N-terminal tails of histones represents the most complex and rapid way of epigenetic regulation of genes. Up to now, numerous such modifications were identified (some of the most common and best studied are listed in **Table 3.2**). These modifications vary not only in their chemical nature, e.g. acetylation or methylation, but also in the effect that these modifications have on gene transcription. For instance, trimethylation of lysine 9 of histone 3 is a very strong repressive mark, while trimethylation of lysine 4 of the same histone leads to increased transcription (Cohen *et al*., 2011; Sadikovic *et al*., 2008; Shi *et al*., 2011; Wu *et al*., 2007).

The enormous complexity of regulation by the histone code is best exemplified by the vast numbers of enzymes – writers, readers, and erasers, each of which might have multiple targets and opposing effects on gene activity (Hake *et al*., 2004).

Table 3.2. Histone modifications and their impact on transcription

Modification	Role in transcription	Modification site	Main regulators
Acetylation	Activation	H3 (K9, K14, K18, K56) H4 (K5, K8, K12, K16) H2B (K6, K7, K16, K17)	Writers: HATs Erasers: HDACs
Methylation	Activation	H3 (K4me2, K4me3, K36me3, K79me2)	Writers: MLLs, SETDs Erasers: KDM1A/B, KDM5A-D, KDM4A-C
Methylation	Repression	H3 (K9me3, K27me3) H4 (K20me3)	Writers: EZH1/2, G9a, SUV4-20H1/2 Erasers: KDM6A/B, JHDM1D
Phosphorylation	Activation	H3 (S10, S28)	Writers: MSK1/2, Aurora-B Erasers: PP1, PP2A

H – histone, K – lysine, S – serine, me – methylation, HAT – histone acetyltransferase, HDAC – histone deacetylase (modified from Boland *et al*., 2014 and Landgrave-gómez *et al*., 2015)

Limited information is available on the mechanisms of EMT regulation by histone modifications, with many studies focusing on E-cadherin (*CDH1*) repression as one of the main events during EMT. This is best exemplified by the EMT regulator Snail, which was shown to cooperate with multiple epigenetic enzymes:

1) In a study by Herranz *et al*., 2008, it was shown that Snail recruits EZH2 and SUZ12 (both polycomb repressor complex 2 members) to the *CDH1* promoter, resulting in H3K27 trimethylation and gene repression;
2) Dong *et al*., 2013 showed that Snail interacts with the histone methyltransferase SUV39H1 that catalyzes H3K9 trimethylation, recruiting it to the *CHD1* promoter and resulting in gene silencing;
3) Snail was identified to recruit the NuRD complex to the *CHD1* promoter (Dong *et al*., 2013), resulting in histone deacetylation (mediated by the HDAC1/2 enzymes, which are part of the NuRD complex).

While histone modifications are believed to be the fastest epigenetic mechanism of controlling gene activity, DNA methylation – the other complementary type of epigenetic regulation – is associated with long term stable gene repression (Mathot *et al*., 2017; Yang *et al*., 2014). Unlike the numerous regulators involved in histone modification, the process

of DNA methylation and demethylation is regulated by a much smaller number of enzymes with the primary regulators belonging to two gene families (**Fig. 3.6**):

1) DNA methyltransferases (DNMTs) – enzymes that actively methylate cytosines at CpG sites. Three DNMTs are involved in methylation in mammals: the maintenance methyltransferase DNMT1 and two *de novo* methyltransferases – DNMT3A and DNMT3B (Rhee *et al*., 2002);
2) Ten-eleven translocation enzymes (TETs) – named after the fusion oncoprotein between *TET1* and *MLL* originally identified in acute myeloid leukemia (Kim *et al*., 2017). These enzymes are Fe(II) and α-ketoglutarate dependent dioxygenases catalyzing the oxidation of 5-methylcytosines to 5-hydroxymethylcytosines, followed by oxidation to 5-formylcytosines and 5-carboxylcytosines. The sequential rounds of oxidation lead to base excision repair (BER) reverting the methylation state (Kim *et al*., 2017; Kohli and Zhang, 2013; Williams *et al*., 2011).

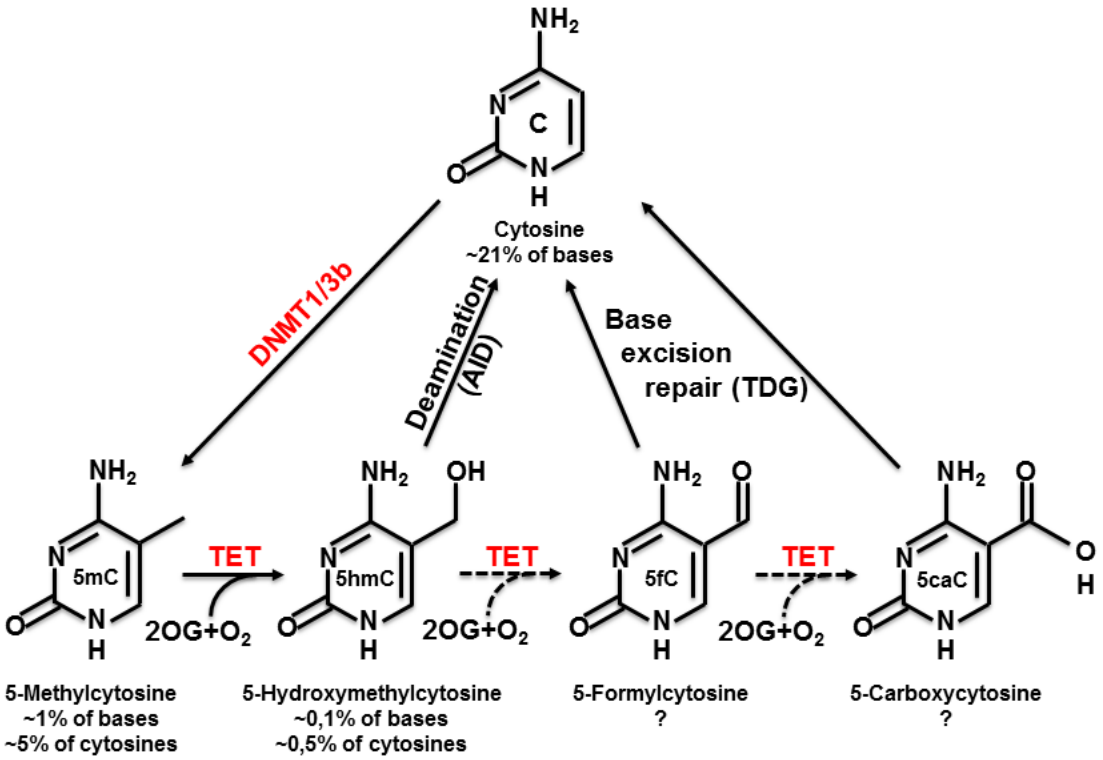

Fig. 3.6. Regulation of DNA methylation. Two groups of enzymes – the TET family of oxygenases and the DNA methyltransferases (DNMTs) – are the main regulators of DNA methylation. While DNMTs can directly transfer the methyl groups onto cytosines, the process of demethylation is more complex and involves a series of oxygenation steps mediated by TET1-3 enzymes, typically followed by the base excision repair as the final step in reversing the methylated state (modified from Koh and Rao, 2013).

Historically, DNA demethylation was the first epigenetic modification to be discovered in cancer, followed by numerous studies either contradicting or supporting the initial finding. Until now, it is well established that tumors employ DNA hypermethylation to silence some tumor suppressor genes (first shown on the *RB* gene), while the consensus is that a slight decrease in DNA methylation is observed overall (Bernardino *et al*., 1997; Ehrlich, 2002; Frigola *et al*., 2005; Hansen *et al*., 2011; Stirzaker *et al*., 1997).

Very limited information is available on the role of methylation in EMT and metastasis. So far, it was shown that increased methylation of the tumor suppressor *VHL* can promote EMT by stimulating hypoxia (McRonald *et al*., 2009; Moore *et al*., 2011), while other studies showed a correlation between hypoxia and genome-wide DNA demethylation (e.g. in breast cancer; Guo *et al*., 2002; Lu *et al*., 2011). Of special interest is the study by Mariani *et al*., 2014 that showed that not only TET1 was upregulated by hypoxia, but that this was also associated with increased levels of 5-hMeC at hypoxia-inducible genes. Yet, these effects were observed only in the case of neuroblastomas, but not other cancers. Overall, despite the recent insights into the epigenetics of EMT, these mechanisms remain largely elusive, especially concerning the contribution of epigenetics to tumor invasion and metastasis.

3.2.2.2. Cancer stem cells and their role in metastasis

Hypoxia- and TGFβ-induced EMT significantly contribute to the acquisition of stem cell characteristics by tumor cells (Asiedu *et al*., 2011; Covello, KL., Kehler, J., Yu, H., Gordan, JD., Arsham, AM., Hu, C., Labosky, PA., Simon, MC., Keith, 2006; Polyak and Weinberg, 2009; Seidel *et al*., 2010). Cancer stem cells (CSCs) represent a distinct subpopulation in tumors that, similarly to stem cells in normal tissues, possesses a high capacity for self-renewal. CSCs were first identified in leukemias, but solid tumors were also shown to possess CSCs (Welte *et al*., 2010).

CSCs can be identified by the expression of specific markers, like CD133, CD44, Sox2, Nanog, Maml3, Oct4, etc., yet the exact gene profile is dependent of the specific tumor type. For example, breast cancer CSCs bear a $CD44^{high}/CD24^{low}$ profile (Chen *et al*., 2008; Horimoto *et al*., 2016; Li *et al*., 2017; Tirino *et al*., 2009). High self-renewal capacity of CSCs has been demonstrated *in vitro* in, for example, a colony or sphere formation assays, and *in vivo*, based on more efficient tumor initiation and faster tumor growth in animals transplanted with CSC marker-expressing cells compared to non-CSC cells (Agro and O'Brien, 2015; Seidel *et al*., 2010; Zhu *et al*., 2018).

Hypoxia and TGFβ greatly enhance the CSC phenotype in tumors (Asiedu *et al*., 2011; Covello *et al*., 2006; Louie *et al*., 2010; Seidel *et al*., 2010). For instance, $CD44^{high}/CD24^{low}$ breast cancer cells possess high expression of EMT markers, like N-cadherin and laminin, and decreased E-cadherin (Liu *et al*., 2014). As another example, cells in perinecrotic, and thus hypoxic, areas in glioblastomas have high expression of CSC markers (Seidel *et al*., 2010). In addition, Oct4 – a well-established CSC marker – is also known to be regulated by HIF2 (Covello *et al.*, 2006). Similarly to hypoxia, TGFβ was also shown to regulate the CSC phenotype in tumor cells (e.g. TGFβ-induced expression of *CD133* via DNMT repression and DNA demethylation in hepatocellular carcinoma cells; You *et al*., 2010). Moreover, based on the connection between EMT and metastasis, a direct link has been proposed between CSC characteristics and metastatic tumor dissemination (Mani *et al*., 2008). In addition, CSC are believed to play a significant role in dormancy, tumor recurrence, and chemoresistance, highlighting the importance of developing new approaches to target this specific tumor cell population (Dean *et al*., 2005; Magee *et al*., 2012; Singh and Settleman, 2010).

3.3. Anti-angiogenic therapy

"…There is enough evidence to suggest that if neovascularization is prevented many solid tumors might remain fixed at this tiny [2-3 mm] diameter."

J. Folkman, Annals of Surgery, 1971

The fact that tumor growth is dependent on the blood supply naturally leads to the idea of blocking angiogenesis as means of treatment for patients with cancer. The concept of anti-angiogenic therapy was pioneered by Judah Folkman in the 1970s and at that time evoked many hopes for its effectiveness in clinics (Folkman, 1972).

Curiously, a more basic version of the idea of "starving" the tumor by blocking its blood supply can be traced back to ancient times: Archigenes of Apamea, a Roman surgeon practicing in 1-2 centuries AD, is credited to be the first to suggest vessel occlusion by ligation before surgical resection of the tumor (Papavramidou *et al*., 2010). In addition, he suggested applying "cups" to the tumors, which is nowadays believed to have stimulated tumor vein thrombosis (i.e. a forerunner to embolization of the vascular supply of a tumor). The practice of closing major vessels feeding the tumor was further developed and improved

by many surgeons thereafter, yet Folkman was the first to suggest blocking the ingrowing vessels rather than dealing with the already established vascular supply.

At the dawn of the anti-angiogenesis era high expectations were fueled by the solid theoretical background behind the approach (Folkman, 1972; Yang *et al*., 2017):

1) As endothelial cells lining the vessel walls were the primary targets of anti-angiogenic therapy, it was expected that no issues with drug delivery would be encountered;
2) Endothelial cells are non-transformed cells lacking the heterogeneity and genetic instability of tumor cells, thus no resistance mechanisms were expected to develop;
3) Since many layers of tumor cells depend on scarce vessels, it was believed that targeting tumor vessels would result in massive death of cancer cells;
4) Tumor vasculature was known to be in a different (activated) state than the quiescent vasculature in normal tissues, raising hopes for developing tumor vessel-specific agents;
5) Angiogenesis was long known to accompany tumor metastasis; therefore, it was believed that anti-angiogenic therapy would diminish tumor dissemination.

At that time, newly discovered endogenous anti-angiogenic agents (e.g. statins and thrombospondins) fueled the interest in anti-angiogenesis and urged clinical trials. Pre-clinical data showed that endostatin, a 20 kDa fragment of collagen XVIII, could block endothelial cell proliferation, migration, vascular sprouting, and tumor growth in mice. Alas, the first phase I and II clinical trials proved disappointing, showing little to no survival benefits in patients with advanced tumors (Hansma *et al*., 2005). Despite the fact that later on a new formulation of recombinant endostatin (Endostar) did show survival benefits in non-small-cell lung cancer (NSCLC) patients, the initial failure was followed by intense research in the field of vascular biology and tumor angiogenesis, which in turn spurred the search for other anti-angiogenic agents (Fu *et al*., 2008; Sun *et al*., 2013).

Real advance in anti-angiogenesis came about after the discovery of factors driving tumor vessel formation, especially – identification and cloning of VEGF (Keck *et al*., 1989; Leung *et al*., 1989; Senger *et al*., 1983). This progress in understanding the molecular basis of tumor angiogenesis resulted in the development of the first clinically approved anti-angiogenic agent – bevacizumab (BVZ; Presta *et al*., 1997). BVZ is a humanized monoclonal IgG antibody against VEGFA that was developed by Roche (commercial name – Avastin). In contrast to the previous failed clinical trials with endogenous inhibitors, BVZ significantly increased progression free survival and to a lesser extent – overall survival in

patients with metastatic colorectal carcinomas, renal cell carcinomas, and ovarian carcinomas (Escudier *et al*., 2010; Perren *et al*., 2011; Yamazaki *et al*., 2016). For example, a randomized phase III clinical trial of BVZ in combination with irinotecan, 5-fluorouracil, and leucovirin (IFL), in patients with metastatic colorectal carcinoma revealed a significant increase in progression free survival (PFS) from 6.2 months in the control cohort (without BVZ, but with IFL) to 10.6 months in the test group (Hurwitz *et al*., 2004). Overall survival (OS) – arguably, the most important criteron of drug efficacy – was also significantly higher in patients receiving BVZ+IFL than in the IFL group (20.3 vs 15.6 months, respectively). Another phase III trial of BVZ in combination with paclitaxel and carboplatin in patients with non-small cell lung cancer showed a more modest, but nevertheless significant improvement in PFS (6.2 vs 4.5 months) and OS (12.3 vs 10.3 months; Hurwitz *et al*., 2004). Interestingly, the initial US FDA approval of BVZ in 2004 also recommended BVZ to be used in combination with paclitaxel to treat patients with metastatic breast carcinomas. This recommendation was based on the results of a phase III trial showing an increase in PFS from 5.8 months in the control (only paclitaxel) to 11.3 months in the cohort receiving BVZ in addition to paclitaxel (no changes in OS were observed in that trial; Miller *et al*., 2007). However, another phase III trial could not support the initial findings (Gray *et al*., 2009): combination of BVZ and capecitabine did not show any significant improvements either in PFS (4.86 vs 4.17 months), or in OS (15.1 vs 14.5 months). This led to a withdrawal of the FDA permission to use BVZ for treating breast cancer patients.

Such modest results obtained with BVZ in the clinics raised questions regarding the sufficiency of targeting just one molecule, especially considering the constantly growing list of novel pro-angiogenic factors and their contribution to tumor angiogenesis. Thus, the idea of targeting multiple signaling pathways involved in angiogenesis was conceived resulting in the development of multi-targeted agents. Most of these agents belong to the class of small molecule inhibitors that target receptor and non-receptor tyrosine kinases (Broekman, 2011; Chow and Eckhardt, 2007; Wilhelm *et al*., 2006). Some of the early and typical representatives of this class of anti-angiogenic drugs are sorafenib and sunitinib. Both share many commonly targeted receptors like VEGFR2, PDGFRs, c-Kit, etc. In contrast to BVZ, significant clinical improvements were achieved using monotherapy with these RTK inhibitors (Llovet JM *et al*., 2008; Motzer *et al*., 2007). In 2005, sorafenib became the first FDA approved anti-angiogenic RTK inhibitor for use in metastatic renal cell carcinomas (later also extended to hepatocellular carcinomas and thyroid cancer), with sunitinib approval following in 2006 for renal cell carcinomas (RCC), and later – for pancreatic

neuroendocrine tumors (PNETs) and gastrointestinal stromal tumors (GIST) tumors. Evidence for clinical benefits of these drugs were further confirmed in multiple subsequent studies. For instance, sorafenib monotherapy in patients with advanced RCC increased OS to 17.8 months in contrast to 14.3 months in the placebo group (Escudier *et al*., 2009), while phase III trial with sunitinib in comparison to IFNα (the standard of treatment for advanced RCCs) in patients with metastatic RCC revealed significantly increased OS in the sunitinib-treated group (26.4 vs 21.8 months, respectively; Escudier *et al*., 2009). It should be noted that several of the targets of these RTK inhibitors are expressed not only on blood vessel cells, but also on other stromal cells and on tumor cells. Therefore, the benefits of RTK inhibitors in tumor patients may be attributable to a combination of effects on their various molecular and cellular targets

Since the time the first RTK inhibitors were introduced into the clinics multiple novel anti-angiogenic drugs have been developed and tested in pre-clinical and clinical trials. **Table 3.3.** lists the anti-angiogenic drugs that have been approved by the FDA and EMA for use in the clinics. The list is still growing with new drugs added almost every year. Most of the new agents are RTK inhibitors which are recommended for use in combination with conventional chemotherapy or after previous attempts with chemotherapy have failed (Jayson *et al*., 2016; Vasudev and Reynolds, 2014). Interestingly, combination of anti-angiogenic and conventional cytotoxic chemotherapy proved to be beneficial due to an unexpected side effect of anti-angiogenesis in tumors – transient vessel normalization which improves perfusion, resulting in improved delivery of chemotherapeutics (Batchelor *et al*., 2007; Chae *et al*., 2010; Winkler *et al*., 2004).

Table 3.3. Anti-angiogenic drugs approved for clinical use

Agent	Drug class / Target	Year of first approval, FDA/EMA	Clinical use
Bevacizumab	mAb against VEGFA	2004/2005	Metastatic colorectal cancer, NSCL cancer, RCC, ovarian carcinoma
Sorafenib	Tyrosine kinase inhibitor targeting B-Raf, VEGFR, PDGFR	2005/2006	HCC, RCC, thyroid cancer

Agent	Drug class / Target	Year of first approval, FDA/EMA	Clinical use
Sunitinib	RTK inhibitor targeting VEGFRs, PDGFRs, c-Kit	2006/2007	RCC, PNET
Pazopanib	RTK inhibitor targeting FGFR, VEGFRs, PDGFRs, c-Kit	2009/2009	RCC, soft tissue sarcoma
Vandetanib	Kinase inhibitor targeting VEGFR2, EGFR, RET	2011/2012	RCC
Axitinib	Tyrosine kinase inhibitor targeting VEGFRs, PDGFR, c-KIT, and Bcr-Abl	2012/2012	RCC
Aflibercept	VEGF trap, binds to VEGFA, VEGFB, and PlGF	2012/2013	Colorectal cancer
Cabozantinib	Tyrosine kinase inhibitor targeting c-Met, VEGFR2, AXL, RET	2012/2014	Thyroid cancer, RCC
Regorafenib	Tyrosine kinase inhibitor targeting VEGFRs, TIE2, c-KIT, RET, B-Raf, PDGFR, FGFR	2013/2013	Metastatic colorectal cancer
Nintedanib	RTK inhibitor targeting VEGFRs, PDGFR, FGFR	- / 2014	NSCL cancer
Ramucirumab	mAb against VEGFR2	2014/2014	Gastric cancer, NSCL cancer, metastatic colorectal cancer
Lenvatinib	RTK inhibitor targeting VEGFRs, FGFR2, PDGFR, c-KIT, RET	2015/2015	Thyroid cancer

FDA – Food and Drug Administration, EMA – European Medicines Agency, mAb – monoclonal antibody, NSCLC – non-small cell lung cancer, RCC – renal cell carcinoma, HCC – hepatocellular carcinoma, PNET – pancreatic neuroendocrine tumors; modified from Jayson *et al*., 2016.

Nonetheless, it is worth noting that only a limited number of tumors is currently recommended for treatment with anti-angiogenic therapy. This can partially be explained by the heavy side-effects of anti-angiogenic drugs (e.g. hemorrhages, thromboembolism,

hypertension, and bowel perforation in patients with colorectal carcinoma receiving BVZ; Yamazaki *et al*., 2016). However, the main obstacle is the lack of antitumor efficacy of these drugs in other tumor types (for instance, failed phase III trials of the RTK inhibitor vatalanib in colorectal carcinoma patients; Los *et al*., 2007). In most cases, less than 50% of patients in clinical trials responded to anti-angiogenic therapy (Jayson *et al*., 2016). Moreover, in the majority of patients showing positive effects of the therapy, the antitumor response to anti-angiogenic drugs was never curative but rather transient and mostly short-lived (Ebos *et al*., 2009b; Griffioen *et al*., 2012).

A more detailed analysis of the response of tumors to anti-angiogenic therapy revealed the presence of various mechanisms of tumor resistance against anti-angiogenic therapy that significantly limit the clinical application of this treatment approach (Bottsford-Miller *et al*., 2012).

3.4. Modes of resistance to anti-angiogenic therapy

“Judah Folkman is going to cure cancer in two years.”

J. Watson, The New York Times, 1998

[In later years J. Watson claimed to have been misquoted by the reporter]

“If you have cancer and you are a mouse, we can take good care of you.”

J. Folkman, interview, 1998

Disillusionment following initial clinical trials of the first anti-angiogenic agents was quickly replaced by investigations of the mechanisms of tumor resistance to the therapy. The very first resistance mechanism to be discovered reflected the enormous redundancy in angiogenic signaling in tumors: in clinical studies with BVZ, various pro-angiogenic factors became upregulated following VEGFA neutralization, like PlGF, HGF, and FGF2 (Casanovas *et al*., 2005; Kopetz *et al*., 2010). Moreover, some tumors were not responsive to BVZ from the beginning, indicating that such tumors were intrinsically resistant to anti-VEGFA therapy (Kindler *et al*., 2010). On the other hand, the transient nature of antitumor effects in sensitive tumors hinted at some mechanisms that actively developed in response to the therapy (acquired resistance). One possible explanation for the rapid regrowth of vessels following anti-angiogenic therapy raised in multiple studies is the therapy-induced

hypoxia which stimulates the secretion of alternative pro-angiogenic factors (PlGF, ANGPT1, PDGF, etc.; Giuliano and Pagès, 2013; Han *et al*., 2015; Rapisarda and Melillo, 2009). The dichotomy into intrinsic and acquired resistance mechanisms laid the foundation for classification of the modes of resistance to anti-angiogenic therapy (**Fig. 3.7**; Bergers and Hanahan, 2008). Several distinct molecular and cellular mechanisms have been proposed to explain both intrinsic and acquired resistance.

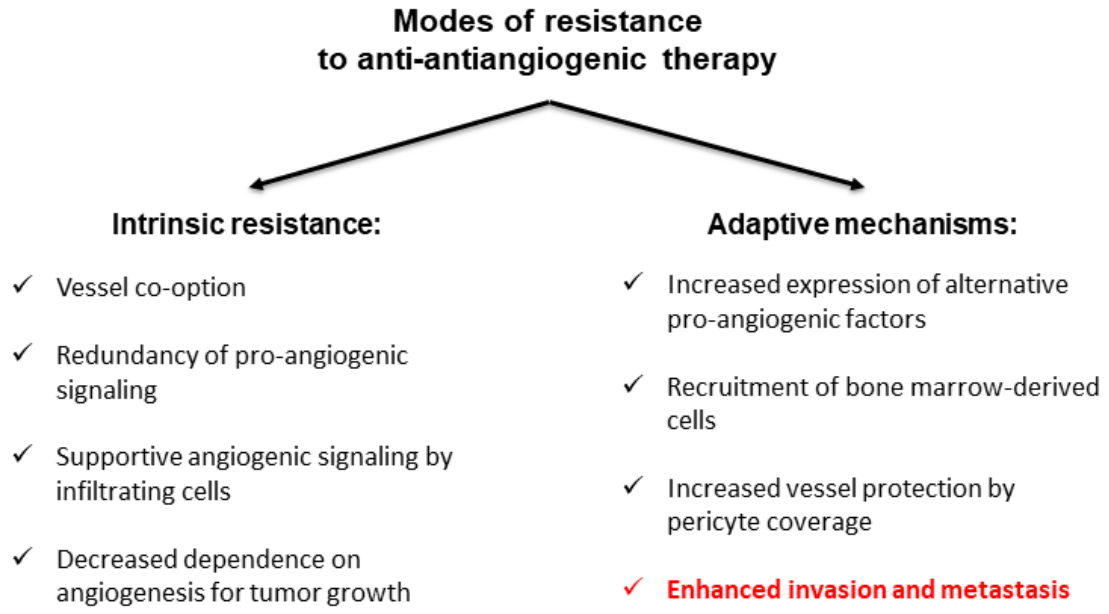

Fig. 3.7. Classification scheme of modes of tumor resistance to anti-angiogenic therapy. Mechanisms of tumor resistance to anti-angiogenic therapy can be classified into two main groups: 1) intrinsic resistance, pre-existing before the application of therapy; 2) mechanisms that evolve in response to therapy, i.e. adaptive resistance. Amid the adaptive mechanisms, a separate subgroup can be outlined that lead to increased tumor cell migration and invasion, the so called evasive resistance (modified from Bergers and Hanahan, 2008).

Beside the pre-existing redundancy of alternative pro-angiogenic factors, vessel co-option represents another example of intrinsic resistance (Bridgeman *et al*., 2017; Prager *et al*., 2012). Some tumor types, e.g. GBMs or melanomas, primarily rely on vessel co-option in contrast to angiogenesis and show a characteristic pattern of growth along the vessels (Dme *et al*., 2002; Xue *et al*., 2017). Beyond co-option, some tumors, as melanomas or GBMs, possess even a more exceptional way of acquiring sufficient blood supply – vasculogenic mimicry (El Hallani *et al*., 2010; Vartanian *et al*., 2007). This process is characterized by tumor cell transdifferentiation into endothelial-like cells that can form vessel-like structures to support blood flow. In this case melanoma cells acquired the ability to express endothelial

cell markers, like VE-cadherin, ephrin A2, TIE1, etc. Nonetheless, this phenotypic change did not render these tumor cells responsive to anti-angiogenic therapy with endostatin or anginex (van der Schaft *et al*., 2004).

On top of the above-mentioned intrinsic resistance mechanisms, some tumors are less dependent on vascularization in general (e.g. pancreatic ductal carcinomas, cholangiocarcinomas or chondrosarcomas), which may reflect their better adaptation to hypoxic conditions and the poor responsiveness to anti-angiogenesis (Casanovas *et al*., 2005; Kawahara *et al*., 1998; Kubo *et al*., 2013).

Another type of tumor resistance to anti-angiogenic therapy is mediated by infiltrating myeloid and lymphoid cells, often referred to as bone marrow-derived cells (BMDCs). Among the multiple distinct types of non-cancerous cells residing in human tumors, BMDCs – including myeloid-derived suppressor cells (MDSC), tumor associated macrophages (TAMs), T helper type 17 cells (Th17), etc. – directly contribute to tumor angiogenesis by secretion of pro-angiogenic factors (VEGFs, FGFs, EGF) and ECM remodeling enzymes, like MMPs (Chung *et al*., 2013; Finke *et al*., 2011; Hotchkiss *et al*., 2003). A separate group of BMDCs, endothelial progenitor cells (EPCs), become incorporated into the newly formed tumor vessels enhancing the resistance to anti-angiogenesis (Rafii *et al*., 2002). In some tumors the dazzling diversity of BMDCs secrete such a complex mix of alternative angiogenic factors that any attempts at blocking angiogenesis by targeting one or few factors or signaling pathways remain futile (Casanovas, 2011; Han *et al*., 2015). Other tumors in response to anti-angiogenic therapy start to secrete factors like SDF1, VEGF, or G-CSF, that initiate mobilization and recruitment of BMDCs into the tumor stroma (Crawford and Ferrara, 2009; Griffioen *et al*., 2012; Orimo *et al*., 2005).

For most of the above-mentioned intrinsic and acquired resistance mechanisms compelling evidence is available from both experimental and clinical studies. Yet, much less clinical data are available for one unique group of acquired resistance mechanisms that result in enhanced tumor migration and metastasis, despite the potentially grave implications for the patients. This distinct group of mechanisms is generally referred to as evasive resistance (Bergers and Hanahan, 2008; Dey *et al*., 2015). So far, in several *in vivo* studies with human tumor xenografts (lung, breast, and renal carcinomas, melanoma) and genetically engineered mouse models (pancreatic tumors of RIP1-Tag2 mice) applying RTK inhibitors as anti-angiogenic therapy resulted in increased metastasis to the lungs or liver (Crawford and Ferrara, 2009; Ebos *et al*., 2009b; Orimo *et al*., 2005; Pàez-Ribes *et al*., 2009a; Singh

et al., 2012; Welti *et al*., 2012). Even though these effects were dose- and regimen-dependent for some specific agents, such as sunitinib, in most cases the results could be reproduced by many independent studies.

As multiple pathways converge on the regulation of tumor cell migration, invasion, and metastasis, the exact mechanisms underlying evasive resistance remain to be fully elucidated. One of the possible explanations implicates hypoxia as a trigger for increased invasion and metastasis (Cooke *et al*., 2012; Rapisarda and Melillo, 2009; Tejpar *et al*., 2012). Anti-angiogenic therapy has long been speculated to induce strong hypoxia in tumors as a natural consequence of limiting the availability of oxygen-delivering blood. Indeed, experiments with the hypoxyprobe pimonidazole revealed the presence of highly hypoxic regions in primary tumors of mice treated with sunitinib, anti-VEGFR2 Ab, or after pericyte ablation (Casanovas *et al*., 2005; Cooke *et al*., 2012; Han *et al*., 2015; Pàez-Ribes *et al*., 2009a). In line with the theory that hypoxia stimulates EMT, tumors in mice receiving anti-angiogenic therapy had high levels of EMT regulators Snail, Twist1, and Zeb2, and a typical change in the EMT markers: decreased E-cadherin and increased N-cadherin and vimentin. Furthermore, it was shown that targeting vessels with sunitinib, BVZ, or by pericyte ablation increased tumor HIF1α levels (Cooke *et al*., 2012; Depner *et al*., 2016).

Some more mechanistic insights into evasive resistance to anti-angiogenic therapy are available from GBM studies. So far, this is also the tumor type for which clinical data exits to support the concept: BVZ treatment of patients with GBM was shown to induce a highly infiltrative growth of tumors following tumor resection (Norden *et al*., 2008). Experimental studies of GBM response to anti-angiogenic therapy confirmed the increased invasion of these tumors following BVZ treatment. Moreover, some molecular mechanisms of the acquired resistance were explored:

1) in a study by Lu *et al*., 2012, it was shown that VEGFR2 forms heterodimers with c-Met and that subsequent binding of VEGF to heterodimers results in decreased c-Met phosphorylation. Thus, in a situation where VEGF signaling was inhibited (either with BVZ or in VEGF knockout cells), c-Met became activated contributing to cell invasion *in vitro* and enhanced invasion *in vivo*;
2) in another investigation Depner and co-authors showed that loss of ephrinB2 increases glioma growth and invasion (Depner *et al*., 2016). Under conditions of aggravated hypoxia, i.e. during bevacizumab anti-angiogenic therapy, upregulated HIF1α was identified to significantly repress ephrinB2. The repression mechanism

was shown to involve HIF1α-dependent transcriptional upregulation of the EMT regulator Zeb2, which repressed ephrinB2 expression. Targeting Zeb2 blocked the increased invasion of glioma cells following BVZ treatment *in vivo*.

Unlike the few abovementioned investigations into the response of GBM to anti-angiogenesis, studies in carcinoma have not provided direct evidence for a possible involvement of hypoxia as a trigger for the development of resistance. Moreover, in study by Ebos and co-authors, the whole concept of tumor cell specific mechanisms behind resistance to anti-angiogenesis was challenged by showing that administration of sunitinib for one week before transplantation of tumor cells also leads to increased metastasis (Ebos *et al*., 2009). Such results hint at the possibility that the accelerated metastasis following anti-angiogenic therapy may be the result of damaged vessels and disrupted vascular barriers, or other systemic effects.

Taken together, it can be summarized that the molecular mechanisms driving tumor cell invasion and metastasis in response to anti-angiogenic therapy in carcinomas remain elusive.

3.5. Aim of the study

Despite the many hopes and encouraging pre-clinical results, the concept of anti-angiogenesis as means of treatment for patients with cancer has not produced drastic improvements in the clinics. Anti-angiogenic therapy remains limited to the treatment of a short list of cancers, producing relatively limited clinical benefits. *In vivo* studies with various carcinoma models showed increased invasion and metastasis of tumors following anti-angiogenic therapy. So far, the mechanisms driving this type of evasive resistance are poorly understood, although some studies have hinted at hypoxia as the culprit behind the increased invasion and metastasis. Hence, we set out to elucidate the hypoxia-mediated mechanisms, HIF downstream signaling targets and upstream regulators, that together fuel the evasive resistance of tumors against anti-angiogenic therapy.

First, we set out to establish several *in vivo* models, in which anti-angiogenic therapy with various agents induced enhanced metastasis. Next, we re-isolated tumor cells from tumors of control and sunitinib-treated tumors and showed that cells re-isolated from treated tumors acquire a stable EMT, invasive, and metastatic phenotype.

To examine the role that hypoxia plays in acquisition of this phenotype, we first showed that *in vivo* anti-angiogenic therapy with sunitinib leads to an increased hypoxic response. Then, using an *in vitro* model we demonstrated that intermittent hypoxia is sufficient for the acquisition of an invasive EMT phenotype and increased metastasis *in vivo*.

Finally, enhanced response to hypoxia and specifically increased HIF2α, were identified as the main characteristics that tumor cells acquire after anti-angiogenic therapy *in vivo* and intermittent hypoxia *in vitro*. The EMT regulator Snail was shown to be the primary HIF-downstream target driving the increased invasion of tumor cells, and TET1 to be the upstream regulator of HIF2α, that via DNA demethylation of *HIF2A* (*EPAS1*) creates a feed-forward loop driving the increased hypoxia response of tumors during anti-angiogenesis.

4. Results

4.1. Anti-angiogenic therapy *in vivo* leads to increased metastasis

To study the mechanisms underlying the evasive resistance of tumors to anti-angiogenic therapy, we first had to establish an *in vivo* model that would closely resemble the clinical situation. To this end, we assessed different anti-angiogenic agents and regimen of treatment for their capacity to increase metastasis. We employed xenograft models, in which athymic nude mice were transplanted with human carcinoma cells. For these initial experiments, two different human carcinoma lines were used:

1) A549VI cells derived from the human lung adenocarcinoma line A549, enriched for cells with invasive potential by six rounds of selection in a modified Boyden chamber. These cells were transplanted subcutaneously;
2) MDA-Br – a highly metastatic variant of the parental breast carcinoma line MDA-MB-231. These cells were transplanted orthotopically in the mammary fat pad.

Three different anti-angiogenic agents (all being currently prescribed in the clinics; Jayson *et al*., 2016) were used to test the hypothesis that the antitumor effect following treatment would be accompanied by increased metastasis: two small molecule inhibitors – sunitinib and sorafenib and the first clinically approved anti-angiogenic agent – bevacizumab (BVZ; Ebos *et al*., 2009a; Lu and Bergers, 2013; Pàez-Ribes *et al*., 2009). BVZ scavenges the human VEGFA (Bukowski, 2012; Ferrara *et al*., 2005; Shukla S, Robey RW, Bates SE, 2009). Sunitinib and sorafenib target the VEGF receptors, but also other receptor tyrosine kinases (RTKs), e.g. Kit, PDGFRs and others (Gotink and Verheul, 2010).

The chosen small molecule inhibitors bind with similar efficiencies both human and mouse RTKs (Fendrich *et al*., 2012; Tanaka *et al*., 2011). By contrast, BVZ is known to target only human, but not mouse VEGFA (Yu *et al*., 2008). Thus, considering the nature of the drugs, different degrees of tumor response to applied therapies were expected.

In all animal experiments, therapy was initiated only after the tumors reached a size of approx. 200 mm^3. This was done to test the therapy on established tumors and thus to better adapt the model to the actual clinical situation. All agents were administered daily until the end of the experiment at the following doses: 60 mg/kg sunitinib and sorafenib orally, and 20 mg/kg BVZ and Gamunex (the control human IgG antibody) via an i.p. injection.

When tumors reached the legally set maximal size of 2000 mm^3, the mice were sacrificed, and the number of superficial lung metastases was assessed.

Fig. 4.1. depicts some of the observed antitumor, but pro-metastatic effects in animals receiving anti-angiogenic therapy. In all studies, the therapy produced a visible decrease in tumor volume even after a short period of treatment (**Fig. 4.1, A**). In addition, tumors of animals receiving therapy often appeared to have characteristic whitish color, a clear indication of dysfunctional blood perfusion (**Fig. 4.1, B**). Importantly, and in line with clinical observations, inspection of the lungs of treated animals revealed a significantly increased incidence of superficial lung metastases in animals receiving anti-angiogenic therapy (**Fig. 4.1, C**).

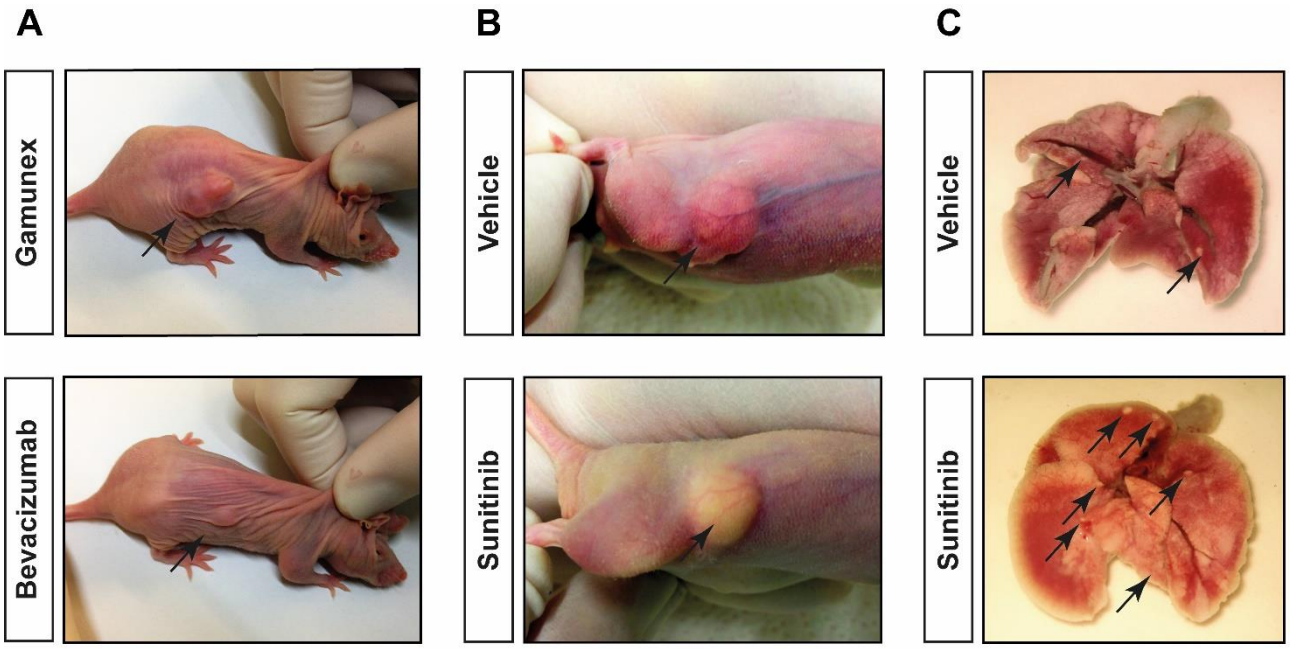

Fig. 4.1. *In vivo* treatment with anti-angiogenic therapy recapitulates the clinical observations. **A**, Significant reduction in tumor volume was observed in animals treated with bevacizumab (black arrows point at the subcutaneous tumors). **B**, Sunitinib treatment results in decreased blood perfusion of tumors, as evidenced by the pale white color of the tumor tissue. **C**, Anti-angiogenic therapy with sunitinib leads to an increase in the number of superficial lung metastasis.

Similar anti-tumor effects were observed with all tested anti-angiogenic agents in both tumor lines (**Fig. 4.2, A-D**). Most importantly, treatment with these drugs significantly increased metastasis formation in the lungs (**Fig. 4.2, E-H**).

The data presented above demonstrate that the established *in vivo* models reconstitute key findings related to enhanced metastasis following anti-angiogenic therapy, leading to further studies on the mechanisms underlying tumor resistance to anti-angiogenesis.

4.2. Anti-angiogenic therapy induces the acquisition of a stable phenotype, characterized by enhanced EMT, cancer stem cell traits, invasion, and metastasis

Once we confirmed that anti-angiogenic therapy stimulates metastasis *in vivo*, we set out to investigate whether the treatment could induce changes in the phenotype of tumor cells. To this end, A549VI cells were re-isolated from tumor-bearing mice (**Fig. 4.2, A**). By means of enzymatic digestion of tumor tissue, we released the tumor cells from the ECM and brought them back into culture. Two lines were generated: 1) A549-CO, isolated from control tumors and 2) A549-SU, cells of which were isolated from tumors of sunitinib treated animals. It is important to note that in all further experiments cells of the A549-SU line were cultured in sunitinib-free medium, thus all stable changes in the phenotype (if detected) were not due to exposure to the drug in culture, but were acquired *in vivo*.

Intriguingly, we observed a strikingly altered morphology of A549-SU cells in comparison to the control line (**Fig. 4.3, A**). While re-isolated control cells did not show any significant morphological changes in comparison to the original A549VI line (not shown), sunitinib cells acquired a mesenchymal, spindle-cell shape typical of cells undergoing EMT; these morphological differences were especially clearly visible after TGBβ1 treatment or hypoxia.

Indeed, real-time PCR revealed a remarkable shift in the expression of EMT markers in A549-SU in comparison with A549-CO cells (**Fig. 4.3, B**). In particular, the A549-SU line showed a strong downregulation in the main marker for EMT, E-cadherin, along with another epithelial marker, T-cadherin. In contrast, expression of mesenchymal and invasion markers was significantly enhanced (e.g. N-cadherin and MMPs).

The observed shift towards mesenchymal phenotype in the A549-SU line can be attributed to a markedly increased expression of major EMT regulators. As shown by the mRNA analysis (**Fig. 4.3, C**), expression of several major EMT regulators, such as Snail, Slug, Zeb1/2 and Twist1 (Zheng and Kang, 2014), was upregulated in A549-SU cells.

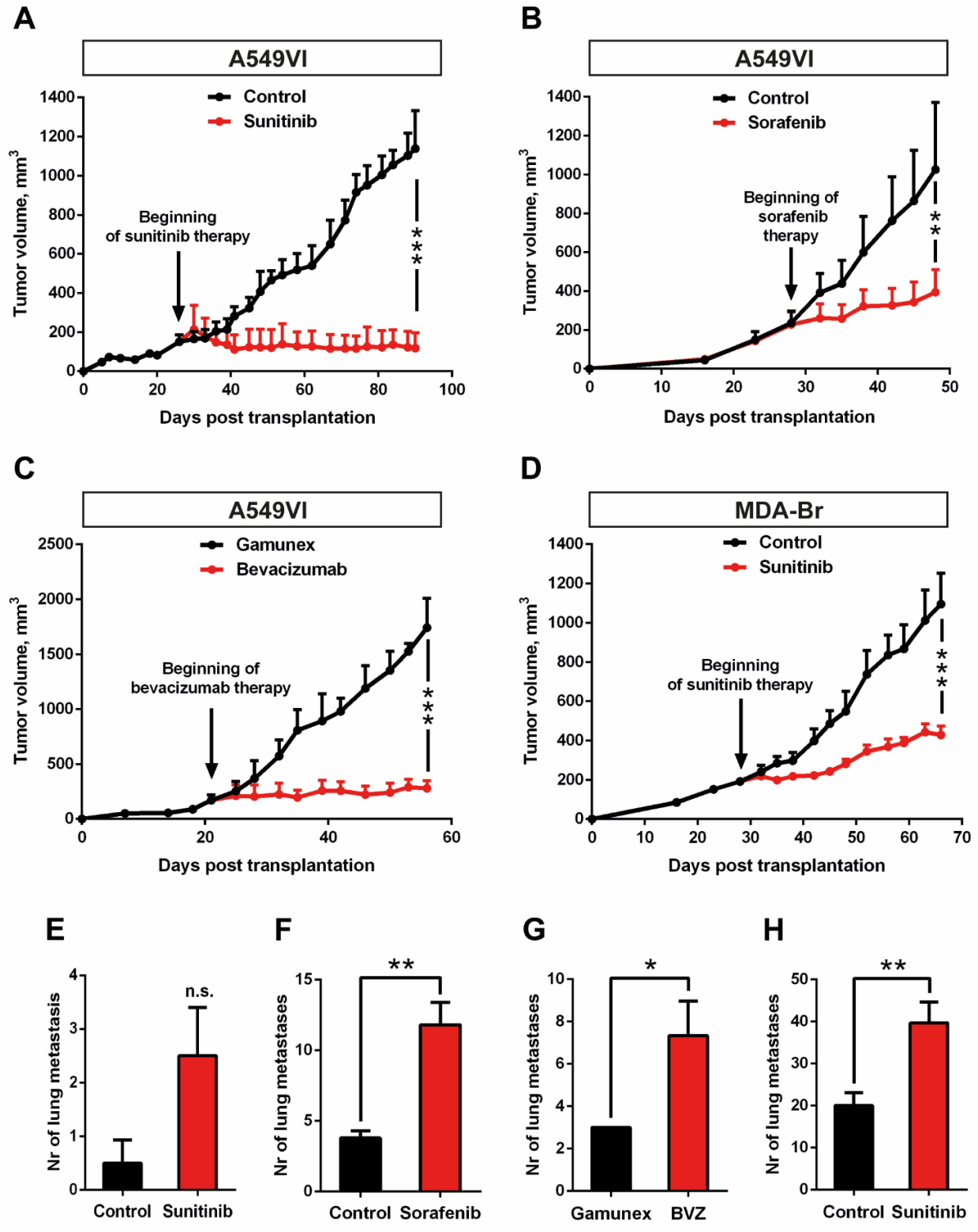

Fig. 4.2. Anti-angiogenic treatment *in vivo* leads to increased metastasis. A-D, Animals transplanted with human tumor lines (A549VI or MDA-Br) showed a significant reduction in primary tumor growth following anti-angiogenic therapy with sunitinib, sorafenib, or bevacizumab. **E-H**, Quantification of the number of lung metastasis reveals increased metastasis in animals after anti-angiogenic therapy (E-G represent metastasis in animals transplanted with A549VI cells, while in H mice were transplanted with cells of the MDA-Br line). Quantification represents the average number of metastases in four animals per group in **E**, and ten animals per each group in **F-H**. Experiments performed in collaboration with Angel Cuesta. n.s. – not significant, *p<0.05, **p<0.01, ***p<0.001.

These changes in mRNA levels were further corroborated by immunoblotting (**Fig. 4.4**). In this experiment cells were treated with TGFβ1 to induce EMT. In line with the observed mRNA changes, protein levels of E- and T-cadherin were significantly reduced in sunitinib cells in comparison to the control line. By contrast, mesenchymal markers (N-cadherin and vimentin) were significantly elevated in A549-SU cells already without TGFβq treatment, with N-cadherin reaching a peak expression level in sunitinib cells that could not be further induced even by TFGβ1 (**Fig. 4.4**).

Immunoblotting showed that Snail was strongly induced in sunitinib cells, while the levels of other EMT regulators were only slightly increased in the absence of TGFβ1 treatment in comparison to the control line (**Fig.4.4**).

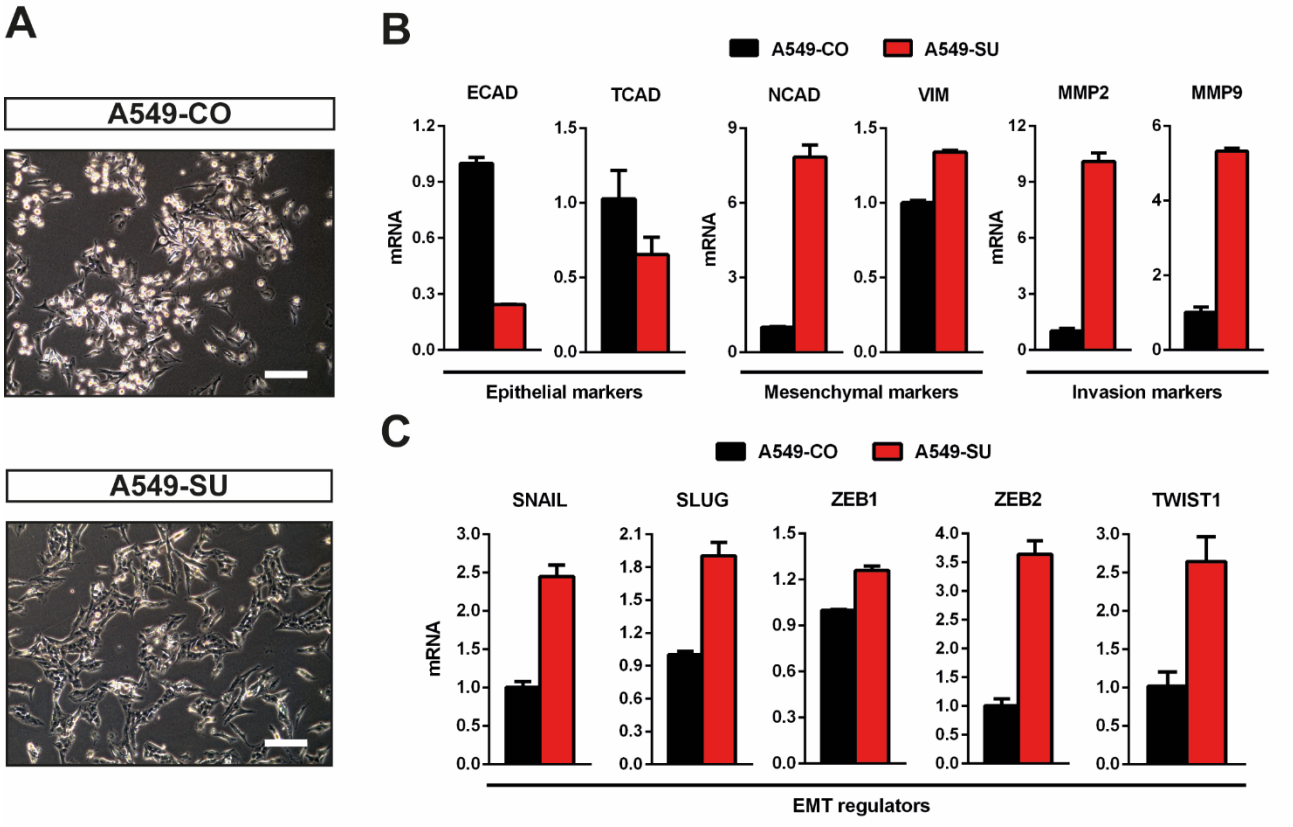

Fig. 4.3. Tumor cells acquire a stable EMT phenotype following anti-angiogenic treatment with sunitinib. A, Cells isolated from sunitinib-treated tumor-bearing mice acquire a mesenchymal morphology. Scale bars represent 100 µm. A549-SU cells show an EMT shift, as evidenced by changes in mRNA levels of key EMT markers (**B**) and regulators (**C**); one representative image from three independent experiments is shown in **B** and **C**.

Among a plethora of factors that can trigger EMT, hypoxia and TGFβ have been reported to be some of the most potent stimuli (Lenferink *et al*., 2010; Lundgren *et al*., 2009; Zheng and

Kang, 2014). As cells re-isolated from tumors of animals treated with sunitinib showed a prominent induction of EMT, we assessed the state of TGFβ signaling in these cells.

First, we analyzed phosphorylation of SMADs, which represent the canonical TGFβ pathway (Wiercinska *et al*., 2011; Xu *et al*., 2009). Western blot analysis showed an increased phospho-SMAD2/3 expression in the A549-SU line compared to the control line (**Fig. 4.5, A**). Considering that no changes in total SMAD2/3 were observed, increased pSMAD2/3 may be attributed to higher activity of the TGFβ signaling pathway. To corroborate this hypothesis, we performed a dual luciferase assay with a construct in which expression of Firefly luciferase was driven by a promoter containing four SMAD binding elements (SBEs), rendering it responsive to TGFβ signaling. Indeed, activity of Firefly luciferase in the A549-SU line was significantly increased (**Fig. 4.5, B**).

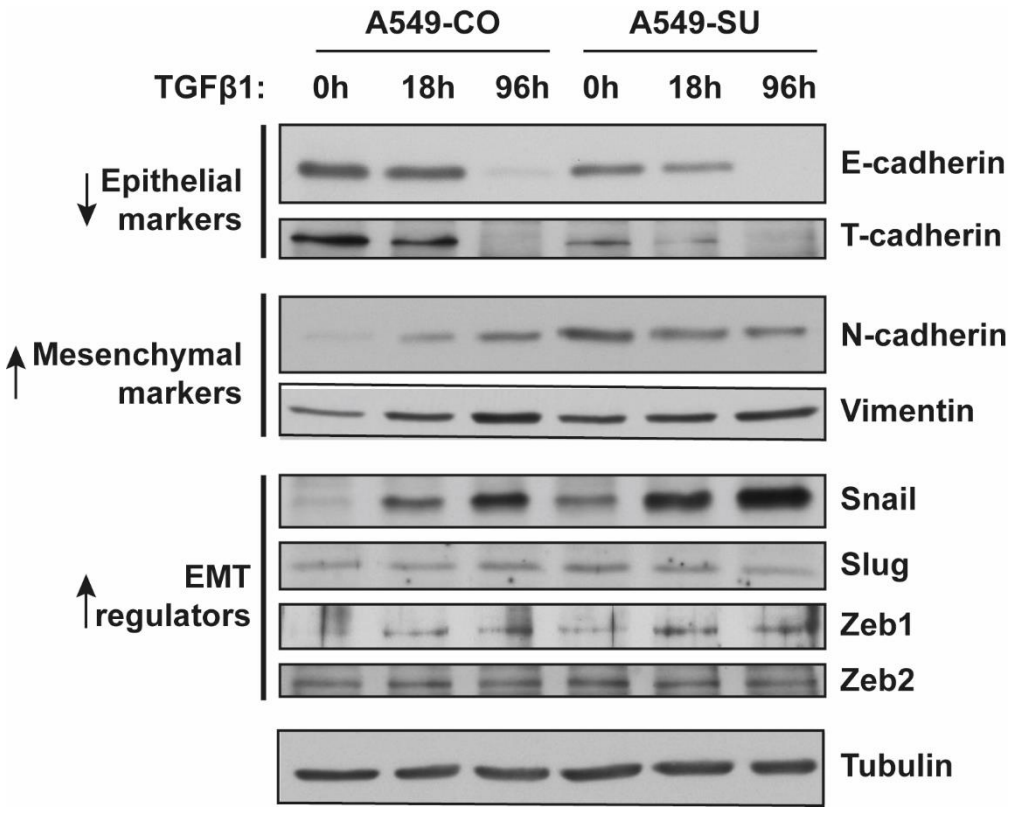

Fig. 4.4. Tumor cells isolated from sunitinib treated animals show an EMT shift in the expression of EMT markers and regulators. Sunitinib cells show a decrease in the expression of epithelial markers (E-, T-cadherin), contrasted by an increase in mesenchymal markers (N-cadherin and vimentin) and EMT regulators (e.g. Snail) when analyzed by Western blotting. One representative image from three independent experiments is shown.

Enhanced TGFβ signaling observed in sunitinib cells might be explained by several alternative hypotheses: either by increased expression of TGFβ ligands or by elevated TGFβ

receptor levels/activity. First, we proceeded to analyze the expression of TGFβ1-3. qPCR results showed only a moderate increase in expression of two of the three ligands in the A549-SU line (**Fig. 4.5, D**).

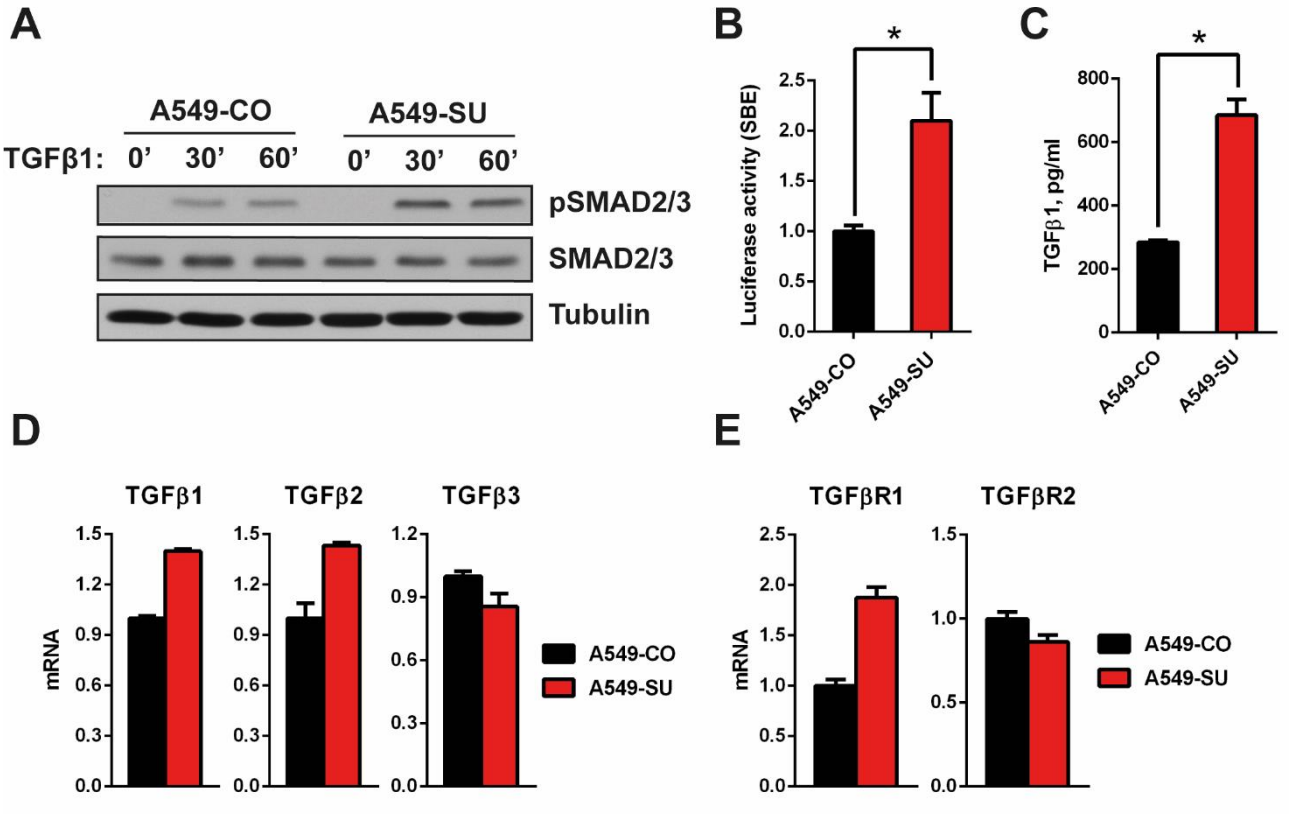

Fig. 4.5. The TGFβ-pathway is activated in cells derived from sunitinib-treated tumors. **A**, Western blotting analysis revealed higher levels of phosphorylated Smad2/3 in A549-SU cells, indicating increased expression/activity of the TGFβ receptors. **B**, In line with elevated pSmad2/3 levels, activity of the luciferase reporter harboring four SMAD-binding elements (SBEs) in the promoter was enhanced in the A549-SU line in comparison to control cells. **C**, ELISA results showing that A549-SU cells secrete significantly more mature TGFβ1 than control cells. Real-time PCR analysis for *TGFB1-3* expression revealed only marginally increased mRNAs of *TGFB1* and *TGFB2* in A549-SU cells (**D**), while significantly more *TGFBR1* (but not TGFBR2) was detected in sunitinib cells (**E**). Relative quantification presents averages with SEMs from triplicates in **B** and **C**, while one representative image from three independent experiments is shown in **D** and **E**.*p<0.05.

As the amount of TGFβ is regulated not only at the mRNA level, but also at the level of ligand maturation and secretion, we next examined the mature secreted TGFβ1 by ELISA. Surprisingly, in contrast to the moderate changes in expression detected by qPCR, ELISA analysis of the conditioned medium showed that A549-SU cells secreted almost three times more of the mature TGFβ1 ligand than control cells, which could contribute to the EMT shift in these cells (**Fig. 4.5, C**).

Next, we assessed with a real-time PCR if expression of *TGFBR1/2* was altered in sunitinib cells. Indeed, in addition to increased ligand production, A549-SU cells also showed

increased *TGFBR1* mRNA (**Fig. 4.5, E**). Interestingly, TGFβR1 is the isoform containing the serine/threonine protein kinase domain (absent in TGFβR2). These results suggest that increased expression of TGFβR1, in combination with elevated expression of its ligands, can form an autocrine stimulatory loop in the A549-SU line that renders the cells sensitive to an EMT shift.

TGFβ-signaling is one of the critical pathways determining cell migration and invasion (Padua and Massagué, 2009; Tsai *et al*., 2012). Therefore, we next examined invasion of the A549-SU line in a modified Boyden chamber assay (**Fig. 4.6, A**). While the A549-SU cells showed similar invasion rates to the control line under baseline conditions (i.e. without induction of EMT), stimulation of cells with TGFβ1 resulted in enhanced invasion of the A549-SU cells.

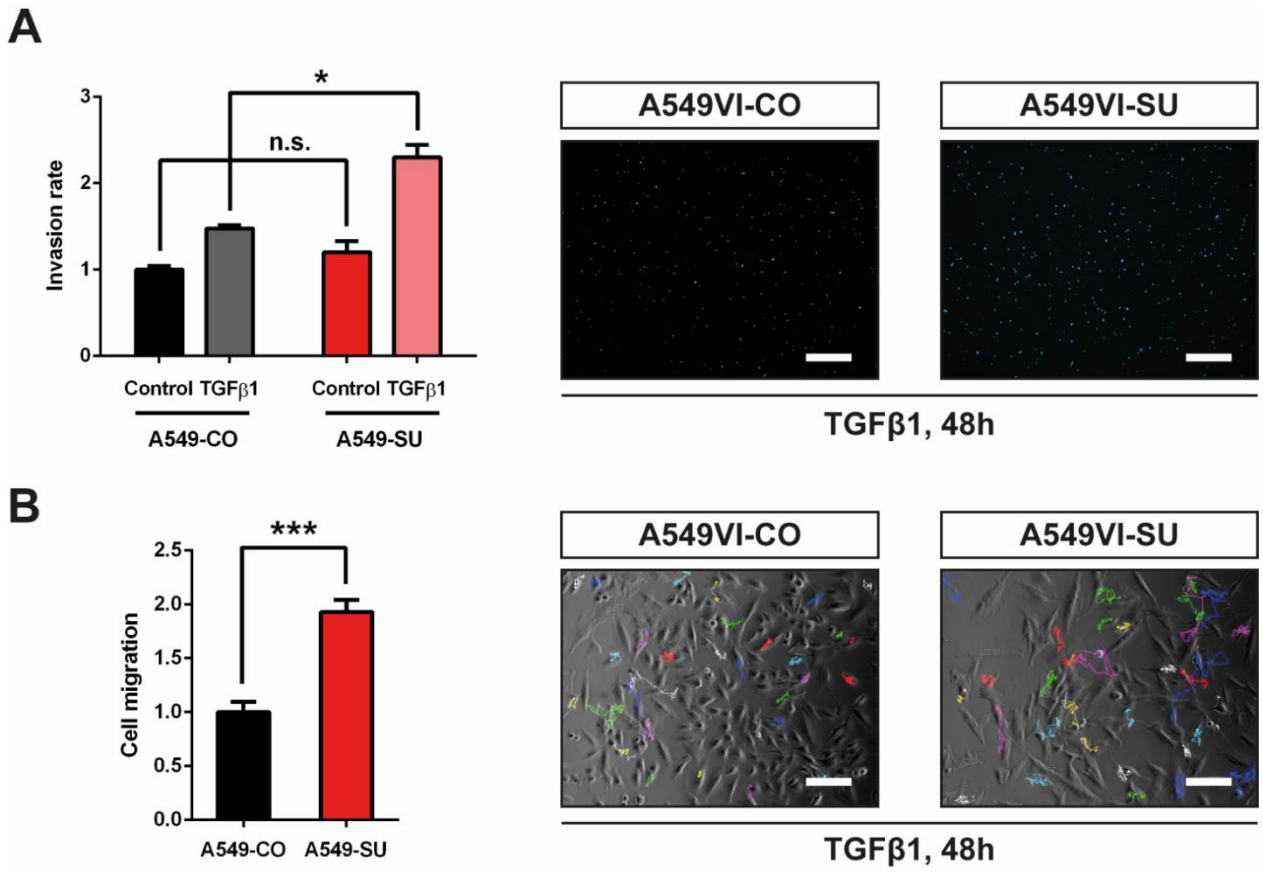

Fig. 4.6. Anti-angiogenic therapy leads to the acquisition of an invasive phenotype. A, Upon EMT stimulation with TGFβ1, sunitinib cells were more invasive in the modified Boyden chamber assay than control cells. Pictures represent DAPI-stained nuclei of cells that invaded to the lower side of the membrane in the chamber. Data present average values of three independent repeats with standard errors of the mean (SEM). Scale bars represent 400 μM. **B**, Time-lapse microscopy revealed increased migration of A549-SU cells. Migratory tracks of individual cells are presented on the micrographs as jagged colored lines (a representative picture from three independent experiments); relative quantification presents average migration of 30 cells with SEM. Experiments in **B** performed in collaboration with Angel Cuesta Scale bars represent 100 μM. n.s. – not significant, *p<0.05, ***p<0.001.

To corroborate these finding, the motility of cells was assessed in a 2D migration assay, where cells were tracked with the help of time-lapse microscopy (**Fig. 4.6, B**). The jagged color lines in the micrographs represent the tracks of individual cells that were quantified with ImageJ software. In line with their pro-invasive capacity, A549-SU cells were significantly more motile in comparison to the control line.

In several studies it was shown that human tumor cells with EMT features often have high expression of cancer stem cell (CSC) markers (Mani *et al*., 2008; Morel *et al*., 2008). Given the EMT shift in A549-SU cells, we were interested to assess their self-renewal capacity. First, we analyzed the expression of a panel of established cancer stem cell markers, such as *CD133*, *Sox2*, *Nanog*, etc. (**Fig. 4.7, A**). In line with previous reports, A549-SU cells exhibited elevated mRNA levels of all the tested CSC markers. In addition, A549-SU cells formed a significantly higher numbers of colonies. Thus, we could show that anti-angiogenic therapy *in vivo* induces acquisition of stable cancer stem cell traits in tumor cells, which is maintained after re-isolation of cells from the tumors.

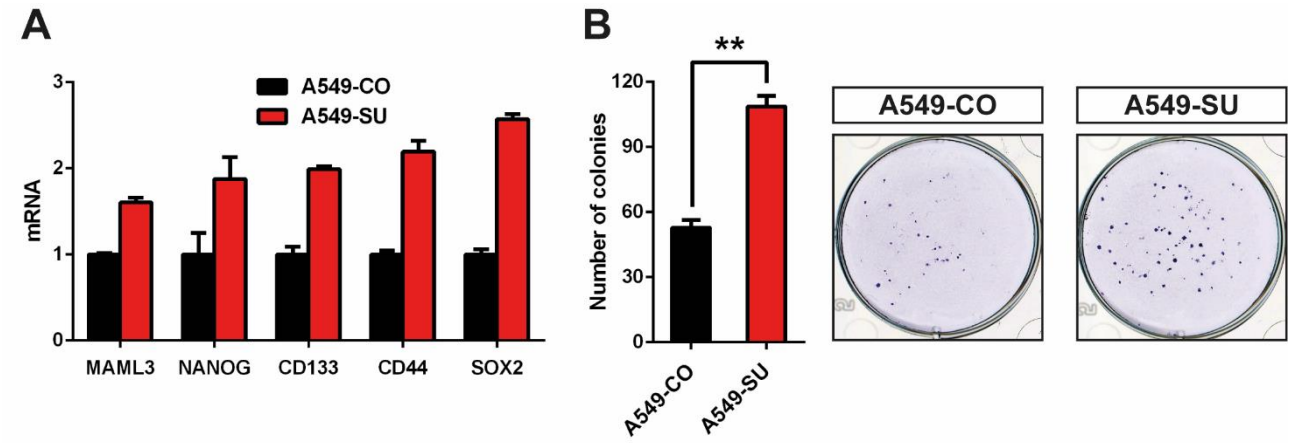

Fig. 4.7. Tumor cells isolated from sunitinib treated animals show enhanced cancer stem cell traits. A, mRNA analysis revealed higher expression of cancer stem cell markers in A549-SU cells in comparison to the control line. One representative image from two independent experiments is presented. **B**, Tumor cells re-isolated from sunitinib treated tumors form significantly more colonies, which indicates their higher self-renewal capacity. Quantification presents average of six replicates with SEM. **p<0.01.

Taking together the enhanced EMT and CSC traits of A549-SU cells and their increased invasion rate, it was tempting to hypothesize that this stable phenotype would be maintained *in vivo*, leading to increased metastasis. To investigate this hypothesis, we transplanted A549-CO and A549-SU cells subcutaneously into athymic nude mice and measured primary tumor growth and metastasis (**Fig. 4.8**). To compare the phenotype of sunitinib cells to acute

sunitinib treatment, animals transplanted with the A549-CO line were subdivided into two groups, receiving sunitinib or control vehicle. The third group represented mice transplanted with A549-SU cells and receiving control vehicle.

Similar to the previous experiments, sunitinib treatment of mice transplanted with A549-CO cells resulted in significantly diminished growth of subcutaneous tumors and increased metastasis in comparison to vehicle treated control animals (**Fig. 4.8, A, B**). Primary tumors of animals transplanted with the A549-SU line or animals transplanted with A549-CO cells and treated with sunitinib showed strongly upregulated expression of Snail. Interestingly, the primary tumor growth in mice transplanted with A549-SU cells and treated with vehicle control was similar to A549-CO tumors of animals receiving sunitinib therapy, and the A549-SU line also produced a significantly higher number of lung metastases compared to the vehicle-treated A549-CO cells.

Taken together, these results demonstrate that anti-angiogenic therapy with sunitinib did not only cause a shift towards EMT and increased CSC traits, but that this altered phenotype remained stable throughout *in vitro* culture and a second round of *in vivo* transplantation, resulting in significantly higher metastasis.

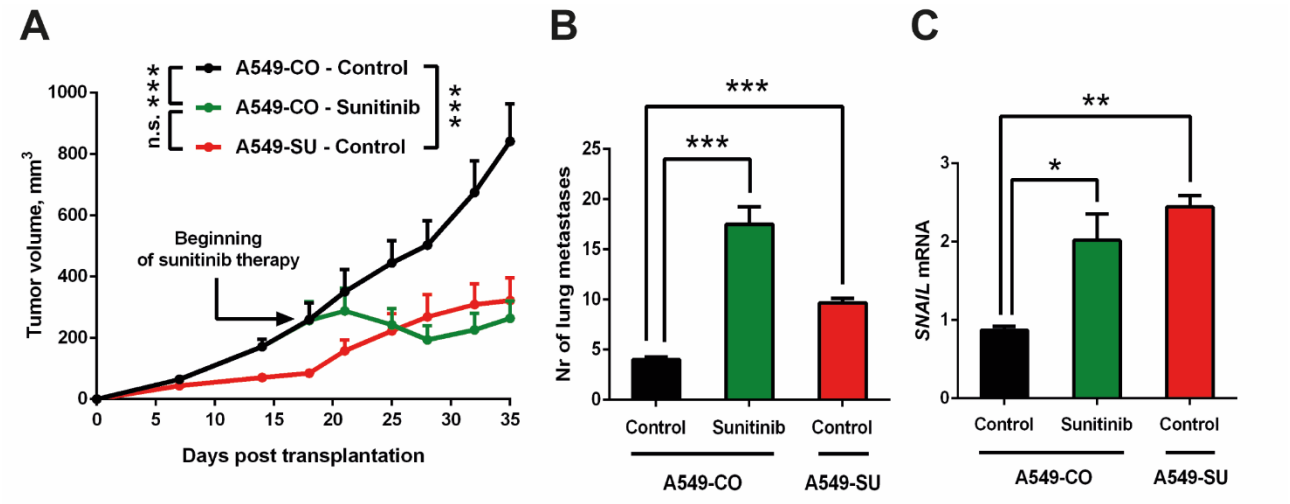

Fig. 4.8. Anti-angiogenic therapy leads to the acquisition of a stable metastatic phenotype. A, *In vivo* study with animals transplanted either with control (with and without sunitinib administration) and A549-SU cells (treated with control vehicle) revealed that primary tumor growth of the vehicle-treated A549-SU line was similar to the sunitinib-treated control group. **B**, Significantly higher numbers of superficial lung metastases were observed in both sunitinib-treated animals transplanted with the control line, and vehicle-treated mice transplanted with the A549-SU line. **C**, qPCR analysis of RNA isolated from tumors showed that control tumors treated with sunitinib and tumors formed by vehicle-treated A549-SU cells had a significant increase in mRNA of the EMT regulator Snail. Experiments performed in collaboration with Angel Cuesta. n.s. – not significant; *p<0.05, **p<0.01, ***p<0.001.

4.3. Snail is required for maintenance of the invasive phenotype induced by anti-angiogenic therapy

So far, we showed that anti-angiogenic therapy induces the acquisition of a highly invasive EMT phenotype in tumor cell. Yet, it remained unclear what is driving the EMT phenotype of sunitinib cells. EMT regulators are well documented to be playing a role in cancer migration, invasion, and metastasis. Thus, considering the elevated expression of several EMT regulators in the A549-SU line, we speculate that some of these transcription factors might mediate the aggressive phenotype of these cells. To resolve this question, a series of lentivirus-mediated shRNA knockdowns (KDs) against the main EMT regulators were generated in A549-SU cells. qPCR analysis showed that a significant reduction in mRNA was achieved in all KD lines (**Fig. 4.9, A**).

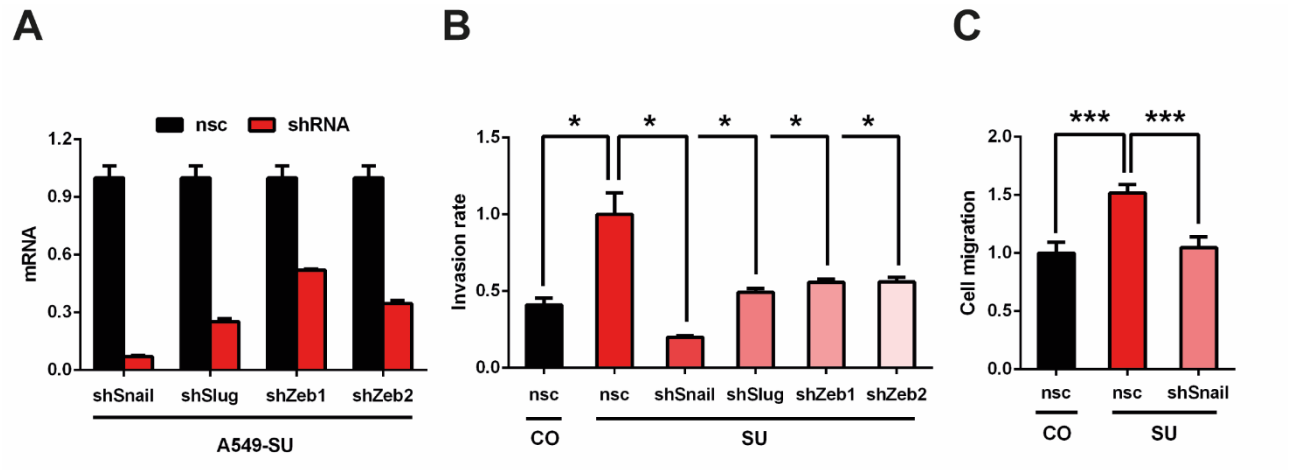

Fig. 4.9. Snail is the dominant EMT regulator responsible for maintenance of the invasive phenotype in sunitinib cells. A, Real-time PCR results showing KD efficiency of the targeted mRNA, respectively, in a series of lentivirus-mediates shRNA knockdown lines generated against the main EMT regulators, whose expression was upregulated in the A549-SU line. **B**, A modified Boyden chamber invasion assay revealed that silencing of every one of the EMT regulators results in a marked decrease in invasion of A549-SU cells, with the most dramatic effects observed with the Snail KD. **C**, Knockdown of Snail reversed cell migration of the A549-SU line, bringing it back to the level of control cells, as assessed by time-lapse microscopy. In **A** and **B** one representative picture of two independent experiments is shown. Relative quantification in **C** presents average migration of 30 cells with SEM. *p<0.05, ***p<0.001.

Next, we proceeded to assess invasion and migration of the generated cells. Diminished invasion in the modified Boyden chamber was observed in all KD cells in comparison to the non-silencing control, with the most prominent reduction in invasion rate being detected in cells expressing the Snail shRNA (**Fig. 4.9, B**). This is in line with our finding that Snail is the most strongly upregulated and, thus, dominant EMT regulator in the A549-SU line. Yet,

we cannot completely exclude the possibility that this is due to the highest knockdown efficiency (compared to other shRNA constructs).

In line with the Boyden chamber invasion results, A549-SU cells bearing the Snail KD showed a marked reduction in migration when analyzed by time-lapse microscopy (**Fig. 4.9, C**). In fact, the migration rate of KD cells was reversed to that of the control line. In summary, we show that EMT regulators, and in particular Snail, play an important role in the maintenance of invasive phenotype in A549-SU cells.

4.4. *In vitro* selection for sunitinib resistance does not lead to the acquisition of an EMT phenotype

We next considered two types of possible mechanisms, through which the A59-SU cells may acquire their invasive phenotype after the *in vivo* exposure to sunitinib. First, it is conceivable that the direct action of sunitinib on tumor cells rendered the cells resistant to the drug, which might mediate the increased invasiveness, e.g. through changes in RTK signaling. An alternative possibility is that sunitinib affected the invasiveness of tumor cells indirectly, through changes in the tumor microenvironment, e.g. due to the suppression of angiogenesis.

To address whether A549-SU cells had acquired classical resistance to sunitinib after *in vivo* exposure, sensitivity of the A549-SU line to the drug was tested in an methylthiazolyldiphenyl-tetrazolium bromide (MTT) cell viability assay (**Fig. 4.10, A**). Interestingly, despite the prolonged *in vivo* treatment (approx. 60 days), no difference in sensitivity to sunitinib between the control and A549-SU lines was observed *in vitro*.

Next, to further explore if *in vivo* treatment with sunitinib altered the activity of RTKs, we performed an RTK array. For this experiment, cells were starved overnight and then stimulated with serum-containing medium to assure sufficient RTK phosphorylation, and thus enhance the sensitivity of the RTK array. In line with the MTT assay, RTK array results revealed that none of the 49 tested RTKs showed any pronounced changes between A549-SU and A549-CO cells. Indeed, even the activity of primary targets of the drug – VEGFRs, PDGFRs, c-KIT, and c-RET – was unaltered (**Fig. 4.10, C**).

These results indicate that the observed EMT phenotype of sunitinib cells is not caused by sunitinib resistance *per se*, but most probably is a result of action of some other factors in the tumor microenvironment that are altered as a result of the sunitinib treatment.

To conclusively rule out the possibility that the EMT-phenotype of A549-SU cells is the result of the direct action of the drug on the tumor cells, we generated a sunitinib-resistant line – A549-SunRES. To this end, A549VI cells were exposed *in vitro* to gradually increasing concentrations of sunitinib in the growth medium. Sunitinib resistance of the generated line was confirmed in an MTT assay (**Fig. 4.11, A**), showing that IC_{50} was almost twice as high in A549-SunRES cells in comparison to the control cells. In subsequent experiments, we compared the phenotype of the classically resistant A549-SunRES line with the A549-SU line.

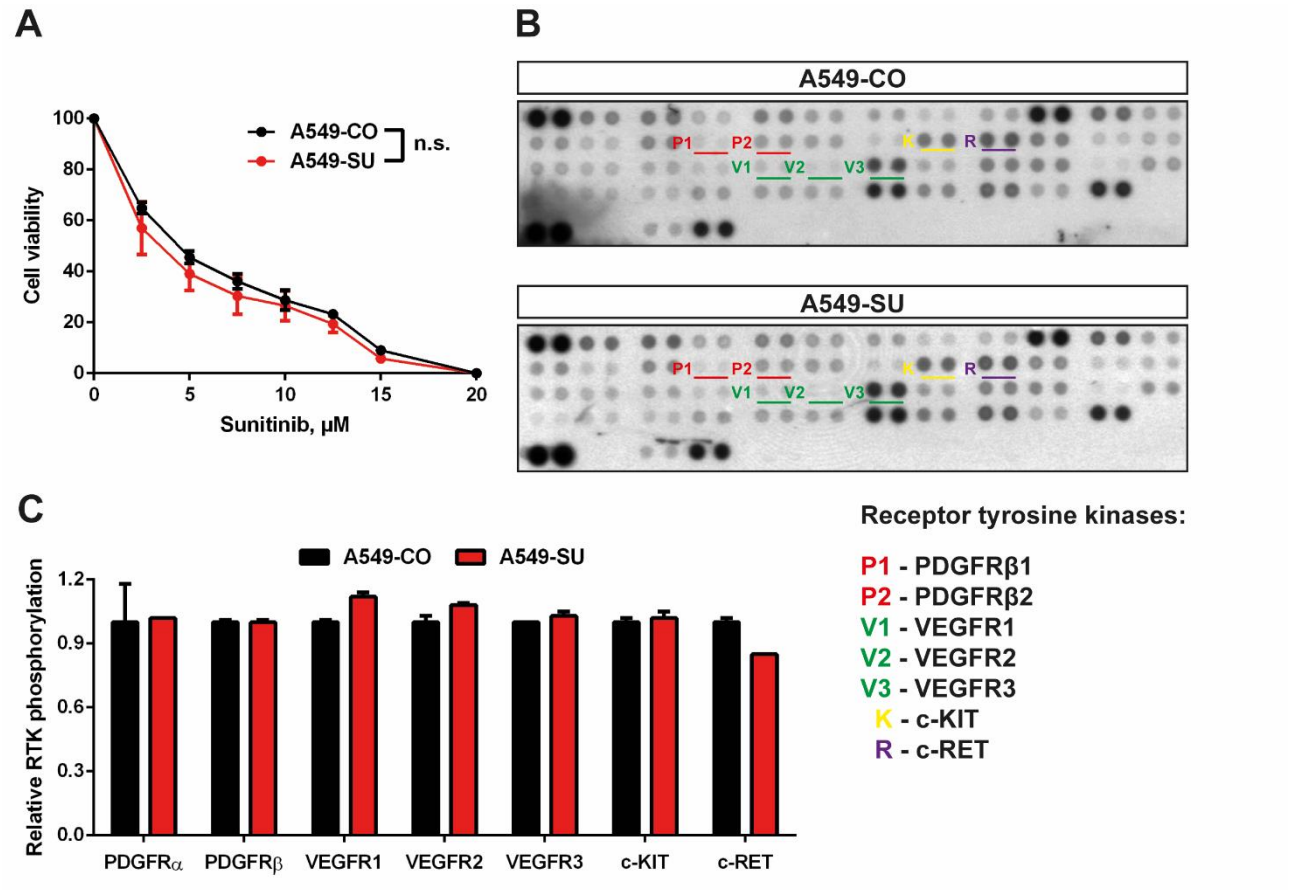

Fig. 4.10. Sunitinib anti-angiogenic therapy *in vivo* does not alter the sensitivity of cells to the drug or induce changes in phosphorylation of receptor tyrosine kinases. A, MTT assay showing that re-isolated A549-SU cells possess similar sensitivity to the drug in comparison to the control line. **B**, RTK array results revealed no changes in phosphorylation of RTKs in A549-SU cells compared to the control line. Two spots for each RTK were present on the array, serving as technical replicates; the position of the main sunitinib targets – PDGFRs, VEGFRs, c-KIT, and c-RET – are indicated. **C**, Quantification of the phosphorylation of the main RTKs targeted by sunitinib showed no major difference between the lines. Relative quantification presents averages of two points for each receptor in an array with SEM. n.s. – not significant.

Results of immunoblotting showed that the phenotype of A549-SunRES cells was unlike that of the A549-SU line: no changes were detected in the levels of E-cadherin or Snail levels (**Fig. 4.11, B**). Moreover, upon TGFβ1 stimulation the A549-SunRES line showed a downregulation of Snail in comparison to the control.

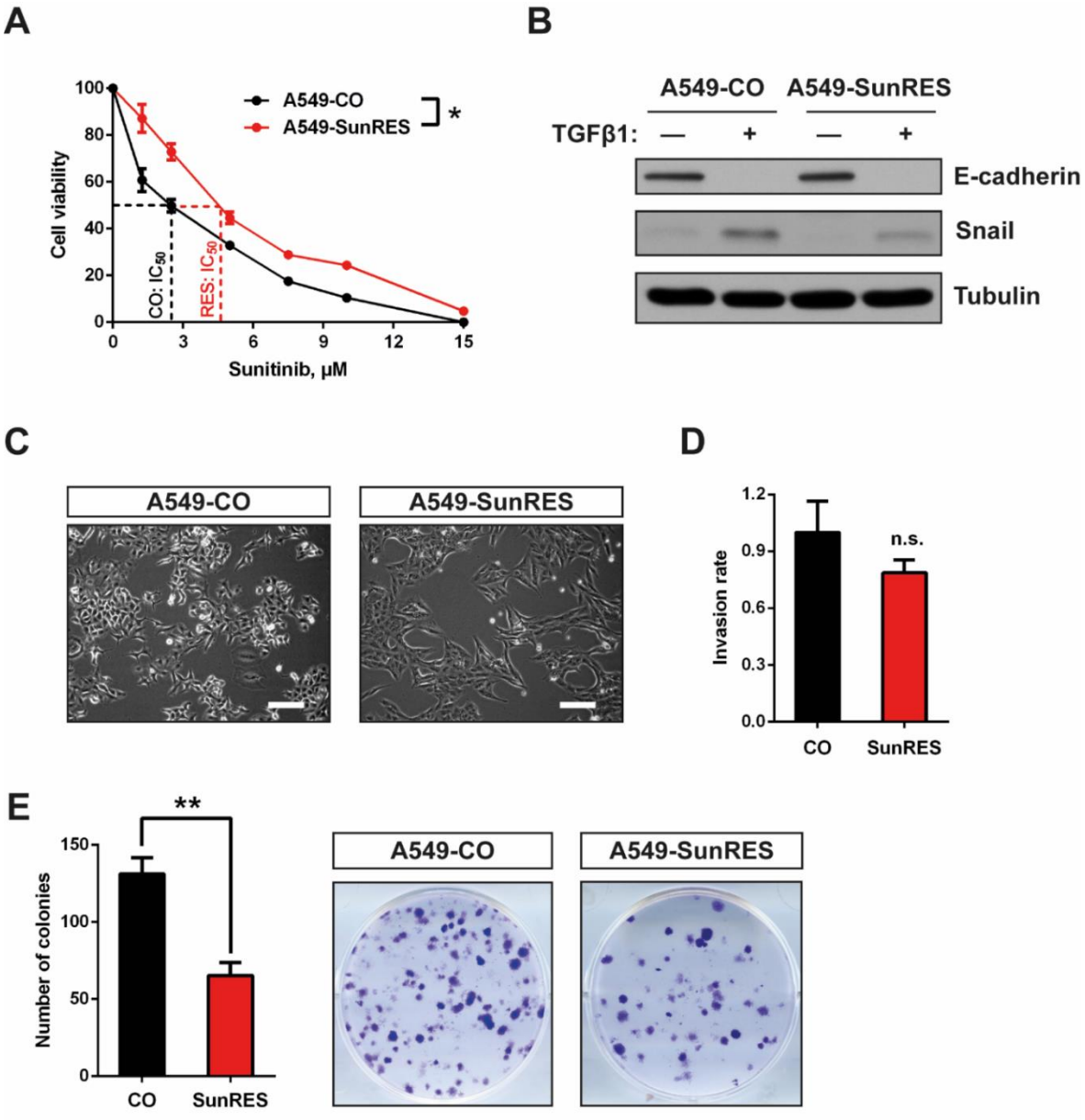

Fig. 4.11. Sunitinib-resistant cells do not acquire the EMT-phenotype observed after *in vivo* anti-angiogenic treatment. A, Culturing cells *in vitro* in the presence of increasing concentrations of sunitinib in the growth medium induces sunitinib resistance; represented are the MTT assay results with the control and sunitinib resistant lines. Dashed lines indicate IC_{50} values. **B**, Western blot analysis shows no changes in expression of E-cadherin or Snail in the A549-SunRES line. Despite the seemingly mesenchymal morphology of the sunitinib resistant cells (**C**), no increase in invasion was detected using the modified Boyden chamber assay (**D**). In contrast to A549-SU cells, classically resistant A549-SunRES cells form significantly less colonies in the colony formation assay (**E**). In **D** bars represent averages with SEMs of three replicates, while in **E** six replicates were used for quantification. Scale bars represent 100 μm, n.s. – not significant, *p<0.05, **p<0.01.

Despite the more mesenchymal appearance of A549-SunRES cell (**Fig. 4.11, C**), the invasion rate of the cells remained unaltered when tested in the Boyden chamber assay (**Fig. 4.11, D**). Furthermore, these cells exhibited significantly decreased colony formation capacity (**Fig. 4.11, E**).

In summary, our results show that selection for cells resistant to sunitinib does not lead to the acquisition of an EMT phenotype similar to that after anti-angiogenic therapy with sunitinib *in vivo*. This led us to propose that changes in the tumor microenvironment induced by anti-angiogenic therapy are responsible for the stable changes in the invasive behavior of the A549-SU tumor cells.

4.5. Generation of a stable tumor line expressing a luciferase reporter to monitor hypoxia *in vivo*

Anti-angiogenic therapy suppresses the growth of the tumor vasculature and thus induces ischemia – a physiological state characterized by lack of oxygen (hypoxia) and nutrients. Therefore, it is tempting to speculate that hypoxia, a known regulator of EMT and invasion, could be a major trigger for the onset of evasive resistance in tumors against anti-angiogenic therapy. To explore this hypothesis and to test to which extent anti-angiogenic therapy induces hypoxia, we generated a novel lentivirus-based dual luciferase reporter system for visualization of hypoxia *in vivo* by bioluminescence imaging.

A lentiviral transfer plasmid, which encodes two luciferase proteins under the transcriptional control of strong viral promoters, was generated (**Fig.4.12, A**). The luciferase reporter proteins were:

1) A fusion protein between firefly luciferase and the oxygen dependent degradation domain (ODD) of HIF2α, as a reporter for hypoxia (Safran *et al*., 2006).
2) *Renilla* luciferase (RLuc), a reporter used to estimate the number of viable tumor cells.

Based on the reporter proteins used, we named the resulting plasmid POR, which stands for **p**Lenti6-**O**DD-**R**Luc.

While RLuc activity is oxygen-independent, stability of the firefly luciferase fusion protein depends on oxygen availability due to the presence of the ODD domain (**Fig. 4.12, B**): under normoxia (~21% O_2), prolyl hydroxylases (PHD1-3) hydroxylate the fusion protein at the ODD domain, marking it for proteasomal degradation. On the contrary, upon reduced

oxygen availability (0-5% O_2, hypoxia conditions), activity of PHDs would become reduced, leading to stabilization of the fusion protein and greatly enhanced luciferase activity.

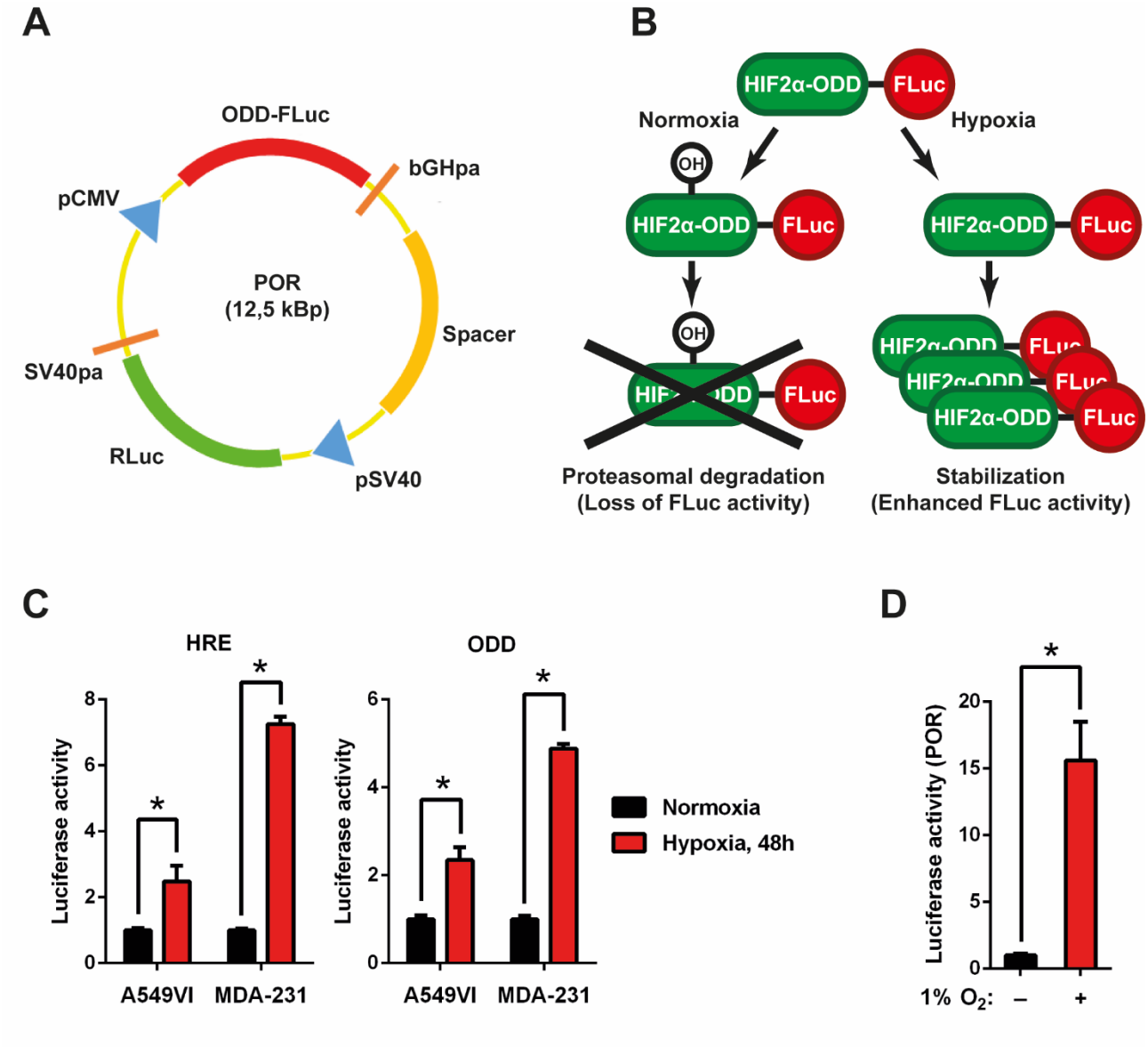

Fig. 4.12. Generation of a reporter line expressing a dual luciferase system for hypoxia sensing *in vivo*. A, Map of the lentiviral transfer plasmid encoding the two components of the luciferase system for hypoxia detection: *Renilla* luciferase (RLuc) for imaging viable tumor cells, and the Firefly luciferase-ODD fusion protein (ODD-FLuc), as a reporter for hypoxia. **B**, Under normoxic conditions, the fusion protein becomes hydroxylated by PHDs at the oxygen dependent degradation domain, which marks it for proteasomal degradation. Under hypoxic conditions, hydroxylation is inhibited, leading to increased stability of the protein and high levels of luciferase activity. **C**, Results of a dual luciferase reporter assay with two distinct reporters for hypoxia (one with hypoxia response elements and the other – with an FLuc-ODD construct) show that human breast cancer line MDA-MB-231 has a much stronger response to hypoxia than A549 human lung carcinoma cells. **D**, A significant increase in luciferase activity upon hypoxia treatment was detected in a luciferase assay using a MDA-MB-231 cell clone stably transduced with the POR construct. Relative quantification in **C** and **D** presents averages with SEMs from three replicates. *p<0.05.

To select a tumor cell line with a robust hypoxic response for transduction with the POR construct, we first performed a dual luciferase reporter assay with transient transfection of two hypoxia-responsive reporters:

1) HRE – a Firefly luciferase plasmid with nine hypoxia response elements (HREs) in the promoter;
2) ODD – plasmid with the pdDNA3 backbone containing the same FLuc-ODD fusion protein used in the POR construct.

With both of the above constructs, Renilla luciferase in a separate plasmid was cotransfected as an internal control.

Luciferase assay results showed that in both cases (with HRE and ODD reporters) the human breast cancer line MDA-MB-231 had an approximately two- to three-fold stronger response to hypoxia than A549 human lung cancer cells (**Fig. 4.12, C**).

We transduced the MDA-MB-231 cells with the POR lentiviruses and selected a single-cell clone that showed a strong and stable induction of FLuc activity under hypoxia (**Fig.4.12, D**). This line – MDA-POR – was then used in subsequent *in vivo* experiments.

4.6. Sunitinib anti-angiogenic therapy increases the tumor hypoxic response in an orthotopic model of breast cancer

To assess the extent to which anti-angiogenic therapy induces hypoxia in tumor tissue, MDA-POR cells were transplanted orthotopically into the mammary fat pad of athymic nude mice. When tumors reached 200 mm^3, 60 mg/kg/day sunitinib was administered orally. In line with previous experiments, soon after the beginning of sunitinib therapy a significant reduction of the primary tumor growth was observed in the treated group in comparison to the control (**Fig. 4.13, A**).

The strong antitumor effect of the therapy was confirmed during tumor resection: the weight of the tumors from sunitinib-treated mice was significantly lower compared to control tumors (**Fig. 4.13, B**). Interestingly, a clear difference in perfusion of the tumor tissue could be seen: tumors of sunitinib-treated mice were much less vascularized than those from control mice. This confirms that the applied treatment regimen indeed results in decreased tumor vessel formation and leads to diminished tumor growth.

We made use of the dual luciferase reporter used for this *in vivo* experiment and performed several bioluminescence imaging sessions to assess the hypoxic response in the tumors. For this, mice were injected on two subsequent days of each session with the corresponding luciferase substrates (coelentherazine for *Renilla* luciferase and luciferin for FLuc).

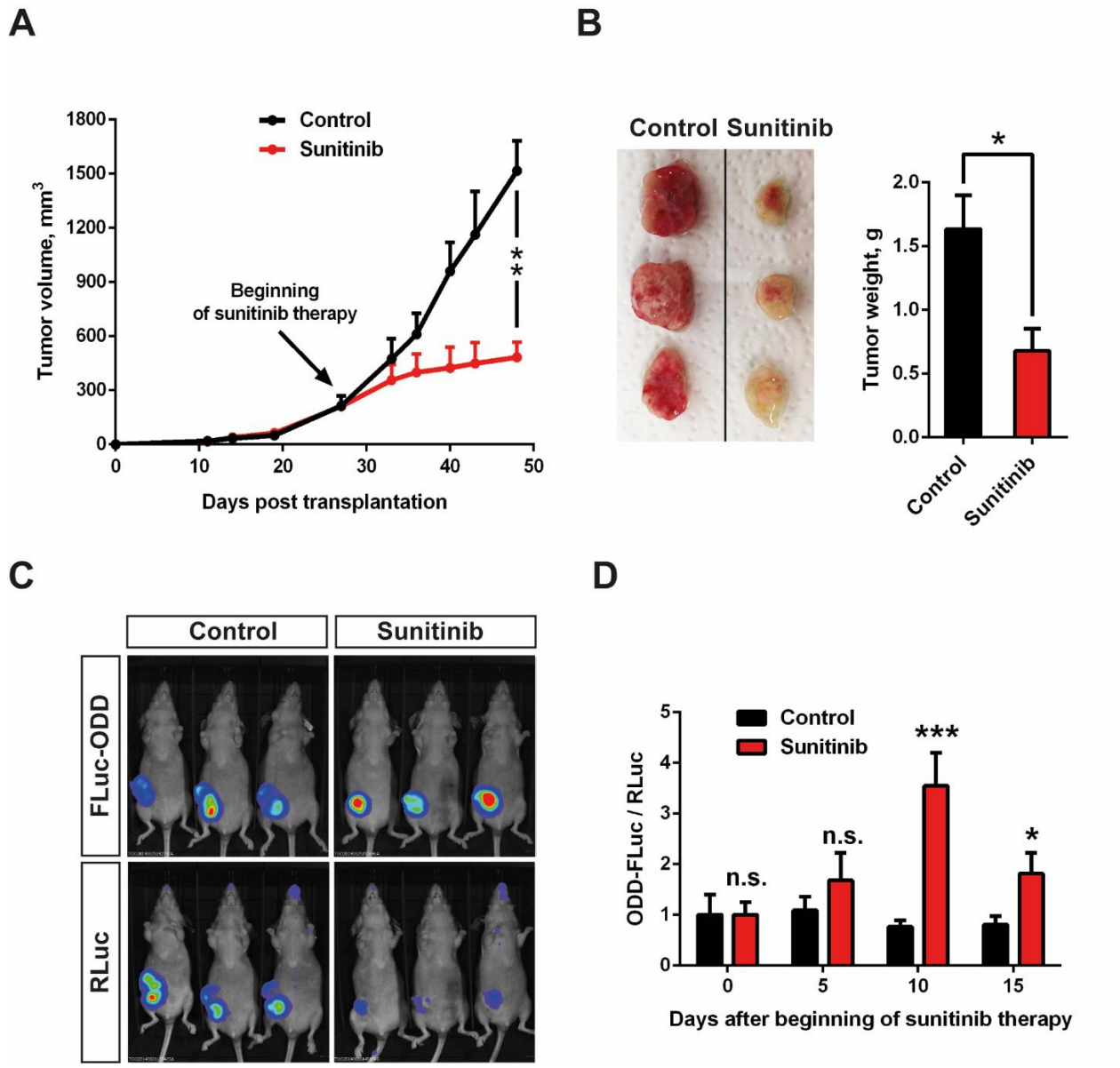

Fig. 4.13. Sunitinib anti-angiogenic therapy increases the tumor hypoxic response. A, In line with the previous *in vivo* studies (**Fig. 4.2**), administration of sunitinib anti-angiogenic therapy to animals, transplanted orthotopically with the MDA-POR line, resulted in a significant reduction in primary tumor growth. **B**, Photograph depicting resected tumors from control and sunitinib treated animals. A clear decrease in tumor size and blood perfusion, as well as weight (shown in the graph on the right), were observed in sunitinib treated mice. **C**, Bioluminescence *in vivo* imaging (day 10) revealing higher Firefly luciferase activity in the sunitinib treated group in comparison to the control; in contrast, RLuc activity was decreased in treated animals. Representative picture for each group is presented. **D**, Quantification of the Firefly to *Renilla* ratio showed a significant increase in the hypoxic response of tumors in the sunitinib-treated group in comparison to control animals. Each bar presents an average with SEM of ten imaged animals. Experiments performed in collaboration with Angel Cuesta. n.s. – not significant, *p<0.05, **p<0.01, ***p<0.001.

Bioluminescence readings were acquired with the help of an IVIS imager (*In Vivo* Imaging System, PerkinElmer). **Fig. 4.13, C** shows representative bioluminescence images taken at day ten after the beginning of sunitinib treatment. While a clearly lower RLuc signal was observed in the treated animals, in agreement with the reduced tumor size, the signal of the firefly luciferase, as a measure of tumor hypoxia, was significantly stronger. Quantification of the FLuc/RLuc ratio revealed that sunitinib anti-angiogenic therapy indeed strongly induced the tumor hypoxic response, with the peak difference between control and treated groups reaching approx. 3.5-fold (**Fig. 4.13, D**).

In this *in vivo* study, sunitinib therapy was discontinued after the resection of primary tumors and animals were observed for another four weeks. This was done to increase the chances of detecting metastasis, in accordance with the clinical observations that metastases are often detected after some time following primary tumor resection (Tohme *et al*., 2017). As in previous experiments, we observed a significantly higher incidence of lung metastasis in the treated group (the number of superficial lung metastasis was three times higher than in the control group, **Fig. 4.14, A**). A representative photo indicating the lung metastasis is depicted in **Fig. 4.14, B**, with a hematoxylin-eosin staining of a lung section showing a metastasis **Fig. 4.14, C**.

In summary, we could show that anti-angiogenic therapy significantly enhanced the tumor hypoxic response, which was accompanied by increased metastasis in an orthotopic breast cancer model. Next, we investigated if sunitinib therapy also induced an invasive phenotype in breast cancer cells, similarly to what we observed with the A549VI line.

4.7. Breast cancer cells acquire a stable EMT and cancer stem cell phenotype, and become more responsive to hypoxia after anti-angiogenic therapy *in vivo*

Six lines per group were re-isolated and cultured *in vitro* from the resected tumors of control and sunitinib-treated mice. As in previous experiments, cells re-isolated from the sunitinib-treated animals were further maintained in sunitinib-free medium.

In line with the findings from the A549-SU line, cells isolated from sunitinib-treated MDA-POR tumors (MDA-SU cells) proved to be more invasive in the modified Boyden invasion assay compared to cells isolated from control vehicle-treated mice (MDA-CO cells; **Fig. 4.15, A**). Moreover, MDA-SU lines had a higher expression of cancer stem cell markers like

NANOG and SOX2 (**Fig. 4.15, B**) and formed more colonies in the colony formation assay (**Fig. 4.15, C**).

Thus, we could show that *in vivo* anti-angiogenic therapy induces an invasive and CSC phenotype in two distinct human tumor lines of different origin.

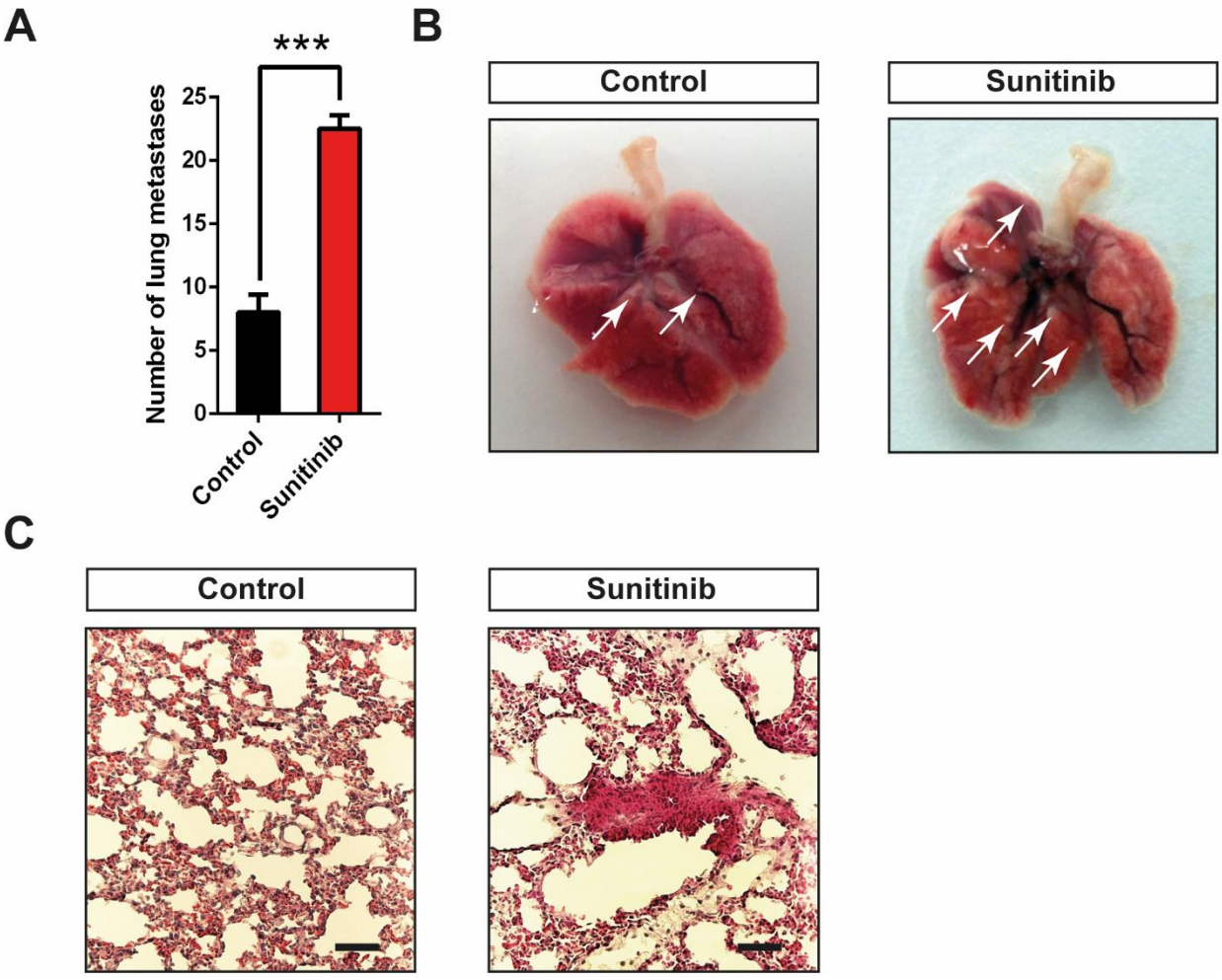

Fig. 4.14. Sunitinib anti-angiogenic therapy increases metastasis in an orthotopic xenograft model of breast cancer. A, Quantification of superficial lung metastases showed that sunitinib treatment of animals orthotopically transplanted with the human breast carcinoma line MDA-POR significantly increases metastasis. Quantification represents the average number of metastases in ten animals in each group. **B**, Representative pictures of lungs from control and sunitinib treated animals (arrows indicate the lung metastasis). **C**, Micrograph of a hematoxylin/eosin stained lung section showing a micrometastasis in an animal from the treated group. Scale bars represent 400 µM. Experiments performed in collaboration with Angel Cuesta. ***p<0.001.

Surprisingly, in addition to the observed changes in the EMT phenotype, MDA-SU cells were more responsive to hypoxia. Specifically, after culturing cells at 1% O_2, MDA-SU lines showed significantly elevated expression of HIF2α compared to control cells both at the protein (**Fig. 4.16, A**) and mRNA level (**Fig. 4.16, B**).

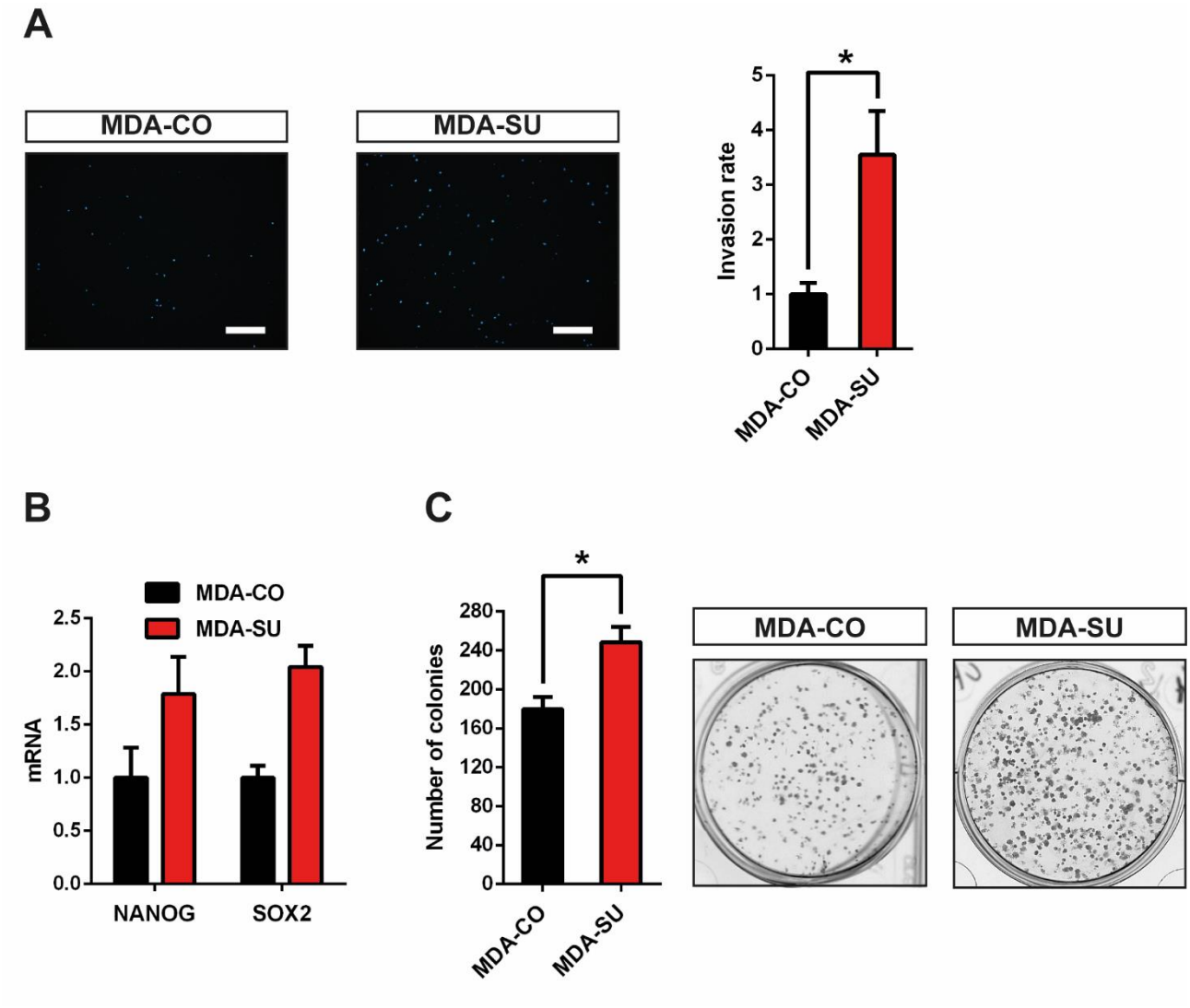

Fig. 4.15. Human breast cancer cells re-isolated from tumors of sunitinib-treated animals acquire enhanced EMT- and cancer stem cell traits. A, Modified Boyden chamber assay results show that MDA-SU cells are more invasive than control lines. Relative quantification of three replicates is presented. Scale bars represent 400 µm. **B**, qPCR analysis of MDA-SU cells revealed higher expression of cancer stem cell markers in comparison to the control. One representative picture of two independent experiments is presented. **C**, MDA-SU cells form more colonies in the colony formation assay. Averages represent quantification of six replicates. In all experiments cells were analyzed after exposure to hypoxia for 48h. (experiments were performed by Steffen Gretser). *p<0.05.

Taken together, the results described so far suggest that the hypoxia engendered by anti-angiogenic therapy could drive a novel regulatory loop that leads to increased invasion and metastasis. Our next aim was to determine if exposure to hypoxia is sufficient to produce a stable invasive phenotype in tumor cells.

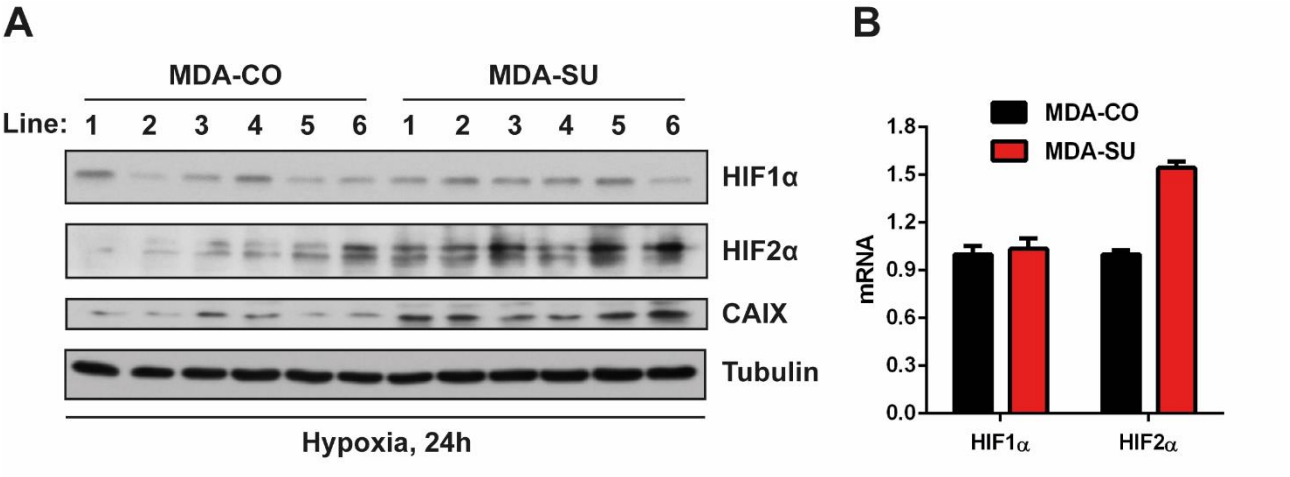

Fig. 4.16. Sunitinib anti-angiogenic therapy *in vivo* increases HIF2α expression in tumor cells. **A**, Western blot analysis of cells re-isolated from tumors of animals treated with sunitinib showing increased level of HIF2α and the hypoxia response marker CAIX. **B**, Increased HIF2α (but not HIF1α) mRNA was detected in MDA-SU lines by qPCR. One representative picture of two independent experiment is presented (Western blots and qPCR analysis were done by Steffen Gretser).

4.8. Intermittent hypoxia leads to the acquisition of a stable EMT- and CSC-phenotype, and enhanced response to hypoxia

To investigate if the hypoxic tumor microenvironment is sufficient to induce an EMT/invasive phenotype, we subjected the tumor cells to repeated hypoxia / re-oxygenation cycles (intermittent hypoxia). This approach was adopted in an attempt to mimic the microenvironment of tumors, where blood perfusion of the tumor tissue constantly fluctuates (Brurberg *et al*., 2007; Gonçalves *et al*., 2015).

MDA-POR cells were exposed to 15 cycles of hypoxia (1% O_2) for 48h each, followed by re-oxygenation (21% O_2) for 48h, and afterwards were cultured under normoxic conditions to produce intermittent hypoxia (IH) lines; control (CO) lines were cultured under normoxia (21% O_2) for the same period of time. As can be seen from micrographs in **Fig. 4.17, A**, intermittent hypoxia (IH) cells had a more spindle-shaped morphology, a clear sign of EMT. In addition, IH cells were almost 25-fold more invasive than the control line (**Fig. 4.17, B**). This striking capacity for invasion was maintained after prolonged culturing: even after 30 additional passages under normoxia *in vitro*, the IH line was significantly more invasive than the control (**Fig. 4.17, C**). Collectively, these results show that intermittent hypoxia not only induced an invasive phenotype, but that these changes remained stable over a long time.

Next, we analyzed the molecular phenotype of the generated IH line. Immunoblotting revealed higher levels of the EMT regulators Snail and Slug in IH cells (**Fig. 4.18, A**). Moreover, in line with the results from MDA-SU lines, IH cells also showed markedly

increased expression of HIF2α (but not HIF1α) and the hypoxia-response gene CAIX (**Fig. 4.18, A**).

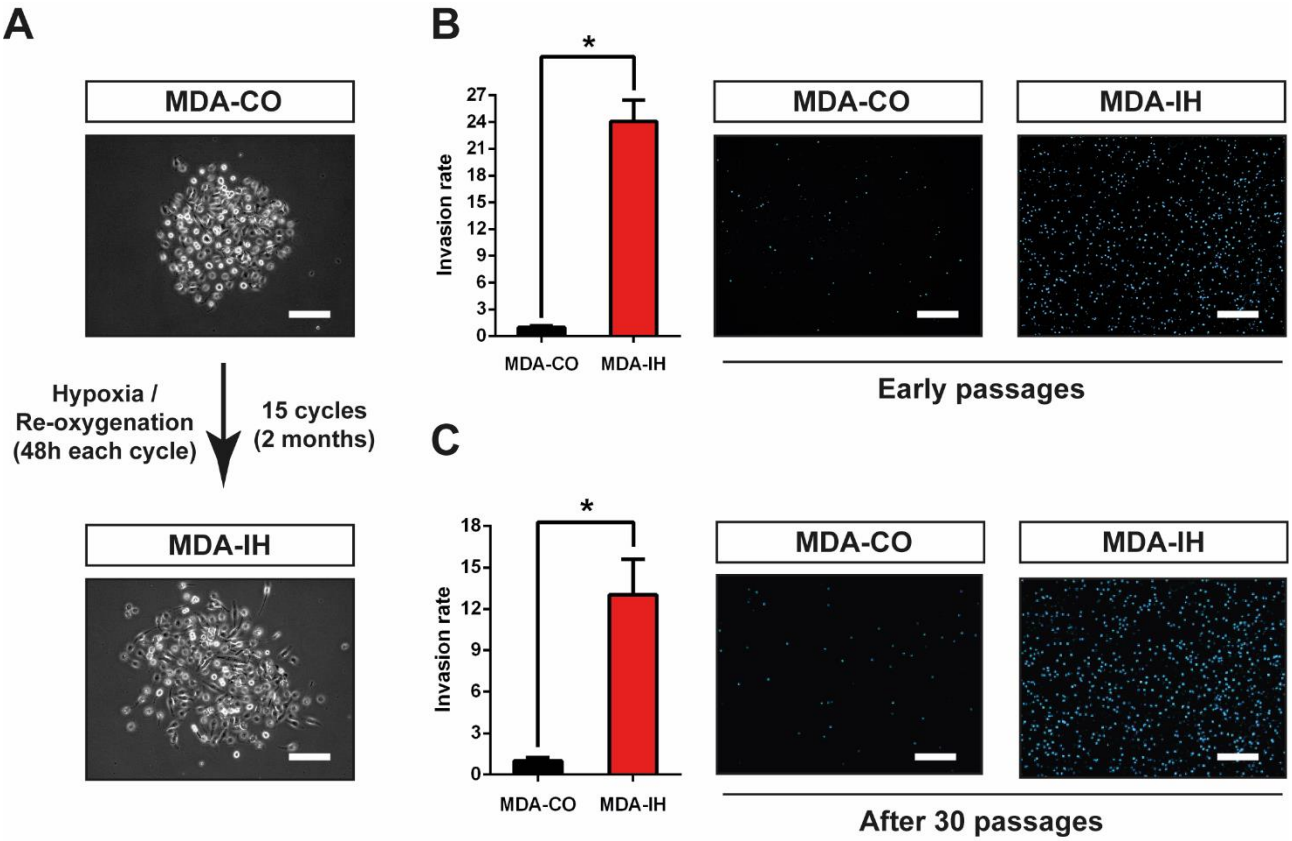

Fig. 4.17. Intermittent hypoxia promotes the acquisition of a stable invasive phenotype. **A**, Tumor cells that underwent 15 cycles of hypoxia/re-oxygenation (48h/48h) acquired a mesenchymal morphology and formed less cell-to-cell contacts. Scale bars represent 100 µm. **B**, Modified Boyden chamber invasion results revealed that IH cells are significantly more invasive than the control line. **C**, The highly invasive phenotype of IH cells is maintained throughout multiple passaging *in vitro* without repeated exposures to hypoxia. Relative quantification of three replicates is presented in **B** and **C**. In **B** and **C** cells were analyzed after exposure to hypoxia for 48h. Experiments were performed in collaboration with Steffen Gretser. Scale bars represent 400 µm, *p<0.05.

qPCR analysis showed that, in addition to increased Snail and Slug, the mRNA levels of several hypoxia response genes (CAIX, VEGFA, and GLUT1) and invasion markers (MMP2 and MMP9) were also significantly increased in IH cells (**Fig. 4.18, B**).

In line with the findings in the SU cells, the EMT phenotype of IH cells was accompanied by increased CSC traits: the IH line showed higher mRNA levels of the CSC markers OCT4, SOX2, and MAML3 (**Fig. 4.18, C**). Intermittent hypoxia cells also formed significantly more colonies (**Fig. 4.18, D**).

The observed alterations induced by intermittent hypoxia were further verified by immunofluorescence microscopy: IH cells showed markedly increased levels of transcription factors HIF2α and Snail (**Fig. 4.19, A**) and hypoxia and EMT markers - CAIX and vimentin, respectively (**Fig. 4.19, B**).

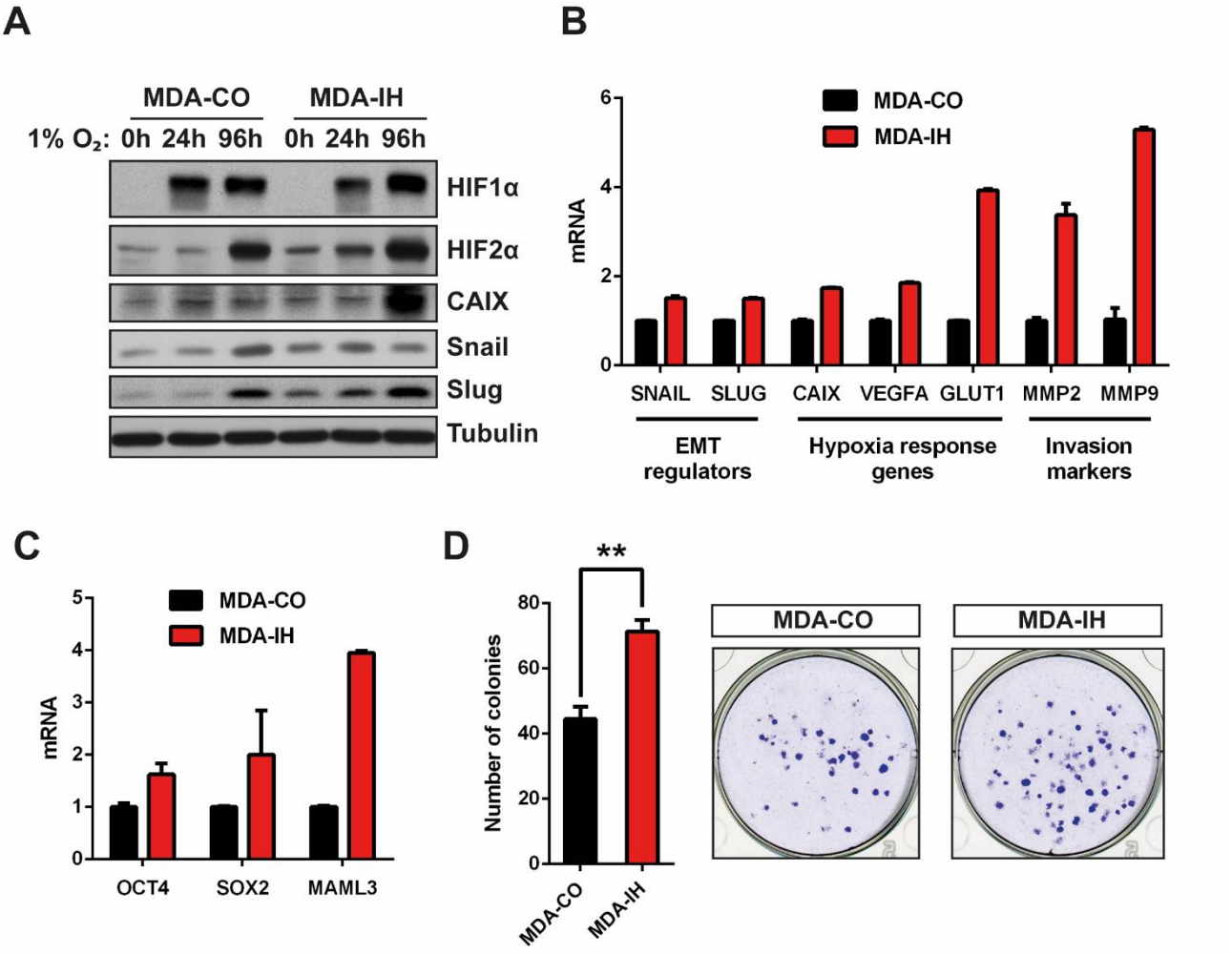

Fig. 4.18. IH cells show an enhanced response to hypoxia and augmented cancer stem cell traits. A, Immunoblotting revealed significantly higher levels of HIF2α, as well as the hypoxia response marker CAIX in the IH line. In addition, EMT regulators Snail and Slug were also induced by intermittent hypoxia. **B**, Real-time PCR analysis showed several hypoxia response and invasion markers (CAIX, VEGFA, and MMP2/9), in addition to Snail and Slug, to be upregulated by intermittent hypoxia. Similarly to SU cells, the IH line had increased expression of cancer stem cell genes (**C**) and colony forming capacity (**D**). In **B** and **C** a representative picture from three independent experiments is presented. **D** represents quantification of six replicates. In **B-D** cells were analyzed after exposure to hypoxia for 48h. Experiments were performed in collaboration with Steffen Gretser. **p<0.01.

To elucidate the mechanism driving the increased hypoxic response of the IH line, we analyzed the expression of the genes involved in HIFα stability and activity. Surprisingly, considering that HIFs are primarily regulated at the posttranslational level, Western blotting

revealed no significant changes in expression of pVHL, nor of PHD1 and PHD2 (**Fig. 4.20, A**). We observed an increase in PHD3 levels, which cannot explain the higher hypoxia response in IH cells, as PHD3 would promote HIF degradation. Instead, the increased PHD3 level is likely the consequence of its HIF-driven upregulation (Minamishima *et al*., 2009). Furthermore, the levels of additional HIF regulators, including factor inhibiting HIF (FIH) and the hypoxia associated factor (HAF), were also unchanged.

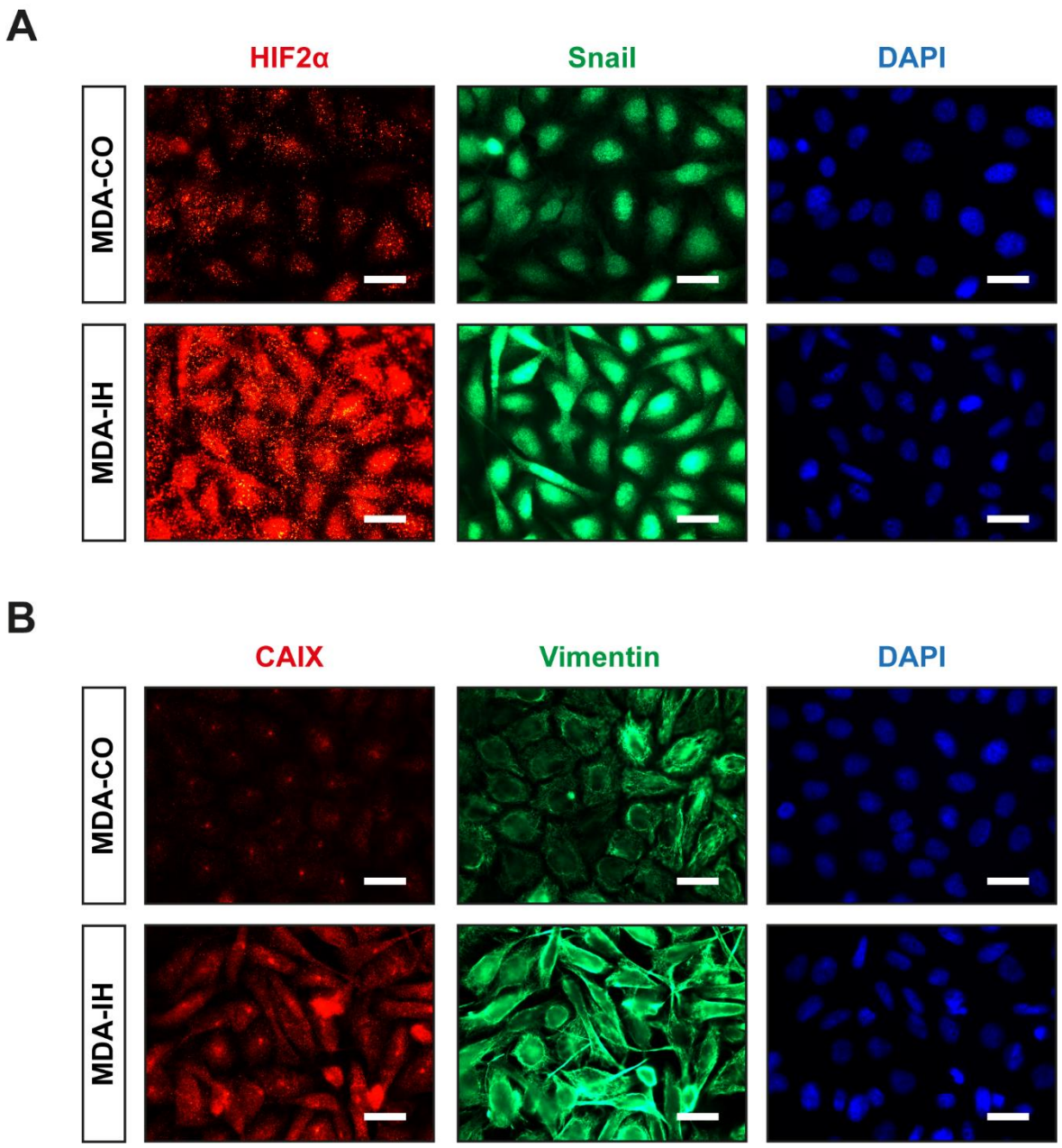

Fig. 4.19. Intermittent hypoxia cells show enhanced EMT and increased response to hypoxia. **A**, **B**, Immunofluorescence staining revealed increased expression of the two transcription factors, HIF2α and Snail, and their corresponding downstream target genes – CAIX and vimentin. Scale bars represent 30 μm. Cells were analyzed after exposure to hypoxia for 48h. Depicted are representative images from three independent experiments.

Since MDA-POR cells were used to generate the IH line, we performed a dual luciferase assay to assess PHD activity. Surprisingly, results of the luciferase assay showed even higher activity of PHDs (i.e. lower Firefly luciferase) in IH cells compared to the control. This result would fit the observed increase in PHD3, but does not explain higher HIF2α level.

Lack of changes in expression of the main HIF regulators indicated that HIF level may be regulated at a level other than the post-translational. Therefore, we next analyzed HIF1α, HIF2α, and HIF1β mRNA in control and IH cells. qPCR analysis revealed significantly increased HIF2α mRNA level (and to a smaller degree – HIF1A and HIF1β) in the IH line, while again no significant changes in the expression of HIF regulators were detected (**Fig. 4.20, C**).

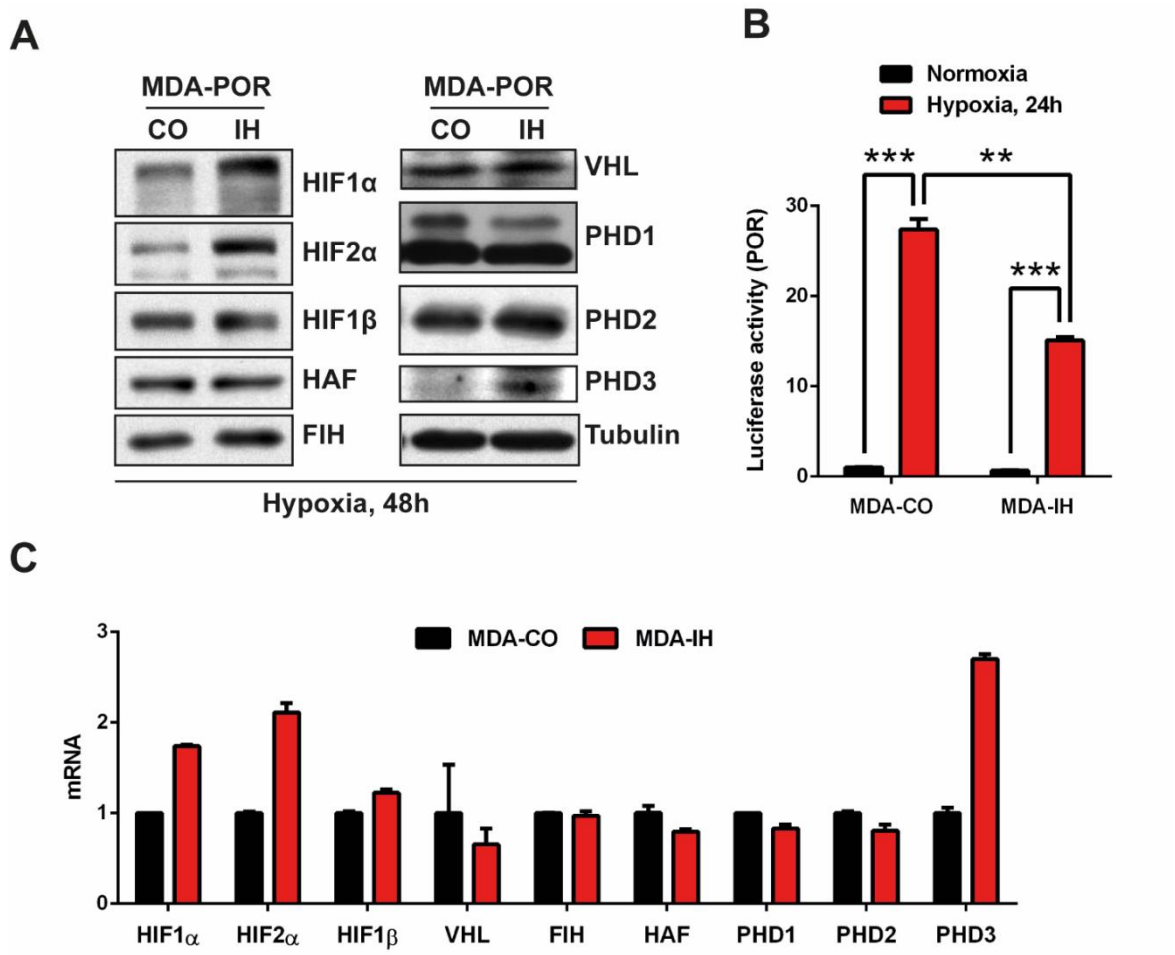

Fig. 4.20. Intermittent hypoxia induces *HIF2A* at the transcriptional level. A, Western blot showing minor to no changes in expression of major regulators of HIF stability and activity (e.g. VHL, PHDs, FIH, or HAF) in cells after IH cycling. **B**, Luciferase assay results showing decreased activation of the POR reporter in the IH line, which excludes decreased enzymatic activity of PHDs as a possible explanation for the enhanced hypoxic response in cells after intermittent hypoxia. Each bar represents relative quantification of three replicates. **C**, qPCR analysis showing a significant increase in *HIF2A* mRNA in IH cells, while no significant changes in mRNA of HIF-regulators were present after exposure of cells to 48h of hypoxia. One image of two independent experiments is presented. **p<0.01, ***p<0.001.

Besides the enhanced response to hypoxia and in agreement with the findings in SU cells, IH cells showed increased activation of the TGFβ pathway. Immunoblotting revealed higher phosphorylation of SMAD2/3 after TGFβ1 treatment in IH cells in comparison to the control (**Fig. 4.21, A**). However, in this case total SMAD2/3 levels were also slightly increased in the IM line.

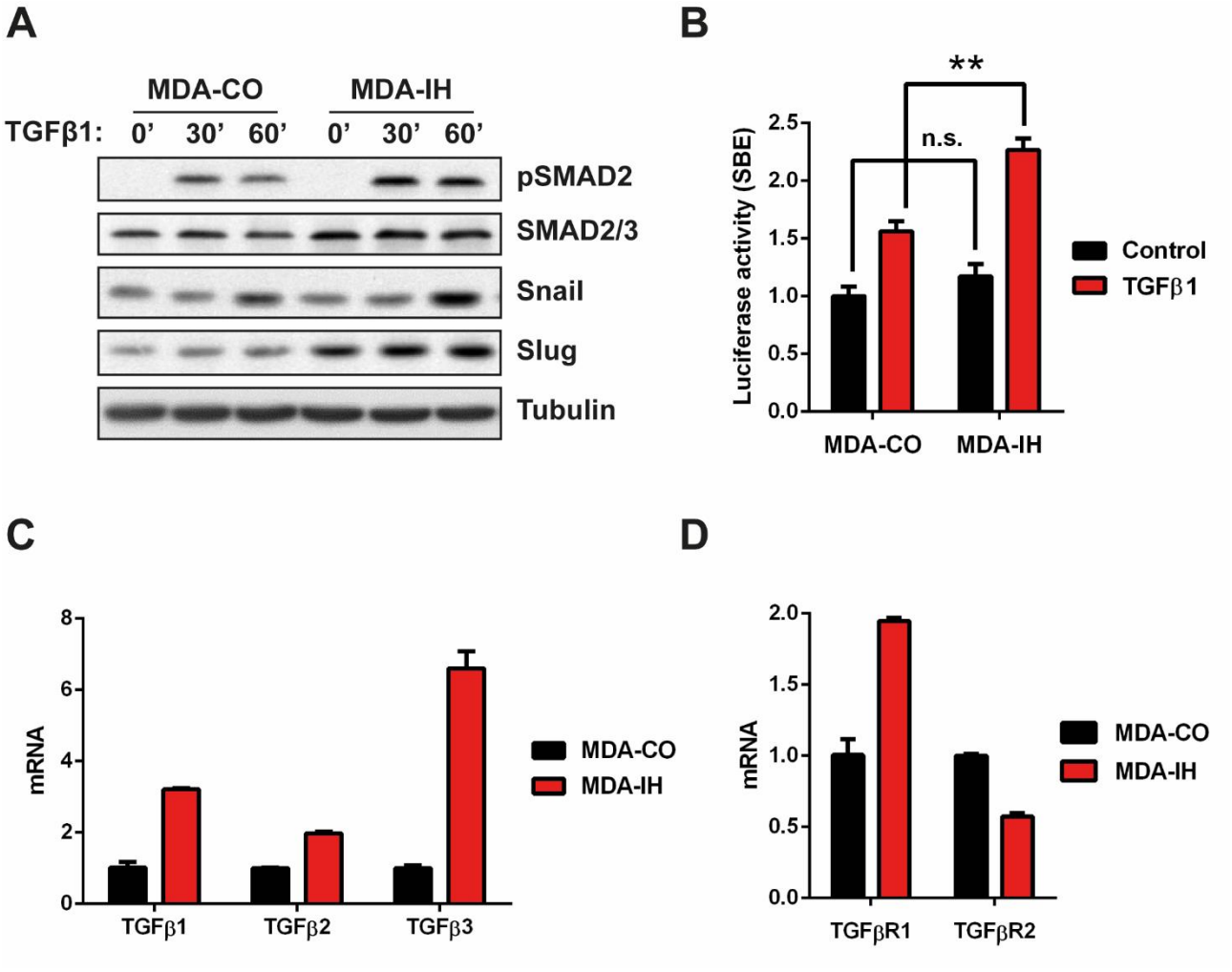

Fig. 4.21. The intermittent hypoxia phenotype is characterized by enhanced TGFβ signaling. **A**, Western blot showing higher expression of total and phosphorylated SMAD2/3 in IH cells in contrast to the control line upon TGFβ1 stimulation. **B**, Dual luciferase performed using the Firefly luciferase construct containing SMAD-binding elements (SBE) in the promoter, revealed higher FLuc activity in the IH line upon treatment with TGFβ1. Each bar represents relative quantification of three replicates. **C**, **D**, qPCR analysis showed increased levels of TGFβ1-3 and TGFβR1-2 in intermittent hypoxia cells. One image from three experiments is presented **p<0.01.

Employing a dual luciferase assay, in which FLuc transcription is under the control of SBEs, we observed increased activation of TGFβ signaling in IH cells compared with the control line, following stimulation with TGFβ1 (**Fig. 4.21, B**).

In accordance with the results from the SU lines, qPCR analysis of IH cells also revealed higher mRNA levels of the three TGFβ ligands (**Fig. 4.21, C**), as well as TGFBR1 (**Fig. 4.21, D**).

Taken together, the changes in TGFβ signaling in IH cells could in part explain the enhanced EMT phenotype of this line.

Collectively, our data show that exposing cells to intermittent hypoxia induces a stable phenotype that is characterized by EMT features, such as an increase invasive capacity, as well as enhanced HIF2α levels. Yet, the question remained open if these were cell line specific results, or these observations held true in a broader range of tumors. To address this issue, we generated two more intermittent hypoxia lines using the same protocol:

1) A549-IH – from the human lung adenocarcinoma line A549VI;
2) G55-IH – from the human glioblastoma cell line G55TL.

Both of the above-mentioned IH lines demonstrated a significant increase in invasion in comparison to respective control cells, as assessed by the modified Boyden chamber invasion assay (**Fig. 4.22, A, D**). In line with the phenotype of MDA-IH cells, both A549-IH and G55-IH lines showed higher HIF2α and Snail mRNA levels (**Fig. 4.22, B, E**), and a stronger response to hypoxia (as indicated by enhanced HIF2α and CAIX in Western blots, **Fig. 4.22, C, F**).

4.9. HIF2α and Snail are required for the maintenance of the invasive phenotype induced by intermittent hypoxia

So far, we showed that intermittent hypoxia is sufficient to trigger the acquisition of an EMT and invasive phenotype in several human tumor lines and that this phenotype is characterized by increased HIF2α and Snail. While these transcription factors are both reported to be playing an important role in regulation of tumor cell invasion and metastasis, the question whether HIF2α and Snail are responsible for the maintenance of the EMT phenotype of IH cells remained open.

To address the question whether HIF2α is required for the maintenance of the invasive phenotype, we generated a lentivirus-mediated shRNA knockdown of HIF2α in MDA-CO and MDA-IH cells. KD efficiency was verified both at the mRNA (**Fig. 4.23, A**) and protein (**Fig. 4.23, B**) levels under hypoxic conditions.

Having confirmed that HIF2α expression was sufficiently reduced in IH cells, we proceeded to analyze the invasion capacity of the generated lines in the modified Boyden chamber assay (**Fig. 4.23, C**). While no changes in invasion rate were observed in the control cells, targeting HIF2α in the intermittent hypoxia line resulted in significantly reduced invasion. Thus, we conclude that HIF2α indeed plays a major role in the maintenance of the EMT phenotype in IH cells.

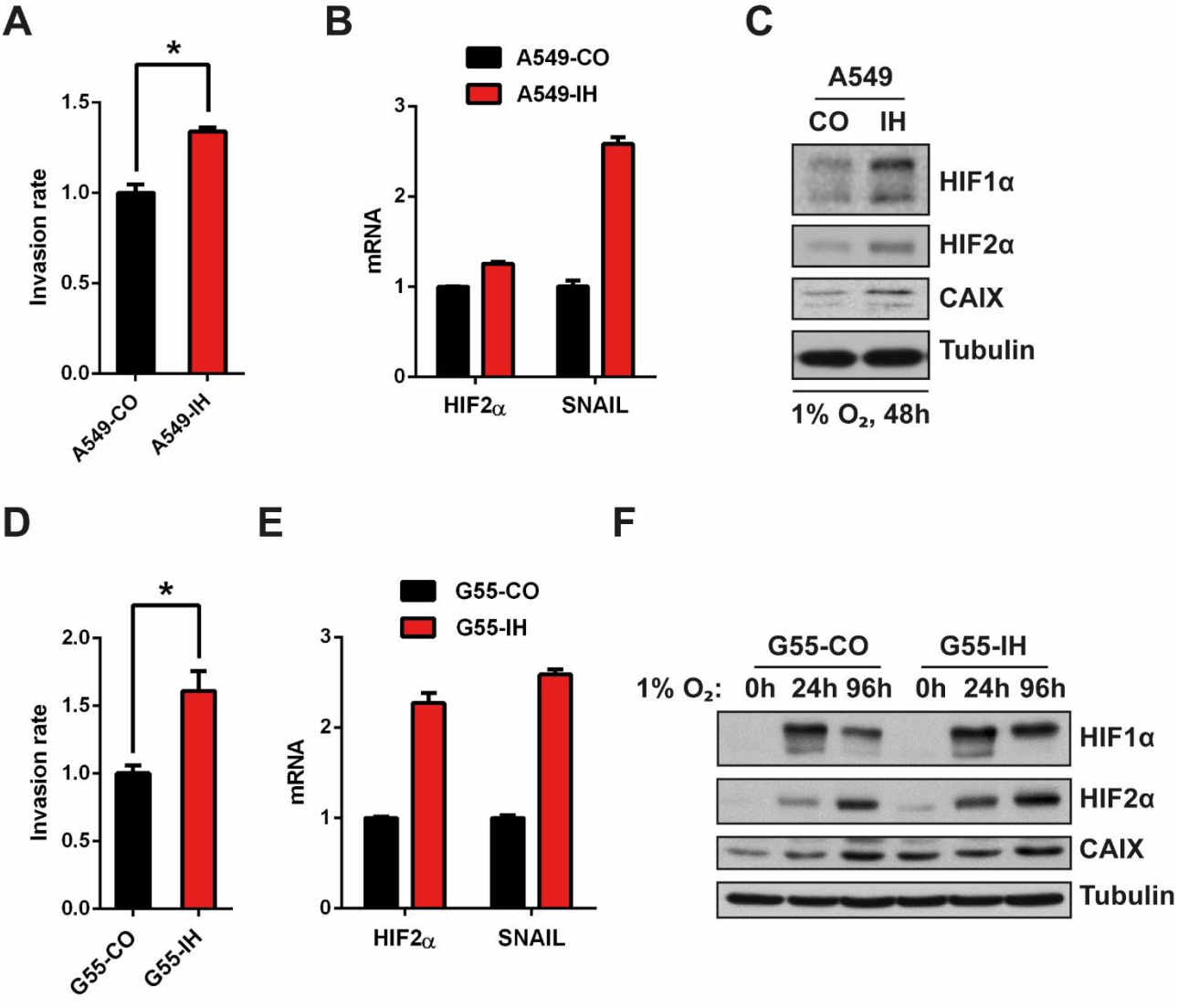

Fig. 4.22. The IH phenotype is reproducible in human tumor lines of different origin. A, Boyden chamber invasion assay showing increased invasion of IH cells generated from the human lung adenocarcinoma line A549VI. **B**, mRNA analysis by qPCR revealed increased expression of HIF2α and Snail in A549-IH cells. **C**, Western blot presenting increased HIFα levels in the IH line in comparison with the control. **D**, **E**, **F**, Like MDA-IH and A549-IH lines, intermittent hypoxia cells derived from the human glioblastoma line G55 were more invasive in a Boyden chamber assay, and showed increased levels of Snail and HIF2α. Each bar in **A** and **D** represents quantification of three replicates; one image from two independent experiments is presented in **B** and **E**. Experiments in **A**, **B**, **D**, and **E** performed after exposure of cells to 48h of hypoxia. *p<0.05.

In a similar way, we assessed the role of Snail, one of the primary EMT regulators that was highly expressed in SU and IH lines. shRNA-mediated knockdowns were generated in the control and intermittent hypoxia lines. We confirmed the KD efficiency by Western blot analysis in cells under TGFβ1 treatment, where a clear reduction of Snail was detected in both control and IH cells (**Fig. 4.24, A**). Next, we proceeded to assess the invasion capacity of generated KD cells.

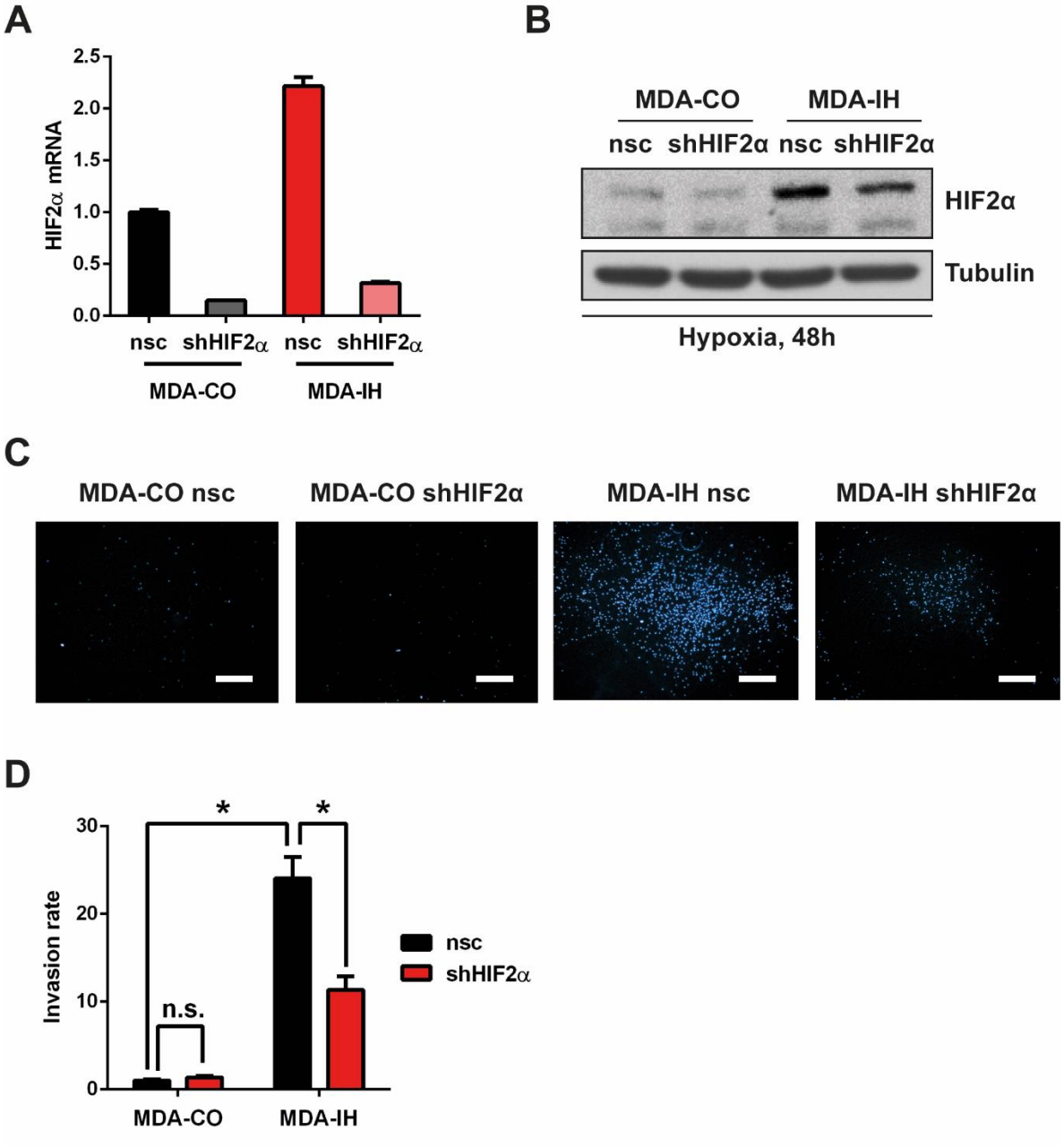

Fig. 4.23. HIF2α is required for maintenance of the invasive phenotype of intermittent hypoxia cells. HIF2α knockdown efficiency was confirmed by qPCR (**A**), and in Western blot (**B**). One picture is presented from three independent experiments. **C**, **D**, Boyden chamber invasion assay showed that HIF2α knockdown in the IH line significantly reduces invasion. Scale bars represent 400 μm. Each bar represents quantification of three replicates. In all experiments cells were analyzed after exposure to hypoxia for 48h. Experiments were performed in collaboration with Steffen Gretser. *p<0.05.

Targeting Snail had a major impact on invasion (**Fig. 4.24, B, C**). While in the presence of TGFβ1 we observed a threefold higher invasion of IH cells in comparison to the control line, Snail knockdown greatly reduced the invasion rate of IM cells. These results support the hypothesis that Snail is also involved in determining invasion in the IH line.

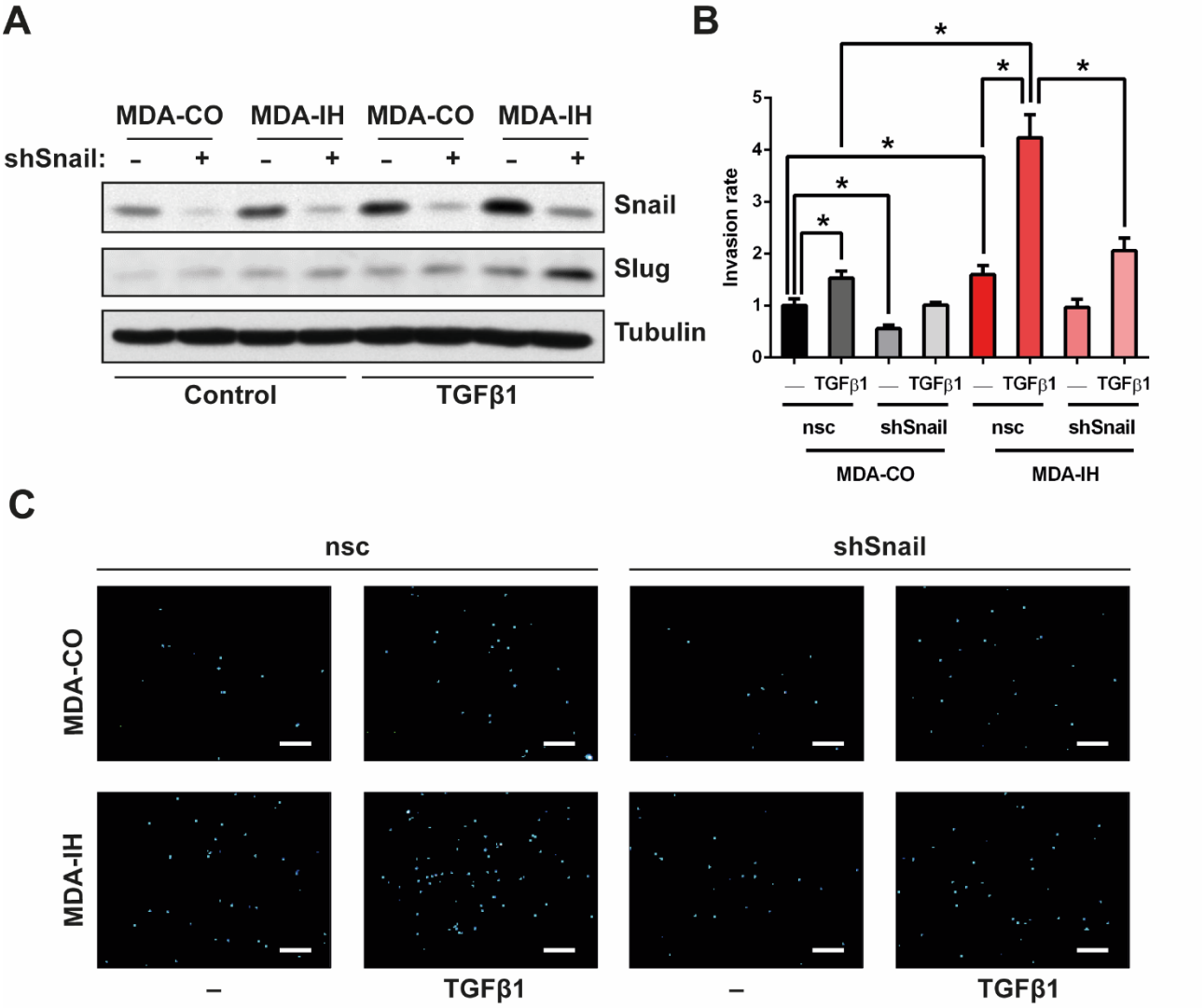

Fig. 4.24. Snail is required for maintenance of the invasive phenotype induced by intermittent hypoxia. A, Western blot showing a significant reduction of Snail in knockdown IH and control cells. **B**, **C**, Snail knockdown significantly impairs invasion of cells in a Boyden chamber assay, reverting the invasion rate of the IH line to the level of control cells. Each bar represents quantification of three replicates. Scale bars represent 400 μm, *p<0.05.

As a next step, we wanted to explore if targeting HIF2α or Snail would affect the development of metastasis. For this, we conducted an *in vivo* study in which athymic nude mice were orthotopically transplanted with the generated non-silencing control and KD cells (**Fig. 4.25, A**).

Interestingly, while neither of the knockdowns had a major influence on primary tumor growth, the growth rate of the IM lines was significantly lower in comparison to control cells.

Strikingly, however, we could demonstrate that intermittent hypoxia indeed drives the acquisition of a metastatic phenotype, as IH cell-derived tumors produced approximately three-fold more superficial lung metastases (**Fig. 4.25**, **B**). Moreover, in accordance with the Boyden chamber invasion assay results, targeting HIF2α in the IM line significantly reduced metastasis to the level of control cells.

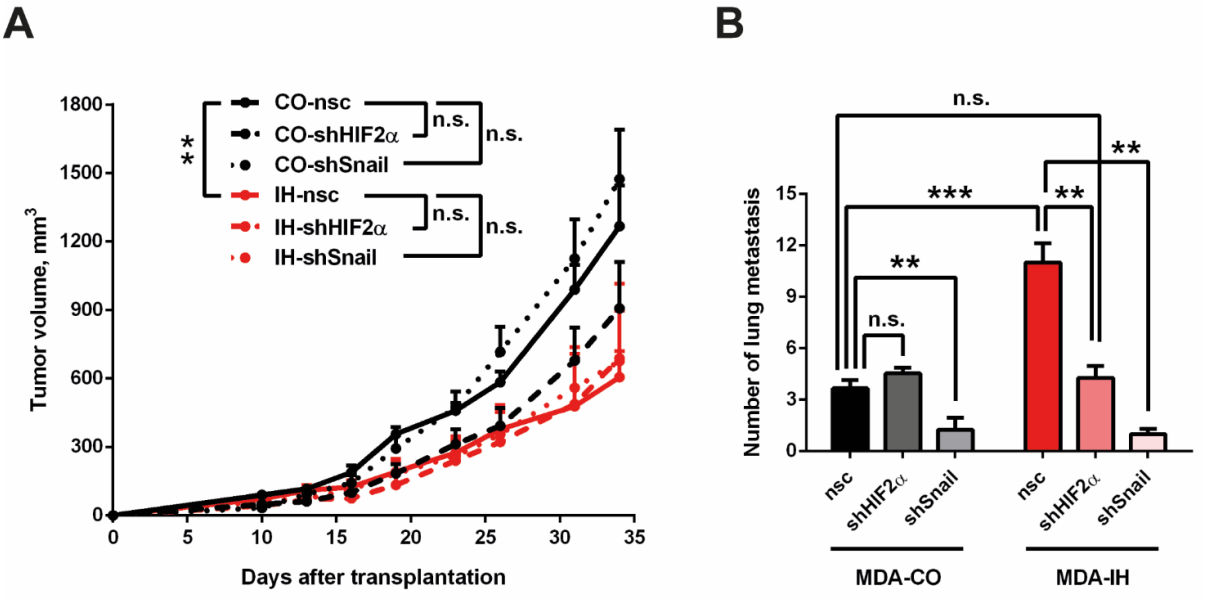

Fig. 4.25. HIF2α and Snail are required for maintenance of the metastatic phenotype of intermittent hypoxia cells. While primary tumor growth was unaffected by HIF2α or Snail knockdown (**A**), animals transplanted with knockdown lines showed a significant reduction in the number of superficial lung metastases (**B**). Specifically, targeting HIF2α resulted in a reversal of metastasis of IH cells, while not affecting the control line. Snail KD significantly decreased metastasis numbers in both control and IH cells. Number of metastasis in each group is presented as an average with SEM of ten animals. Experiments performed in collaboration with Angel Cuesta. n.s. – not significant, **p<0.01, ***p<0.001.

A similar picture was also observed upon Snail KD, which markedly reduced metastases formation in control and to an even higher extent in IH cell-derived tumor cells. These results confirm that this EMT regulator is indeed contributing to the intermittent hypoxia phenotype, as IH cells appeared to be more dependent upon Snail (reduction from an average of eleven to one metastasis per lung), than the control line (reduction from three to one).

Taken together, these results show that increased HIF2α and Snail levels are clearly required for maintenance of the highly invasive and metastatic phenotype of IH cells.

4.10. HIF2α is required for acquisition of the invasive phenotype of intermittent hypoxia cells

We could show that HIF2α is required for maintenance of the IH phenotype. However, the role that this transcription factor plays in the acquisition of intermittent hypoxia phenotype remained unclear. To address this question, we generated CRISR/Cas9-mediated knockout cells for HIF2α. **Fig. 4.26, A** shows Western blotting results with single cell-derived KO clones and the control pool of cells. In several of the selected single-cell KO clones, a total absence of HIF2α can be observed.

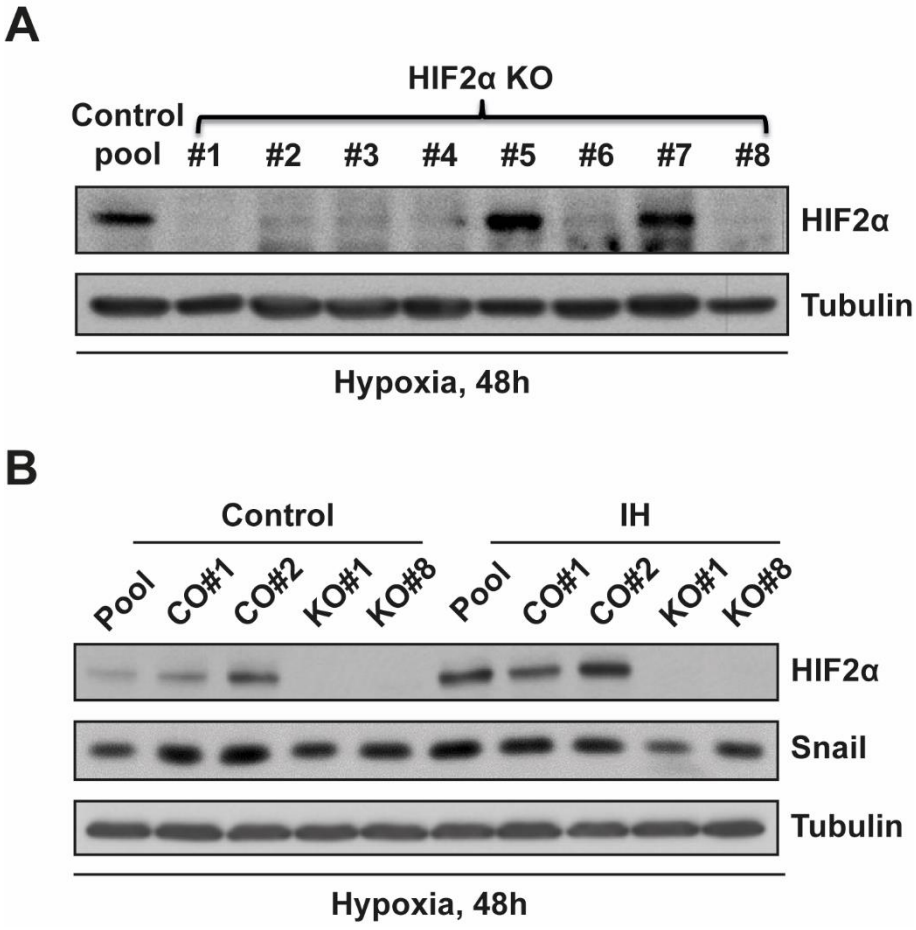

Fig. 4.26. Selection of CRISPR/Cas9 HIF2α KO clones in MDA-MB-231 cells. A, Western blot analysis of CRISPR/Cas9 KO single cell-derived clones showing several lines with a complete lack of HIF2α. **B**, IH lines generated from HIF2α KO lines show reduction in Snail protein level.

After selection, two of the HIF2α KO clones (Nr. 1 and 8), along with the control cell pool (transfected with empty vector) and two control single-cell clones, were subjected to the IH protocol with cycling hypoxia.

First, we performed Western blot analysis with the generated lines (**Fig. 4.26, B**) and confirmed the complete absence of HIF2α in KO clones 1 and 8 after IH selection. Moreover, in line with the previous findings, intermittent hypoxia induced HIF2α in all the control lines (in the polyclonal pool and single-cell clones). Interestingly, IH lines generated from control cell pools also showed increased Snail; such an increase was not apparent in the control clones, which may be due to the fact that the selected clones already had highly increased levels of Snail under normoxic conditions. By contrast, Snail was downregulated in HIF2α knockout cells following intermittent hypoxia selection.

Next, we assessed the invasive capacity of the control and HIF2α KO clones selected with the intermittent hypoxia protocol using the Boyden chamber assay (**Fig. 4.27, A, B**). First, as a control for the IH selection protocol, we observed an increase in the invasion of the polyclonal control pool of cells following cycling hypoxia. Second, IH cells harboring the HIF2α KO proved to be significantly less invasive that the control IH lines. Together, these results suggest that HIF2α plays a central role in the induction of the invasive phenotype of cells during intermittent hypoxia.

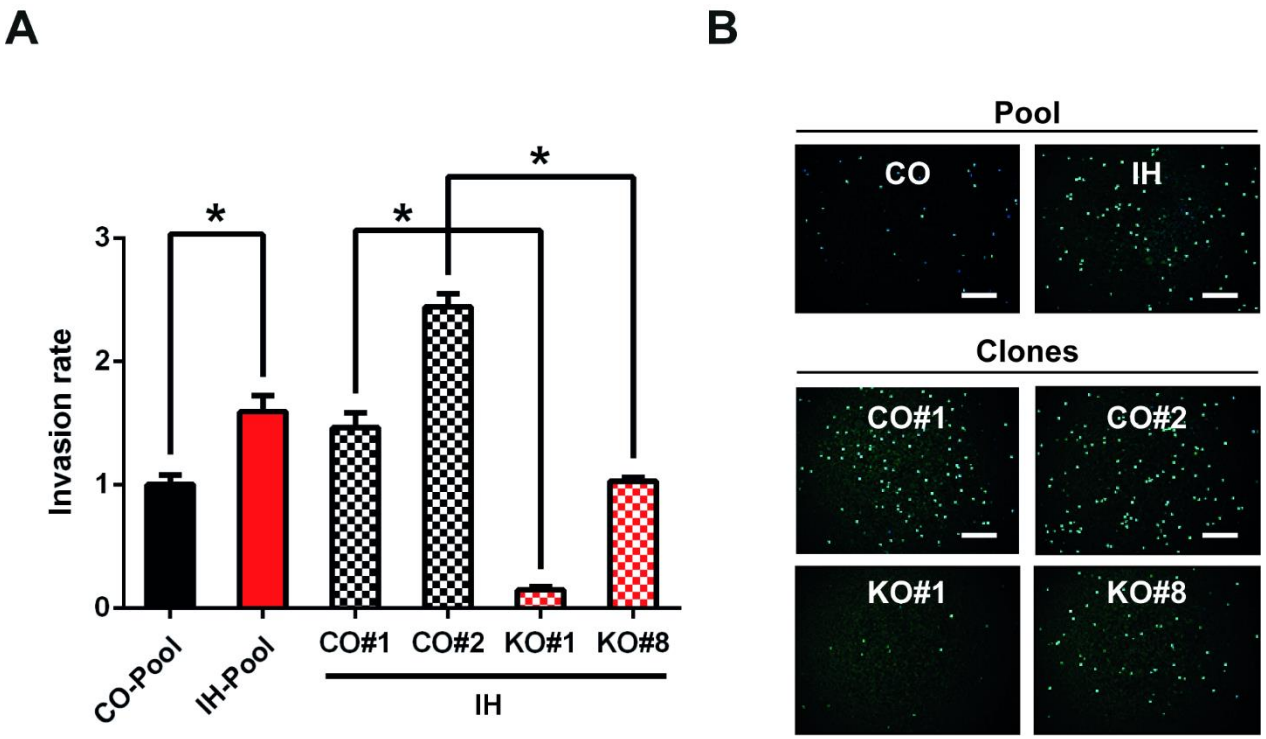

Fig. 4.27. HIF2α is required for acquisition of the invasive phenotype induced by intermittent hypoxia. A, **B**, Modified Boyden chamber invasion results show that knocking out HIF2α prevents the acquisition of an invasive phenotype in cells following intermittent hypoxia cycling. Each bar represents quantification of three replicates. Invasion analyzed after exposure of the cells to hypoxia for 48h. Scale bars represent 500 μm, *p<0.05.

4.11. HIF2α expression is regulated by DNA methylation

Our findings so far established that HIF2α plays a key role in the acquisition and maintenance of the IH phenotype. Moreover, data from the SU and IM lines indicated that elevated HIF2α was the result of increased transcription. Nonetheless, the exact mechanisms driving stronger transcription of HIF2α in SU and IH cells remained elusive.

Among the many ways of transcriptional regulation of gene expression in eukaryotic cells, epigenetic mechanisms play a significant role in cancer development and progression (Fleischer *et al*., 2017; Ha *et al*., 2017; Hanley *et al*., 2017). Considering recent reports describing the impact of DNA methylation on HIF1α expression (Pierre *et al*., 2015a; Rawłuszko-Wieczorek *et al*., 2014; Walczak-Drzewiecka *et al*., 2010a), we were interested to investigate if methylation was also involved in regulating HIF2α transcription in intermittent hypoxia cells.

First, we tested whether HIF2α can be regulated by methylation. For this, MDA-MB-231 cells were treated with a pan-inhibitor of DNA methyl-transferases (DNMTs) – azacytidine (azaC), after which we assessed expression of HIF2α. **Fig. 4.28, A** shows the result of a genomic DNA dot blot for 5-methylcytosine (5-MeC). As expected, azaC treatment reduced methylation of total genomic DNA. Furthermore, supporting our hypothesis, HIF2α expression was significantly upregulated at both the mRNA (**Fig. 4.28, B**) and protein (**Fig. 4.28, C**) levels.

In addition, we performed immunofluorescent staining for 5-methylcytosine and HIF2α in azaC-treated cells exposed to hypoxia. Using immunofluorescence analysis, we could confirm that azaC treatment leads to a reduction in 5-MeC (**Fig. 4.28, C**), which was accompanied by a significant increase in HIF2α.

Thus, we conclude that HIF2α is a target for epigenetic regulation by DNA methylation. Next, we proceeded to analyze expression of enzymes that regulate DNA methylation in IH and SU cells *in vitro*.

4.12. Anti-angiogenic treatment and intermittent hypoxia upregulate TET1

Two main groups of enzymes are known to regulate DNA methylation:

1. DNA methyl-transferases (DNMTs) – enzymes that transfer methyl groups to cytosines. In human, this group of enzymes is represented by three isoforms, among

which DNMT1 is the maintenance methyl-transferase, whereas DNMT3A and DNMT3B are the *de novo* methyl-transferases.

2. Ten-eleven translocation (TET) methyl-cytosine dioxygenases – a family of three enzymes (TET1-3) that catalyze the conversion of methylcytosines to hydroxymethylcytosines, the first step of active DNA demethylation (see **Fig. 3.6**).

First, the mRNA of these enzymes in SU and IH lines was analyzed. Interestingly, we observed significantly higher TET1 mRNA levels in both SU and IH cells (**Fig. 4.29, A, B**). In contrast, the other TET members were either not altered or even slightly downregulated.

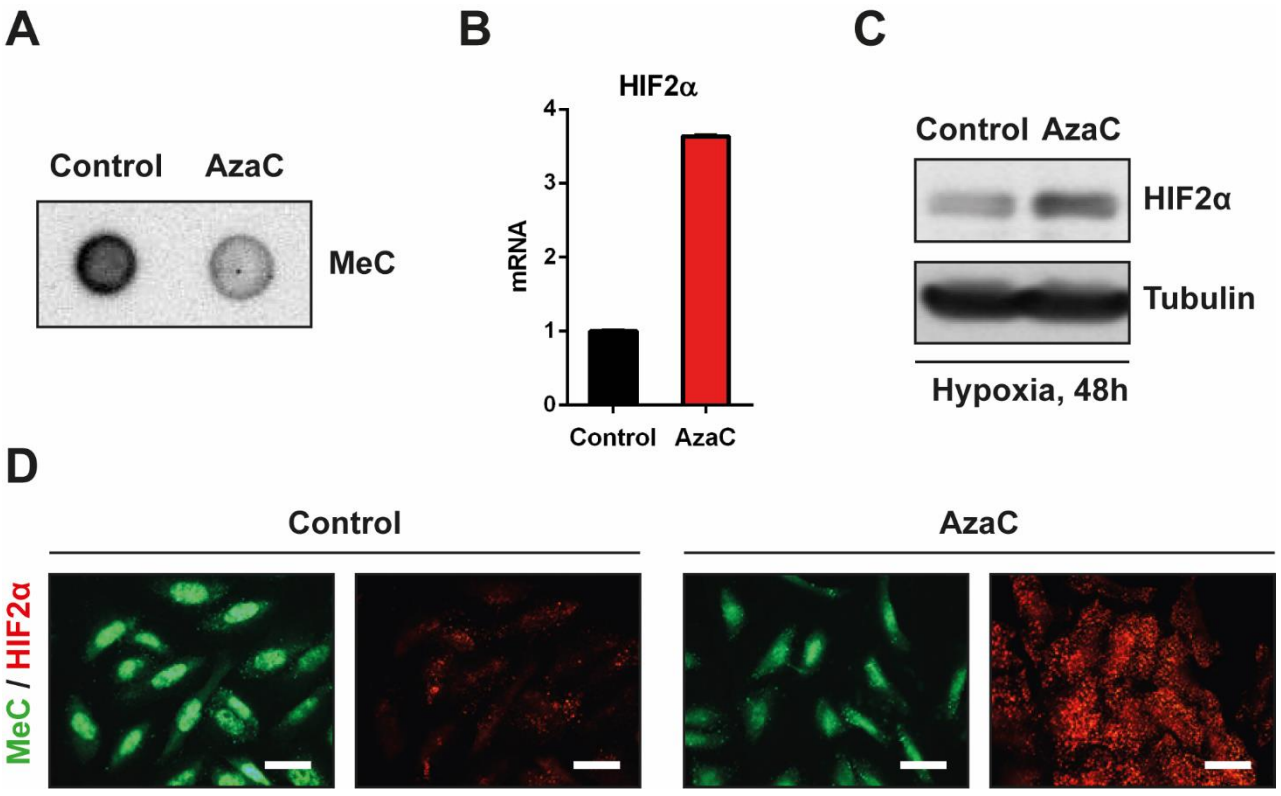

Fig. 4.28. HIF2A expression is epigenetically regulated by DNA methylation. A, DNA dot blot showing a significant reduction in methylation of genomic DNA in azacytidine treated cells. Azacytidine treatment leads to enhanced expression of HIF2α at the mRNA (**B**) and protein (**C**) levels. **D**, Immunofluorescence analysis revealed a reduction in methylated cytosines in azaC treated cells, which was accompanied by an increase in HIF2α. One picture from two independent experiments is presented. Scale bars represent 50 µm. In all experiments cells were exposed to hypoxia for 48h. Experiments in **A**-**C** were performed in collaboration with Steffen Gretser.

Real-time PCR analysis of DNMTs revealed a slight decrease in expression of the *de novo* methyl-transferase DNMT3B in SU lines. IH cells, by contrast, showed a slight upregulation of DNMT3B, while mRNA of the maintenance methyl-transferase DNMT1 remained largely unchanged in either sunitinib or IH cells.

Taken together, these results hint at the possibility that TET1 might be responsible for the increased transcription of HIF2α in SU and IM cells.

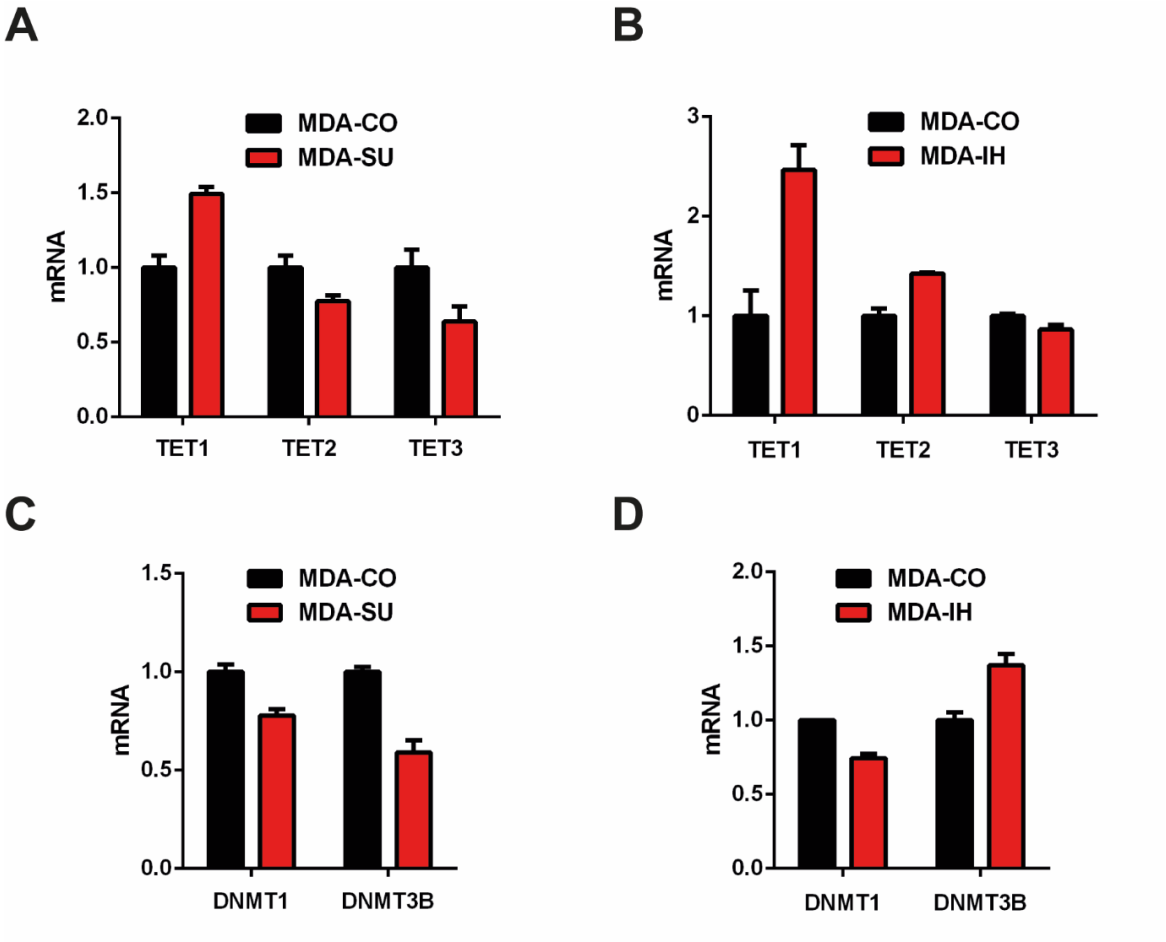

Fig. 4.29. Anti-angiogenic therapy and intermittent hypoxia upregulate TET1. A, **B**, qPCR results show significantly increased TET1 mRNA in both SU and IH lines. **C**, **D**, Real-time PCR analysis showed no consistent changes in the expression of DNA methyltransferases (DNMT1 and DNMT3B) in either SU or IH cells. One picture from two independent experiments is presented. Experiments were performed in collaboration with Steffen Gretser.

Next, we performed immunoblotting for TET1 in IH and SU lines. Indeed, in line with qPCR results, a significant increase of TET1 levels was observed in SU (**Fig. 4.30, A**) and IH cells (**Fig. 4.30, B**) in comparison to the corresponding controls. Moreover, TET1 was induced by hypoxia in both control and IH lines, further strengthening our hypothesis.

Western blot results were then corroborated by immunofluorescence showing that intermittent hypoxia upregulated TET1. Co-staining for vimentin, a classical EMT marker, confirmed the enhanced EMT phenotype of the IH line (**Fig. 4.30, C**).

Moreover, staining for 5-hydroxymethylcytosine (5-hMeC), the direct product of TET1 catalytic activity, nicely correlated with TET1 expression, with a significant increase in 5-hMeC in the IH line (**Fig. 4.30, D**).

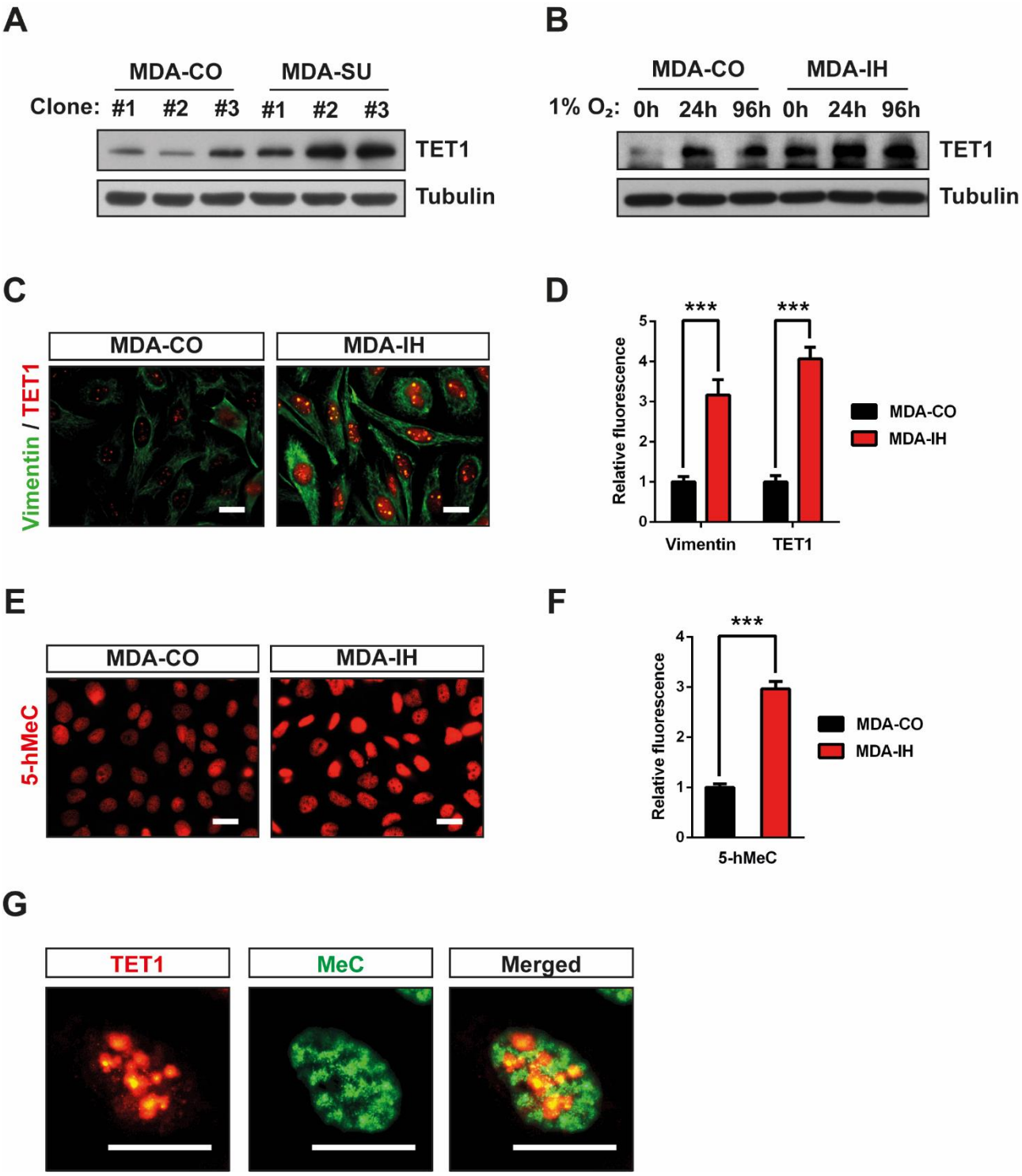

Fig. 4.30. Increased levels of TET1 and DNA demethylation in intermittent hypoxia cells. Western blot analysis revealed increased TET1 in SU (**A**) and IH cells (**B**). **C**, **D**, Immunofluorescence staining showed elevated TET1 and vimentin in IH cells. **E**, **F**, Enhanced immunofluorescent staining for 5-hydroxymethylcytosine in the IH line indicates higher TET activity. **G**, In the nuclei of IH cells TET1 co-localized with hypomethylated areas of DNA, as shown by IF co-staining with MeC. In **A**-**E** one picture from two independent experiments is presented. In **E** three images per coverslip were used for quantification Scale bars represent 20 μm (Western blot analysis in **A** performed by Steffen Gretser).

A connection between TET1 and DNA demethylation in the IH line was further strengthened by the results of immunofluorescence staining of methylcytosine (MeC) and TET1 (**Fig. 4.30, E**) showing a colocalization of TET1 with hypomethylated areas in the cell nuclei.

In line with the results from MDA-IH cells, similar changes were observed in the other two intermittent hypoxia lines – A549-IH and G55-IH. Specifically, immunofluorescence staining revealed significantly increased TET1 and 5-hMeC in both IM lines (**Fig. 4.31, A-D**).

Taken together, these results show that intermittent hypoxia drives an elevated, constitutive TET1 expression and leads to DNA demethylation in tumor cells. Therefore, we hypothesized that DNA demethylation mediated by TET1 contributes to the EMT/invasive phenotype in tumor cells. To test this hypothesis, we generated two different sets of cells – TET1 loss-of-function and TET1 overexpression – and analyzed their phenotype.

4.13. TET1 promotes the EMT and a cancer stem cell phenotype

To establish the functional connection between TET1 and HIF2α, we first silenced TET1 by shRNA mediated knockdown in the MDA-MB-231 cell line. Knockdown efficiency was assessed by qPCR, where we observed a 40% reduction in TET1 mRNA (**Fig. 4.32, A**). In addition to decreased TET1, knockdown cells also expressed less HIF2α.

Interestingly, using MDA-MB-231 cells in which HIF2α was knocked down, we could show that not only TET1 regulates HIF2α, but also that HIF2α controls TET1 expression, as mRNA analysis of HIF2α KD cells revealed significantly reduced TET1 (**Fig. 4.32, B**).

Immunoblots with TET1 KD cells showed that despite the relatively moderate decrease in TET1, HIF2α was significantly downregulated (**Fig. 4.32, C**), in line with real-time PCR findings. HIF2α KD also led to a decrease in TET1 protein levels, although the reduction was less pronounced than the one seen at the mRNA level.

Next, we set out to investigate if TET1 overexpression could induce an EMT/invasive phenotype. For this, MDA-MB-231 cells were transduced with lentiviruses containing a TET1 overexpression cassette. Overexpression was confirmed by real-time PCR (**Fig. 4.33, A**) and immunoblotting (**Fig. 4.33, B**).

Interestingly, TET1-overexpressing cells showed also higher HIF2α mRNA levels. Immunoblotting results revealed a similar picture, where TET1-overexpressing cells had increased HIF2α, as well as Snail protein levels.

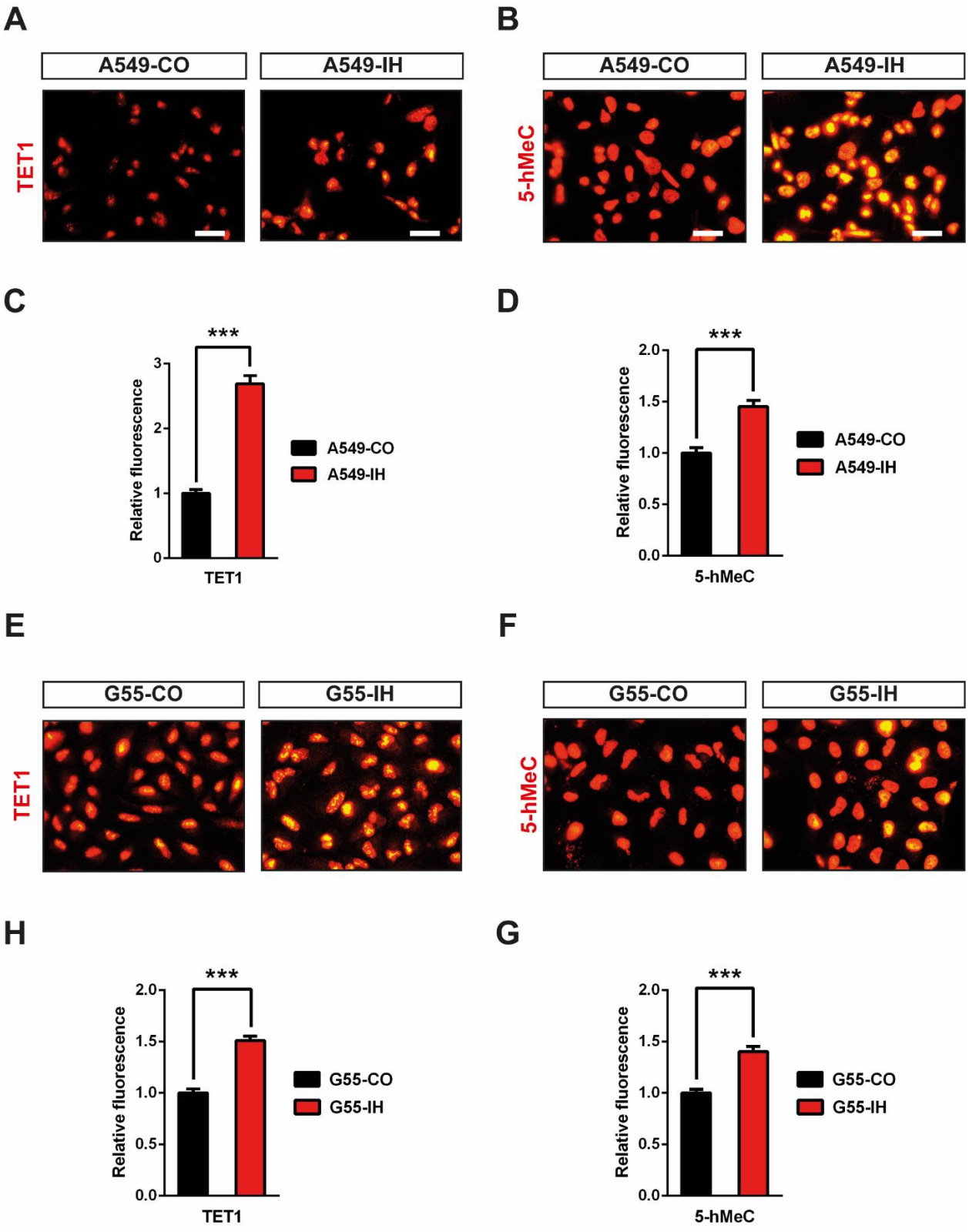

Fig. 4.31. Intermittent hypoxia promotes TET1 expression and increases 5-hydroxymethylcytosine in human tumor lines of different origin. Immunofluorescence analysis showed increased TET1 and 5-hMeC levels in the human lung carcinoma line A549 (**A**-**D**) and in the human glioblastoma line G55 (**E**-**G**) following intermittent hypoxia selection. One picture from two independent experiments is presented. In **C**, **D**, **H**, and **G** three images per coverslip were used for quantification. Scale bars represent 30 µm.

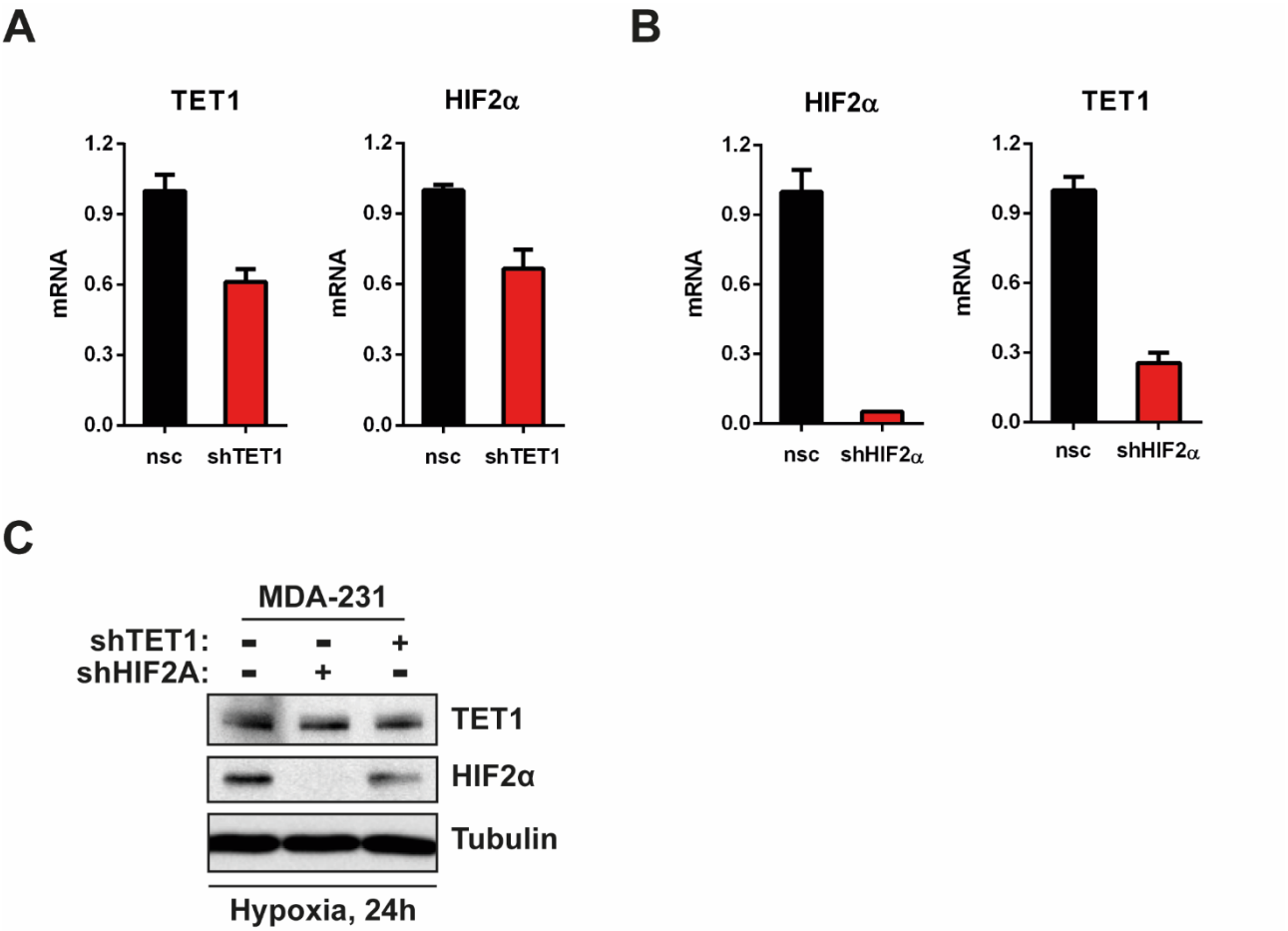

Fig. 4.32. TET1 regulates HIF2α expression. A, Real-time PCR showed that targeting TET1 with shRNA leads to decreased HIF2α levels. **B**, Vice versa, mRNA analysis of cells expressing shRNA against HIF2α revealed decreased TET1 levels. **C**, Western blotting confirmed that TET1 KD cells express less HIF2α, and that HIF2α KD cells have lower levels of TET1, although the latter change was less dramatic than that seen at the mRNA level. One picture from two independent experiments is presented in **A**-**C**.

Analysis of the generated cell line in a Boyden chamber assay showed increased invasion of TET1 overexpressing cells (**Fig. 4.33, C**). In addition to TET1 overexpression, we generated loss of function cells by transfecting MDA-MB-231 cells with siRNA against TET1. In contrast to TET1 overexpression, knockdown cells showed a significant (more than 50%) reduction of invasion (**Fig. 4.33, D**).

Taken together, these results show that TET1 is an upstream regulator of HIF2α, through which it regulates EMT and cell invasion.

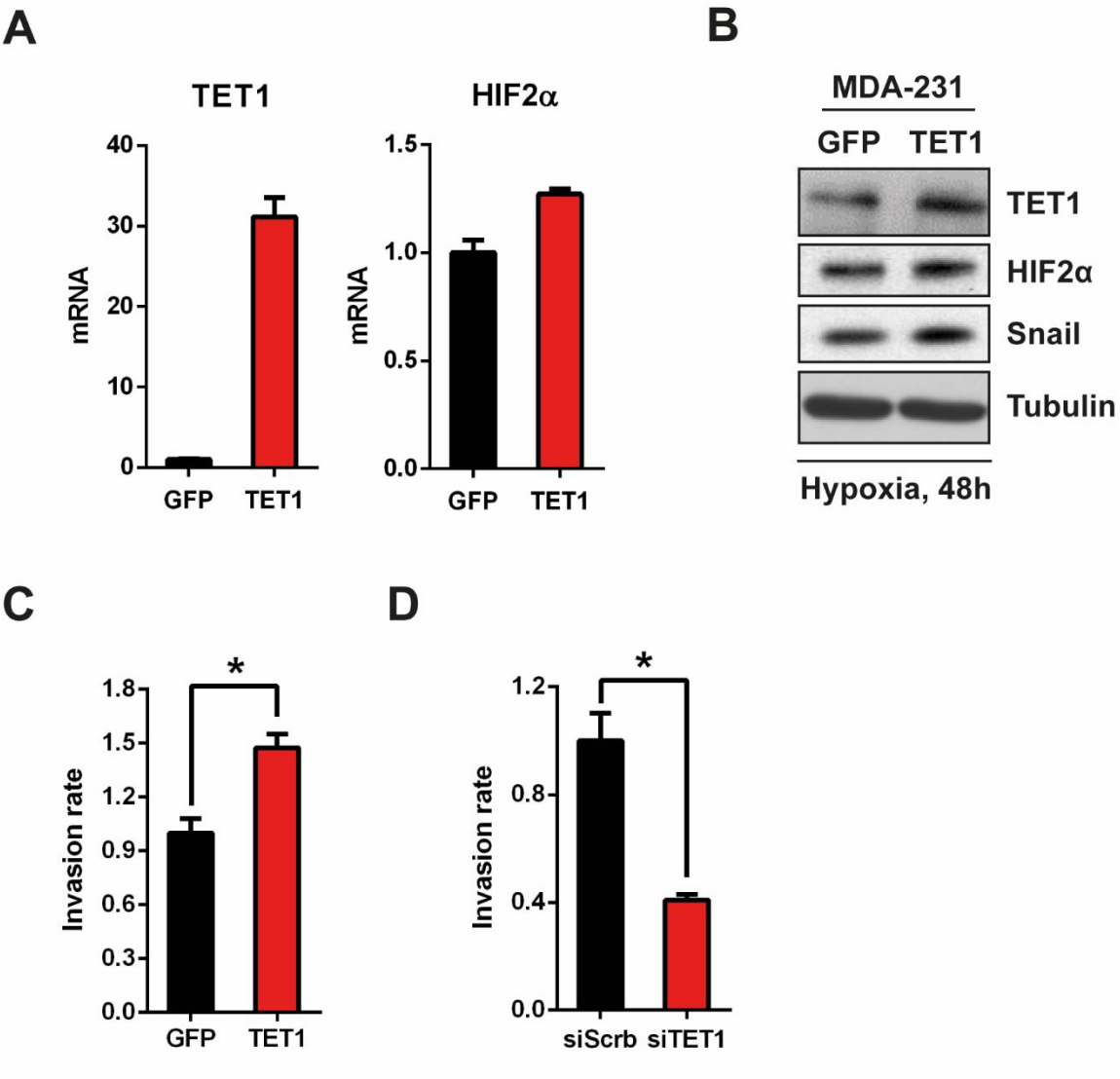

Fig. 4.33. TET1 promotes the invasive cell phenotype. **A**, qPCR results demonstrate that overexpression of TET1 results in increased HIF2α mRNA levels. **B**, Immunoblotting results show that cells overexpressing TET1 show higher HIF2α and Snail levels in comparison to the GFP control line. **C**, **D**, TET1 overexpression stimulates invasion of cells in a modified Boyden assay (**C**), while siRNA knockdown significantly reduces the invasion rate (**D**). In **A** and **B** one picture from two independent experiments is presented; each bar presents average with SEM of three replicates. Experiments in **A**-**C** were performed in collaboration with Steffen Gretser. *p<0.05.

4.14. TET1 is associated with a hypoxic gene expression profile in patients with lung adenocarcinoma and breast invasive carcinoma

The findings that TET1 regulates HIF2α expression suggest that TET1 may also be involved in regulating the hypoxic response in human tumors. To assess this possibility, we analyzed the publicly available patient datasets with RNA sequencing data from The Cancer Genome Atlas (TCGA). For this, mRNA z-scores of TET1, HIFs, cancer stem cell markers, and various hypoxia-response genes were retrieved through the cBioPortal for patients with lung

adenocarcinoma (LUAD) and breast invasive carcinoma (BIC). In total, expression data from 456 tumors of lung cancer patients and 787 tumors of breast cancer patients were analyzed.

To assess the influence of TET1 on the phenotype of the analyzed tumors, patients in each group were stratified into two subgroups, depending on the expression of TET1:

1) TET1-low – patients in which TET1 mRNA z-scores were below -0.5;
2) TET1-high – patients with TET1 mRNA z-scores above 0.5.

Cutoff values of -0.5 and 0.5 were chosen with the aim of ensuring a sufficient difference in TET1 expression between the two groups. In addition, selection of the cutoffs was influenced by the availability of case numbers, which had to be analyzed to enable sufficiently powered statistical analysis. Despite the high variation in TET1 mRNA z-scores (from -0.94 to 11.5 in breast cancer patients, and -0.65 to 16.15 in lung cancer patients), the majority of cases lay between -0.5 and 1, with medians at -0.23 and -0.18 for breast invasive carcinoma patients and lung adenocarcinoma patients, respectively.

Thus, after the stratification, we compared the expression of genes of interest between the TET1-high and TET1-low groups. **Fig. 4.34** presents the result of this gene expression analysis. First, as a confirmation, stratification of patients resulted in a significant difference in average TET1 z-scores in in both lung and breast cancer patients (**Fig. 4.34, A, E**).

A strong difference in expression of hypoxia-response genes was noted after stratification (**Fig. 4.34, B, F**): in both, LUAD and BIC patients, TET1-high groups possessed significantly greater z-scores of multiple hypoxia-regulated genes, e.g. *VEGFA*, *NCAD*, etc. Furthermore, lung cancer patients with high TET1 expression had elevated mRNA of *HIF2A*, but not *HIF1A* (**Fig. 4.34, C**). However, an opposite expression pattern was present in BIC patients, with *HIF1A* being significantly upregulated in the TET1-high group, while *HIF2A* was decreased (**Fig. 4.34, G**).

To further explore the significance of TET1 in human tumors, we assessed the expression of several prototype lung and breast cancer stem cell markers (Ferone et al., 2016; Gwak et al., 2017; Levina et al., 2010; Ricardo et al., 2011; Seo et al., 2016; Sin and Lim, 2017; Wang et al., 2013). In agreement with the findings from IH and SU cells, we observed a strong correlation between TET1 and CSC markers in lung and breast cancer patients, such as c-KIT, CD133, etc. (**Fig. 4.34, D, H**).

Thus, the results of the gene expression analysis indicate that in both breast and lung cancer patients, high TET1 expression correlates with an enhanced hypoxic response that can be linked to increased HIFs and a CSC phenotype. Combined, these characteristics are

generally considered to be poor prognostic factors (Van Den Beucken *et al*., 2014; Cleven *et al*., 2008; Hu *et al*., 2017a; Rhee *et al*., 2016).

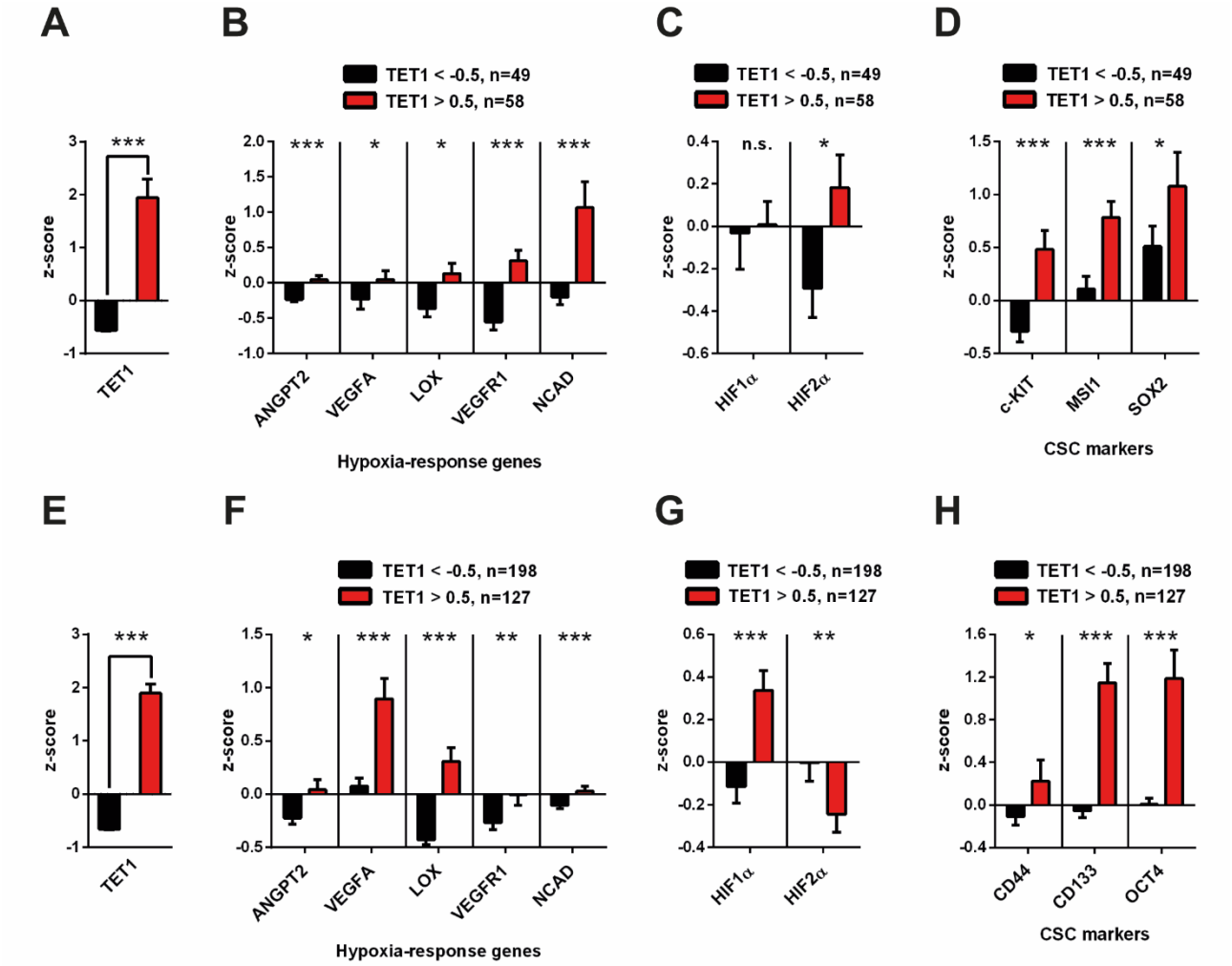

Fig. 4.34. High expression of TET1 correlates with an increased hypoxic response and stem cell traits in patients with lung adenocarcinoma and breast invasive carcinoma. A, Patients with lung adenocarcinoma were stratified into two groups: TET1-low (mRNA z-scores below -0.5) and TET1-high (z-scores above 0.5). **B**, High expression of TET1 in patients with lung cancer correlates with an increased response to hypoxia, as evidenced by increased z-scores for multiple hypoxia response genes, e.g. VEGFR1, NCAD, etc.). **C**, Lung cancer patients with high expression of TET1 showed an increase in the mRNA levels of HIF2α, but not HIF1α. **D**, TET1 correlates with stem cell markers, e.g. c-KIT, SOX2, in patients with lung adenocarcinoma. **E**, Patients with breast invasive carcinoma, like lung cancer patients, were subdivided into TET1-high and TET1-low groups. **F**, BIC patients with high TET1 showed elevated expression of hypoxia response genes, such as LOX, VEGFA, etc. **G**, Unlike patients with lung cancer, breast cancer patients with high TET1 showed increased HIF1α, but not HIF2α mRNA. **H**, TET1 expression correlates with stem cell markers in patients with breast cancer. n – number of cases, n.s. – not significant, *p<0.05, **p<0.01, ***p<0.001.

4.15. High expression of TET1 in patients with lung adenocarcinoma and breast invasive carcinoma is associated with decreased methylation at multiple CpG-sites in *HIF2A*

Having established that TET1 expression correlates with HIF2α mRNA in human tumor samples, we hypothesized that this connection is functional, i.e. that higher TET1 could result in demethylation of *HIF2A*. To explore this hypothesis, we assessed methylation at multiple CpG-sites in the *HIF2A (EPAS1)* gene using the publicly available datasets containing Illumina 450k array results. The 450k methylation array is a chip-based platform for methylation analysis covering more than 485 thousand CpG-sites in the human genome. According to the manufacturer, CpG-sites were selected to cover all genes, promoters, most CpG islands, shores and shelves, and represent sites with the highest variation in methylation.

Data files of lung adenocarcinoma and breast invasive carcinoma patients (the same cohorts used for mRNA expression analysis in section 4.14) containing the methylation β-values were downloaded from the Genomic Data Commons repository (NCI). β-values for CpG sites in the *HIF2A* gene were then retrieved using RStudio. Afterwards, to locate the CpG-sites that play a role in regulating HIF2α transcription, we performed a correlation analysis between HIF2α mRNA z-scores and methylation β-values for each specific CpG site for *HIF2A* in the 450k array.

Fig. 4.35, A depicts a map of the HIF2A gene with annotated exons and the CpG island, which covers a part of the promoter, the first exon, and part of the first intron. Additionally, all the CpG-sites were mapped, at which methylation values were inversely correlated to HIF2α mRNA. In all, 22 such CpG-sites in lung cancer patients and 13 sites in breast cancer patients were identified. Among these, 10 sites were common for both tumor types (approx. 28% of the *HIF2A* CpG sites available for analysis).

Next, we set out to assess if there was any correlation between methylation β-values in the identified CpG-sites and TET1 expression. To achieve this, we stratified the patients according to the TET1 mRNA z-scores (using the same cutoffs as for gene expression analysis). β-values were then compared between TET1-high and TET1-low groups in lung and breast cancer patients. Among all the sites at which methylation was inversely correlated to HIF2α mRNA and common for both lung and breast cancer patients, three CpG-sites (indicated as CpG #1-3 on the map in **Fig. 4.35, A**) were identified where β-values were significantly lower in the TET1-high group in comparison to the TET1-low cohort

(**Fig. 4.35, B**). The observed differences were highly significant in all three cases (Mann-Whitney $p<0.001$ or $p<0.01$), even if the magnitude of the change was moderate: ~10% lower in the TET1-high group compared to the TET1-low cohort for two sites (CpG # 1-2), and ≥20% for CpG #3.

However, the 450k array provides data on methylation of only 36 CpG-sites located in the *HIF2A* gene, which constitutes ~3,1% from the 1 200 CpG sites that this gene contains.

Thus, it could be expected that a more comprehensive analysis of the CpG-sites in *HIF2A* (or at least those in the proximity to the already identified sites) would reveal the full extent to which TET1 is involved in regulating DNA methylation at this gene.

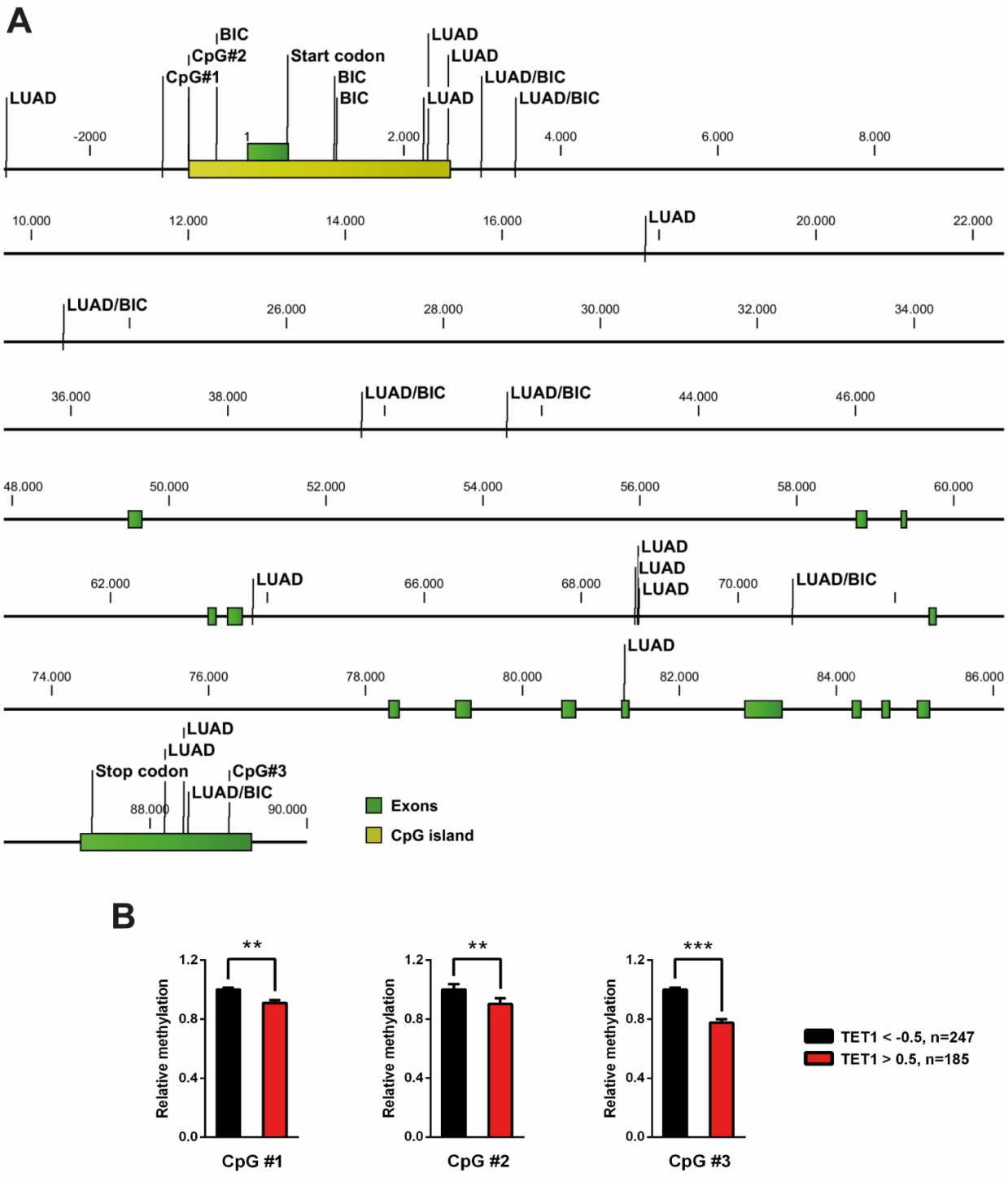

Fig. 4.35. TET1 expression is associated with decreased methylation of *HIF2A* in lung and breast cancer patients. A, Map of the human *HIF2A* gene showing the location of exons (green), start and stop codons, and the CpG island (yellow; numbers represent the distance in base pairs from the transcription start site). Using the publicly available Illumina 450k methylation array datasets for lung and breast cancer patients, CpG-sites were identified, whose methylation inversely correlated with HIF2α expression. Sites specific to either lung of breast cancer patients were annotated with “LUAD” or “BIC”, respectively, while “LUAD/BIC” and “CpG” represent the common sites. **B**, After the patients were stratified according to TET1 expression in “TET1-high” and “TET1-low” subgroups, average methylation β-values were calculated for common CpG-sites. At three such common CpG-sites (CpG #1-3) methylation was significantly reduced in the “TET1-high” group. n – number of patients, **p<0.01, ***p<0.001.

5. Discussion

Initially, anti-angiogenic therapy showed highly promising results in preclinical studies, but nowadays the application in the clinic remains limited to several tumor entities (Jayson *et al*., 2016; Ye, 2016). The reasons for this are primarily related to 1) low efficiency and 2) concerns for increased invasion and metastasis of tumors after the therapy, with both problems being potentially interconnected (van Beijnum *et al*., 2015; Bottsford-Miller *et al*., 2012). Despite the fact that several preclinical studies showed increased invasion and metastasis following *in vivo* administration of various anti-angiogenic agents in models of breast carcinoma, lung cancer, and melanoma (Depner *et al*., 2016; Ebos *et al*., 2009; Helfrich *et al*., 2010; Pàez-Ribes *et al*., 2009), the exact mechanism underlying this phenomenon remained elusive. One common thread uniting these pilot studies and numerous reviews on the topic is the hypothesis which views hypoxia as the key trigger of invasion and metastasis (Bergers and Hanahan, 2008; Crawford and Ferrara, 2009; Rapisarda and Melillo, 2009). Thus, we set out to explore this hypothesis using both *in vivo* and *in vitro* approaches.

Initially, *in vivo* experiments were performed in which nude mice transplanted with human carcinoma lines were treated with established anti-angiogenic agents. In all animal studies, treatment was initiated after the tumors reached an average volume of 100 mm^3, i.e. therapy was administered to animals with established tumors. This was done to make the models as close as possible to the clinical situations, in contrast to numerous preclinical investigations where administration of chemotherapy is initiated very early, in many cases – even on the next day following transplantation (Day *et al*., 2015).

To exclude drug-specific and off-target effects we tested three distinct and clinically approved agents from two different classes of anti-angiogenic drugs: two small-molecule RTK inhibitors – sunitinib and sorafenib, and a humanized monoclonal anti-VEGFA antibody, BVZ. In accordance with previous studies (Ebos *et al*., 2009a; Pàez-Ribes *et al*., 2009a; Welti *et al*., 2012), anti-angiogenic therapy with every one of the tested agents resulted in pronounced reduction in the primary tumor growth in comparison to the control. Remarkably, a significant difference in tumor volume between the treated and control groups was detected already after a few days of treatment with all the tested agents. This result nicely demonstrates why at the dawn of anti-angiogenic therapy so many hopes were raised for the potential of this new approach in the clinic (Folkman, 1972). Sadly, these findings

stand in contrast to the clinical trials where such reduction in tumor volume was never observed even with combination chemotherapy, let alone monotherapy with anti-angiogenic agents (Miller *et al*., 2005; Sun *et al*., 2013; Yamazaki *et al*., 2016).

Nonetheless, despite the strong inhibitory effect on the primary tumor growth, a significant increase in the number of superficial lung metastases was observed. Other sites were not systematically examined because the lung is reported to be the primary site of tumor metastasis in experimental mouse models (Gómez-Cuadrado *et al*., 2017). Indeed, in our experience, metastasis to other organs such as liver, bones, brain, etc., were observed in a very low number of cases. The increase in the number of lung metastases ranged from two to almost four fold, depending on the cell line and the tested anti-angiogenic agent. No significant correlation between the duration of treatment and number of metastases was noted. This results hints at some early factor that is driving evasive resistance after the beginning of anti-angiogenic therapy.

Interestingly, similarly to the RTK inhibitors targeting multiple receptors, enhanced metastasis was observed also in the case of BVZ. This finding is remarkable, considering that this agent was reporter to target specifically the human tumor cell-secreted VEGF (and not VEGF secreted by mouse stromal cells; Ferrara *et al*., 2005). This result suggests that tumor cells are the predominant source of VEGF for angiogenesis in this experimental model.

Collectively, having established a clinically relevant *in vivo* model with anti-angiogenic therapy that reproducibly showed enhanced metastasis, we proceeded to explore the mechanisms underlying this phenomenon.

5.1. Anti-angiogenic therapy increases the tumor hypoxic response and induces a stable EMT and metastatic phenotype in tumor cells

The concept of chemotherapy- and microenvironment-induced genetic and epigenetic alterations resulting in an altered tumor cell phenotype is not new (Brien *et al*., 2016; D'Anselmi *et al*., 2013; Pisco *et al*., 2013; Quail and Joyce, 2013). For example, nowadays it is well established that chemotherapy can lead to increased expression of the multidrug resistance proteins (e.g. MDR-1 and other ABC pumps) via clonal expansion or through transcriptional activation of these genes (van den Heuvel-Eibrink *et al*., 2001; Vaidyanathan *et al*., 2016). Previous investigations into the mechanisms of tumor resistance to anti-angiogenic therapy showed certain changes in the tumor microenvironment, like the

presence of an immunosuppressive microenvironment induced by increased expression of PD-L1 (Liu *et al*., 2015) or increased hypoxia (Depner *et al*., 2016; Ebos *et al*., 2009a). Yet, none of the studies addressed the question if these microenvironmental factors permanently altered the tumor cell phenotype or were merely causing transient effects that would revert after cessation of the therapy.

By analyzing the isolated cells from tumors of treated animals, for the first time we provide evidence that anti-angiogenic therapy is indeed inducing a new, more invasive and most importantly - stable tumor cell phenotype characterized by a shift in expression of EMT markers and regulators. One possible explanation for the acquired EMT-phenotype in SU cells is the much stronger activation of TGFβ-signaling (due to both increased expression of the TGFβ1 and the TGFβ1R). Increased activity of the TGFβ pathway might also explain the dramatic upregulation of the EMT regulator expression, especially Snail, which we could single out in an shRNA screen as the major regulator of invasion in SU cells. Besides the phenotypic alterations, SU cells also showed accompanying functional changes: they were more invasive and had a higher self-renewal capacity than CO cells.

Importantly, this complex phenotype remained stable for numerous passages after isolation (tested after 15 passages *in vitro*; data not shown), which was further confirmed *in vivo*. Curiously, primary tumor growth kinetics of the SU line was similar to CO tumors treated with sunitinib, which may be explained by the EMT shift in SU cells: it's an established fact that cells undergoing EMT show decreased proliferation (Tsai *et al*., 2012). Nonetheless, SU line produced the double amount of lung metastasis in comparison to the CO cells. Thus, we could show that anti-angiogenic therapy induces a stable EMT and metastatic phenotype in tumor cells, which is an unexpected finding, considering that the primary target of this systemic therapy are endothelial cells of the ingrowing vessels.

These results might also explain the low clinical efficacy of anti-angiogenic therapy, as in addition to the EMT-shift, increased invasion and metastasis, SU cells showed enhanced CSC characteristics and elevated resistance to cisplatin (data on chemotherapy resistance not shown as this line of evidence was not further pursued). Thus, we may conclude that anti-angiogenic therapy is inducing a multi-faceted phenotype in tumors that may simultaneously affect many of the hallmarks of cancer.

Such striking alterations in the cells raised the question of the mechanism driving this phenomenon. As this was a pharmacologically induced phenotype, we were naturally interested to know if the SU cells became more resistant to the drug, similar to the classic

studies with alkylating chemotherapeutic agents, such as cisplatin or 5-fluorouracil (De Angelis *et al*., 2006; Teicher *et al*., 1990; Yoo *et al*., 2009). Surprisingly, SU cells showed similar sensitivity to sunitinib as CO cells and had no changes in the activation of the RTKs targeted by sunitinib. Taken together, these results hint at a different mechanism of resistance than observed in the case of classic chemotherapeutics. Another confirmation that the acquired phenotype of SU cells is independent of the direct effect of the drug was obtained by analyzing the SunRES cells – true sunitinib resistant cells generated *in vitro*. In contrast to the re-isolated SU line, SunRES cells showed no increase in invasion, a decreased colony forming capacity and an unaltered EMT profile. Similar results were obtained also with the MDA-SunRES line (data not shown). These findings prompted us to speculate that the anti-angiogenic therapy-induced microenvironment may be a key trigger for the stable EMT phenotype of SU cells.

Although Stephen Paget first raised interest in the tumor microenvironment (the fertile “soil” for the metastatic “seed”) at the end of the 19th century (Paget, 1889), this area of cancer biology started to be truly explored only in the last decades. This is mainly because of the experimental challenges and the multidimensional nature of the tumor microenvironment, which combines multiple physical factors (e.g., high interstitial pressure observed in tumors, atypical dynamics of blood flow; Ferretti *et al*., 2009; Hofmann *et al*., 2006; Jain, 1988), complex physiological environment (like variable carbon dioxide and oxygen levels, acidosis; Corbet and Feron, 2017; Höckel *et al*., 1996; Riemann *et al*., 2017), and multiple cellular components (ECM composition, tumor-associated macrophages, cancer associated fibroblasts, etc.; Su *et al*., 2013; Takahashi *et al*., 2018; Tan *et al*., 2011). While some hallmarks of cancer were shown to be driven by an interaction of different components of the microenvironment (e.g. enhanced CSC phenotype in GBM cells exposed to acidosis and hypoxia; Filatova *et al*., 2016), even one factor might be enough to trigger a significant change in the behavior of tumor cells. Thus, considering the vast amount of data on the impact of hypoxia on tumor invasion and metastasis, we explored the mechanism that links evasive resistance and HIF signaling in tumor cells.

While several previous studies could show higher levels of hypoxia in tumors of animals treated with anti-angiogenic agents (for example, by pimonidazole staining; Cooke *et al*., 2012; Pàez-Ribes *et al*., 2009a), to our best knowledge no kinetic data on hypoxia were presented so far *in vivo*. To study hypoxic kinetics, we designed a novel lentivirus-based dual luciferase system that would enable us to monitor the tumor hypoxic response *in vivo*

by bioluminescence imaging. Activity of the FLuc/HIF2α ODD fusion protein served as the primary surrogate readout for hypoxia, as this synthetic fusion protein reporter undergoes similar stability regulation – hydroxylation by PHDs, ubiquitination by VHL, and proteasomal degradation – as HIFs (Danhier *et al*., 2015). It is important to stress that this system allows only for indirect measurement of tumor hypoxia as the final readout depends on the activity of multiple enzymes in the cell, excluding the possibility of distinguishing between decreased function of a particular enzyme group and actual tissue oxygen tension. Nonetheless, testing of the FLuc/ODD reporter in transient transfection of two carcinoma lines – MDA-MB-231 and A549VI – exposed to hypoxia *in vitro*, showed a strong correlation with another well-established reporter that is based on HIF transcriptional activity – the HRE reporter. Interestingly, a clear difference in the response to hypoxia was observed with the tested cell lines: the MDA-MB-231 breast carcinoma showed a significantly higher increase of the hypoxic response in comparison to the A549 lung adenocarcinoma line. These observations are in accordance with previous studies, where the MDA-MB-231 line was shown to express higher levels of HIFs and hypoxia response genes upon stimulation (DelNero *et al*., 2015; Jung *et al*., 2017). Therefore, we generated the POR reporter line using the more hypoxia-sensitive MDA-MB-231 cells and proceeded to an *in vivo* study with sunitinib anti-angiogenic therapy, where we could show using kinetic non-invasive optical imaging that anti-angiogenic therapy is indeed stimulating the hypoxic response in tumors.

Surprisingly, no significant changes in the kinetics of the tumor hypoxic response were observed in the control group. This finding is contradictory to the previous reports describing the development of hypoxia as the result of the tumor cells outgrowing the capabilities of the vasculature to supply oxygen, e.g. near the necrotic areas of a tumor (Höckel and Vaupel, 2001). A possible explanation can be found in the biology of the reporter: both luciferases (FLuc and RLuc) must be constantly synthetized in cells and are dependent on ATP. Therefore, these reporter proteins can function only in living cells with abundance of energy and substrate, which might not be the case in dying cells in necrotic areas (in one of the experiments we conducted *ex vivo* luciferase imaging of vibratome cut tumor slices, where luminescence was observed only in peripheral areas of the tumor, and not the central necrotic regions; data not shown). Thus, it is possible that the unchanging levels of luminescence in the control group represented the dynamic equilibrium reached between cell death and proliferation. Nonetheless, the developed POR dual-luciferase system proved to be a reliable tool for monitoring hypoxia *in vivo* and can be further used in tumor-drug response studies or for studying the role of hypoxia in tumor physiology.

Similar to the previous experiment with the A549VI line, analysis of the re-isolated MDA-MB-231 cell lines from the mammary fat pad tumors of sunitinib treated animals showed significantly enhanced invasion and CSC traits. Due to the lack of expression of most of the well-established EMT markers (none to very low expression of cadherins, most of the EMT regulators, etc.), we could not profile the MDA-SU cells in a similar way to the A549-SU line. Nonetheless, based on the functional results it is highly tempting to speculate that anti-angiogenic therapy can induce a more aggressive phenotype in tumor cells irrespective of the tumor type. Nevertheless, to truly generalize this result, further studies are needed, including additional testing on other tumor types (e.g. RCCs) and with several other anti-angiogenic agents.

The most striking observation in this experiment was the strongly upregulated expression of HIF2α and the hypoxia response gene CAIX in MDA-SU cells. Interestingly, expression of HIF1α was unaltered in the sunitinib lines. Despite the shared consensus sequence, HIF1 and HIF2 are known to have selective downstream target genes depending on the context and cell type (Hu *et al*., 2003). For example, it is believed that HIF1 preferentially regulates the metabolic switch to anaerobic glycolysis, activation of EMT and cell migration, while HIF2 is mainly responsible for the CSC phenotype and angiogenesis. Yet, numerous reports can be found in the literature ascribing the same function or downstream target genes either to HIF1, or HIF2. Despite the significant redundancy in gene activity regulation by HIFs, it is well established that the two alpha isoforms maintain a distinct temporal mode of action. Thus, HIF1α is believed to be the predominant isoform during acute hypoxia, being active for a relatively short time, while HIF2α activity is associated with chronic hypoxia (Koh *et al*., 2011). In light of this model, increased levels of HIF2α in sunitinib lines would reflect the long-term exposure to hypoxia created by the anti-angiogenic therapy *in vivo*, which would also fit the kinetic *in vivo* imaging data obtained with the reporter line.

Based on the obtained data we speculate about a plausible model of how anti-angiogenic therapy leads to increased metastasis: by blocking the ingrowing vessel formation anti-angiogenic therapy is modulating the tumor microenvironment that leads to an increased hypoxic response, tumor cell invasion, and enhanced CSC traits, that in turn results in increased metastasis. The principal distinction of the suggested model from the highly debated hypothesis of tumor-associated hypoxia driving EMT is that we propose a cell-intrinsic mechanism that is reprogramming the tumor cells, resulting in a permanently altered and more aggressive phenotype that remains stable even after re-introduction of the cells in

a different microenvironment, e.g. into cell culture or after cessation of the treatment. The suggested model, however, posed two questions that we further explored in the study: 1) is hypoxia sufficient to cause such a drastic change in tumor cells and 2) what is the mechanism that drives this aggressive phenotype?

5.2. Tumor cells exposed to intermittent hypoxia *in vitro* acquire a similar phenotype to that induced by anti-angiogenic therapy *in vivo*, characterized by mesenchymal traits and increased metastasis

To address the first of the above-mentioned questions, if hypoxia is sufficient to reprogram the tumor cells, we employed a novel *in vitro* model of intermittent hypoxia, whereby cells were exposed to repeated cycles of hypoxia and reoxygenation. The regimen of 48h hypoxia followed by 48h reoxygenation was chosen based on the typically observed HIF1/2α kinetics *in vitro* (48h represents the midpoint at which both isoforms are detectable in most of the tested tumor cell lines; data not shown). The main rationale behind this model was to mimic the constantly fluctuating perfusion observed in human tumors as the result of aberrant angiogenesis (Brurberg *et al*., 2007). Importantly, this cycling protocol resulted in a significant change in the cell phenotype, which shared many common traits with cells isolated from animals treated with sunitinib anti-angiogenic therapy. For example, the IH cells proved to be significantly more invasive, showed enhanced CSC characteristics, and increased expression of EMT markers and regulators. Interestingly, similarly to MDA-SU, IH cells exhibited a significantly stronger response to hypoxia, and specifically – high expression of HIF2α, but not HIF1α. In addition to the above-mentioned similarities in the phenotype between MDA-IH and MDA-SU lines, the IH line also showed a significantly activated TGFβ signaling (e.g. increased levels of phosphorylated SMADs, TGFβ ligands, and the TGFβR1). Thus, IH cells replicate not only the functional phenotype of MDA-SU cells, but also acquire an enhanced EMT profile similar to A549-SU cells. Importantly, this complex phenotype remained stable for an extensive time of passaging in culture. Moreover, to generalize the obtained results we generated IH lines using two other cell lines, A549-IH and G55-IH. These lines exhibited similar changes in their phenotype when compared to the respective control lines, as those observed in the MDA-IH line. Combined, these results provide evidence that cycling hypoxia is sufficient to permanently reprogram the cells in an analogous manner to anti-angiogenic therapy *in vivo* (**Fig. 5.1**).

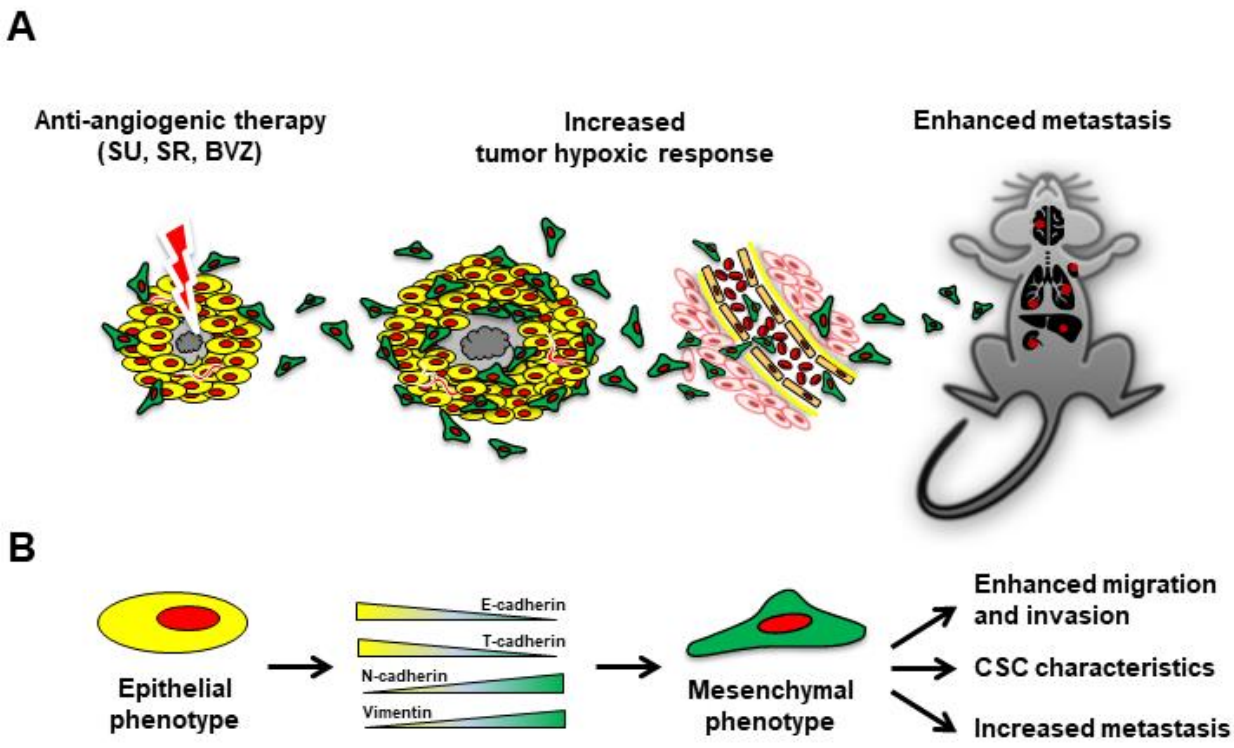

Fig. 5.1. Anti-angiogenic therapy *in vivo* and intermittent hypoxia *in vitro* drive the acquisition of a stable EMT and metastatic phenotype in tumor cells. A, Administration of anti-angiogenic therapy to mice or exposure of tumor cells to intermittent hypoxia *in vitro* increases the tumor hypoxic response, which enhances tumor cell invasion and metastatic dissemination. **B**, SU and IH cells acquire a stable EMT phenotype characterized by a typical change in expression of EMT markers and acquisition of CSC trains, increased migration and metastasis forming capacity. SU, sunitinib; SR, sorafenib; BVZ, bevacizumab.

In general, the phenomenon of intermittent hypoxia and its physiological consequences are much less studied in comparison to prolonged and uninterrupted chronic hypoxia. In the last decades, intermittent hypoxia has been primarily explored in connection with obstructive sleep apnea (Almendros *et al*., 2013; Semenza, 2013). Specifically, it was shown that *in vivo* intermittent hypoxia can stimulate metastasis formation in the lungs: recently Chen and co-authors showed that *in vitro* exposure of a syngenic mouse mammary tumor line to several cycles of hypoxia-reoxygenation (24h each for 9 days) resulted in increased metastasis to the lung in a passive metastasis model (Chen *et al*., 2018). Curiously, immediately following the cycling in hypoxia the cells showed enhanced expression of HIF1α (but not HIF2α) and enhanced expression of some hypoxia response and CSC genes. Yet, in this study the authors did not analyze the drivers of the observed phenotype. Nonetheless, Chen and co-authors managed to show that even *in vitro* exposure of cells to cycling hypoxia increases metastasis, which was previously only reported in tumor bearing animals exposed to intermittent hypoxia (Cairns *et al*., 2001; Rofstad *et al*., 2010).

Unlike the above-cited investigations, we observed that exposure of the cells to intermittent hypoxia *in vitro* led to a prominent sensitization of tumor cells to hypoxia, a strong increase in the expression of HIF2α, and acquisition of a permanently changed phenotype. The differences between our results and those of the above-mentioned study, might be explained by the significantly longer exposure to cycling hypoxia in the present study. Unfortunately, in the study by Chen *et al*., 2018 the authors did not raise the question if the cycling hypoxia induced a stable phenotype in the cells, but it is possible that a short term cycling protocol would produce a weaker and a transient phenotype. For example, in some preliminary experiments we could see that even three cycles of hypoxia (48 h)-reoxygenation (48 h) induced a more invasive phenotype in A549VI cells (data not shown).

The study by Verduzco and co-authors represents another example of an investigation addressing the role of intermittent hypoxia in tumor physiology (Verduzco *et al*., 2015). Despite the fact, that the authors propose the hypothesis that hypoxia can genetically reprogram tumor cells, the presented data must be taken with caution as the IH phenotype was analyzed on cell clones selected after a prolonged period of hypoxia cycling (from two to four months). In spite of the argument by the authors that clonal selection is beneficial in terms of identifying the clones that have adapted to the IH, multiple publications show significant variation between the selected single-cell clones inside established cell lines even without any treatments (Burrell and Swanton, 2014; Nguyen *et al*., 2016). Additionally, we observed a significant variation (up to four fold) in the expression of HIF2α between the initially selected control single-cell clones, which were selected for the KO experiment (for the current study, two clones which had HIF2α levels closest to the cell pool were selected; data not shown). Thus, as no results with polyclonal IH cells were presented by Verduzco *et al*. a selection bias cannot be excluded. Nonetheless, the authors speculate that IH could drive the acquisition of a new stable phenotype through some epigenetic alterations.

Collectively, based on the results with both SU and IH cells, it is highly tempting to speculate that at some stage of exposure to intermittent hypoxia tumor cells reach a point of no return, at which their aggressive phenotype becomes imprinted via some genetic or epigenetic changes. Yet, it remained unclear what are the principal signaling cascades responsible for the maintenance of the invasive/EMT phenotype and the nature of the genetic or epigenetic changes that stabilize such a cell state.

5.3. HIF2α and Snail are the key transcription factors regulating the EMT and metastatic phenotype of SU and IH cells

Among the most consistent changes in the cell phenotype between the generated IH and lines were increased invasion, a shift in EMT markers, and the significantly enhanced hypoxia signaling. Moreover, high expression of the two transcription factors – HIF2α and Snail – was common in IH and SU lines. Both proteins are known to be controlling the expression of multiple downstream targets contributing to cell migration and invasion, EMT transition, angiogenesis, etc. Thus, to examine the role of these two master regulators in the maintenance of the observed aggressive cell phenotype we generated knock-down (KD) cells. Confirming the role as key regulators of the IH phenotype, KD lines showed significantly reduced invasion, which was used as the primary functional readout of the IH phenotype. Interestingly, while strongly reducing invasion in the IH line, HIF2α KD did not affect the invasion rate of control cells. The significance of HIF2α in intermittent hypoxia was also tested in CRISPR KO cells, where we could show that HIF2α is required not only for the maintenance but also for acquisition of the IH phenotype. Knockdown of Snail, however, caused a significant reduction in invasion even in the CO line. These results indicate that the function of Snail is not strictly limited to the IH phenotype, but that it is a stronger and a more general regulator of invasion than HIF2α.

Despite the fact that a connection between Snail and tumor cell invasion and metastasis is well established (Kudo-Saito *et al*., 2009; Mikami *et al*., 2011; Wu *et al*., 2009b), the upstream signaling that induces the expression of this transcription factor remains poorly understood. TGFβ is one of the strongest inducers of Snail and the underlying mechanism is well known (Argast *et al*., 2011; David *et al*., 2016; Peinado *et al*., 2003). Indeed, in both IH and SU cells we observed enhanced TGFβ signaling due to increased expression of the ligands and TGFβR1.

Additionally, in several recent publications, hypoxia and TGFβ signaling were shown to synergize in promoting EMT in cancer and normal cells. For example, in the studies by Hanna *et al*., 2013 and Mingyuan *et al*., 2018 hypoxia and TGFβ signaling were shown to be interdependent: hypoxia treatment increased TGFβ1 secretion, while inhibition of the TGFβRs or silencing of SMADs resulted in decreased expression of HIFs. Investigation by Han *et al*., 2013 showed that in renal tubular cells TGFβ1 treatment decreases PHD2, resulting in enhanced stabilization of HIFs. In another recent study by Dopeso et al., 2018

the authors showed that TGFβ induced depletion of PHD3 in lung tumors, leading to enhanced EMT and metastasis mediated by HIF-dependent upregulation of TGFα.

Moreover, some investigations implicate hypoxia as a direct factor driving Snail expression. For example, it was shown that Snail is a direct target of HIF1α in hepatocellular carcinoma (Zhang *et al*., 2013), coronary endothelial cells (Xu *et al*., 2015), or of both HIF1α and HIF2α, in colorectal cancer (Santoyo-Ramos *et al*., 2014). The majority of studies connecting hypoxia to Snail point at HIF1α as the main driver of Snail transcription. Nonetheless, due to a wide overlap of the downstream targets between the HIF isoforms, it seems plausible that in our model HIF2α is enhancing TGFβ-mediated activation of Snail. Indeed, HIF2α KD decreased Snail expression in IH tumor cells. However, further experiments are required to address how precisely HIF2α drives EMT and invasion in the IH cells, for example by performing ChIP-sequencing to cover the full spectrum of the involved downstream target genes.

Beyond the functional alterations, the question remained opened as to the nature of the reprogramming process that led to the acquisition of the IH phenotype: were these genetic or epigenetic alterations, and what were the exact mechanisms behind these alterations? Since HIF2α was identified as one of the factors that is responsible not only for maintenance but also acquisition of the IH phenotype, we focused on investigating the mechanisms that activate expression of this gene.

None of the typical regulators of HIF2α stability that we tested – PHDs, FIH, HAF, pVHL – were changed in the IH line in a way that would explain the high levels of the protein. Even though post-translational regulation is believed to be the primary mechanism of controlling HIF2α expression (Huang *et al*., 1998; Tian *et al*., 2011), in some tumors *EPAS1* was shown to be regulated on the mRNA level, e.g. in neuroblastoma cells (Hamidian et al., 2015; Mohlin et al., 2013). Curiously, the only consistent change in the generated IH cells that would explain the high HIF2α was the increased mRNA. HIF1α mRNA was not found to be systematically upregulated in the IH lines which also translated into no or more modest increase of HIF1α protein levels in most IH lines.

Numerous mechanisms can contribute to increased gene expression, including transcription factor-mediated transcriptional activation, increased stability and decreased degradation of mRNA, and permissive chromatin states (Reményi *et al*., 2004; Sproul *et al*., 2005). In several previous investigations, it was shown that expression of HIF1α can be regulated at the level of transcription, specifically by DNA methylation (Pierre *et al*., 2015b; Walczak-

Drzewiecka *et al*., 2010b). Additionally, evidence exists that hypoxia can activate both DNA methylation (Lu *et al*., 2011; Thienpont *et al*., 2016a) and DNA demethylation (Liu *et al*., 2011; Mariani *et al*., 2014b; Shahrzad *et al*., 2007). Thus, we hypothesized that during intermittent hypoxia the *HIF2A* gene becomes demethylated leading to a permanently enhanced hypoxia signaling and consequently to the acquisition of the IH phenotype.

5.4. Intermittent hypoxia induces epigenetic reprogramming of tumor cells by TET1-mediated DNA demethylation, resulting in enhanced response to hypoxia and invasion

To investigate the role of epigenetic regulation of HIF2α during IH, we first explored the impact of methylation on expression of this gene. In a recent report, Nakazawa and co-authors identified HIF2α as a tumor suppressor in soft tissue sarcomas, with the gene being silenced by histone deacetylases, but not methylation (Nakazawa *et al*., 2016). Yet, no reports could be found that would show increased expression of HIF2α due to DNA demethylation in tumors.

To establish the role of methylation in HIF2α expression cells were treated with the DNA methyltransferase inhibitor azadeoxycytidine, resulting in a significant increase in HIF2α mRNA and protein levels. Nonetheless, despite the reassuring results with AzaC, we could not rule out the possibility that the observed increase in HIF2α expression was indirect and mediated by multiple upstream regulators, as AzaC affects methylation of practically all genes.

Next, we proceeded to analyze the role of DNA methylation in the IH and SU lines. No changes in global DNA methylation between the respective CO and IH or SU lines were observed when analyzed by 5MeC stainings and dot-blots (data not shown). However, staining for 5-hydroxymethylcytosine (5-hMeC), the direct product of TET catalytic activity, revealed significantly upregulated levels of 5-hMeC in IH cells derived from three different tumor lines, which confirms that IH is indeed enhancing genomic DNA demethylation. Nonetheless, we could not draw any definitive conclusions about the impact on the methylation of the *HIF2A* gene specifically, as hypoxia was reported to be able to simultaneously elicit both hypo- and hypermethylation at distinct regions. Thus, these crude methods of detecting DNA methylation may not have provided the required sensitivity and specificity. However, mRNA analysis of the two main groups of enzymes involved in regulating DNA methylation identified upregulation of TET1 in both SU and IH lines (DNMT1

was slightly downregulated in the lines, although this was not further pursued). These findings were further supported by Western blot analysis and immunofluorescent staining, where we also showed that TET1 clusters were co-localized with hypomethylated areas in cell nuclei (to our knowledge, this would be the first report showing TET1 localization in correlation to DNA methylation in a co-staining).

Analysis of shRNA cells revealed TET1 and HIF2α expression to be interconnected. This prompted us to speculate about the existence of a TET1-HIF2α regulatory loop by which cells can become sensitized to hypoxia: first, hypoxia through HIF2α increases TET1 levels leading to DNA demethylation, including demethylation of the *HIF2A* gene, which in turn leads to enhanced HIF signaling. Based on the proposed model, it becomes also possible to explain the stronger impact of HIF2α KD on TET1 expression, than TET1 KD on HIF2α expression: as opposed to the direct transcriptional activation mediated by HIF2α, DNA demethylation is generally regarded as a much slower process, requiring several cell divisions and/or base excision repair to shed the methylated marks (Kohli and Zhang, 2013).

In accordance with the KD results, we could show that overexpression of TET1 increased HIF2α mRNA levels, albeit to a smaller extent. As a possible explanation, the overexpressing cells might not have had sufficient time to undergo significant changes in methylation, or some other TET1 cofactors could have been absent that are required to initiate demethylation at specific loci. However, in line with a key role of TET1 in controlling the pro-invasive IH phenotype, TET1 overexpression significantly promoted the invasion of tumor cells.

Further evidence in support of our hypothesis was obtained by analyzing expression data from TCGA datasets of patients with breast invasive carcinoma and lung adenocarcinoma. In accordance with the obtained *in vitro* and *in vivo* data, patients with high TET1 mRNA levels had significantly increased expression of hypoxia response genes and CSC markers. Interestingly, lung adenocarcinoma patients with high TET1 had significantly higher HIF2α mRNA levels, although expression of HIF1α was unaltered. In the case of breast cancer patients, we observed an opposite situation with HIF1α being significantly upregulated in TET1-high patients, but not HIF2α. This discrepancy might be due to the tumor type specific effects of TET1 on the expression of the different HIF isoforms, which may differ between tumors and cell lines in culture.

The link between hypoxia, TET1, and DNA methylation was further strengthened by analyzing methylation with the TCGA datasets of lung and breast cancer patients. Patients

with high expression of TET1 had significantly decreased methylation levels near the first and the last exons of *HIF2A*. Additionally, some of the identified CpG sites in *HIF2A* gene showing decreased methylation in TET1-high patients were clustering within the CpG island that overlaps with the first exon and part of the *HIF2A* promoter. Based on these findings, we conclude that methylation indeed plays a significant role in regulating HIF2α expression.

The current study is not the first one to investigate the connection between hypoxia and DNA methylation. In fact, this question was already raised in two recent publications by Mariani *et al.*, 2014 and Thienpont *et al*., 2016, yielding discrepant results. Mariani and co-authors could show that hypoxia leads to a TET1-mediated increase in 5hMeC levels in hypoxia-regulated genes (Mariani *et al.*, 2014). Moreover, by using KD lines the authors linked the hypoxia-induced increase of TET1 in neuroblastoma cells to HIF1α. In contrast, in the study by Thienpont *et al* the authors show that severely decreased oxygen levels of 0.5% that are often registered in solid tumors (Höckel and Vaupel, 2001) lead to a downregulation of TET1 activity and as a result to increased DNA methylation in different tumor lines (Thienpont *et al*., 2016). In fact, Thienpont *et al*. show that the actual availability of oxygen (i.e. the hypoxic tumor microenvironment) is the main factor behind decreased TET1 activity, rather than changes in TET1 expression.

The present study does not completely fall in line with either of the investigations mentioned above, yet several important reasons might account for the discrepancies:

1) In our models, tumor cells were exposed to intermittent (cycling) hypoxia, as opposed to the acute hypoxia treatments used in both above-mentioned investigations (longest hypoxia exposure times in the papers were 72 or 96 hours). As discussed previously, there are indications that IH has drastically different effects from prolonged or chronic hypoxia, with several reports showing heightened adaptation and sensitization of cells to the low oxygen conditions (Chen *et al*., 2018; Chou *et al*., 2012; Thews *et al*., 2004; Verduzco *et al*., 2015). Thus, IH hypoxia might lead to other physiological consequences than chronic hypoxia.
2) Previous reports show sharply opposing effects of hypoxia on net genomic DNA methylation, with evidence for both hyper- and hypomethylation in different tumor lines / patient tumor samples (Hattori *et al*., 2015; Hu *et al*., 2017; Liu *et al*., 2011; McDonnell *et al*., 2016; Robinson *et al*., 2012; Shahrzad *et al*., 2007). Curiously, while the earlier studies tend to focus more on total genomic DNA methylation, in more current reports methylation at specific sites is more often analyzed. For example, in

a recent study Bhandari *et al*., 2017 could show that reversal of tumor hypoxia *in vivo* by administration of oxygen nanobubbles not only significantly delayed tumor progression, but also resulted in *BRCA1* promoter hypermethylation. Thus, in view of the previous reports on the impact of hypoxia on DNA methylation, we can assume that both DNA methylation and demethylation occur in human tumors in parallel and in a site-specific manner. Another support for this hypothesis can be found in the data from Thienpont *et al*., 2016, showing that only 10 000 sites of the approximately 290 000 analyzed (3.45%) had decreased 5hMeC levels, which would surely be not enough to explain the observed DNA hypermethylation in former studies.

3) Similar to the study by Mariani *et al.*, 2014, Thienpont *et al*., 2016 showed that in neuroblastoma lines TET1 mRNA is increased, while in some other tumor lines either nonsignificant changes or decreased TET1 levels are observed upon hypoxia treatment. Thus, based on the distribution of TET1 expression in the different tumor lines and the rather expected finding that TET1 activity is dependent upon oxygen supply (after all, TETs were shown to belong to the class of oxygen-dependent dioxygenases; Iyer *et al*., 2009), it is difficult to judge how general the conclusions are and whether a subclassification approach based on the tumor type would have been more reasonable. Moreover, in a study by Laukka et al., 2016, Michaelis constant (Km) value of TET1 for oxygen was estimated to be 30±10 μM, which is significantly lower in comparison to other 2-oxoglutarate dependent dioxygenases (e.g. Km of PHD2 for oxygen is 250 μM; Hirsilä et al., 2003). Thus, decreased TET1 activity could be expected only at extremely low oxygen concentrations (close to anoxic conditions), which are typically limited to very small areas in tumors (e.g. necrotic regions).
4) Our findings with TET1 KD lines are in line with the report by Mariani *et al.*, 2014, where shTET1 was shown to decrease the hypoxic response in neuroblastoma cells. Nonetheless, the authors implicate HIF1α as the factor driving TET1, based on higher expression of HIF1α and results from HIF1 KD experiments. In our model, however, only HIF2α was consistently upregulated in the IH and SU lines and HIF2α KD decreased TET1 expression. This might be explained by the differential roles that these isoforms play in the cellular response to chronic and intermittent hypoxia, although further studies are required to investigate the HIF1/2 switch during intermittent hypoxia.

Thus, we speculate that the single time-point measurements by Mariani *et al.*, 2014 and Thienpont *et al*., 2016 does not accurately reflect the dynamics of tumor hypoxia but focuses on one aspect of hypoxia: prolonged or chronic hypoxia. It is tempting to speculate that the phenotype we observed to be induced following intermittent hypoxia might become particularly apparent once tumor cells migrate out of the severe hypoxic area to more oxygenated tumor or tissue areas (within the metastatic cascade) which would allow the increased TET1 levels to become fully operative. Our results we obtained from analyzing the phenotypes of SU and IH lines from three different tumor lines fall the closest to the findings in neuroblastoma lines of the published reports. Perhaps, the neuroblastoma lines, shown in both studies to upregulate TET1 in response to hypoxia, have a significantly lower threshold for epigenetic reprogramming triggered by hypoxia (i.e. requiring much less cycles to obtain the same result as with IH hypoxia). Yet, the question regarding the possible trigger (or the epigenetic state) that defines the cells' capability to undergo epigenetic reprogramming remains unresolved and requires further investigation.

5.5.Summary and perspectives

In the current study we investigated the mechanisms that drive tumor invasion and metastasis following anti-angiogenic therapy. As hypothesized in previously published reviews (Azam *et al*., 2010; Bergers and Hanahan, 2008; Dey *et al*., 2015; Giuliano and Pagès, 2013; Hlushchuk *et al*., 2011; Rapisarda and Melillo, 2009), we could indeed confirm the significant role of hypoxia in the resistance to anti-angiogenesis. Moreover, we established a link between intermittent hypoxia and epigenetic reprogramming that leads to the acquisition of a new, more aggressive tumor cell phenotype.

Collectively, based on the obtained results we suggest the following model that could potentially explain the low clinical efficacy of current anti-angiogenic approaches and the plausible underlying mechanism driving tumor progression in response to the therapy (**Fig. 5.2**): blocking tumor angiogenesis increases the tumor hypoxia, resulting in HIF2α-mediated upregulation of TET1. TET1, in turn, fuels the epigenetic reprogramming of tumor cells, sensitizing them to subsequent hypoxic events through demethylation of the *HIF2A* gene. Ultimately, in the context of intermittent hypoxia, HIF2α and TET1 form a loop that operates to promote EMT, tumor cell migration, and metastasis through *SNAIL*.

The presented model of tumor response to anti-angiogenic therapy is based on extensive experimentation with three distinct tumor types – lung cancer, breast cancer and GBM. On

the one hand, converging result obtained with different tumor lines make it highly tempting to generalize the conclusions to cancer at large, yet further investigations are required to establish the validity of the suggested model for other types of cancer. For example, *in vivo* studies with TET1 KD lines and various anti-angiogenic approaches and tumor models to establish the impact on tumor hypoxic response and metastasis would significantly strengthen the conclusions. Additionally, it would be highly interesting to investigate the role of TET1 and DNA demethylation in renal cell carcinomas, which due to a loss of VHL are known to have high HIF2α expression (Razorenova *et al*., 2011; Zimmer *et al*., 2004).

In addition, while highly reproducible in functional assays and in some molecular characteristics, the SU and IH phenotypes remain insufficiently characterized on a more comprehensive genome-wide level. This could be addressed, for example, by DNA-methylation arrays, RNA-sequencing or SILAC mass spectrometry analysis, that would significantly broaden our understanding of the full complexity behind these phenotypes.

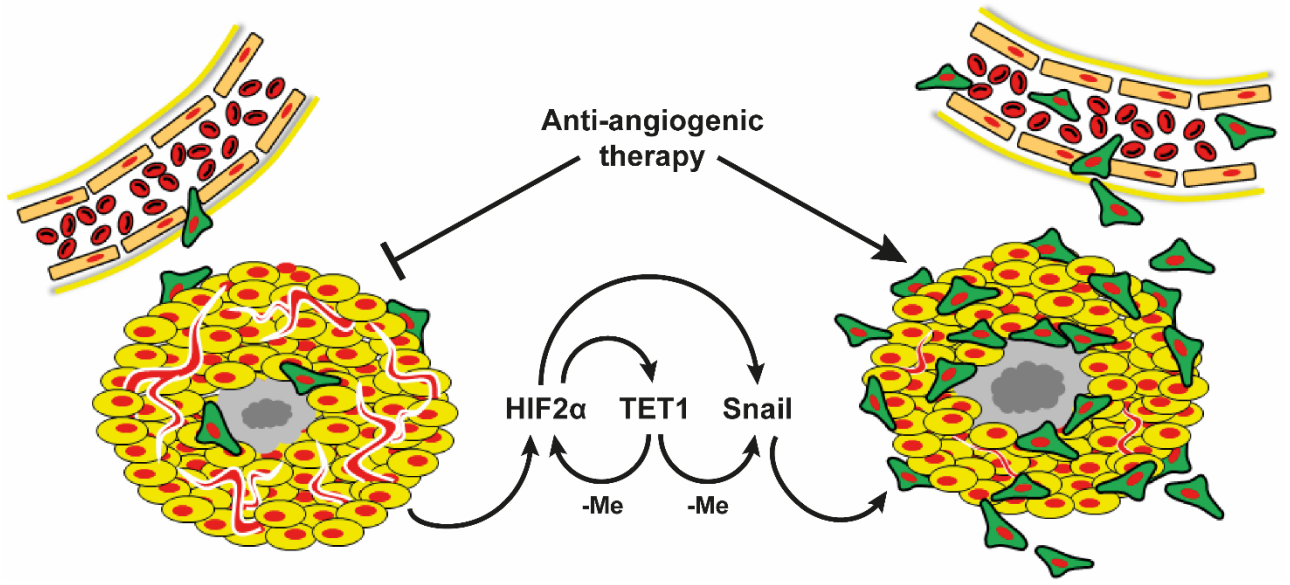

Fig. 5.2. Hypoxia-driven epigenetic reprogramming of tumor cells following anti-angiogenic therapy. Anti-angiogenic therapy-associated hypoxia drives epigenetic reprogramming of tumor cells by stimulating DNA demethylation mediated by TET1. Increased TET1 expression is induced by HIF2α in conditions of intermittent hypoxia (e.g. in regions of tumors where changes of blood perfusion take place). HIF2α and TET1 form a feed-forward loop that potentiates the tumor hypoxic response and Snail-mediated EMT and results in increased invasion and metastasis. Me, DNA methylation.

Considering the observed changes in TET1 expression and activity, high density methylation arrays or methylation sequencing would be another high-throughput method that would aid in characterizing the intermittent hypoxia- and therapy-induced epigenetic changes. In

particular, the full spectrum of CpG sites in *HIF2A* that become demethylated in IH and SU cells remain to be identified (several attempts at bisulfite sequencing were undertaken to identify these sites, but due to technical difficulties did not yield conclusive results; data not shown). Additionally, TET1 ChIP-sequencing could be used as a supplementary approach to methylation sequencing to identify the downstream target genes that become demethylated during IH hypoxia.

Notwithstanding the abovementioned limitations, the current study not only broadens our understanding of the underlying mechanisms of evasive resistance but also opens new directions to overcoming tumor resistance to anti-angiogenesis. Since we identified the TET1-HIF2α loop to be a driving force behind the highly aggressive phenotype, the question remains open whether early interference with this cycle could improve the clinical outcomes in patients receiving anti-angiogenic therapy. To move beyond a proof-of-concept exploration, it is necessary to conduct pharmacological studies with inhibitors, which would also significantly raise the clinical relevance of the findings.

Until now no specific TET1 (or TET2/3) inhibitors exist. In some recent publications the α-ketoglutarate analogue DMOG (Zhang *et al*., 2015) and NSC-311068 and NSC-370284 (both STAT3/5 inhibitors) were shown to partially reduce TET1 activity or expression, respectively. Nonetheless, none of the inhibitors is specific to the TET enzymes, and their multiple off-targets makes their clinical application highly unlikely (e.g. DMOG is known to inhibit the PHDs, thus resulting in increased, rather than the desired decrease in the hypoxic response; Siddiq *et al*., 2009). Thus, TET1 represents an important target for the development of novel inhibitors.

Unlike TET1, multiple HIF inhibitors were developed over the last decades; **Table 5.1** (Martínez-Sáez *et al*., 2017; Wallace *et al*., 2016; Wigerup *et al*., 2016). These can be subclassified according to the mechanism of action (inhibition of HIF transcription, translation, or dimerization), or by their isoform specificity (most primarily targeting HIF1 or both isoforms). Interestingly, two of the newly developed inhibitors were designed to specifically target HIF2α, with the primary intent of treating RCC patients (Cho *et al*., 2016; Wallace *et al*., 2016). Despite the very promising preclinical results (e.g. significantly reduced growth of xenograft tumors), the impact on tumor cell invasion and metastasis remains unknown.

In 2014 a clinical trial was initiated (NCT02293980, *ClinicalTrials.gov*) to test the antitumor efficacy of the PT2385 inhibitor in RCC patients as monotherapy or in combination with cytotoxic and anti-angiogenic therapy. Thus, in the nearest future the role of HIF2α in

invasive response to anti-angiogenic therapy might be explored in a clinical setting. Specifically, considering our preclinical studies, analysis of the tumor samples from these patients for TET1 expression and DNA methylation could potentially be the ultimate test of our hypothesis.

Table 5.1. Inhibitors of HIFs

Agent	Mechanism of action	Selectivity	Other known targets
Echinomycin	Inhibition of HIF1 binding to DNA	HIF1	Notch1, AKT, mTOR, PTEN
EZN-2968	Inhibition of HIF1α mRNA	HIF1	-
Aminoflavone	Inhibition of HIF1α mRNA	HIF1	-
EZN-2208	Inhibition of HIF translation	HIF1	Topoisomerase I
PX-478	Inhibition of HIF translation	HIF1	-
Anthracyclines	Inhibition of HIF1 binding to DNA	HIF1/HIF2	Topoisomerase II
Chetomin	Inhibition of HIF transcriptional activity	HIF1/HIF2	-
Bortezomib	Inhibition of HIF transcriptional activity	HIF1/HIF2	Proteasome
Digoxin	Inhibition of HIF translation	HIF1/HIF2	Na+/K+ ATPase, topoisomerase I/II
Topotecan	Inhibition of HIF translation	HIF1/HIF2	Topoisomerase I, NF-κB
CRLX101	Inhibition of HIF translation	HIF1/HIF2	Topoisomerase I
PT2385	Inhibitor of HIF2α dimerization with HIFβ	HIF2	-
PT2399	Inhibitor of HIF2α dimerization with HIFβ	HIF2	-

Modified from Martínez-Sáez *et al*., 2017 and Wigerup *et al*., 2016

Eighteen years passed since the first edition of “The hallmarks of cancer” by Hanahan and Weinberg, 2000, when angiogenesis and metastasis were recognized as two of the six principal characteristics of malignant tumors. Since then numerous investigations prompted a review of the basic features of cancer cell resulting in the addition of four new hallmarks,

namely, evasion of immune destruction, tumor-associated inflammation, altered energetics, and genome instability, in the second review (Hanahan and Weinberg, 2011). In light of the numerous reports of the last years and our own data showing the role of the tumor microenvironment and epigenetics in tumor growth, progression and metastasis, it is tempting to speculate that in the next revision of “The hallmarks” tumor hypoxia and epigenetic alterations will be recognized as the other key characteristics, warranting further exploration of these traits and development of novel treatment modalities.

6. Materials and methods

6.1. Materials

6.1.1. Antibiotics

All stock solutions were sterilized by filtration (0.22µm).

Table 6.1. Antibiotics for selection of bacterial cells

Antibiotic name	Stock solution	Working concentration
Ampicillin (Cat# A-9518, Sigma-Aldrich)	100 mg/ml in dist. H_2O	100 µg/ml
Kanamycin (Cat# T832.1, Carl Roth)	50 mg/ml in dist. H_2O	50 µg/ml

Table 6.2. Antibiotics for selection of mammalian cells

Antibiotic name	Stock solution	Working concentration
Puromycin (Cat# P9620, Sigma-Aldrich)	10 mg/ml in HEPES buffer (ready to use)	A549VI:2 µg/ml MDA-231: 1 µg/ml
Blasticidin S HCl (Cat# R210-01, Invitrogen)	6 mg/ml in PBS	6 µg/ml

6.1.2. Antibodies

Table 6.3. Primary antibodies for Western (WB) / dot (DB) blots and immunofluorescence (IF)

Antigen	Host species / Type	Dilution	Manufacturer
5-hMeC	Rabbit / polyclonal	DB: 1:1000 IF: 1:100	Active Motif, Cat# 39770
5-MeC	Mouse / monoclonal	DB: 1:1000 IF: 1:200	Millipore, Cat# MABE146
CAIX	Rabbit / polyclonal	WB: 1:2000 IF: 1:200	Novus, Cat# NB-100-417
E-cadherin	Mouse / monoclonal	WB: 1:20000	BD, Cat# 610181
FIH	Rabbit / polyclonal	WB: 1:1000	Novus, Cat# NB-100-428
HAF	Rabbit / polyclonal	WB: 1:1000	Novus, Cat# NB-P2-14836
HIF1α	Rabbit / polyclonal	WB: 1:2000	Cayman, Cat# 10006421

Antigen	Host species / Type	Dilution	Manufacturer
HIF2α	Rabbit / polyclonal	WB: 1:1000 IF: 1:200	Novus, Cat# NB-100-122
HIF2α	Rabbit / monoclonal	WB: 1:1000	Cell Signaling, Cat# 7096
N-cadherin	Mouse / monoclonal	WB: 1:1000	BD, Cat# 10920
PHD1	Rabbit / polyclonal	WB: 1:2000	Novus, Cat# NB-100-310
PHD2	Rabbit / polyclonal	WB: 1:2000	Novus, Cat# NB100-137
PHD3	Rabbit / polyclonal	WB: 1:1000	Novus, Cat# NB-100-303
pSMAD2/3	Rabbit / monoclonal	WB: 1:1000	Cell Signaling, Cat# 138D4
Slug	Rabbit / polyclonal	WB: 1:1000	Abcam, Cat# ab38551
SMAD2/3	Rabbit / polyclonal	WB: 1:1000	Cell Signaling, Cat# 3102
Snail	Rat / monoclonal	WB: 1:1000 IF: 1:200	Cell Signaling, Cat# 4719
T-cadherin	Mouse / monoclonal	WB: 1:2000	Santa Cruz, Cat# sc-166875
TET1	Rabbit / polyclonal	WB: 1:1000 IF: 1:100	GeneTex, Cat# GTX124207
TET1	Mouse / monoclonal	WB: 1:1000	GeneTex, Cat# GTX627420
Tubulin	Mouse / monoclonal	WB: 1:20000	Dianova, Cat# DLN09992
VHL	Rabbit / polyclonal	WB: 1:1000	Santa Cruz, Cat# sc-5575
Vimentin	Mouse / monoclonal	WB: 1:5000 IF: 1:500	Dako, Cat# M0725
Zeb1	Rabbit / polyclonal	WB: 1:1000	Santa Cruz, Cat# sc-25388
Zeb2	Rabbit / polyclonal	WB: 1:1000	Santa Cruz, Cat# sc-48789

Table 6.4. Secondary antibodies for Western / dot blots and immunofluorescence

Antigen	Dilution	Manufacturer
Goat anti-mouse IgG, Alexa Fluor 488	IF: 1:200	Invitrogen, Cat# A-11029
Goat anti-mouse IgG, Alexa Fluor 568	IF: 1:200	Invitrogen, Cat# A-11031
Goat anti-rabbit IgG, Alexa Fluor 568	IF: 1:200	Invitrogen, Cat# A-11036
Goat anti-rat IgG, Alexa Fluor 488	IF: 1:200	Invitrogen, Cat# A-11006
F(ab')2 rat IgG antibody peroxidase conjugated	WB: 1:2500	Rockland, Cat# 721-1333
Peroxidase-conjugated AffiniPure goat anti mouse IgG	WB: 1:2500	Dianova, Cat# 115-035-146
Peroxidase-conjugated AffiniPure goat anti rabbit IgG	WB: 1:2500	Dianova, Cat# 111-035-144

6.1.3. Plasmids

pCI-VSVG-Env: lentiviral packaging plasmid (2nd generation) that encodes the vesicular stomatitis virus glycoprotein G, used for pseudotyping of recombinant lentiviruses (Addgene, Cat# 1733)

psPAX2: lentiviral packaging plasmid (2nd generation) coding the Gag and Pol genes (Addgene, Cat# 12260)

pGIPZ-nsc: (non-silencing control; Open Biosystems, RHS4346)**:** lentiviral expression vector coding the non-targeting hairpin; hairpin sequence:

TGCTGTTGACAGTGAGCGATCTCGCTTGGGCGAGAGTAAGTAGTGAAGCCACAGATG
TACTTACTCTCGCCCAAGCGAGAGTGCCTACTGCCTCGGA

pGIPZ-shSnail: lentiviral expression vector coding the shRNA against human *SNAIL*; hairpin sequence (Open Biosystems, V2LS_199873):

TGCTGTTGACAGTGAGCGCAAAGGTACACTGGTATTTATATAGTGAAGCCACAGATGT
ATATAAATACCAGTGTACCTTTATGCCTACTGCCTCGGA

pGIPZ-shSlug: lentiviral expression vector coding the shRNA against human *SLUG*; hairpin sequence (Open Biosystems, V2LHS_153126):

TGCTGTTGACAGTGAGCGACGAAGCCAAATGACAAATAAATAGTGAAGCCACAGATG
TATTTATTTGTCATTTGGCTTCGGTGCCTACTGCCTCGGA

pGIPZ-shZeb1: lentiviral expression vector coding the shRNA against human *ZEB1*; hairpin sequence (Open Biosystems, V2LHS_116663):

TGCTGTTGACAGTGAGCGCCCTGAACCAGGCAAAGTAAATTAGTGAAGCCACAGATG
TAATTTACTTTGCCTGGTTCAGGATGCCTACTGCCTCGGA

pGIPZ-shZeb2: lentiviral expression vector coding the shRNA against human *ZEB2*; hairpin sequence (Open Biosystems, V2LHS_268826):

TGCTGTTGACAGTGAGCGCGGAGACAGATCAGTAATATAATAGTGAAGCCACAGATG
TATTATATTACTGATCTGTCTCCTTGCCTACTGCCTCGGA

pGIPZ-shHIF2α: lentiviral expression vector coding the shRNA against human *ZEB2*; hairpin sequence (Open Biosystems, V2LHS_113750):

TGCTGTTGACAGTGAGCGCCCAGACTGAATCCCTGTTCAATAGTGAAGCCACAGATG
TATTGAACAGGGATTCAGTCTGGTTGCCTACTGCCTCGGA

pGIPZ-shTET1: lentiviral expression vector coding the shRNA against human *ZEB2*; hairpin sequence (Dharmacon, V3LHS_399496):

TGCTGTTGACAGTGAGCGAGGATAGAAATAGTAGTGTTAGTGAAGCCACAGATGTAA
CACTACTATTTCTATCCTTGCCTACTGCCTCGGA

Hairpin sequence color code (as given by the manufacturer)**:** miR-30 derived sequence, mature sense, loop, mature antisense, miR-30 derived sequence.

SBE4-Luc: Firefly luciferase reporter vector with four SMAD binding elements (4SBE) in the promoter; reporter for TGFβ signaling (Addgene, Cat# 16495)

pcDNA3-9HRE-Luc: Firefly luciferase (FLuc) reporter vector with nine hypoxia response elements (9HRE) in the promoter (kindly provided by Prof. Massimiliano Mazzone, Leuven Center for Cancer Biology)

pcDNA3-ODD-Luc: Firefly luciferase reporter vector coding the FLuc-ODD (oxygen dependent degradation domain of HIF2α) fusion protein under a CMV promoter; stability of the fusion protein is regulated by oxygen availability through PHDs, rendering the FLuc activity responsive to hypoxia (kindly provided by Prof. Richard Bruick, UT Southwestern; Safran *et al*., 2006)

pRL-SV40: *Renilla* luciferase (RLuc) control reporter vector (Promega, Cat# E2231)

pENTR4: Gateway entry vector containing the attL recombination sites (Invitrogen, Cat# A10465)

pLenti6/V5-DEST: Gateway lentiviral expression vector with the CMV promoter (Invitrogen, Cat# V49610)

POR (pLenti6-CMVp-ODD/FLuc-SV40p-RLuc): dual luciferase hypoxia reporter vector containing two expression cassettes: 1) RLuc under the control of a SV40 promoter (the control reporter); 2) FLuc-ODD fusion protein under a CMV promoter (hypoxia reporter). A map of the generated plasmid is represented in **Fig. 4.12, A**. The plasmid was cloned in three steps: 1) introduction of the SV40p-RLuc-SV40pa cassette from pRL-SV40 into pEntr4 at *SmaI* / *XhoI* cloning sites using the RLuc For / Rev primers (see **Table 6.6.**); 2) cloning of the CMVp-FLuc/ODD-bGHpa cassette from pcDNA3-ODD-Luc into the pEntr4-RLuc vector at *SalI* / *KpnI* cloning sites using the ODD For / Rev primers; 3) Gateway recombination of pEntr4-CMVp-FLuc/ODD-SV40p-RLuc with pLenti6/V5-DEST

pENTR4-tGFP: Gateway entry vector coding turboGFP; generated by cloning the tGFP from pGIPZ-nsc (generated in the Giessen Institute of Neuropathology)

pLenti6-tGFP: lentiviral expression vector coding turboGFP. Generated by recombining the pENTR4-tGFP with pLenti6/V5-DEST (generated in the Giessen Institute of Neuropathology); overexpression control

pLenti6-TET1: lentiviral expression vector coding human *TET1*; generated by subcloning the TET1 ORF from FH-TET1-pEF (Addgene, Cat# 49792) into pEntr4 at *KpnI* and *XbaI* cloning sites, followed by Gateway recombination of the resulting pENTR4-TET1 with pLenti6/V5-DEST

PX459: expression vector coding the Cas9 nuclease (Addgene, Cat# 62988) without a targeting sgRNA; control vector

PX459-sgHIF2α: expression vector coding the Cas9 nuclease and a sgRNA targeting *HIF2A*; sgRNA was cloned at the *BpiI* site using HIF2α KO For / Rev primers (see **Table 6.6**).

6.1.4. Short interfering RNAs (siRNAs)

siRNA control: ON-TARGETplus Non-targeting pool siRNA (Dharmacon, Cat# D-001810)
siRNA targeting human TET1: SMART pool ON-TARGETplus siRNA to TET1 (Dharmacon, Cat# L-014635-03-0005); target sequences: 1) GAGAAUAGGUAUGGU-CAAA, 2) CUGUCUUGAUCGAGUUAUA, 3) CCUUAACUCGAGAAGAUAA, 4) GCACGC-AUGAAUUUGGAUA.

6.1.5. Bacterial cells

One Shot Stbl3 chemically competent *Escherichia coli* cells (Invitrogen, Cat# C737303) were used for plasmid propagation and all cloning purposes.

6.1.6. Human cell lines

A549: established human lung adenocarcinoma line, ATCC Cat# CCL-185

A549VI: cell line enriched for invasive clones, derived from the parental A549 line after six rounds of selection in the modified Boyden chamber: cells seeded in Matrigel were allowed to invade and cross the membrane with 8 µm pores, next the invaded cells were detached with trypsin and cultured until enough could be collected for the next round of selection (Abdelkarim *et al*., 2011; Kao *et al*., 2008)

MDA-MB-231: established human breast carcinoma line, ATCC Cat# HTB-26

MDA-Br: highly invasive variant of the parental MDA-MB-231, obtained by serial transplantations into the brain and re-isolation (Wang *et al*., 2012); kindly provided by Prof. Frank Winkler (DKFZ)

G55TL: established human glioblastoma line

A549-SU / MDA-SU: lines re-isolated from resected tumors of mice that were receiving sunitinib anti-angiogenic therapy. After re-isolation the lines were maintained *in vitro* without the presence of sunitinib in the growth medium. Respective control lines - A549-CO / MDA-CO – were re-isolated from tumors of control animals (receiving the vehicle) (generated as a part of this thesis).

A549-SunRES: line selected *in vitro* to become resistant to sunitinib by culturing cells in gradually increasing concentrations of the drug in growth medium (beginning from 0,5 μM sunitinib, followed by a 1-2 μM increase in the concentration every two weeks; selection was stopped after cells were able to grow at 10 μM sunitinib in the medium). Control cells – A549-CO – were maintained in culture at basic conditions (without sunitinib) for the duration of selection of the resistant line (generated as a part of this thesis).

A549-IH / MDA-IH / G55-IH: lines generated by exposing the parental cells to 15 cycles of hypoxia (for 48 h) and re-oxygenation (for 48 h) – the intermittent hypoxia (IH) protocol. In the end of the IH protocol cells were maintained under basic conditions, i.e. in the incubator in normoxia, at 37°C and 5% CO_2. Control lines (A549-CO / MDA-CO / G55-CO) are the respective parental cells that were maintained in culture at basic conditions for the duration of IH cycling (this was done to exclude the possibility of any artifacts coming from prolonged passaging of cells *in vitro*) (generated as a part of this thesis).

HEK293T: established cell line derived from the embryonic human kidney line HEK293 by stable transfection of the large T antigen, ATCC Cat# CRL-3216.

Table 6.5. Knockdown (KD), knockout, (KO), and overexpression (o/e) lines

(All cell lines have been generated in frames of this thesis)

Line name	Construct, manufacturer	Genetic modification (transient/stable, MOI, KD/KO/o-e)	Selection
A549-SU nsc	pGIPZ-nsc, non-silencing control (Dharmacon)	Lentiviral transduction, stable, MOI 100, control	Puromycin

Line name	Construct, manufacturer	Genetic modification (transient/stable, MOI, KD/KO/o-e)	Selection
A549-SU shSnail	pGIPZ-shSnail (Dharmacon)	Lentiviral transduction, stable, MOI 100, KD	Puromycin
A549-SU shSlug	pGIPZ-shSlug (Dharmacon)	Lentiviral transduction, stable, MOI 100, KD	Puromycin
A549-SU shZeb1	pGIPZ-shZeb1 (Dharmacon)	Lentiviral transduction, stable, MOI 100, KD	Puromycin
A549-SU shZeb2	pGIPZ-shZeb2 (Dharmacon)	Lentiviral transduction, stable, MOI 100, KD	Puromycin
MDA-POR (Clone #8)	POR	Lentiviral transduction, stable, MOI 10, o/e, single-cell clone	Blasticidin
MDA-CO nsc	pGIPZ-nsc, non-silencing control (Dharmacon)	Lentiviral transduction, stable, MOI 100, control	Puromycin
MDA-CO shHIF2α	pGIPZ-shHIF2α (Dharmacon)	Lentiviral transduction, stable, MOI 100, KD	Puromycin
MDA-IH nsc	pGIPZ-nsc, non-silencing control (Dharmacon)	Lentiviral transduction, stable, MOI 100, control	Puromycin
MDA-IH shHIF2α	pGIPZ-shHIF2α (Dharmacon)	Lentiviral transduction, stable, MOI 100, KD	Puromycin
MDA-CO nsc	pGIPZ-nsc, non-silencing control (Dharmacon)	Lentiviral transduction, stable, MOI 100, control	Puromycin
MDA-CO shSnail	pGIPZ-shSnail (Dharmacon)	Lentiviral transduction, stable, MOI 100, KD	Puromycin
MDA-IH nsc	pGIPZ-nsc, non-silencing control (Dharmacon)	Lentiviral transduction, stable, MOI 100, control	Puromycin
MDA-IH shSnail	pGIPZ-shSnail (Dharmacon)	Lentiviral transduction, stable, MOI 100, KD	Puromycin
MDA-MB-231 CRISPR/Cas9 control pool	PX459, empty (Addgene)	Transient transfection of Cas9, control cell pool	Puromycin
MDA-MB-231 CRISPR/Cas9 control Clone #1	PX459, empty (Addgene)	Transient transfection of Cas9, control, single-cell clone	Puromycin
MDA-MB-231 CRISPR/Cas9 control Clone #2	PX459, empty (Addgene)	Transient transfection of Cas9, control, single-cell clone	Puromycin
MDA-MB-231 CRISPR/Cas9 HIF2α KO Clone #1	PX459-sgHIF2α	Transient transfection of Cas9 and sgRNA, stable KO, single-cell clone	Puromycin

Line name	Construct, manufacturer	Genetic modification (transient/stable, MOI, KD/KO/o-e)	Selection
MDA-MB-231 CRISPR/Cas9 HIF2α KO Clone #8	PX459-sgHIF2α	Transient transfection of Cas9 and sgRNA, stable KO, single-cell clone	Puromycin
MDA-MB-231 nsc	pGIPZ-nsc, non-silencing control (Dharmacon)	Lentiviral transduction, stable, MOI 100, control	Puromycin
MDA-MB-231 shTET1	pGIPZ-shTET1 (Dharmacon)	Lentiviral transduction, stable, MOI 100, KD	Puromycin
MDA-MB-231 shHIF2α	pGIPZ-shHIF2α (Dharmacon)	Lentiviral transduction, stable, MOI 100, KD	Puromycin
MDA-MB-231 GFP	pLenti6-tGFP	Lentiviral transduction, stable, MOI 100, control	Blasticidin
MDA-MB-231 TET1	pLenti6-TET1	Lentiviral transduction, stable, MOI 100, o/e	Blasticidin
MDA-MB-231 siScrb	ON-TERGETplus Non-targeting pool siRNA (D-001810-10-05; Dharmacon)	Transient transfection of siRNA, control	-
MDA-MB-231 siTET1	SMART pool ON-TARGETplus siRNA to TET1 (L-014635-03-0005; Dharmacon)	Transient transfection of siRNA, KD	-

6.1.7. Primers

Table 6.6. Cloning and sequencing primers

Primer name	Sequence	Cloning site	Application
pENTR4 For	GACGGATGGCCTTTTTGCGTTTCTAC	-	Sequencing of inserts in pEntr4
CMV For	CGCAAATGGGCGGTAGGCGTG	-	Sequencing of inserts in pLenti6
ODD For	GTATGGTCGACTCAAGCTTGGCATTCCGGTACTGT	SalI	Cloning of the POR plasmid
ODD Rev	AATAAGGTACCGAGCCATAGAGCCCACCGCATCC	KpnI	
RLuc For	TAATACCCGGGATGCGCAGCACCATGGCCTGAAATA	SmaI	
RLuc Rev	GGGCGCTCGAGGTTACCACATTTGTAGAGGTTTTACTTG	XhoI	
HIF2α KO For	CACCGATTGCCAGTCGCATGATGG	-	Cloning of HIF2α sgRNA into PX459
HIF2α KO Rev	AAACCCATCATGCGACTGGCAATC	-	

Table 6.7. qPCR primers

Gene	Forward / reverse sequence	Gene function / Group
ECAD	For: CGAGAGCTACACGTTCACGG Rev: GGGTGTCGAGGGAAAAATAGG	EMT and invasion markers
TCAD	For: AGCGATGGCGGCTTAGTTG Rev: CCCCGACAATCACGAGTTCTG	
NCAD	For: GGTGGAGGAGAAGAAGACCAG Rev: GGCATCAGGCTCCACAGT	
VIM	For: GAGGAGATGCTTCAGAGAGAGG Rev: AGATTCCACTTTGCGTTCAAG	
MMP2	For: TACAGGATCATTGGCTACACACC Rev: GGTCACATCGCTCCAGACT	
MMP9	For: CAGTCCACCCTTGTGCTCTT Rev: ATCTCTGCCACCCGAGTGTA	
SNAIL	For: CTTCCAGCAGCCCTACGAC Rev: CGGTGGGGTTGAGGATCT	EMT regulators
SLUG	For: CGGACCCACACATTACCTTG Rev: CAAATGCTCTGTTGCAGTGAG	
ZEB1	For: CCTGAAGAGGACCAGAGG Rev: TATCACAATATGGACAGGTGAG	
ZEB2	For: AACAAGCCAATCCCAGGAG Rev: ACCGTCATCCTCAGCAATATG	EMT regulators
TWIST1	For: CTACGCCTTCTCGGTCTGG Rev: CTCCTTCTCTGGAAACAATGAC	
TGFB1	For: CACCGCCGAGCCCTGGAC Rev: CCCGAGGCAGAAGTTGGCATGG	TGFβ ligands and receptors
TGFB2	For: AGCGTGCTTTGGATGCGGC Rev: AGAAGTTGGCATTGTACCCTTTGGG	
TGFB3	For: TGACACTGTGCGTGAGTGGCTG Rev: TTGTCCACGCCTTTGAATTTGATTTCC	
TGFBR1	For: ACGGCGTTACAGTGTTTCTG Rev: GCACATACAAACGGCCTATCTC	
TGFBR2	For: GTAGCTCTGATGAGTGCAATGAC Rev: CAGATATGGCAACTCCCAGTG	
MAML3	For: CAGCAGGTCAATCAGTTTCAAG Rev: GGTTCTGGGAGGGTCCTATTC	Stem cell markers
NANOG	For: GCAGAAGGCCTCAGCACCTA Rev: AGGTTCCCAGTCGGGTTCA	
CD133	For: TTGACCGACTGAGACCCAAC Rev: AGGTGCTGTTCATGTTCTCCAAC	
CD44	For: TGGCACCCGCTATGTCCAG Rev: GTAGCAGGGATTCTGTCTG	
SOX2	For: GCCGGCGGCAACCAGAAAAACAG Rev: CCGCCGGGGCCGGTATTTAT	

Gene	Forward / reverse sequence	Gene function / Group
OCT4	For: GCTCGAGAAGGATGTGGTCC Rev: CGTTGTGCATAGTCGCTGCT	
HIF1A	For: CCATTAGAAAGCAGTTCCGC Rev: TGGGTAGGAGATGGAGATGC	Hypoxia inducible factors and hypoxia responsive genes
HIF2A	For: CGAACACACAAGCTCCTCTC Rev: GTCACCACGGCAATGAAAC	
HIF1B	For: CGCCGCTTAATAGCCCTCTG Rev: CTGCCAACCCCGAAATGACAT	
CAIX	For: AAGAAGAGGGCTCCCTGAAG Rev: TAGCGCCAATGACTCTGGTC	
VEGFA	For: AGCCTTGCCTTGCTGCTCTA Rev: GTGCTGGCCTTGGTGAGG	
GLUT1	For: GATTGGCTCCTTCTCTGTGG Rev: CAGGATCAGCATCTCAAAGG	
VHL	For: GGGAACGGGGTGGGTTTAG Rev: GCTCGCGTGAGTTCACAGA	Regulators of HIF stability and activity
FIH	For: TTTAAGCCGAGGTCCAACAG Rev: ACAATCTTCCTGCCCACAG	
HAF	For: CCAGCTCCAAAACTAGCTCAG Rev: AAGGCCATAGGGTTGATGACA	
PHD1	For: CGCTGCATCACCTGTATCTATTAC Rev: GTCAAAGAGTGGCTCGATGTTG	
PHD2	For: AATGGAACGGGTTATGTACGTC Rev: ATACCTCCACTTACCTTGGCATC	Regulators of HIF stability and activity
PHD3	For: CTACGTCAAGGAGAGGTCTAAGG Rev: GATAGTAGATGCAGGTGATGCAG	
TET1	For: CAGAACCTAAACCACCCGTG Rev: TGCTTCGTAGCGCCATTGTAA	Enzymes regulating DNA methylation
TET2	For: GATAGAACCAACCATGTTGAGGG Rev: TGGAGCTTTGTAGCCAGAGGT	
TET3	For: GCCGGTCAATGGTGCTAGAG Rev: CGGTTGAAGGTTTCATAGAGCC	
DNMT1	For: AGAACGGTGCTCATGCTTACA Rev: CTCTACGGGCTTCACTTCTTG	
DNMT3B	For: CCCAGCTCTTACCTTACCATCG Rev: GGTCCCCTATTCCAAACTCCT	
HPRT	For: TATGGCGACCCGCAGCCC Rev: GCAAGACGTTCAGTCCTGTCCAT	Housekeeping gene

6.1.8. Anti-angiogenic drugs and other agents

Table 6.8. Drugs and other reagents

Reagent	Solvent	Manufacturer	Application, concentration
Sunitinib malate	0.5 M citrate buffer, pH 3.5 / DMSO	LC Laboratories, Cat# S-8803	In vivo: 60 mg/kg In vitro: 10 μM
Sorafenib	0.5 M citrate buffer, pH 3,5	LC Laboratories, Cat# S-8599	In vivo: 60 mg/kg
Gamunex	Saline	Grifols	In vivo: 20 mg/kg
Bevacizumab (Avastin)	Saline	Roche	In vivo: 20 mg/kg
TGFβ1 (transforming growth factor β1)	10 mM Tris, pH 7.6; 0.1% BSA	PeproTech, Cat# 100-21C	In vitro: 5 ng/ml
D-Luciferin potassium salt	DPBS	Regis Tech, Cat# RE-1-360222-200	In vivo: 150 mg/kg
Coelentherazine H	Ready to use	PerkinElmer, Cat# 760506	In vivo: 0.5 mg/kg
AzaC (5-Aza-2-Deoxycytidine)	PBS	Sigma-Aldrich, Cat# A3656	In vitro: 10 μM

6.1.9. DNA and protein ladders

1 Kb Plus DNA ladder was used to estimate the size of DNA fragments in agarose gels (Thermo Fisher, Cat# 10787018).

PageRuler Prestained Protein ladder (Thermo Fisher, Cat# 26616) was used for estimating low molecular weight proteins, while Spectra Multicolor High Range Protein ladder (Thermo Fisher, Cat# 26625) – for proteins with high molecular weight.

6.1.10. Buffers, media, and other supplies

6.1.10.1. Western blot / dot blot / agarose gel electrophoresis / IF / luciferase assay

Laemmli lysis buffer: 10 mM Tris-HCl (pH 7,5), 2% SDS, 2 mM EGTA, 20 mM NaF, in deionized water (dH_2O)

Sample buffer: 4% SDS, 160 mM Tris (pH 7,5), 20% glycerol, in dH_2O; stored aliquoted at -20°C

TEMED (tetramethylenediamine): Applichem, Cat# A1148

Ammonium persulfate (APS): 1% APS (Carl Roth, Cat# 9592.1) dissolved in dH_2O; aliquoted solution stored at -20°C

Acrylamide: Rotiphorese NF-Acrylamide/Bis-solution (30%), Carl Roth, Cat# A124.2

Upper buffer: 0.5 M Tris base, 0.4% SDS, in dH_2O; pH adjusted to 6.8

Lower buffer: 1.5 M Tris base, 0.4% SDS, in dH_2O; pH adjusted to 8.8

8% PAGE separating gel: 27% of acrylamide (30%), 26% of the lower buffer, in dH_2O, 0.1% APS, 1:1000 TEMED

12% PAGE separating gel: 40% of acrylamide (30%), 26% lower buffer, in dH_2O, 1:100 0.1% APS, 1:1000 TEMED

PAGE Stacking gel: 6.5% of acrylamide (30%), 13% of the upper buffer, in dH_2O, 1:100 0.1% APS, 1:1000 TEMED

10xRunning buffer: 250 mM Tris base, 2 M glycine, 1% SDS, in dH_2O

10xTransfer buffer: 200 mM Tris base, 1.5 M glycine, 1% SDS, in dH_2O

Washing buffer: 1xPBS, 0.1% Tween 20, in dH_2O

Blocking buffer: 5% milk powder in 1xPBS/Tween 20 (0.1%)

20xPBS: 140 mM NaCl, 2.7 mM KCl, 10 mM Na_2HPO_4, 1.8 mM KH_2PO_4, in dH_2O; pH adjusted to 7.4

PVDF membrane: PVDF membrane 0.45 µm, Thermo Fisher, Cat# 88518

Nitrocellulose membrane: Hybond-ECL nitrocellulose membrane, Amersham, Cat# RPN 2020D

50xTAE (Tris-acetate-EDTA) buffer: 2 M Tris base, 1 M glacial acetic acid, 50 mM EDTA (pH 8.0)

Agarose gel: 0.8% agarose (Carl Roth, Cat# 2326.2) in 1xTAE buffer

Sorensen's glycine buffer: 0.1 M glycine, 0.1 M NaCl; pH adjusted to 10.5

IF blocking solution: 4% normal goat serum, 2% BSA, in DMEM; final solution was filtered sterile, aliquoted, and stored at -20°C

Luciferase reagent A (*in vitro* FLuc substrate): glycylglycine (25 mM), KH_2PO_4 (15 mM), EGTA (4 mM), ATP (2 mM), dithiothreitol (1 mM), $MgSO_4$ (15 mM), coenzyme A (0,1 M), beetle D-luciferin (75 µM, Promega, Cat# E1602)

Luciferase reagent B (*in vitro* RLuc substrate): NaCl (1.1 M), Na_2-EDTA (2.2 mM), KH_2PO_4 (0.22 M), BSA (0.44 mg/ml), NaN_3 (1.3 mM), coelenterazine h (1.5 µM, Promega, S2001)

All chemicals, if not mentioned otherwise, were purchased from Sigma-Aldrich, Carl Roth, or Applichem.

6.1.10.2. Bacterial culture

LB medium: 20 g of LB powder (Carl Roth, Cat# X964.1) were dissolved in 1 l of dH_2O and autoclaved at 120°C for 15 min. Autoclaved medium was stored at 4°C. Antibiotics (kanamycin or ampicillin) were added freshly before inoculation of bacteria.

LB agar: 32 g of ready to use LB agar powder (Carl Roth, Cat# X965.2) were dissolved in 1 l dH_2O, then the solution was immediately autoclaved at 120°C for 15 min. After autoclaving, when the solution cooled down to approx. 40°C, appropriate antibiotics were added and the ready LB agar poured into 10 cm bacterial Petri dishes. Ready plates were stored at 4°C.

6.1.10.3. Cell culture / Tissue dissociation

1xPBS: Gibco, Cat# 10010-056

Trypsin-EDTA (0.05%), phenol red: Gibco, Cat# 25300054

DMEM (Dulbecco's modified Eagle medium), high glucose (4.5 g/l D-glucose), with GlutaMAX, and sodium pyruvate: Gibco, Cat# 31966-021

FBS (fetal bovine serum): Merck, Cat# S0115

Complete growth medium for culturing cells: DMEM with 10% FBS; in case of re-isolated lines – 1:100 of penicillin / streptomycin (Pen/Strep, Gibco, Cat# 15140-122)

Cryoprotective medium: 50% FBS, 45% DMEM, and 5% DMSO (Carl Roth, Cat #A994.1), filtered sterile and stored at 4°C

Matrigel: a gelatinous protein mixture derived from Engelbreth-Holm-Swarm (EHS) mouse sarcoma cells which closely resembles a typical composition of tissue ECM; BD, Cat# 356234

Crystal violet solution: 0.5% crystal violet (Fluka, Cat# 61135), 20% methanol, in dist. H_2O; final solution was filtered through a 0.45 µm PDVF filter and stored at +4°C

$CaCl_2$, 2.5 M: salt dissolved in dist. H_2O, sterilized by filtration through a 0.22 µm filter, and stored at 4°C

Chloroquine, 10 mM: dissolved in dH_2O, filtered sterile, and stored at 4°C

Polybrene (hexadimethrine bromide): dissolved in dH_2O at the concentration of 6 mg/ml, filtered sterile, and stored at -20°C

2xHBS (Hank's buffered saline): 281 mM $NaCl_2$, 100 mM HEPES (Gibco, Cat# 1563-056), 1,5 mM Na_2HPO_4, dissolved in dH_2O; pH adjusted to 7.06. Final solution was sterile filtered and stored aliquoted at -20°C

Papain: stock solution was prepared by dissolving 100mg of papain (Worthington, Cat# LS004194) in 5 ml EBSS (Invitrogen, Cat# 14155.048)

DNase I solution: 100 mg DNase I (Sigma-Aldrich, Cat# DN25-100mg) dissolved in 5 ml of sterile 0.15 M NaCl, stored aliquoted at -20°C

Solution I, for re-isolation of cells from tumor tissue: for 500 ml of Solution I – 50 ml HBSS (Invitrogen, Cat# 14180-046), 9 ml of D-glucose (300 mg/ml), 7.5 ml of 1 M HEPES; pH adjusted to 7.5; volume adjusted to 500 ml with dH_2O. Ready solution was stored aliquoted at -20°C. Before immediate use, 200 µl of papain and 50 µl of DNase I solutions were added, following a 30 min activation period at 37°C

Solution II, for re-isolation of cells from tumor tissue: for 100 ml of Solution II – 70 mg of collagenase I (Worthington, Cat# LS004194), 70 mg of hyaluronidase (Sigma-Aldrich, Cat# H3884-100mg), 100 mg of trypsin (Sigma-Aldrich, Cat# T9935-100mg), volume adjusted to 100 ml by dH_2O; aliquoted solution was stored at -20°C. Before immediate use, 50 µl of DNase I solution were added

6.1.10.4. Animal experiments / Hematoxylin/eosin histology

Experimental animals: immunocompromised mice were used in all animal studies to allow xenotransplantation of human tumor lines (TVA Nr: F42/16). Female 6-8-week-old NMRI-*Foxn1*$^{nu/nu}$ mice were purchased from Janvier and kept in the animal facility of the Department of Molecular and Cellular Neurobiology (BMLS, Goethe University Frankfurt)

Anesthesia: 100 mg/kg ketamine (Bela-Pharm, Cat# FS1670041); 10 mg/kg xylazine (CEVA Tiergesundheit); dissolved in 0.9% NaCl solution; final solution was prepared freshly before each application

PFA (paraformaldehyde) for tissue fixation: 4% PFA dissolved in 1xPBS

Mayer's hematoxylin solution: Applichem, Cat# A4840-500

Eosin solution: eosin Y solution, alcohol-based, Sigma-Aldrich, Cat# HT110116

0.5 M PB buffer: 115 mM NaH_2PO_4, 385 mM Na_2PO_4; pH adjusted to 7.4; stored at room temperature (RT)

Cryoprotection solution (CPS): for 1 l of the final CPS – 500 ml of 0.1 M PB buffer, 250 ml of ethylene glycol (Carl Roth, Cat# 9516.1), and 250 ml of glycerol (Carl Roth, Cat# 3783.1); final solution stored at RT

30% sucrose in 0.1 M PB: for 1 L of the final solution – 200 ml of 0.5 M PB buffer, 300 g of D-sucrose (Fluka, Cat# 84099), volume adjusted to 1 l by dH_2O; after preparation the final solution was filtered sterile and stored at 4°C

6.2. Methods

6.2.1. Cloning: PCR, DNA electrophoresis, isolation of DNA from agarose gels

Phusion high-fidelity DNA polymerase (2 U/µl, Thermo Fisher, Cat# F534L) was used to amplify the fragments of interest. The primers are listed in **Table 6.6**. Composition of a reaction mixture for 20 µl was as following: 0.2 µl Phusion polymerase, 4 µl 5xPhusion green GC buffer, 0.4 µl dNTP mix (10 mM each, NEB, Cat# N0447S), 0.6 µl DMSO, 1 µl For primer (10 µM), and 1 µl Rev primer (10 µM), in DEPC-treated water. Standard cycling program is presented in **Table 6.9** (Tm is the lower melting temperature for the primer in a corresponding primer pair).

Table 6.9. Standard amplification program

Step	Time	Temperature, °C	Nr of cycles
Initial denaturation	5 min	98	1x
Denaturation	30 sec	98	40x
Annealing	30 sec	Tm+3	
Extension	1 min/kB	72	
Final extension	10 min	72	1x

PCR products and restriction fragments were resolved by agarose gel electrophoresis (0.8% agarose in 1xTAE buffer; 8 V/cm over 30 min). Ethidium bromide (Carl Roth, Cat# 2218.1) was used to visualize DNA with a transilluminator (UV-B, 254 nm).

Isolation of DNA fragments from agarose gels was done by using the Qiaquick Gel Extraction Kit (Qiagen, Cat# 28704), following the manufacturer's instructions.

All restriction and modifying (polynucleotide kinase, alkaline phosphatase) enzymes, and the T4 ligase were purchased from Thermo Fisher.

6.2.2. Bacterial transformation, plasmid isolation, and sequencing

Transformation of bacteria: chemically competent Stbl3 *Escherichia coli* cells were incubated with the plasmid/ligation mix on ice for 30 min, followed by a 45 sec heat shock at 42°C and 2 min incubation on ice. Glucose rich SOC medium (Invitrogen, Cat# 1554403) was then added to bacteria, followed by a 30 min incubation in a shaker at 37°C. In the end, transformed bacteria were seeded onto LB agar dishes containing the appropriate antibiotic.

Plasmid isolation: PureLink Miniprep Kit (Invitrogen, Cat# K2100-10) was used to isolate small quantities of plasmid DNA, while for isolation of large quantities we used the HiPure Plasmid Maxiprep Kit (Invitrogen, Cat# K2100-07). All isolation steps were done according to the manufacturer's instructions. DNA concentration was estimated using the NanoDrop spectrophotometer (Thermo Fisher) at 260 nm.

Sequencing: all sequencing reactions were performed by SeqLab (Göttingen, www.microsynth.seqlab.de).

6.2.3. Cell culture

6.2.3.1. Maintenance of lines and passaging

All cell lines were cultured in DMEM supplemented with 10% FBS at 37°C, 5% CO_2 and normoxic conditions (21% O_2) in tissue culture dishes, unless specified otherwise. Lines were maintained in culture no longer than one month after thawing to avoid artifacts related to passaging (after a month in culture fresh aliquots from early passages were brought into culture, if necessary).

In general, cells were subcultured upon reaching 80% confluency. This was achieved by washing the cells with 1xPBS and further digestion with 0.05% trypsin/EDTA solution for 5-8 min. After cells detached from the dish, trypsin was inactivated by addition of full medium (containing FBS) and the cell suspension was centrifuged at 1000 rpm. Next, the supernatant was discarded, cells resuspended in fresh medium and subcultured at ratios ranging between 1:20 and 1:5. For all experiments, a fixed number of cells was seeded at the beginning (400 thousand cells / 10 cm Petri dish for A549 lines, and 300 thousand / dish – for MDA-MB-231 or G55TL). Confluency was never higher than 80% at the moment of lysis.

6.2.3.2. Cryopreservation and thawing of cells

Cryopreservation: cells of the earliest possible passage were taken for cryopreservation. Upon reaching 70-80% confluence in 10 cm Petri dishes, cells were trypsinized, centrifuged at 1000 rpm for 3 min, resuspended in cryomedium (DMEM with 5% DMSO and 50% FBS), and aliquoted in cryovials (1 ml of cell suspension per vial, containing approx. half the cells from one Petri dish). Vials were then gradually cooled in cryoboxes at -80°C and the next day transferred to liquid nitrogen for long term storage.

Thawing: cryopreserved cells were rapidly thawed in a water bath at 37°C, after which cell suspension was transferred to a 15 ml tube with fresh growth medium and centrifuged to remove DMSO. After centrifugation, the supernatant was removed, and cells were resuspended in fresh complete medium and plated in tissue culture dishes. Next day medium was changed to fresh complete medium (in case of transduced cells – with selection antibiotics).

6.2.3.3. Quantification of cell number

Cell number was determined using the Casy automatic cell counter (TT model, Roche, Cat# 5651697). The counting principle is based on the current exclusion method: cells that are passing through a pore of a defined size are generating a resistance signal which is registered by the counter. This approach also allows assessing the vital state of a cell as dead cells display a much weaker resistance due to a disrupted cell membrane.

For counting, 100 µl of cell suspension were diluted in 10 ml of Casy ton (isotonic measurement buffer, Roche, Cat# 5651808) and analyzed with the Casy counter following the manufacturer's recommendations.

6.2.3.4. Isolation of cells from tumor tissue

The protocol of isolating cells by enzymatic digestion of tumor tissue is based on Seidel *et al*., 2015. The whole procedure was carried out in aseptic condition in a laminar cell culture hood. In brief, resected mouse tumors were minced in Petri dishes into pieces smaller than 1 mm in diameter using sterile single-edged razor blades. Minced tissue was then transferred to a 15 ml tube, resuspended in 5 ml of activated Solution I (see section 6.1.10.3), and incubated at 37°C for 30 min (described reagent quantities are sufficient for digestion of one resected tumor of up to approx. 1.5 g). During the incubation time the suspension was frequently triturated by vigorous pipetting to ensure a more efficient digestion. At the end of the incubation, the tube containing the partially digested tumor tissue was centrifuged at 1000 rpm for 4 min, after which the supernatant was discarded. Then, the pellet was resuspended in 5 ml of activated Solution II and incubated for further 30 min at 37°C with frequent trituration. Next, the suspension was centrifuged, and supernatant again discarded.

To remove any remaining red blood cells, the cell pellet was resuspended in 1 ml of the Red blood cell lysis buffer (Roche, Cat# 11814389001) and incubated for 15 min at RT. The suspension was then diluted with DMEM 10% FBS to a volume of 10 ml and filtered through a 70 µm mesh cell strainer (BD, Cat# 352350). In the end, cells were washed twice with fresh medium and plated onto 10 cm tissue culture Petri dishes.

Re-isolated lines were propagated until a few vials could be frozen at the earliest passage possible.

6.2.4. Transfection of cells with plasmids and siRNA

6.2.4.1. Transient transfection of cells with plasmids

Transfection of A549 and MDA-MB-231 cells was performed using the Lipofectamine 2000 reagent (Thermo Fisher, Cat# 11668019). For this, cells were seeded at a density that would ensure a 50-60% confluence on the following day. Then, the following mixture was prepared for transfection of cells in 1 well of a 6-well tissue plate (when necessary, the numbers were scaled appropriately):

Mix 1 – 10 µl of Lipofectamine 2000 reagent diluted in 150 µl of Opti-MEM (reduced serum medium, Thermo Fisher, Cat# 11058021);

Mix 2 – total of 5 µg of DNA were diluted in 150 µl of Opti-MEM.

The final transfection mix was prepared by combining mixtures 1 and 2, followed by a 5 min incubation at RT. Next, the medium of cells to be transfected was changed to fresh complete medium and the final transfection mixture was added. After 5 h of incubation of cells with the transfection mix, the medium was once again changed to fresh culture medium.

6.2.4.2. Transfection of cells with siRNA

Non-targeting control siRNA and si*TET1* were purchased from Dharmacon (see Section 6.1.6). Lyophilized siRNA pools were resuspended in 1x siRNA buffer (Dharmacon, Cat# B-002000-UB-100), aliquoted, and stored frozen at -80°C. Transfection of cells with siRNAs was done using the Oligofectamine reagent (Thermo Fisher, Cat# 12252-011). Cells were transfected, as with plasmids, at 50-60% confluence. Transfection mixture was prepared in three steps (per well of a 6-well plate):

Mixture 1 – 8.5 µl Oligofectamine diluted in 31.5 µl Opti-MEM;

Mixture 2 – 10 µl of reconstituted siRNAs (20 pmol/µl) diluted in 150 µl Opti-MEM.

The final transfection mix was produced by combining mixtures 1 and 2, followed by an incubation period of 20 min at RT. Next, medium of cells was changed to fresh full medium and the final transfection mixture added. Next day the medium was once again changed to fresh culture medium.

6.2.5. Incubation of cells in hypoxic conditions

For each experiment, cells were counted and seeded at specified density (see section 6.4.1). Before exposing the cells to hypoxia, the medium was changed to fresh complete growth medium. Hypoxic incubation of cells was done using a hypoxic chamber (Coy Laboratory, USA), in which cells were incubated at 37°C in the atmosphere of 5% CO_2 and 1% O_2. Cells cultured in the incubator at 21% O_2 and 5% CO_2 served as the corresponding control.

6.2.6. Colony formation assay

To assess stem cell properties of cells, specifically their self-renewal capacity, we performed a colony formation assay. For this purpose, cells were seeded at very low density (300 to 500 cells per well) into a 6-well plate. Colonies were let to grow for 1.5-2 weeks, after which they were stained with crystal violet: crystal violet solution diluted in DMEM in the ratio 1:10, 1 ml per well, staining for 15 min at RT. After incubation, dishes were washed twice with PBS, and the stained colonies counted. Six wells were seeded per condition.

6.2.7. MTT assay

MTT (3-(4,5-dimethylthiazol-2-yl)-2,5-diphenyltetrazolium bromide) assay was employed to assess the sensitivity of cells to drugs of interest. The principle behind the assay lies in the ability of mitochondrial enzymes of living cells to convert the MTT reagent into water-insoluble purple formazan crystals. These crystals, after being dissolved in DMSO, can be spectrophotometrically detected and the OD from treated and untreated cells can be compared to estimate the cytotoxic/cytostatic effect of a test drug on cells.

In brief, at the beginning of the assay 2.5 thousand cells were seeded per well in a 96-well tissue culture plate (8 wells seeded for each condition). The following day medium was changed to fresh growth medium containing a series of dilutions of the test agent (ranging from 0 to 2-3x higher than IC_{50} values for the drug reported in the literature, if available). Cells were expose to the drug for 24 h, after which medium was replaced to fresh medium with MTT (1 mg/ml). Following a 3 h incubation period, the MTT-containing medium was replaced by DMSO. Sorensen's glycine buffer was added to wells to shift the pH to 10.5, at which the spectrum shows only one peak with an absorption max. around 570 nm.

At the end of the assay, OD_{540} was measured using the Tristar LB 941 multimode reader (Berthold). OD values were used to calculate the relative survival rate of cells in wells where the agent was added.

6.2.8. Dual luciferase reporter assay

Activity of the TGFβ and hypoxia pathways was assessed using the dual luciferase reporter assay. For this purpose, cells were co-transfected with two plasmids:

1) a specific reporter plasmid (e.g. FLuc with a promoter containing SMAD binding elements to assess TGFβ pathway activity, or the FLuc-ODD fusion protein for sensing hypoxia);

2) control reporter vector (RLuc coding plasmid with a stable viral promoter – SV40p; used to estimate numbers of viable cells).

Plasmids were co-transfected in the ratio of FLuc to RLuc 50:1 (see section 6.5 for the exact transfection protocol). After the appropriate treatment (e.g. stimulation with TGFβ1 or hypoxia conditions), cells were lysed in 1x passive lysis buffer (Promega, Cat# E1941). Lysates were frozen at -80°C, thawed at RT, and rotated for 15 min on a rotation wheel to insure complete cell lysis. Next, lysates were centrifuged at max. speed for 1 min in a table centrifuge. 10 µl of lysates were transferred into wells of a non-transparent 96-well plate and luciferase activity was automatically measured with a Tristar LB 941 multimode reader: Firefly luciferase was measured first (after the addition of 50 µl luciferase reagent A), followed by addition of 50 µl luciferase reagent B and RLuc activity measurement.

Firefly to *Renilla* ratio was assumed to represent the true reporter activity in a given sample, in accordance with the dual luciferase reporter assay principle.

6.2.9. Modified Boyden invasion assay

The ability of cells to invade was assessed using the modified Boyden chamber assay. The principal difference between the modified version of the protocol and the original assay is that in the modified Boyden chamber assay cells first must invade through an ECM matrix – Matrigel – to migrate through the porous membrane.

To assess invasion, cells were trypsinized, counted, and resuspended in diluted Matrigel (1:10 in DMEM, kept on ice to avoid premature solidification). 30 thousand cells for A549, and 50 thousand for MDA-MB-231 in 100 µl of diluted Matrigel were seeded per one well in

the upper compartment of the insert (Corning, Cat# 3422) in a 24-well plate, on top of the porous membrane (8 µm pores). Four wells were seeded per each condition. Then, the suspension was allowed to polymerize in the incubator at 37°C for 1 h. Next, the polymerized Matrigel containing suspended cells were carefully overlaid with DMEM 1% FBS, while 600 µl of complete growth medium (10% FBS) were added to the lower compartment. This generated a gradient via a difference in the concentration of nutrients and chemokines, effectively stimulating cell migration towards the porous membrane in the lower part of the upper compartment. After 18 h of incubation of inserts in the incubator or the hypoxic chamber, invasion was stopped by replacing the medium in the lower compartment to 70% EtOH. Cells were fixed for 10 min at RT, then the ethanol was replaced with PBS and cells were let to rehydrate for another 10 min.

Next, the nuclei of migrated cells (located on the lower side of the porous membrane) and nuclei of cells remaining suspended in Matrigel were stained with DAPI. For this, PBS from the lower compartment was replaced to a DAPI solution (2.5 µg/ml DAPI in 1xPBS), and the inserts incubated at RT for 10 min. The inserts were then washed for 10 min in PBS, after which pictures were taken of the DAPI stained nuclei in the upper compartment using a fluorescent Leica microscope (Leica BM IL LED) with a 2.5x objective.

In the end, medium was completely removed from the lower and upper compartments, membranes were carefully separated from the insert walls and placed on glass slides with the lower side facing upwards. A drop of fluorescent mounting medium (Dako, Cat# S3023) was placed on top of the membranes, which were then sealed to the slide with a cover glass. Afterwards, fluorescent pictures were taken from the fixed membranes with the 2.5x objective.

The number of cells in the upper compartment and on the membrane were estimated by counting DAPI stained nuclei with ImageJ (v.1.51j8, https://imagej.nih.gov/ij/). Invasion rate was determined as the ratio of invaded cells (on the lower surface of the membrane) to the number of cells in the upper compartment.

6.2.10. Time lapse microscopy-based migration assay

Cell migration was assessed by time-lapse microscopy. For this, cells were seeded in wells of a sterile chambered coverslip (Ibidi, Cat# 80826), and incubated in the culture chamber of the Zeiss Observer.Z1 microscope at 37°C in an atmosphere of 5% CO_2. Phase contrast

images were taken every 15 min for 48 h from 8 locations per each well with a 10x objective. Individual cell tracks were quantified for 30 cells per stack using the manual tracking plug-in in ImageJ.

6.2.11. Immunofluorescent staining of cells on coverslips

For immunofluorescence staining, cells were seeded on sterile glass coverslips placed in 12-well plates. After the appropriate treatment (e.g. hypoxia), cells were washed once with PBS and fixed with 4% PFA for 15 min at RT (at fixation confluency never exceeding 50%), after which the cells were washed twice with PBS. Next, cells were permeabilized with pre-cooled methanol at -20°C for 20 min. Afterwards, methanol was replaced with PBS, and cells incubated at RT for 15 min for rehydration. Coverslips were then placed on parafilm, and the following staining steps performed: 1) 30 min of blocking at RT with the IF blocking solution; 2) 1 h of incubation at RT with the primary antibodies in IF blocking buffer (see **Table 6.3**), followed by 3x washing with PBS; 3) 1 h of incubation in the dark at RT with fluorophore-conjugated secondary antibodies (all used in the dilution 1:1000 in the IF blocking buffer), followed by 3x washing with PBS; 4) 10 min incubation at RT with DAPI (2.5 µg/ml in PBS), followed with 3 final washing steps with PBS, and one – in dH_2O. Afterwards, a drop of fluorescent mounting medium was placed on the coverslips and they were placed on microscope slides. Epifluorescence images were taken using a Leica TCS SPE microscope with the 40x and 63x immersion objectives. Quantification of relative fluorescence was performed using ImageJ, where intensity measurements were taken of at least 15 cells per image. Three images per well were used for quantifying each datapoint.

6.2.12. Lentiviral transduction of cells

6.2.12.1. Production of lentiviruses in HEK293T cells

Recombinant lentiviruses were produced in the S2 facility of Giessen Institute of Neuropathology.

Human embryonic kidney cells HEK293T were used as the producer line. 5 million cells were seeded into 75T flasks the day prior to transfection. Second generation packaging plasmids (pCI-VSVG-Env and psPAX2) were used for virus production (all packaging and

transfer plasmids are listed in section 6.1.5). 25 µg of the transfer plasmid and 12.5 µg of each of the packaging plasmids were co-transfected into the seeded HEK cells using the calcium phosphate transfection method. For this, DNA-Ca-phosphate precipitate was formed by a dropwise addition of Hank's buffered saline (containing Na_2HPO_4) to the DNA-$CaCl_2$ solution under constant agitation. The final transfection mixture was immediately applied to cells, which were then incubated with the mixture for 5 h at 37°C (chloroquine in the final concentration of 10 µM was added to cells immediately before transfection to improve the transfection efficiency). Following the incubation time, medium was replaced to fresh complete growth medium and the virus-containing supernatants were collected 24 h and 48 h after transfection.

Next, virus-containing supernatants were transferred to sterile 38.5 ml ultracentrifuge tubes (Herolab, Cat# 253040), equilibrated, and concentrated by ultracentrifugation at 4°C for 4 h at approx. 52 000 g (20 000 rpm) using the AH-629 swinging bucket rotor in the Sorvall WX 80+ ultracentrifuge (Thermo Fisher). After centrifugation, the supernatant was discarded and virus resuspended in 100-200 µl of DMEM, aliquoted and stored at -80°C until titration or transduction of cells.

6.2.12.2. Virus titration

Human GBM line G55TL was used to titer all generated viruses. Serial dilutions of the concentrated virus (ranging from 10^{-9} to 10^{-2}) were produced, and G55TL cells transduced in medium containing polybrene at 6 µg/ml (used to improve transduction efficiency). The following day after transduction, medium was replaced to fresh complete growth medium and cells cultured for another 5 days (for viruses coding GFP) or 2-3 weeks (in case of viruses without fluorescent tags, under appropriate antibiotic selection) in the incubator at 37°C and 5% CO_2.

In the end, the titer was estimated by counting colonies either with fluorescence (in case of GFP-coding viruses), or after crystal violet staining (crystal violet solution dissolved 1:10 in DMEM, applied to cells for 15 min at RT, with a following 2x wash with PBS).

6.2.12.3. Lentiviral transduction

For transduction 1000 to 30 000 carcinoma cells were seeded per well in a 96- or 48-well plate. The next day, medium was changed to the transduction mix containing polybrene (at

6 µg/ml) and the appropriate volume of the concentrated virus to ensure the desired multiplicity of infection (MOI). 24 h after transduction medium was changed to complete growth medium. Two days after transduction the medium was changed again to fresh complete medium containing the appropriate selection antibiotic (either puromycin, or blasticidin). Transduced cells were grown under constant selection until several vials could be frozen, after which knockdown/overexpression efficiency, as well as the resulting phenotype, were analyzed.

6.2.13. RNA isolation, reverse transcription, and real-time PCR

6.2.13.1. Isolation of RNA from cells in culture

Isolation of total RNA from cells in culture was done using the RNeasy Quiagen Kit (Cat# 74104) following the manufacturer's instructions. In brief, the kit provides a spin column-based platform for RNA isolation which relies on the ability of RNA molecules to reversibly bind silica membranes. Cells were first lysed in a denaturing guanidine-thiocyanate buffer (RLT buffer with addition of β-mercaptoethanol), ethanol was then added to ensure proper RNA binding, and the lysates spun through binding columns containing silica membranes. Contaminants were then removed in several washing steps and highly pure RNA eluted in DEPC-treated water. Upon isolation, RNA concentration was determined using the Nanodrop spectrophotometer. RNA was stored at -20°C until reverse transcription.

6.2.13.2. RNA isolation from tumor tissue

Total RNA isolation from fresh tumor tissue was done using the Roti-Quick kit (Carl Roth, Cat# A979.1) in accordance with the manufacturer's recommendations. The kit is based on the RNA isolation method by a single-step acid guanidinium thiocyanate-phenol-chloroform extraction (Chomczynski, 1987). 0.5 g of fresh tumor tissue were used for RNA extraction.

6.2.13.3. Reverse transcription (RT) and qPCR

Reverse transcription: to generate cDNA from RNA, we used the Bio-Rad cDNA synthesis kit (Cat# 1708891) following the protocol provided by the manufacturer. The iScript mix contained all the necessary components – RNase inhibitor, reverse transcriptase, dNTPs,

and random hexamers. 1 µg of isolated RNA was used for reverse transcription. After synthesis, cDNA was diluted with DEPC-treated water to the final concentration of 5 ng/µl, which was then used for qPCR.

Quantitative PCR (qPCR): analysis of gene expression on mRNA level was done by quantitative PCR using the QuantStudio 3 Real-Time PCR system (Applied Biosystems). All samples were analyzed in triplicates, with reactions containing the following components: 20 ng cDNA, 100 µM forward primer, 100 µM reverse primer (list of all primers is presented in **Table 6.7**), 1x PowerUp SYBR Green master mix (contains the *Taq* polymerase, dNTPs, PCR buffer, and the SYBR green dye, Applied Biosystems, Cat# A25742). The routinely used amplification program is presented in **Table 6.10**.

Analysis of relative gene expression was performed using the 2-delta/delta C(t) method, with target gene mRNA quantity being first normalized to the *HPRT* housekeeping gene, and then – to the respective group control sample. Data in figures containing qPCR results represent an average from three technical replicates with standard error of the mean (SEM).

Table 6.10. Standard qPCR amplification program

Step	Time	Temperature	Nr of cycles
Enzyme activation	2 min	95	1x
Denaturation	30 sec	95	45x
Primer annealing	30 sec	60	
Extension	35 sec	72	
Melt curve	1 min	95	1x
	6 min	60→95, 0,1°C/sec	1x

6.2.14. Western blot

6.2.14.1. Lysis of cells

Adherent cells in dishes were washed once with PBS, and after all the PBS was removed – lysed in 150-300 µl of Laemmli buffer by scraping with a rubber policeman. The lysates were transferred to 1.5 ml eppendorf tubes and heated for 5 min at 95°C. Afterwards, samples were sonicated at 90%-intensity (0.5 sec / 0.5 sec sonication-rest intervals, Sonoplus,

Bandelin), heated again for 5min at 95°C, and stored at -20°C until protein concentration measurements.

6.2.14.2. Quantification of protein concentration

Protein concentration was estimated using the colorimetric DC protein assay kit (Bio-Rad, Cat# 500-0116), which represents a modified Lowry assay. The measurements were done in accordance with the manufacturer's instructions for the microplate assay protocol. Every sample was analyzed in duplicates (5 µl of the lysate per replicate) and the absolute protein quantity was quantified using a calibration curve made by serial dilutions of BSA.

6.2.14.3. SDS-PAGE / Immunoblotting

SDS-polyacrylamide gel electrophoresis (in denaturing conditions) was used to separate the proteins by their size using the mini-protean tetra cell chambers (Bio-Rad, Cat# 1658004EDU). Depending on the size of the proteins to be separated, 8% or 12% separating gels were cast freshly before use. Proteins were separated at 90 V while in the stacking gel, after which – upon reaching the separating gel – the voltage was turned up to 130 V for approx. 1 h.

Next, the separated proteins were transferred from gels to PVDF membranes using the Novex Semi-dry blotter (Invitrogen, Cat# SD1000) at 100 mA/gel for 1.5 h. The membranes were then incubated in the blocking buffer (5% milk in PBS / 0.1%Tween 20) for 1 h at RT to prevent unspecific binding of antibodies, followed by overnight incubation with primary antibodies diluted in the blocking buffer (see **Table 6.3** for the list and dilutions of all primary antibodies used).

On the next day, membranes were washed and incubated with secondary antibodies (see **Table 6.4**) diluted in blocking buffer for 1 h at RT. Afterwards, unbound secondary antibodies were removed by washing, followed by incubation of the membranes with ECL solutions. Depending on protein abundance and antibody performance, three different ECL solutions were used: ECL Western blotting substrate (Pierce, Cat# 32106), Western Lightning Plus-ECL (PerkinElmer, Cat# NEL103E001EA), or ECL Pico/Femto (Thermo Fisher, Cat# 34580/34095). Radiographic film (Thermo Fisher, Cat# 34089) was used for detection of the chemiluminescent signal.

6.2.15. RTK array

The activation state of receptor tyrosine kinases was asses using the Human phosphor-receptor tyrosine kinase array (R&D, Cat# ARY001B) following the manufacturer's instructions. In this assay receptors from lysed cells are bound by antibodies against 49 human RTKs, which are immobilized in specific spots of a nitrocellulose membrane. The phosphorylation state of the receptors is then estimated by HRP-conjugated pan phospho-tyrosine antibodies, followed by chemiluminescent detection.

For this assay, cells were starved overnight in DMEM containing 1% FBS, after which full medium (10% FBS) was applied for 10 min to stimulate most of the RTKs. 300 µg of protein were used from each lysate. Quantification of the relative RTK phosphorylation was done using ImageJ.

6.2.16. gDNA dot blot

6.2.16.1. Isolation of genomic DNA

Total genomic DNA from cells was isolated using the Blood and cell culture DNA mini kit (Qiagen, Cat# 13323) according to the manufacturer's instructions. In brief, this isolation method is subdivided into two phases: isolation of cell nuclei by enzymatic disruption of cells, and binding of DNA to anion-exchange resins (in the column) under low-salt and pH conditions. After DNA binding, contaminants (e.g. RNA, proteins) get removed in several washing steps. In the end, gDNA is eluted with a high-salt buffer and concentrated by isopropanol precipitation. 5 million cells were used for the isolation procedure.

6.2.16.2. Dot blot

0.5 µg of total genomic DNA in 1 µl TE buffer were applied onto a nitrocellulose membrane and left to dry for 30 min. Afterwards, the membrane was processed as in a typical Western blot, i.e. blocking, incubation with primary and secondary antibodies, and detection (all steps same as in section 6.15.3, after the transfer step).

6.2.17. *In vivo* experiments

In all *in vivo* studies each experimental group consisted of ten animals, unless specified otherwise. Such a number was chosen to account for the high variation in the number of lung metastases.

6.2.17.1. Subcutaneous and mammary fat pad transplantation of tumor cells

Prior to the injection of tumor cells, animals were anesthetized with 100 mg/kg ketamine and 10 mg/kg xylazine in 0.2 ml of 0.9% NaCl solution. For subcutaneous transplantation, 100 µl of tumor cell suspension containing 4 million A549 cells per animal were injected subcutaneously into the right flank of NMRI nu/nu mice (Janvier).

For mammary fat pad transplantation, anesthetized mice were placed on the back and under aseptic conditions a small (~1 cm long) incision in the skin was made in the right lower quadrant of the abdomen to expose the mammary fat pad. Next, an injection of 50 µl of a tumor cell suspension containing $4x10^6$ MDA-MB-231 cells per animal was administered in the mammary fat pad, and the wound closed with application of surgical Michel clips (FST, Cat# 12040-01). In the postoperative period animals were administered analgesia (5 mg/kg of carprofen, Rimadyl, Zoetis) for one week after the operation to relieve any pain.

6.2.17.2. Measuring tumor growth kinetics

For estimating the tumor volume, measurements were taken twice weekly with a caliper, and the volume calculated according to the following formula: $\mathbf{V_t = (a \times b^2) / 2}$, where **a** represents the length of the tumor (the longest measurement), and **b** – the tumor width, measured perpendicularly to **a**.

At the end of all experiments (either when the tumor volume reached 2 cm^3 or when other symptoms requiring termination were observed, e.g. cachexia, ulcer formation, etc.), animals were sacrificed by deep anesthesia, after which tumors and lungs were resected and fixed in 4% PFA.

6.2.17.3. Anti-angiogenic treatment

To establish a regimen of anti-angiogenic treatment that would accurately reflect the situation with patients in the clinics, administration of all the tested drugs was initiated only after the tumors were easily measurable and reached the size of approx. 250 mm^3.

Two receptor tyrosine kinase inhibitors – sunitinib and sorafenib – were administered orally to mice using a feeding needle (FST, Cat# 18060-20). Both drugs were dissolved in 0.5 M citrate buffer and administered daily at 60 mg/kg until the end of experiment or tumor resection.

The monoclonal anti-VEGFA antibody bevacizumab (Avastin) and the human IgG control antibody (Gamunex) were diluted in sterile saline and administered daily at 20 mg/kg via an intraperitoneal injection.

6.2.17.4. Resection of mammary fat pad tumors

Animals were anesthetized as described above, and an incision in the skin starting approximately 2-3 mm away from the tumor was made under aseptic conditions. To better expose the tumor, the covering skin was gently retracted. Next, major tumor-supplying arteries were identified and closed by thermocoagulation using a cautery unit (FST, Cat# 18010-00). In order to achieve a complete removal of the tumor, the surrounding mammary fat pad was cut at least 2 mm away from the tumor. Any minor bleeding observed during the tumor resection was stopped by thermocoagulation. Subsequently, the skin wound was closed with application of Michel clips. In the postoperative period animals were administered analgesia (5 mg/kg of carprofen, Rimadyl, Zoetis) for one week after the operation and observed for the next several weeks.

6.2.17.5. *In vivo* bioluminescence imaging

In vivo bioluminescence imaging of the MDA-POR-transplanted mice was performed with the help of the Lumina II *in vivo* imaging system (IVIS Lumina II, PerkinElmer). To assess the activity of both luciferases – Firefly luciferase (the hypoxia reporter) and *Renilla* luciferase (the control reporter for viable tumor cells), every imaging session was performed in two consecutive days to avoid the interference between the signals from the two enzymes.

FLuc imaging was carried out on the first day of every session. In brief, animals were imaged under general anesthesia with isoflurane (1-3%) administered via an inhalational anesthesia system (PerkinElmer). For detection of *in vivo* bioluminescence, 15 min prior to image acquisition mice were given a solution of D-luciferin (RegisTech) by intraperitoneal injection at 150 mg/kg.

Renilla luciferase imaging was performed on the following day after FLuc. 5 min before imaging, RLuc substrate – coelentherazine h – was administered via an i.v. injection at 0.5 mg/kg.

Image analysis was done using the LivingImage 4.2 software (PerkinElmer). FLuc/RLuc ratio, in accordance with the dual luciferase reporter assay principles, was assumed to represent the tumor hypoxic response.

6.2.17.6. Quantification of lung metastases

To assess the metastatic dissemination of tumors, in the end of every *in vivo* experiment superficial lung metastases ware quantified. For this, after being sacrificed by a lethal dose of anesthesia, mice were rapidly dissected, lugs carefully isolated and placed into PBS in Petri dishes. Fresh lung specimens were examined for the presence of superficial lung metastasis by two experimenters: one by the naked eye, the other – with the help of a surgical stereomicroscope (Zeiss) under a low magnification (2-5x). An example of the lung lesions that were quantified is presented in **Fig. 4.1, C**. After quantification of metastases, lungs were fixed in 4% PFA for further analysis by hematoxylin/eosin staining.

6.2.17.7. Hematoxylin/eosin histological staining

To analyze the metastatic dissemination of tumors, we performed hematoxylin/eosin staining of the lungs. PFA-fixed lungs were held immersed in 30% sucrose solution (in 0.1 M PB buffer) for one week to ensure cryoprotection of the tissue during cutting. Next, lung specimens were frozen and cut into 6 µm thick slices with a Leica SM200 R sliding microtome. The cut lung slices were then mounted on glass slides and left to dry overnight. On the following day, the staining procedure was carried out as presented in **Table 6.11**.

Table 6.11. Hematoxylin/eosin staining protocol

Step	Solution	Time
Rehydration	dH2O	2 min
Hematoxylin staining of the nuclei	Mayer's hematoxylin solution	8 min
Washing	dH2O	2 min
Blueing of the hematoxylin stain	Tap water	2 min
Washing	dH2O	2 min
Eosin staining of the cytoplasm	1% eosin in 70%EtOH	6 min
Dehydration	2x 70% EtOH	5-10 sec
	95% EtOH	1 min
	2x Absolute EtOH	5 min
Clearing in xylene	2x xylene	5 min

After xylene, few drops of the Cytoseal XYL (Thermo Fisher, Cat# 8312-4) were applied onto the stained sections, and coverslips were put on top of stained lung slices.

6.2.18. Gene expression analysis using the TCGA database

TCGA (The Cancer Genome Atlas) data for gene expression was retrieved using the cBioPortal (http://www.cbioportal.org/; (Cerami *et al*., 2012; Gao *et al*., 2013)). In brief, after specifying the tumor type – either breast invasive carcinoma (BIC) or lung adenocarcinoma (LUAD) – mRNA z-scores (RNA Seq V2 RSEM) for genes of interest were downloaded and transferred into an Excel table. Then, using the Excel filter function, the retrieved patient dataset was subdivided into two groups, according to TET1 expression: 1) patients with TET1 mRNA z-scores higher than 0.5; 2) patients with TET1 z-scores lower than -0.5. The cutoff values of -0.5 and 0.5 were chosen based on the range of TET1 expression and available numbers of cases to ensure meaningful statistical analysis (in the BIC group TET1 mRNA z-scores ranged from -0.94 to 11.5, with median at -0.23; in LUAD patients TET1 expression ranged from -0.65 to 16.15, with median at -0.18). Patients in the two groups were then compared for the expression of various hypoxia response genes, cancer stem cell markers, etc.

6.2.19. Database analysis of gene methylation

Analysis of *HIF2A* gene methylation was done in the same patients from TCGA for which gene expression data was retrieved (i.e., the same cohort as in section 6.2.18). Methylation

was assessed at a single CpG-site resolution by using publicly available Illumina 450k Array datasets. The 450k Array was designed to cover approx. 485 thousand CpG sites throughout the human genome (sites showing the highest variability in methylation were selected to cover all genes, most promoters, CpG islands, shores, shelves, etc.; Bibikova *et al*., 2011). The array included 36 CpG-sites for the *HIF2A* gene.

Individual patient datafiles containing the 450k Array results were downloaded from the Genomic Data Commons (GDC) portal repository (https://portal.gdc.can-cer.gov/repository; NCI; Grossman *et al*., 2016) with the GDC Data Transfer client (v.1.3.0). β-values, representing methylation at individual CpG-sites, for the *HIF2A* gene were retrieved with the help of RStudio (Version 1.0.143, https://www.rstudio.com/) using the following script, kindly provided by Dr. Gerrit Eichner (Mathematical Institute, Justus-Liebig-University Giessen):

```
“ EPAS1 <- read.csv2("EPAS1.csv")$X
 (Filenames <- list.files("LUAD/BIC", pattern = glob2rx("*.txt", trim.head = TRUE)))
Filepaths <- file.path("LUAD/BIC", Filenames)
names(Filepaths) <- sapply(strsplit(Filenames, "-01A", fixed = TRUE), "[", 1)
# cf <- sapply(Filepaths, function(fp) unique(count.fields(fp, sep = "\t")))
LUAD/BIC <- lapply(Filepaths, read.delim)
output <- lapply(LUAD/BIC, function(pat) pat[match(EPAS1, pat$Composite.Element.REF), 1:11])
BetaValue <- t(sapply(output, "[[", "Beta_value"))
colnames(BetaValue) <- EPAS1
write.csv2(BetaValue, "LUAD/BIC_ BetaValue.csv", quote = FALSE) “,
```

where **EPAS1.csv** contained the IDs of CpG-sites for *HIF2A* in the Illumina 450k Array.

Following the retrieval of β-values, we proceeded to identify the CpG-sites, methylation at which inversely correlated with *HIF2A* mRNA. For this, we calculated the Pearson correlation coefficient between mRNA z-scores of *HIF2A* and β-values of a specific CpG-site and assessed significance of the retrieved correlation.

Next, as with mRNA analysis, the total patient cohort was again stratified into two groups according to TET1 mRNA level: patients having TET1 mRNA z-scores higher than 0.5 and those with z-scores lower than -0.5. Afterwards, β-values were compared between the TET1-high and TET1-low groups, and average methylation at each CpG-site calculated.

6.2.20. Statistical analysis

Throughout the manuscript all bars represent the average with the standard error of the mean. Mann-Whitney U-test was employed in all cases of statistical analysis. Analysis was done using the STATISTICA 8.0 software package (Statsoft). Statistical significance was assumed at the following p-values: $p<0.05$ (*), $p<0.01$ (**), and $p<0.001$ (***).

Literature

Abdelkarim, M., Vintonenko, N., Starzec, A., Robles, A., Aubert, J., Martin, M.L., Mourah, S., Podgorniak, M.P., Rodrigues-Ferreira, S., Nahmias, C., et al. (2011). Invading basement membrane matrix is sufficient for MDA-MB-231 breast cancer cells to develop a stable in vivo metastatic phenotype. PLoS One *6*.

Agro, L., and O'Brien, C.A. (2015). In vitro and in vivo limiting dilution assay for colorectal cancer. Bio-Protocol *5*, 1–11.

Ahmad, S. a, Liu, W., Jung, Y.D., Fan, F., Wilson, M., Reinmuth, N., Shaheen, R.M., Bucana, C.D., and Ellis, L.M. (2001). The effects of angiopoietin-1 and -2 on tumor growth and angiogenesis in human colon cancer. Cancer Res. *61*, 1255–1259.

Almendros, I., Montserrat, J.M., Torres, M., Dalmases, M., Cabañas, M.L., Campos-Rodríguez, F., Navajas, D., and Farré, R. (2013). Intermittent hypoxia increases melanoma metastasis to the lung in a mouse model of sleep apnea. Respir. Physiol. Neurobiol. *186*, 303–307.

De Angelis, P.M., Svendsrud, D.H., Kravik, K.L., and Stokke, T. (2006). Cellular response to 5-fluorouracil (5-FU) in 5-FU-resistant colon cancer cell lines during treatment and recovery. Mol. Cancer *5*, 1–25.

Araos, J., Sleeman, J.P., and Garvalov, B.K. (2018). The role of hypoxic signalling in metastasis: towards translating knowledge of basic biology into novel anti-tumour strategies (Springer Netherlands).

Argast, G.M., Krueger, J.S., Thomson, S., Sujka-Kwok, I., Carey, K., Silva, S., O'Connor, M., Mercado, P., Mulford, I.J., Young, G.D., et al. (2011). Inducible expression of TGFβ, Snail and Zeb1 recapitulates EMT in vitro and in vivo in a NSCLC model. Clin. Exp. Metastasis *28*, 593–614.

Arnoux, V., Nassour, M., L'Helgoualc'h, A., Hipskind, R.A., and Savagner, P. (2008). Erk5 controls Slug expression and keratinocyte activation during wound healing. Mol. Biol. Cell *19*, 4738–4749.

Arreola, A., Cowey, C.L., Coloff, J.L., Rathmell, J.C., and Rathmell, W.K. (2014). HIF1α and HIF2α exert distinct nutrient preferences in renal cells. PLoS One *9*, 1–10.

Asiedu, M.K., Ingle, J.N., Behrens, M.D., Radisky, D.C., and Knutson, K.L. (2011).

TGFbeta/TNFalpha-mediated epithelial-mesenchymal transition generates breast cancer stem cells with a claudin-low phenotype. Cancer Res. *71*, 4707–4719.

Azam, F., Mehta, S., and Harris, A.L. (2010). Mechanisms of resistance to antiangiogenesis therapy. Eur. J. Cancer *46*, 1323–1332.

Baines, C.J., and Ley, D.C. (1962). A preliminary report on the use of 5-fluorouracil in malignant disease. Can. Med. Assoc. J. *86*, 207–210.

Batchelor, T.T., Sorensen, A.G., di Tomaso, E., Zhang, W.T., Duda, D.G.G., Cohen, K.S., Kozak, K.R., Cahill, D.P., Chen, P.J., Zhu, M., et al. (2007). AZD2171, a pan-VEGF receptor tyrosine kinase inhibitor, normalizes tumor vasculature and alleviates edema in glioblastoma patients. Cancer Cell *11*, 83–95.

Bates, D.O., Cui, T.-G., Doughty, J.M., Winkler, M., Sugiono, M., Shields, J.D., Peat, D., Gillatt, D., and Harper, S.J. (2002). VEGF165b, an inhibitory splice variant of vascular endothelial growth factor, is down-regulated in renal cell carcinoma. Cancer Res. *62*, 4123–4131.

Baxter, E., Windloch, K., Gannon, F., and Lee, J.S. (2014). Epigenetic regulation in cancer progression. Cell Biosci. *4*, 1–11.

van Beijnum, J.R., Nowak-Sliwinska, P., Huijbers, E.J.M., Thijssen, V.L., and Griffioen, A.W. (2015). The great escape; the Hallmarks of resistance to antiangiogenic therapy. Pharmacol. Rev. *67*, 441–461.

Benjaminsen, I.C., Graff, B.A., Brurberg, K.G., and Rofstad, E.K. (2004). Assessment of tumor blood perfusion by high-resolution dynamic contrast-enhanced MRI: A preclinical study of human melanoma xenografts. Magn. Reson. Med. *52*, 269–276.

Bentolila, L.A., Prakash, R., Mihic-Probst, D., Wadehra, M., Kleinman, H.K., Carmichael, T.S., Péault, B., Barnhill, R.L., and Lugassy, C. (2016). Imaging of angiotropism/vascular co-option in a murine model of brain melanoma: Implications for melanoma progression along extravascular pathways. Sci. Rep. *6*, 1–11.

Bergers, G., and Benjamin, L.E. (2003). Tumorigenesis and the angiogenic switch. Nat. Rev. Cancer *3*, 401–410.

Bergers, G., and Hanahan, D. (2008). Mode of resistance to anti-angiogenic therapy. Nat. Rev. Cancer *8*, 592–603.

Bernardino, J., Roux, C., Almeida, A., Vogt, N., Gibaud, A., Gerbault-Seureau, M.,

Magdelenat, H., Bourgeois, C.A., Malfoy, B., and Dutrillaux, B. (1997). DNA hypomethylation in breast cancer: An independent parameter of tumor progression? Cancer Genet. Cytogenet. *97*, 83–89.

Van Den Beucken, T., Koch, E., Chu, K., Rupaimoole, R., Prickaerts, P., Adriaens, M., Voncken, J.W., Harris, A.L., Buffa, F.M., Haider, S., et al. (2014). Hypoxia promotes stem cell phenotypes and poor prognosis through epigenetic regulation of DICER. Nat. Commun. *5*, 1–13.

Bhandari, P.N., Cui, Y., Elzey, B.D., Goergen, C.J., Long, C.M., and Irudayaraj, J. (2017). Oxygen nanobubbles revert hypoxia by methylation programming. Sci. Rep. *7*, 1–14.

Bhaskara, V.K., Mohanam, I., Rao, J.S., and Mohanam, S. (2012). Intermittent hypoxia regulates stem-like characteristics and differentiation of neuroblastoma cells. PLoS One *7*, 1–10.

Bibikova, M., Barnes, B., Tsan, C., Ho, V., Klotzle, B., Le, J.M., Delano, D., Zhang, L., Schroth, G.P., Gunderson, K.L., et al. (2011). High density DNA methylation array with single CpG site resolution. Genomics *98*, 288–295.

Bluemn, E.G., Coleman, I.M., Lucas, J.M., Coleman, R.T., Hernandez-Lopez, S., Tharakan, R., Bianchi-Frias, D., Dumpit, R.F., Kaipainen, A., Corella, A.N., et al. (2017). Androgen receptor pathway-independent prostate cancer is sustained through FGF signaling. Cancer Cell *32*, 474–489.

Boland, M.J., Nazor, K.L., and Loring, J.F. (2014). Epigenetic regulation of pluripotency and differentiation. Circ. Res. 311–325.

Bolos, V., Peinado, H., Perez-Moreno, M.A., Fraga, M.F., Esteller, M., and Cano, A. (2016). The transcription factor Slug represses E-cadherin expression and induces epithelial to mesenchymal transitions: a comparison with Snail and E47 repressors. J. Cell Sci. *129*, 1283–1283.

Bonaventure, A., Harewood, R., Stiller, C.A., Gatta, G., Clavel, J., Stefan, D.C., Carreira, H., Spika, D., Marcos-Gragera, R., Peris-Bonet, R., et al. (2017). Worldwide comparison of survival from childhood leukaemia for 1995–2009, by subtype, age, and sex (CONCORD-2): a population-based study of individual data for 89 828 children from 198 registries in 53 countries. Lancet Haematol. *4*, e202–e217.

Bottsford-Miller, J.N., Coleman, R.L., and Sood, A.K. (2012). Resistance and escape from

antiangiogenesis therapy: Clinical implications and future strategies. J. Clin. Oncol. *30*, 4026–4034.

Bridgeman, V.L., Vermeulen, P.B., Foo, S., Bilecz, A., Daley, F., Kostaras, E., Nathan, M.R., Wan, E., Frentzas, S., Schweiger, T., et al. (2017). Vessel co-option is common in human lung metastases and mediates resistance to anti-angiogenic therapy in preclinical lung metastasis models. J. Pathol. *241*, 362–374.

Brien, G.L., Valerio, D.G., and Armstrong, S.A. (2016). Exploiting the epigenome to control cancer-promoting gene-expression programs. Cancer Cell *29*, 464–476.

Broekman, F. (2011). Tyrosine kinase inhibitors: Multi-targeted or single-targeted? World J. Clin. Oncol. *2*, 80.

Brurberg, K.G., Benjaminsen, I.C., Dørum, L.M.R., and Rofstad, E.K. (2007). Fluctuations in tumor blood perfusion assessed by dynamic contrast-enhanced MRI. Magn. Reson. Med. *58*, 473–481.

Bukowski, R.M. (2012). Third generation tyrosine kinase inhibitors and their development in advanced renal cell carcinoma. Front. Oncol. *2*, 1–10.

Burrell, R.A., and Swanton, C. (2014). Tumour heterogeneity and the evolution of polyclonal drug resistance. Mol. Oncol. *8*, 1095–1111.

Cairns, R.A., Kalliomaki, T., and Hill, R.P. (2001). Acute (cyclic) hypoxia enhances spontaneous metastasis of KHT murine tumors. Cancer Res. *61*, 8903–8908.

Casanovas, O. (2011). The adaptive stroma joining the antiangiogenic resistance front. J. Clin. Invest. *121*, 1244–1247.

Casanovas, O., Hicklin, D.J., Bergers, G., and Hanahan, D. (2005). Drug resistance by evasion of antiangiogenic targeting of VEGF signaling in late-stage pancreatic islet tumors. Cancer Cell *8*, 299–309.

Cerami, E., Gao, J., Dogrusoz, U., Gross, B.E., Sumer, S.O., Aksoy, B.A., Jacobsen, A., Byrne, C.J., Heuer, M.L., Larsson, E., et al. (2012). The cBio Cancer Genomics Portal: An open platform for exploring multidimensional cancer genomics data. Cancer Discov. *2*, 401–404.

Chae, S.S., Kamoun, W.S., Farrar, C.T., Kirkpatrick, N.D., Niemeyer, E., De Graaf, A.M.A., Sorensen, A.G., Munn, L.L., Jain, R.K., and Fukumura, D. (2010). Angiopoietin-2 interferes with anti-VEGFR2-induced vessel normalization and survival benefit in mice bearing

gliomas. Clin. Cancer Res. *16*, 3618–3627.

Chen, A., Sceneay, J., Gödde, N., Kinwel, T., Ham, S., Thompson, E.W., Humbert, P.O., and Möller, A. (2018). Intermittent hypoxia induces a metastatic phenotype in breast cancer. Oncogene *37*, 4214–4225.

Chen, Y.C., Hsu, H.S., Chen, Y.W., Tsai, T.H., How, C.K., Wang, C.Y., Hung, S.C., Chang, Y.L., Tsai, M.L., Lee, Y.Y., et al. (2008). Oct-4 expression maintained cancer stem-like properties in lung cancer-derived CD133-positive cells. PLoS One *3*, 1–14.

Cho, H., Du, X., Rizzi, J.P., Liberzon, E., Chakraborty, A.A., Gao, W., Carvo, I., Signoretti, S., Bruick, R.K., Josey, J.A., et al. (2016). On-target efficacy of a HIF-2α antagonist in preclinical kidney cancer models. Nature *539*, 107–111.

Chomczynski, P. (1987). Single-step method of RNA isolation by acid guanidinium thiocyanate-phenol-chlorophorm extraction. Anal. Biochem. *162*, 156–159.

Chou, C.W., Wang, C.C., Wu, C.P., Lin, Y.J., Lee, Y.C., Cheng, Y.W., and Hsieh, C.H. (2012). Tumor cycling hypoxia induces chemoresistance in glioblastoma multiforme by upregulating the expression and function of ABCB1. Neuro. Oncol. *14*, 1227–1238.

Chow, L.Q.M., and Eckhardt, S.G. (2007). Sunitinib: From rational design to clinical efficacy. J. Clin. Oncol. *25*, 884–896.

Chung, A.S., Wu, X., Zhuang, G., Ngu, H., Kasman, I., Zhang, J., Vernes, J.M., Jiang, Z., Meng, Y.G., Peale, F. V., et al. (2013). An interleukin-17-mediated paracrine network promotes tumor resistance to anti-angiogenic therapy. Nat. Med. *19*, 1114–1123.

Cleven, A.H.G., Wouters, B.G., Schutte, B., Spiertz, A.J.G., Van Engeland, M., and De Bruïne, A.P. (2008). Poorer outcome in stromal HIF-2α- and CA9-positive colorectal adenocarcinomas is associated with wild-type TP53 but not with BNIP3 promoter hypermethylation or apoptosis. Br. J. Cancer *99*, 727–733.

Coelho, A.L., Gomes, M.P., Catarino, R.J., Lopes, A.M., Medeiros, R.M., and Manuel, A. (2015). Angiogenesis in NSCLC: is vessel co-option the trunk that sustains the branches? Oncotarget *8*, 39795–39804.

Cohen, I., Poręba, E., Kamieniarz, K., and Schneider, R. (2011). Histone modifiers in cancer: Friends or foes? Genes and Cancer *2*, 631–647.

Cooke, V.G., LeBleu, V.S., Keskin, D., Khan, Z., O'Connell, J.T., Teng, Y., Duncan, M.B., Xie, L., Maeda, G., Vong, S., et al. (2012). Pericyte depletion results in hypoxia-associated

epithelial-to-mesenchymal transition and metastasis mediated by Met signaling pathway. Cancer Cell *21*, 66–81.

Corbet, C., and Feron, O. (2017). Tumour acidosis: From the passenger to the driver's seat. Nat. Rev. Cancer *17*, 577–593.

Covello, KL., Kehler, J., Yu, H., Gordan, JD., Arsham, AM., Hu, C., Labosky, PA., Simon, MC., Keith, B. (2006). HIF-2alfa regulates Oct-4: effects of hypoxia on stem cell function , embryonic development , and tumor growth. Genes Dev. *20*, 557–570.

Craene, B. De, and Berx, G. (2013). Regulatory networks defining EMT during cancer initiation and progression. Nat. Rev. Cancer *13*, 97–110.

Crawford, Y., and Ferrara, N. (2009). Tumor and stromal pathways mediating refractoriness/resistance to anti-angiogenic therapies. Trends Pharmacol. Sci. *30*, 624–630.

Cunningham, J.J., Brown, J.S., Vincent, T.L., and Gatenby, R.A. (2015). Divergent and convergent evolution in metastases suggest treatment strategies based on specific metastatic sites. Evol. Med. Public Heal. *2015*, 76–87.

D'Anselmi, F., Masiello, M.G., Cucina, A., Proietti, S., Dinicola, S., Pasqualato, A., Ricci, G., Dobrowolny, G., Catizone, A., Palombo, A., et al. (2013). Microenvironment promotes tumor cell reprogramming in human breast cancer cell lines. PLoS One *8*, 1–12.

Danhier, P., Krishnamachary, B., Bharti, S., Kakkad, S., Mironchik, Y., and Bhujwalla, Z.M. (2015). Combining optical reporter proteins with different half-lives to detect temporal evolution of hypoxia and reoxygenation in tumors. Neoplasia *17*, 871–881.

David, C.J., Huang, Y.-H., Chen, M., Su, J., Zou, Y., Bardeesy, N., Iacobuzio-Donahue, C.A., and Massagué, J. (2016). TGF-β tumor suppression through a lethal EMT. Cell *164*, 1015–1030.

Dawson, M.A., and Kouzarides, T. (2012). Cancer epigenetics: From mechanism to therapy. Cell *150*, 12–27.

Day, C., Merlino, G., and Van Dyke, T. (2015). Preclinical mouse cancer models: A maze of opportunities and challenges. Cell *163*, 39–53.

Dean, M., Fojo, T., and Bates, S. (2005). Tumour stem cells and drug resistance. Nat. Rev. Cancer *5*, 275–284.

Dekervel, J., Hompes, D., Van Malenstein, H., Popovic, D., Sagaert, X., De Moor, B., Van Cutsem, E., D'Hoore, A., Verslype, C., and Van Pelt, J. (2014). Hypoxia-driven gene

expression is an independent prognostic factor in stage II and III colon cancer patients. Clin. Cancer Res. *20*, 2159–2168.

DelNero, P., Lane, M., Verbridge, S.S., Kwee, B., Kermani, P., Hempstead, B., Stroock, A., and Fischbach, C. (2015). 3D culture broadly regulates tumor cell hypoxia response and angiogenesis via pro-inflammatory pathways. Biomaterials *55*, 110–118.

Dengler, V.L., Galbraith, M.D., and Espinosa, J.M. (2014). Transcriptional regulation by hypoxia inducible factors. Crit. Rev. Biochem. Mol. Biol. *49*, 1–15.

Depner, C., Zum Buttel, H., BögÜrcü, N., Cuesta, A.M., Aburto, M.R., Seidel, S., Finkelmeier, F., Foss, F., Hofmann, J., Kaulich, K., et al. (2016). EphrinB2 repression through ZEB2 mediates tumour invasion and anti-angiogenic resistance. Nat. Commun. *7*, 1–15.

DeVita, V.T., and Chu, E. (2008). A history of cancer chemotherapy. Cancer Res. *68*, 8643–8653.

Dey, N., De, P., and Brian, L.-J. (2015). Evading anti-angiogenic therapy: resistance to anti-angiogenic therapy in solid tumors. Am J Transl Res *7*, 1675–1698.

Dme, B., Paku, S., Somlai, B., and Tmr, J. (2002). Vascularization of cutaneous melanoma involves vessel co-option and has clinical significance. J. Pathol. *197*, 355–362.

Döme, B., Hendrix, M.J.C., Paku, S., Tóvári, J., and Tímár, J. (2007). Alternative vascularization mechanisms in cancer: Pathology and therapeutic implications. Am. J. Pathol. *170*, 1–15.

Dong, C., Wu, Y., Wang, Y., Wang, C., Kang, T., Rychahou, P.G., Chi, Y.I., Evers, B.M., and Zhou, B.P. (2013). Interaction with Suv39H1 is critical for Snail-mediated E-cadherin repression in breast cancer. Oncogene *32*, 1351–1362.

Dong, Z., Radinsky, R., Fan, D., Tsan, R., Bucana, C.D., Wilmanns, C., and Fidler, I.J. (1994). Organ-specific modulation of steady-state mdr gene expression and drug resistance in murine colon cancer cells. J. Natl. Cancer Inst. *86*, 913–920.

Dopeso, H., Jiao, H., Cuesta, A.M., Henze, A., Jurida, L., Kracht, M., Acker-Palmer, A., Garvalov, B.K., and Acker, T. (2018). PHD3 controls lung cancer metastasis and resistance to EGFR inhibitors through TGFα. Cancer Res. *78*, 1805–1819.

Drake, C.J., LaRue, A., Ferrara, N., and Little, C.D. (2000). VEGF regulates cell behavior during vasculogenesis. Dev. Biol. *224*, 178–188.

Ebos, J.M.L., Lee, C.R., Cruz-Munoz, W., Bjarnason, G.A., Christensen, J.G., and Kerbel, R.S. (2009a). Accelerated metastasis after short-term treatment with a potent inhibitor of tumor angiogenesis. Cancer Cell *15*, 232–239.

Ehrlich, M. (2002). DNA methylation in cancer: Too much, but also too little. Oncogene *21*, 5400–5413.

Escudier, B., Eisen, T., Stadler, W.M., Szczylik, C., Oudard, S., Staehler, M., Negrier, S., Chevreau, C., Desai, A.A., Rolland, F., et al. (2009). Sorafenib for treatment of renal cell carcinoma: Final efficacy and safety results of the phase III treatment approaches in renal cancer global evaluation trial. J. Clin. Oncol. *27*, 3312–3318.

Escudier, B., Bellmunt, J., Négrier, S., Bajetta, E., Melichar, B., Bracarda, S., Ravaud, A., Golding, S., Jethwa, S., and Sneller, V. (2010). Phase III trial of bevacizumab plus interferon alfa-2a in patients with metastatic renal cell carcinoma (AVOREN): Final analysis of overall survival. J. Clin. Oncol. *28*, 2144–2150.

Eskelin, S., Pyrhönen, S., Hahka-Kemppinen, M., Tuomaala, S., and Kivelä, T. (2003). A prognostic model and staging for metastatic uveal melanoma. Cancer *97*, 465–475.

Facciabene, A., Peng, X., Hagemann, I.S., Balint, K., Barchetti, A., Wang, L., Gimotty, P.A., Gilks, C.B., Lal, P., Zhang, L., et al. (2011). Tumour hypoxia promotes tolerance and angiogenesis via CCL28 and Treg cells. Nature *475*, 226–230.

Fagiani, E., Lorentz, P., Kopfstein, L., and Christofori, G. (2011). Angiopoietin-1 and -2 exert antagonistic functions in tumor angiogenesis, yet both induce lymphangiogenesis. Cancer Res. *71*, 5717–5727.

Faguet, G.B. (2015). A brief history of cancer: Age-old milestones underlying our current knowledge database. Int. J. Cancer *136*, 2022–2036.

Fang, H., Hughes, R., Murdoch, C., Coffelt, S.B., Biswas, S.K., Harris, A.L., Johnson, R.S., Imityaz, H.Z., Simon, M.C., Fredlund, E., et al. (2018). Hypoxia-inducible factors 1 and 2 are important transcriptional effectors in primary macrophages experiencing hypoxia. Blood *114*, 844–860.

Farber, S., Diamond, L.K., Mercer, R.D., Sylvester, R.F., and Wolff, J.A. (1948). Temporary remissions in acute leukemia in children produced by folic acid antagonist, 4-aminopteroyl-glutamic acid (Aminopterin). N. Engl. J. Med. *238*, 787–793.

Feinberg, A.P., and Tycko, B. (2004). The history of cancer epigenetics. Nat. Rev. Cancer

4, 143–153.

Fendrich, V., Maschuw, K., Rehm, J., Buchholz, M., Holler, J.P., Slater, E.P., Bartsch, D.K., and Waldmann, J. (2012). Sorafenib inhibits tumor growth and improves survival in a transgenic mouse model of pancreatic islet cell tumors. Sci. World J. *2012*, 1–7.

Fernando, R.I., Castillo, M.D., Litzinger, M., Hamilton, D.H., and Palena, C. (2011). IL-8 signaling plays a critical role in the epithelial-mesenchymal transition of human carcinoma cells. Cancer Res. *71*, 5296–5306.

Ferone, G., Song, J., Sutherland, K.D., Proost, N., Gargiulo, G., Berns, A., Ferone, G., Song, J., Sutherland, K.D., Bhaskaran, R., et al. (2016). SOX2 is the determining oncogenic switch in promoting lung squamous cell carcinoma from different cells of origin article SOX2 is the determining oncogenic switch in promoting lung squamous cell carcinoma from different cells of origin. Cancer Cell *30*, 519–532.

Ferrara, N., Hillan, K.J., and Novotny, W. (2005). Bevacizumab (Avastin), a humanized anti-VEGF monoclonal antibody for cancer therapy. Biochem. Biophys. Res. Commun. *333*, 328–335.

Ferretti, S., Allegrini, P.R., Becquet, M.M., and McSheehy, P.M.J. (2009). Tumor interstitial fluid pressure as an early-response marker for anticancer therapeutics. Neoplasia *11*, 874–881.

Filatova, A., Seidel, S., Böğürcü, N., Gräf, S., Garvalov, B.K., and Acker, T. (2016). Acidosis acts through HSP90 in a PHD/ VHL-independent manner to promote HIF function and stem cell maintenance in glioma. Cancer Res. *76*, 5845–5856.

Finke, J., Ko, J., Rini, B., Rayman, P., Ireland, J., and Cohen, P. (2011). MDSC as a mechanism of tumor escape from sunitinib mediated anti-angiogenic therapy. Int. Immunopharmacol. *11*, 853–858.

Fleischer, T., Tekpli, X., Mathelier, A., Wang, S., Nebdal, D., Dhakal, H.P., Sahlberg, K.K., Schlichting, E., Sauer, T., Geisler, J., et al. (2017). DNA methylation at enhancers identifies distinct breast cancer lineages. Nat. Commun. *8*, 1–14.

Folkman, J. (1972). Anti-angiogenesis: new concept for therapy of solid tumors. Ann. Surg. *175*, 409–416.

Frentzas, S., Simoneau, E., Bridgeman, V.L., Vermeulen, P.B., Foo, S., Kostaras, E., Nathan, M.R., Wotherspoon, A., Gao, Z.H., Shi, Y., et al. (2016). Vessel co-option mediates

resistance to anti-angiogenic therapy in liver metastases. Nat. Med. *22*, 1294–1302.

Friedl, P., and Alexander, S. (2011). Cancer invasion and the microenvironment: Plasticity and reciprocity. Cell *147*, 992–1009.

Friedl, P., Hegerfeldt, Y., and Tusch, M. (2004). Collective cell migration in morphogenesis and cancer. Int. J. Dev. Biol. *48*, 441–449.

Frigola, J., Solé, X., Paz, M.F., Moreno, V., Esteller, M., Capellà, G., and Peinado, M.A. (2005). Differential DNA hypermethylation and hypomethylation signatures in colorectal cancer. Hum. Mol. Genet. *14*, 319–326.

Fu, Y., Wu, X., Han, Q., Liang, Y., He, Y., and Luo, Y. (2008). Sulfate stabilizes the folding intermediate more than the native structure of endostatin. Arch. Biochem. Biophys. *471*, 232–239.

Gale, N.W., Thurston, G., Hackett, S.F., Renard, R., Wang, Q., McClain, J., Martin, C., Witte, C., Witte, M.H., Jackson, D., et al. (2002). Angiopoietin-2 is required for postnatal angiogenesis and lymphatic patterning, and only the latter role is rescued by angiopoietin-1. Dev. Cell *3*, 411–423.

Gao, J., Aksoy, B.A., Dogrusoz, U., Dresdner, G., Gross, B., Sumer, S.O., Sun, Y., Jacobsen, A., Sinha, R., Larsson, E., et al. (2013). Integrative analysis of complex cancer genomics and clinical profiles using the cBioPortal. Sci. Signal. *6*, 1–19.

Gavert, N., and Ben-Ze'ev, A. (2008). Epithelial-mesenchymal transition and the invasive potential of tumors. Trends Mol. Med. *14*, 199–209.

Gerber, H.-P., Condorelli, F., Park, J., and Ferrara, N. (1997). Differential transcriptional regulation of the two vascular endothelial growth factor receptor genes. J. Biol. Chem. *272*, 23659–23667.

Giuliano, S., and Pagès, G. (2013). Mechanisms of resistance to anti-angiogenesis therapies. Biochimie *95*, 1110–1119.

Gómez-Cuadrado, L., Tracey, N., Ma, R., Qian, B., and Brunton, V.G. (2017). Mouse models of metastasis: progress and prospects. Dis. Model. Mech. *10*, 1061–1074.

Gonçalves, M.R., Johnson, S.P., Ramasawmy, R., Pedley, R.B., Lythgoe, M.F., and Walker-Samuel, S. (2015). Decomposition of spontaneous fluctuations in tumour oxygenation using BOLD MRI and independent component analysis. Br. J. Cancer *113*, 1168–1177.

Gordan, J.D., Bertout, J.A., Hu, C.J., Diehl, J.A., and Simon, M.C. (2007). HIF-2α promotes

hypoxic cell proliferation by enhancing c-Myc transcriptional activity. Cancer Cell *11*, 335–347.

Gotink, K.J., and Verheul, H.M.W. (2010). Anti-angiogenic tyrosine kinase inhibitors: what is their mechanism of action? Angiogenesis *13*, 1–14.

Gray, R., Bhattacharya, S., Bowden, C., Miller, K., and Comis, R.L. (2009). Independent review of E2100: A phase III trial of bevacizumab plus paclitaxel versus paclitaxel in women with metastatic breast cancer. J. Clin. Oncol. *27*, 4966–4972.

Greene, H.S. (1941). Heterologous transplantation of mammalian tumors II: The transfer of human tumors to alien species. J. Exp. Med. *73*, 475–486.

Griffioen, A.W., Mans, L.A., de Graaf, A.M.A., Nowak-Sliwinska, P., de Hoog, C.L.M.M., de Jong, T.A.M., Vyth-Dreese, F.A., van Beijnum, J.R., Bex, A., and Jonasch, E. (2012). Rapid angiogenesis onset after discontinuation of sunitinib treatment of renal cell carcinoma patients. Clin. Cancer Res. *18*, 3961–3971.

Grossman, R.L., Heath, A.P., Ferretti, V., Varmus, H.E., Lowy, D.R., Kibbe, W.A., and Staudt, L.M. (2016). Toward a shared vision for cancer genomic data. N. Engl. J. Med. *375*, 1109–1112.

Guo, Y., Pakneshan, P., Gladu, J., Slack, A., Szyf, M., and Rabbani, S.A. (2002). Regulation of DNA methylation in human breast cancer: Effect on the urokinase-type plasminogen activator gene production and tumor invasion. J. Biol. Chem. *277*, 41571–41579.

Gupta, G.P., Nguyen, D.X., Chiang, A.C., Bos, P.D., Kim, J.Y., Nadal, C., Gomis, R.R., Manova-Todorova, K., and Massagué, J. (2007). Mediators of vascular remodelling co-opted for sequential steps in lung metastasis. Nature *446*, 765–770.

Gwak, J.M., Kim, M., Kim, H.J., Jang, M.H., and Park, S.Y. (2017). Expression of embryonal stem cell transcription factors in breast cancer: Oct4 as an indicator for poor clinical outcome and tamoxifen resistance. Oncotarget *8*, 36305–36318.

Ha, K., Kim, H.-G., and Lee, H. (2017). Chromatin marks shape mutation landscape at early stage of cancer progression. Genomic Med. *9*, 1–8.

Hake, S.B., Xiao, A., and Allis, C.D. (2004). Linking the epigenetic “language” of covalent histone modifications to cancer. Br. J. Cancer *90*, 761–769.

El Hallani, S., Boisselier, B., Peglion, F., Rousseau, A., Colin, C., Idbaih, A., Marie, Y., Mokhtari, K., Thomas, J.L., Eichmann, A., et al. (2010). A new alternative mechanism in

glioblastoma vascularization: Tubular vasculogenic mimicry. Brain *133*, 973–982.

Hamidian, A., Von Stedingk, K., Munksgaard Thorén, M., Mohlin, S., and Påhlman, S. (2015). Differential regulation of HIF-1α and HIF-2α in neuroblastoma: Estrogen-related receptor alpha (ERRα) regulates HIF2A transcription and correlates to poor outcome. Biochem. Biophys. Res. Commun. *461*, 560–567.

Han, K.S., Raven, P.A., Frees, S., Gust, K., Fazli, L., Ettinger, S., Hong, S.J., Kollmannsberger, C., Gleave, M.E., and So, A.I. (2015). Cellular adaptation to VEGF-targeted antiangiogenic therapy induces evasive resistance by overproduction of alternative endothelial cell growth factors in renal cell carcinoma. Neoplasia *17*, 805–816.

Han, W.-Q., Zhu, Q., Hu, J., Li, P.-L., Zhang, F., and Li, N. (2013). Hypoxia-inducible factor prolyl-hydroxylase-2 mediates transforming growth factor beta 1-induced epithelial–mesenchymal transition in renal tubular cells. Biochim. Biophys. Acta - Mol. Cell Res. *1833*, 1454–1462.

Hanahan, D., and Weinberg, R.A. (2000). The hallmarks of cancer. Cell *100*, 57–70.

Hanahan, D., and Weinberg, R.A. (2011). Hallmarks of cancer: The next generation. Cell *144*, 646–674.

Hanley, M.P., Hahn, M.A., Li, A.X., Wu, X., Lin, J., Wang, J., Choi, A.H., Ouyang, Z., Fong, Y., Pfeifer, G.P., et al. (2017). Genome-wide DNA methylation profiling reveals cancer-associated changes within early colonic neoplasia. Oncogene *36*, 5035–5044.

Hanna, S.C., Krishnan, B., Bailey, S.T., Moschos, S.J., Kuan, P.F., Shimamura, T., Osborne, L.D., Siegel, M.B., Duncan, L.M., O'Brien, E.T., et al. (2013). HIF1α and HIF2α independently activate SRC to promote melanoma metastases. J. Clin. Invest. *123*, 2078–2093.

Hansen, K.D., Timp, W., Bravo, H.C., Sabunciyan, S., Langmead, B., McDonald, O.G., Wen, B., Wu, H., Liu, Y., Diep, D., et al. (2011). Increased methylation variation in epigenetic domains across cancer types. Nat. Genet. *43*, 768–775.

Hansma, A.H.G., Broxterman, H.J., van der Horst, I., Yuana, Y., Boven, E., Giaccone, G., Pinedo, H.M., and Hoekman, K. (2005). Recombinant human endostatin administered as a 28-day continuous intravenous infusion, followed by daily subcutaneous injections: A phase I and pharmacokinetic study in patients with advanced cancer. Ann. Oncol. *16*, 1695–1701.

Hattori, M., Yokoyama, Y., Hattori, T., Motegi, S. ichiro, Amano, H., Hatada, I., and Ishikawa,

O. (2015). Global DNA hypomethylation and hypoxia-induced expression of the ten eleven translocation (TET) family, TET1, in scleroderma fibroblasts. Exp. Dermatol. *24*, 841–846.

Helfrich, I., Scheffrahn, I., Bartling, S., Weis, J., von Felbert, V., Middleton, M., Kato, M., Ergün, S., Augustin, H.G., and Schadendorf, D. (2010). Resistance to antiangiogenic therapy is directed by vascular phenotype, vessel stabilization, and maturation in malignant melanoma. J. Exp. Med. *207*, 491–503.

Henze, A.T., and Acker, T. (2010). Feedback regulators of hypoxia-inducible factors and their role in cancer biology. Cell Cycle *9*, 2749–2763.

Henze, A.T., Garvalov, B.K., Seidel, S., Cuesta, A.M., Ritter, M., Filatova, A., Foss, F., Dopeso, H., Essmann, C.L., Maxwell, P.H., et al. (2014). Loss of PHD3 allows tumours to overcome hypoxic growth inhibition and sustain proliferation through EGFR. Nat. Commun. *5*, 1–12.

Herranz, N., Pasini, D., Diaz, V.M., Franci, C., Gutierrez, A., Dave, N., Escriva, M., Hernandez-Munoz, I., Di Croce, L., Helin, K., et al. (2008). Polycomb complex 2 is required for E-cadherin repression by the Snail1 transcription factor. Mol. Cell. Biol. *28*, 4772–4781.

van den Heuvel-Eibrink, M.M., Wiemer, E.A., de Boevere, M.J., van der Holt, B., Vossebeld, P.J., Pieters, R., and Sonneveld, P. (2001). MDR1 gene-related clonal selection and P-glycoprotein function and expression in relapsed or refractory acute myeloid leukemia. Blood *97*, 3605–3611.

Hirota, K., and Semenza, G.L. (2006). Regulation of angiogenesis by hypoxia-inducible factor 1. Crit. Rev. Oncol. Hematol. *59*, 15–26.

Hirsilä, M., Koivunen, P., Günzler, V., Kivirikko, K.I., and Myllyharju, J. (2003). Characterization of the human prolyl 4-hydroxylases that modify the hypoxia-inducible factor. J. Biol. Chem. *278*, 30772–30780.

Hlushchuk, R., Makanya, A.N., and Djonov, V. (2011). Escape mechanisms after antiangiogenic treatment, or why are the tumors growing again? Int. J. Dev. Biol. *55*, 563–567.

Hockel, M., Schlenger, K., Aral, B., Mitze, M., Schaffer, U., and Vaupel, P. (1996). Association between tumor hypoxia and malignant progression in advanced cancer of the uterine cervix. Cancer Res. *56*, 4509–4515.

Höckel, Mi., and Vaupel, P. (2001). Tumor hypoxia: Definitions and current clinical, biologic,

and molecular aspects. J. Natl. Cancer Inst. *93*, 266–276.

Hofmann, M., Guschel, M., Bernd, A., Bereiter-Hahn, J., Kaufmann, R., Tandi, C., Wiig, H., and Kippenberger, S. (2006). Lowering of tumor interstitial fluid pressure reduces tumor cell proliferation in a xenograft tumor model. Neoplasia *8*, 89–95.

Hofmann, U.B., Eggert, A.A.O., Blass, K., Bröcker, E.B., and Becker, J.C. (2003). Expression of matrix metalloproteinases in the microenvironment of spontaneous and experimental melanoma metastases reflects the requirements for tumor formation. Cancer Res. *63*, 8221–8225.

Holle, A.W., Kalafat, M., Ramos, A.S., Seufferlein, T., Kemkemer, R., and Spatz, J.P. (2017). Intermediate filament reorganization dynamically influences cancer cell alignment and migration. Sci. Rep. *7*, 1–14.

Horbelt, D., Denkis, A., and Knaus, P. (2012). A portrait of transforming growth factor β superfamily signalling: Background matters. Int. J. Biochem. Cell Biol. *44*, 469–474.

Horimoto, Y., Arakawa, A., Sasahara, N., Tanabe, M., Sai, S., Himuro, T., and Saito, M. (2016). Combination of cancer stem cell markers CD44 and CD24 is superior to ALDH1 as a prognostic indicator in breast cancer patients with distant metastases. PLoS One *11*, 1–11.

Hotchkiss, K.A., Ashton, A.W., Klein, R.S., Lenzi, M.L., Zhu, G.H., and Schwartz, E.L. (2003). Mechanisms by which tumor cells and monocytes expressing the angiogenic factor thymidine phosphorylase mediate human endothelial cell migration. Cancer Res. *63*, 527–533.

Hu, C., Wang, L., Chodosh, L. a, Keith, B., and Simon, M.C. (2003). Differential roles of hypoxia-inducible factor 1 alpha (HIF-1 alpha) and HIF-2 alpha in hypoxic gene regulation. Mol. Cell. Biol. *23*, 9361–9374.

Hu, J., Li, G., Zhang, P., Zhuang, X., and Hu, G. (2017a). A CD44v+ subpopulation of breast cancer stem-like cells with enhanced lung metastasis capacity. Cell Death Dis. *8*, 1–9.

Hu, X.-Q., Chen, M., Dasgupta, C., Xiao, D., Huang, X., Yang, S., and Zhang, L. (2017b). Chronic hypoxia upregulates DNA methyltransferase and represses large conductance Ca2+-activated K+channel function in ovine uterine arteries. Biol. Reprod. *96*, 424–434.

Huang, L.E., Gu, J., Schau, M., and Bunn, H.F. (1998). Regulation of hypoxia-inducible factor 1 is mediated by an O2-dependent degradation domain via the ubiquitin-proteasome

pathway. Proc. Natl. Acad. Sci. *95*, 7987–7992.

Hurwitz, H., Fehrenbacher, L., Novotny, W., Cartwright, T., Hainsworth, J., Heim, W., Berlin, J., Baron, A., Griffing, S., Holmgren, E., et al. (2004). Bevacizumab plus irinotecan, fluorouracil, and leucovorin for metastatic colorectal cancer. N. Engl. J. Med. *350*, 2335–2342.

Im, J.H., Fu, W., Wang, H., Bhatia, S.K., Hammer, D. a, Kowalska, M.A., and Muschel, R.J. (2004). Coagulation facilitates tumor cell spreading in the pulmonary vasculature during early metastatic colony formation. Cancer Res. *64*, 8613–8619.

Iyer, L.M., Tahiliani, M., Rao, A., and Aravind, L. (2009). Prediction of novel families of enzymes involved in oxidative and other complex modifications of bases in nucleic acids. Cell Cycle *8*, 1698–1710.

Jahangiri, A., Nguyen, A., Chandra, A., Sidorov, M.K., Yagnik, G., Rick, J., Han, S.W., Chen, W., Flanigan, P.M., Schneidman-Duhovny, D., et al. (2017). Cross-activating c-Met/β1 integrin complex drives metastasis and invasive resistance in cancer. Proc. Natl. Acad. Sci. 201701821.

Jain, R.K. (1988). Determinants of tumor blood flow: A review determinants of tumor blood flow. Cancer Res. *3890*, 2641–2658.

Jayson, G.C., Kerbel, R., Ellis, L.M., and Harris, A.L. (2016). Antiangiogenic therapy in oncology: current status and future directions. Lancet *388*, 518–529.

Jeong, H.-W., Hernández-Rodríguez, B., Kim, J., Kim, K.-P., Enriquez-Gasca, R., Yoon, J., Adams, S., Schöler, H.R., Vaquerizas, J.M., and Adams, R.H. (2017). Transcriptional regulation of endothelial cell behavior during sprouting angiogenesis. Nat. Commun. *8*, 726.

Jubb, A.M., Buffa, F.M., and Harris, A.L. (2010). Assessment of tumour hypoxia for prediction of response to therapy and cancer prognosis. J. Cell. Mol. Med. *14*, 18–29.

Jung, H.S., Han, J., Shi, H., Koo, S., Singh, H., Kim, H.J., Sessler, J.L., Lee, J.Y., Kim, J.H., and Kim, J.S. (2017). Overcoming the limits of hypoxia in photodynamic therapy: A carbonic anhydrase IX-targeted approach. J. Am. Chem. Soc. *139*, 7595–7602.

Kantarjian, H., Brien, S.O., Jabbour, E., Garcia-manero, G., Shan, J., Rios, M.B., Ravandi, F., Faderl, S., Kadia, T., Borthakur, G., et al. (2012). Improved survival in chronic myeloid leukemia since the introduction of imatinib therapy: a single-institution historical experience Improved survival in chronic myeloid leukemia since the introduction of imatinib therapy : a

single-institution historica. Blood *119*, 1981–1987.

Kao, W. Te, Lin, C.Y., Lee, L.T., Lee, P.P.H., Hung, C.C., Lin, Y.S., Chen, S.H., Ke, F.C., Hwang, J.J., and Lee, M.T. (2008). Investigation of MMP-2 and -9 in a highly invasive A431 tumor cell sub-line selected from a boyden chamber assay. Anticancer Res. *28*, 2109–2120.

Kaplan, R.N., Rafii, S., and Lyden, D. (2006). Preparing the “soil”: The premetastatic niche. Cancer Res. *66*, 11089–11093.

Kawahara, N., Ono, M., Taguhi, K.I., Okamoto, M., Shimada, M., Takenaka, K., Hayashi, K., Mosher, D.F., Sugimachi, K., Tsuneyoshi, M., et al. (1998). Enhanced expression of thrombospondin-1 and hypovascularity in human cholangiocarcinoma. Hepatology *28*, 1512–1517.

Keck, P., Hauser, S., Krivi, G., Sanzo, K., Warren, T., Feder, J., and Connolly, D. (1989). Vascular permeability factor, an endothelial cell mitogen related to PDGF. Science (80-.). *246*, 1309–1312.

Kim, H.-S., Oh, S.H., Kim, J.-H., Kim, J.-Y., Kim, D.-H., Lee, S.-J., Choi, S.-U., Park, K.M., Ryoo, Z.Y., Park, T.S., et al. (2017). MLL-TET1 fusion protein promotes immortalization of myeloid progenitor cells and leukemia development. Haematologica *102*, e434–e437.

Kim, I., Kim, H.G., Moon, S.O., Chae, S.W., So, J.N., Koh, K.N., Ahn, B.C., and Koh, G.Y. (2000). Angiopoietin-1 induces endothelial cell sprouting through the activation of focal adhesion kinase and plasmin secretion. Circ. Res. *86*, 952–959.

Kim, J. -w., Gao, P., Liu, Y.-C., Semenza, G.L., and Dang, C. V. (2007). Hypoxia-inducible factor 1 and dysregulated c-Myc cooperatively induce vascular endothelial growth factor and metabolic switches hexokinase 2 and pyruvate dehydrogenase kinase 1. Mol. Cell. Biol. *27*, 7381–7393.

Kim, L.S., Huang, S., Lu, W., Lev, D.C., and Price, J.E. (2004). Vascular endothelial growth factor expression promotes the growth of breast cancer brain metastases in nude mice. Clin. Exp. Metastasis *21*, 107–118.

Kim, M.Y., Oskarsson, T., Acharyya, S., Nguyen, D.X., Zhang, X.H.F., Norton, L., and Massagué, J. (2009). Tumor self-seeding by circulating cancer cells. Cell *139*, 1315–1326.

Kindler, H.L., Niedzwiecki, D., Hollis, D., Sutherland, S., Schrag, D., Hurwitz, H., Innocenti, F., Mulcahy, M.F., O’Reilly, E., Wozniak, T.F., et al. (2010). Gemcitabine plus bevacizumab compared with gemcitabine plus placebo in patients with advanced pancreatic cancer:

Phase III trial of the Cancer and Leukemia Group B (CALGB 80303). J. Clin. Oncol. *28*, 3617–3622.

Klein, C.A. (2009). Parallel progression of primary tumours and metastases. Nat. Rev. Cancer *9*, 302–312.

Koh, K.P., and Rao, A. (2013). DNA methylation and methylcytosine oxidation in cell fate decisions. Curr. Opin. Cell Biol. *25*, 152–161.

Koh, M.Y., Lemos, R., Liu, X., and Powis, G. (2011). The hypoxia-associated factor switches cells from HIF-1α- to HIF-2α-dependent signaling promoting stem cell characteristics, aggressive tumor growth and invasion. Cancer Res. *71*, 4015–4027.

Kohli, R.M., and Zhang, Y. (2013). TET enzymes, TDG and the dynamics of DNA demethylation. Nature *502*, 472–479.

Kopetz, S., Hoff, P.M., Morris, J.S., Wolff, R.A., Eng, C., Glover, K.Y., Adinin, R., Overman, M.J., Valero, V., Wen, S., et al. (2010). Phase II trial of infusional fluorouracil, irinotecan, and bevacizumab for metastatic colorectal cancer: Efficacy and circulating angiogenic biomarkers associated with therapeutic resistance. J. Clin. Oncol. *28*, 453–459.

Kubo, T., Shimose, S., Fujimori, J., Arihiro, K., and Ochi, M. (2013). Diversity of angiogenesis among malignant bone tumors. Mol. Clin. Oncol. *1*, 131–136.

Kudo-Saito, C., Shirako, H., Takeuchi, T., and Kawakami, Y. (2009). Cancer metastasis is accelerated through immunosuppression during Snail-induced EMT of cancer cells. Cancer Cell *15*, 195–206.

Landgrave-Gomez, J., Mercado-Gomez, O., and Guevara-Guzman, R. (2015). Epigenetic mechanisms in neurological and neurodegenerative diseases. Front. Cell. Neurosci. *9*, 1–11.

Laukka, T., Mariani, C.J., Ihantola, T., Cao, J.Z., Hokkanen, J., Kaelin, W.G., Godley, L.A., and Koivunen, P. (2016). Fumarate and succinate regulate expression of hypoxia-inducible genes via TET enzymes. J. Biol. Chem. *291*, 4256–4265.

Lee, S., Chen, T.T., Barber, C.L., Jordan, M.C., Murdock, J., Desai, S., Ferrara, N., Nagy, A., Roos, K.P., and Iruela-Arispe, M.L. (2007). Autocrine VEGF signaling is required for vascular homeostasis. Cell *130*, 691–703.

Lenferink, A.E.G., Cantin, C., Nantel, A., Wang, E., Durocher, Y., Banville, M., Paul-Roc, B., Marcil, A., Wilson, M.R., and O'Connor-Mccourt, M.D. (2010). Transcriptome profiling of a

TGF-B-induced epithelial-to-mesenchymal transition reveals extracellular clusterin as a target for therapeutic antibodies. Oncogene *29*, 831–844.

Leung, D., Cachianes, G., Kuang, W., Goeddel, D., and Ferrara, N. (1989). Vascular endothelial growth factor is a secreted angiogenic mitogen. Science (80-.). *246*, 1306–1309.

Levina, V., Marrangoni, A., Wang, T., Parikh, S., Su, Y., Herberman, R., Lokshin, A., and Gorelik, E. (2010). Elimination of human lung cancer stem cells through targeting of the stem cell factor-c-Kit autocrine signaling loop. Cancer Res. *70*, 338–346.

Li, M.C., Hertz, R., and Bergenstal, D.M. (1958). Therapy of choriocarcinoma and related trophoblastic tumors with folic acid and purine antagonists. N. Engl. J. Med. *259*, 66–74.

Li, W., Ma, H., Zhang, J., Zhu, L., Wang, C., and Yang, Y. (2017). Unraveling the roles of CD44/CD24 and ALDH1 as cancer stem cell markers in tumorigenesis and metastasis. Sci. Rep. *7*, 1–15.

Liu, Q., Liu, L., Zhao, Y., Zhang, J., Wang, D., Chen, J., He, Y., Wu, J., Zhang, Z., and Liu, Z. (2011). Hypoxia induces genomic DNA demethylation through the activation of HIF-1 and transcriptional upregulation of MAT2A in hepatoma cells. Mol. Cancer Ther. *10*, 1113–1123.

Liu, S., Cong, Y., Wang, D., Sun, Y., Deng, L., Liu, Y., Martin-Trevino, R., Shang, L., McDermott, S.P., Landis, M.D., et al. (2014). Breast cancer stem cells transition between epithelial and mesenchymal states reflective of their normal counterparts. Stem Cell Reports *2*, 78–91.

Liu, X.-D., Hoang, A., Zhou, L., Kalra, S., Yetil, A., Sun, M., Ding, Z., Zhang, X., Bai, S., German, P., et al. (2015). Resistance to antiangiogenic therapy is associated with an immunosuppressive tumor microenvironment in metastatic renal cell carcinoma. Cancer Immunol. Res. *3*, 1017–1029.

Llovet JM, Ricci S, Mazzaferro V, Hilgard P, Gane E, Blanc JF, de Oliveira AC, Santoro A, Raoul JL, Forner A, et al. (2008). Sorafenib in advanced hepatocellular carcinoma. N Engl J Med *359*, 378–390.

Lombaerts, M., Van Wezel, T., Philippo, K., Dierssen, J.W.F., Zimmerman, R.M.E., Oosting, J., Van Eijk, R., Eilers, P.H., Van De Water, B., Cornelisse, C.J., et al. (2006). E-cadherin transcriptional downregulation by promoter methylation but not mutation is related to epithelial-tomesenchymal transition in breast cancer cell lines. Br. J. Cancer *94*, 661–671.

Los, M., Roodhart, J.M.L., and Voest, E.E. (2007). Target practice: Lessons from phase III

trials with bevacizumab and vatalanib in the treatment of advanced colorectal cancer. Oncologist *12*, 443–450.

Louie, E., Nik, S., Chen, J. suei, Schmidt, M., Song, B., Pacson, C., Chen, X.F., Park, S., Ju, J., and Chen, E.I. (2010). Identification of a stem-like cell population by exposing metastatic breast cancer cell lines to repetitive cycles of hypoxia and reoxygenation. Breast Cancer Res. *12*.

Lu, K. V, and Bergers, G. (2013). Mechanisms of evasive resistance to anti-VEGF therapy in glioblastoma. CNS Oncol. *2*, 49–65.

Lu, K. V., Chang, J.P., Parachoniak, C.A., Pandika, M.M., Aghi, M.K., Meyronet, D., Isachenko, N., Fouse, S.D., Phillips, J.J., Cheresh, D.A., et al. (2012). VEGF inhibits tumor cell invasion and mesenchymal transition through a MET/VEGFR2 complex. Cancer Cell *22*, 21–35.

Lu, Y., Chu, A., Turker, M.S., and Glazer, P.M. (2011). Hypoxia-induced epigenetic regulation and silencing of the BRCA1 promoter. Mol. Cell. Biol. *31*, 3339–3350.

Lundgren, K., Nordenskjöld, B., and Landberg, G. (2009). Hypoxia, Snail and incomplete epithelial-mesenchymal transition in breast cancer. Br. J. Cancer *101*, 1769–1781.

Magee, J.A., Piskounova, E., and Morrison, S.J. (2012). Cancer stem cells: Impact, heterogeneity, and uncertainty. Cancer Cell *21*, 283–296.

Malladi, S., Macalinao, D.G., Jin, X., He, L., Basnet, H., Zou, Y., de Stanchina, E., and Massagué, J. (2016). Metastatic latency and immune evasion through autocrine inhibition of WNT. Cell *165*, 45–60.

Mani, S.A., Guo, W., Liao, M.J., Eaton, E.N., Ayyanan, A., Zhou, A.Y., Brooks, M., Reinhard, F., Zhang, C.C., Shipitsin, M., et al. (2008). The epithelial-mesenchymal transition generates cells with properties of stem cells. Cell *133*, 704–715.

Manrow R., C.R. (2010). Cancer fact sheet (National Institutes of Health).

Mariani, C.J., Vasanthakumar, A., Madzo, J., Yesilkanal, A., Bhagat, T., Yu, Y., Bhattacharyya, S., Wenger, R.H., Cohn, S.L., Nanduri, J., et al. (2014a). TET1-mediated hydroxymethylation facilitates hypoxic gene induction in neuroblastoma. Cell Rep. *7*, 1343–1352.

Martínez-Sáez, O., Gajate Borau, P., Alonso-Gordoa, T., Molina-Cerrillo, J., and Grande, E. (2017). Targeting HIF-2 α in clear cell renal cell carcinoma: A promising therapeutic strategy.

Crit. Rev. Oncol. Hematol. *111*, 117–123.

Mathot, P., Grandin, M., Devailly, G., Souaze, F., Cahais, V., Moran, S., Campone, M., Herceg, Z., Esteller, M., Juin, P., et al. (2017). DNA methylation signal has a major role in the response of human breast cancer cells to the microenvironment. Oncogenesis *6*, e390.

Maxwell, P.H., Wlesener, M.S., Chang, G.W., Clifford, S.C., Vaux, E.C., Cockman, M.E., Wykoff, C.C., Pugh, C.W., Maher, E.R., and Ratcliffe, P.J. (1999). The tumour suppressor protein VHL targets hypoxia-inducible factors for oxygen-dependent proteolysis. Nature *399*, 271–275.

McDonnell, F., Irnaten, M., Clark, A.F., O'Brien, C.J., and Wallace, D.M. (2016). Hypoxia-induced changes in DNA methylation alter RASAL1 and TGFβ1 expression in human trabecular meshwork cells. PLoS One *11*, 1–24.

McRonald, F.E., Morris, M.R., Gentle, D., Winchester, L., Baban, D., Ragoussis, J., Clarke, N.W., Brown, M.D., Kishida, T., Yao, M., et al. (2009). CpG methylation profiling in VHL related and VHL unrelated renal cell carcinoma. Mol. Cancer *8*, 1–11.

Mendez, M.G., Kojima, S.I., and Goldman, R.D. (2010). Vimentin induces changes in cell shape, motility, and adhesion during the epithelial to mesenchymal transition. FASEB J. *24*, 1838–1851.

Mikami, S., Katsube, K.I., Oya, M., Ishida, M., Kosaka, T., Mizuno, R., Mukai, M., and Okada, Y. (2011). Expression of snail and slug in renal cell carcinoma: E-cadherin repressor snail is associated with cancer invasion and prognosis. Lab. Investig. *91*, 1443–1458.

Miller, K., Wang, M., Gralow, J., Dickler, M., Cobleigh, M., Perez, E.A., Shenkier, T., Cella, D., and Davidson, N.E. (2007). Paclitaxel plus bevacizumab versus paclitaxel alone for metastatic breast cancer. N. Engl. J. Med. *357*, 2666–2676.

Miller, K.D., Chap, L.I., Holmes, F.A., Cobleigh, M.A., Marcom, P.K., Fehrenbacher, L., Dickler, M., Overmoyer, B.A., Reimann, J.D., Sing, A.P., et al. (2005). Randomized phase III trial of capecitabine compared with bevacizumab plus capecitabine in patients with previously treated metastatic breast cancer. J. Clin. Oncol. *23*, 792–799.

Minamishima, Y.A., Moslehi, J., Padera, R.F., Bronson, R.T., Liao, R., and Kaelin, W.G. (2009). A feedback loop involving the Phd3 prolyl hydroxylase tunes the mammalian hypoxic response in vivo. Mol. Cell. Biol. *29*, 5729–5741.

Mingyuan, X., Qianqian, P., Shengquan, X., Chenyi, Y., Rui, L., Yichen, S., and Jinghong,

X. (2018). Hypoxia-inducible factor-1a activates transforming growth factor-b/Smad signaling and increases collagen deposition in dermal fibroblasts. Oncotarget *9*, 3188–3197.

Minn, A.J., Gupta, G.P., Siegel, P.M., Bos, P.D., Shu, W., Giri, D.D., Viale, A., Olshen, A.B., Gerald, W.L., and Massagué, J. (2005). Genes that mediate breast cancer metastasis to lung. Nature *436*, 518–524.

Mohlin, S., Hamidian, A., and Pahlman, S. (2013). HIF2A and IGF2 expression correlates in human neuroblastoma cells and normal immature sympathetic neuroblasts. Neoplasia *15*, 328-IN38.

Montgomery, R.B., Mostaghel, E. a, Vessella, R., Hess, D.L., Kalhorn, T.F., Higano, C.S., True, L.D., and Nelson, P.S. (2008). Maintenance of intratumoral androgens in metastatic prostate cancer: A mechanism for castration-resistant tumor growth. Cancer Res. *68*, 4447–4454.

Moore, L.E., Nickerson, M.L., Brennan, P., Toro, J.R., Jaeger, E., Rinsky, J., Han, S.S., Zaridze, D., Matveev, V., Janout, V., et al. (2011). Von Hippel-Lindau (VHL) inactivation in sporadic clear cell renal cancer: Associations with germline VHL polymorphisms and etiologic risk factors. PLoS Genet. *7*.

Morel, A.-P., Lièvre, M., Thomas, C., Hinkal, G., Ansieau, S., and Puisieux, A. (2008). Generation of breast cancer stem cells through epithelial-mesenchymal transition. PLoS One *3*, e2888.

Motzer, R.J., Hutson, T.E., Tomczak, P., Michaelson, M.D., Bukowski, R.M., Rixe, O., Oudard, S., Negrier, S., Szczylik, C., Kim, S.T., et al. (2007). Sunitinib versus interferon alfa in metastatic renal-cell carcinoma. N. Engl. J. Med. *356*, 115–124.

Nakaya, Y., Sukowati, E.W., Wu, Y., and Sheng, G. (2008). RhoA and microtubule dynamics control cell-basement membrane interaction in EMT during gastrulation. Nat. Cell Biol. *10*, 765–775.

Nakazawa, M.S., Eisinger-Mathason, T.S.K., Sadri, N., Ochocki, J.D., Gade, T.P.F., Amin, R.K., and Simon, M.C. (2016). Epigenetic re-expression of HIF-2α suppresses soft tissue sarcoma growth. Nat. Commun. *7*, 1–13.

Nguyen, A., Yoshida, M., Goodarzi, H., and Tavazoie, S.F. (2016). Highly variable cancer subpopulations that exhibit enhanced transcriptome variability and metastatic fitness. Nat. Commun. *7*, 1–13.

Nguyen, D.X., Bos, P.D., and Massagué, J. (2009). Metastasis: From dissemination to organ-specific colonization. Nat. Rev. Cancer *9*, 274–284.

Nissen, N.N., Polverini, P.J., Koch, A.E., Volin, M. V, Gamelli, R.L., and DiPietro, L.A. (1998). Vascular endothelial growth factor mediates angiogenic activity during the proliferative phase of wound healing. Am. J. Pathol. *152*, 1445–1452.

Noman, M.Z., Desantis, G., Janji, B., Hasmim, M., Karray, S., Dessen, P., Bronte, V., and Chouaib, S. (2014). PD-L1 is a novel direct target of HIF-1α, and its blockade under hypoxia enhanced MDSC-mediated T cell activation. J. Exp. Med. *211*, 781–790.

Norden, A.D., Young, G.S., Setayesh, K., Muzikansky, A., Ciampa, A.S., Ebbeling, L.G., Levy, B., Drappatz, J., Kesari, S., and Wen, P.Y. (2008). Bevacizumab for recurrent malignant gliomas: Efficacy, toxicity, and patterns of recurrencesymbol. Neurology *70*, 779–787.

Nowak, D.G., Woolard, J., Amin, E.M., Konopatskaya, O., Saleem, M.A., Churchill, A.J., Ladomery, M.R., Harper, S.J., and Bates, D.O. (2008). Expression of pro- and anti-angiogenic isoforms of VEGF is differentially regulated by splicing and growth factors. J. Cell Sci. *121*, 3487–3495.

Nowell, P.C., and Hungerford, D.A. (1961). Chromosome studies in human leukemia. II. Chronic granulocytic leukemia. J. Natl. Cancer Inst. *27*, 1013–1035.

O'Reilly, M.S., Boehm, T., Shing, Y., Fukai, N., Vasios, G., Lane, W.S., Flynn, E., Birkhead, J.R., Olsen, B.R., and Folkman, J. (1997). Endostatin: an endogenous inhibitor of angiogenesis and tumor growth. Cell *88*, 277–285.

Ogunwobi, O.O., Puszyk, W., Dong, H.J., and Liu, C. (2013). Epigenetic upregulation of HGF and c-Met drives metastasis in hepatocellular carcinoma. PLoS One *8*, 1–12.

Okuno, Y., Nakamura-Ishizu, A., Kishi, K., Suda, T., and Kubota, Y. (2011). Bone marrow-derived cells serve as proangiogenic macrophages but not endothelial cells in wound healing. Blood *117*, 5264–5272.

Orimo, A., Gupta, P.B., Sgroi, D.C., Arenzana-Seisdedos, F., Delaunay, T., Naeem, R., Carey, V.J., Richardson, A.L., and Weinberg, R.A. (2005). Stromal fibroblasts present in invasive human breast carcinomas promote tumor growth and angiogenesis through elevated SDF-1/CXCL12 secretion. Cell *121*, 335–348.

Otrock, Z.K., Hatoum, H.A., Awada, A.H., Ishak, R.S., and Shamseddine, A.I. (2009).

Hypoxia-inducible factor in cancer angiogenesis: Structure, regulation and clinical perspectives. Crit. Rev. Oncol. Hematol. *70*, 93–102.

Padua, D., and Massagué, J. (2009). Roles of TGFβ in metastasis. Cell Res. *19*, 89–102.

Pàez-Ribes, M., Allen, E., Hudock, J., Takeda, T., Okuyama, H., Viñals, F., Inoue, M., Bergers, G., Hanahan, D., and Casanovas, O. (2009a). Antiangiogenic therapy elicits malignant progression of tumors to increased local invasion and distant metastasis. Cancer Cell *15*, 220–231.

Paget, S. (1889). The distribution of secondary growths in cancer of the breast. Lancet *133*, 571–573.

Pantel, K., and Brakenhoff, R.H. (2004). Dissecting the metastatic cascade. Nat. Rev. Cancer *4*, 448–456.

Papavramidou, N., Papavramidis, T., and Demetriou, T. (2010). Ancient Greek and Greco-Roman methods in modern surgical treatment of cancer. Ann. Surg. Oncol. *17*, 665–667.

Peinado, H., Quintanilla, M., and Cano, A. (2003). Transforming growth factor β-1 induces Snail transcription factor in epithelial cell lines. Mechanisms for epithelial mesenchymal transitions. J. Biol. Chem. *278*, 21113–21123.

Pellikainen, J.M. (2004). Expression of matrix metalloproteinase (MMP)-2 and MMP-9 in breast cancer with a special reference to activator protein-2, HER2, and prognosis. Clin. Cancer Res. *10*, 7621–7628.

Perren, T.J., Swart, A.M., Pfisterer, J., Ledermann, J.A., Pujade-Lauraine, E., Kristensen, G., Carey, M.S., Beale, P., Cervantes, A., Kurzeder, C., et al. (2011). A phase 3 trial of bevacizumab in ovarian cancer. N. Engl. J. Med. *365*, 2484–2496.

Pierre, C.C., Longo, J., Bassey-Archibong, B.I., Hallett, R.M., Milosavljevic, S., Beatty, L., Hassell, J.A., and Daniel, J.M. (2015a). Methylation-dependent regulation of hypoxia inducible factor-1 alpha gene expression by the transcription factor Kaiso. Biochim. Biophys. Acta - Gene Regul. Mech. *1849*, 1432–1441.

Pisco, A.O., Brock, A., Zhou, J., Moor, A., Mojtahedi, M., Jackson, D., and Huang, S. (2013). Non-Darwinian dynamics in therapy-induced cancer drug resistance. Nat. Commun. *4*.

Polyak, K., and Weinberg, R.A. (2009). Transitions between epithelial and mesenchymal states: Acquisition of malignant and stem cell traits. Nat. Rev. Cancer *9*, 265–273.

Poole, T.J., Finkelstein, E.B., and Cox, C.M. (2001). The role of FGF and VEGF in angioblast

induction and migration during vascular development. Dev. Dyn. *220*, 1–17.

Prager, G.W., Poettler, M., Unseld, M., and Zielinski, C.C. (2012). Angiogenesis in cancer: Anti-VEGF escape mechanisms. Transl. Lung Cancer Res. *1*, 14–25.

Presta, L., Chen, H., O'Connor, S., Chisholm, V., Meng, Y., Krummen, L., Winkler, M., and Ferrara, N. (1997). Humanization of an anti-vascular endothelial growth factor monoclonal antibody for the therapy of solid tumors and other disorders. Cancer Res. *57*, 4593–4599.

Qian, X., Anzovino, A., Kim, S., Suyama, K., Yao, J., Hulit, J., Agiostratidou, G., Chandiramani, N., McDaid, H.M., Nagi, C., et al. (2014). N-cadherin/FGFR promotes metastasis through epithelial-tomesenchymal transition and stem/progenitor cell-like properties. Br. Dent. J. *217*, 3411–3421.

Qin, N., De Cubas, A.A., Garcia-Martin, R., Richter, S., Peitzsch, M., Menschikowski, M., Lenders, J.W.M., Timmers, H.J.L.M., Mannelli, M., Opocher, G., et al. (2014). Opposing effects of HIF1α and HIF2α on chromaffin cell phenotypic features and tumor cell proliferation: Insights from MYC-associated factor X. Int. J. Cancer *135*, 2054–2064.

Quail, D., and Joyce, J. (2013). Microenvironmental regulation of tumor progression and metastasis. Nat. Med. *19*, 1423–1437.

Rafii, S., Lyden, D., Benezra, R., Hattori, K., and Heissig, B. (2002). Vascular and haematopoietic stem cells: Novel targets for anti-angiogenesis therapy? Nat. Rev. Cancer *2*, 826–835.

Rapisarda, A., and Melillo, G. (2009). Role of the hypoxic tumor microenvironment in the resistance to anti-angiogenic therapies. Drug Resist. Updat. *12*, 74–80.

Raval, R.R., Lau, K.W., Tran, M.G.B., Sowter, H.M., Mandriota, S.J., Li, J.-L., Pugh, C.W., Maxwell, P.H., Harris, A.L., and Ratcliffe, P.J. (2005). Contrasting properties of hypoxia-inducible factor 1 (HIF-1) and HIF-2 in von Hippel-Lindau-associated renal cell carcinoma. Mol. Cell. Biol. *25*, 5675–5686.

Rawłuszko-Wieczorek, A.A., Horbacka, K., Krokowicz, P., Misztal, M., and Jagodziński, P.P. (2014). Prognostic potential of DNA methylation and transcript levels of HIF1A and EPAS1 in colorectal cancer. Mol. Cancer Res. *12*, 1112–1127.

Razorenova, O. V., Finger, E.C., Colavitti, R., Chernikova, S.B., Boiko, A.D., Chan, C.K.F., Krieg, A., Bedogni, B., LaGory, E., Weissman, I.L., et al. (2011). *VHL* loss in renal cell carcinoma leads to up-regulation of CUB domain-containing protein 1 to stimulate PKCδ-

driven migration. Proc. Natl. Acad. Sci. *108*, 1931–1936.

Reményi, A., Schöler, H.R., and Wilmanns, M. (2004). Combinatorial control of gene expression. Nat. Struct. Mol. Biol. *11*, 812–815.

Rhee, H., Nahm, J.H., Kim, H., Choi, G.H., Yoo, J.E., Lee, H.S., Koh, M.J., and Park, Y.N. (2016). Poor outcome of hepatocellular carcinoma with stemness marker under hypoxia: Resistance to transarterial chemoembolization. Mod. Pathol. *29*, 1038–1049.

Rhee, I., Bachman, K.E., Park, B.H., Jair, K.W., Yen, R.W.C., Schuebel, K.E., Cui, H., Feinberg, A.P., Lengauer, C., Kinzler, K.W., et al. (2002). DNMT1 and DNMT3b cooperate to silence genes in human cancer cells. Nature *416*, 552–556.

Ricardo, S., Vieira, A.F., Gerhard, R., Leitao, D., Pinto, R., Cameselle-Teijeiro, J.F., Milanezi, F., Schmitt, F., and Paredes, J. (2011). Breast cancer stem cell markers CD44, CD24 and ALDH1: expression distribution within intrinsic molecular subtype. J. Clin. Pathol. *64*, 937–946.

Riemann, A., Reime, S., and Thews, O. (2017). Tumor acidosis and hypoxia differently modulate the inflammatory program: Measurements in vitro and in vivo. Neoplasia *19*, 1033–1042.

Robinson, C.M., Neary, R., Levendale, A., Watson, C.J., and Baugh, J.A. (2012). Hypoxia-induced DNA hypermethylation in human pulmonary fibroblasts is associated with Thy-1 promoter methylation and the development of a pro-fibrotic phenotype. Respir. Res. *13*, 1–9.

Rofstad, E.K., Gaustad, J.V., Egeland, T.A.M., Mathiesen, B., and Galappathi, K. (2010). Tumors exposed to acute cyclic hypoxic stress show enhanced angiogenesis, perfusion and metastatic dissemination. Int. J. Cancer *127*, 1535–1546.

Rosenberg, B., Van Camp, L., Trosko, J.E., and Mansour, V.H. (1969). Platinum compounds: a new class of potent antitumour agents. Nature *222*, 385–386.

Sadikovic, B., Andrews, J., Carter, D., Robinson, J., and Rodenhiser, D.I. (2008). Genome-wide H3K9 histone acetylation profiles are altered in benzopyrene-treated MCF7 breast cancer cells. J. Biol. Chem. *283*, 4051–4060.

Safran, M., Kim, W.Y., O'Connell, F., Flippin, L., Gunzler, V., Horner, J.W., DePinho, R.A., and Kaelin, W.G. (2006). Mouse model for noninvasive imaging of HIF prolyl hydroxylase activity: Assessment of an oral agent that stimulates erythropoietin production. Proc. Natl.

Acad. Sci. *103*, 105–110.

Sakurai, Y., Ohgimoto, K., Kataoka, Y., Yoshida, N., and Shibuya, M. (2005). Essential role of Flk-1 (VEGF receptor 2) tyrosine residue 1173 in vasculogenesis in mice. Proc. Natl. Acad. Sci. *102*, 1076–1081.

Santoyo-Ramos, P., Likhatcheva, M., García-Zepeda, E.A., Cristina Castañeda-Patlan, M., and Robles-Flores, M. (2014). Hypoxia-inducible factors modulate the stemness and malignancy of colon cancer cells by playing opposite roles in canonical Wnt signaling. PLoS One *9*.

van der Schaft, D.W.J., Seftor, R.E.B., Seftor, E.A., Hess, A.R., Gruman, L.M., Kirschmann, D.A., Yokoyama, Y., Griffioen, A.W., and Hendrix, M.J.C. (2004). Effects of angiogenesis inhibitors on vascular network formation by human endothelial and melanoma cells. J. Natl. Cancer Inst. *96*, 1473–1477.

Scharpfenecker, M. (2005). The Tie-2 ligand Angiopoietin-2 destabilizes quiescent endothelium through an internal autocrine loop mechanism. J. Cell Sci. *118*, 771–780.

Schmierer, B., and Hill, C.S. (2007). TGFβ-SMAD signal transduction: Molecular specificity and functional flexibility. Nat. Rev. Mol. Cell Biol. *8*, 970–982.

Schoumacher, M., Goldman, R.D., Louvard, D., and Vignjevic, D.M. (2010). Actin, microtubules, and vimentin intermediate filaments cooperate for elongation of invadopodia. J. Cell Biol. *189*, 541–556.

Seidel, S., Garvalov, B.K., Wirta, V., Von Stechow, L., Schänzer, A., Meletis, K., Wolter, M., Sommerlad, D., Henze, A.T., Nistér, M., et al. (2010). A hypoxic niche regulates glioblastoma stem cells through hypoxia inducible factor 2α. Brain *133*, 983–995.

Seidel, S., Garvalov, B.K., and Acker, T. (2015). Isolation and culture of primary glioblastoma cells from human tumor specimens. In Methods in Molecular Biology (Clifton, N.J.), pp. 263–275.

Semenza, G.L. (2010). HIF-1: upstream and downstream of cancer metabolism. Curr. Opin. Genet. Dev. *20*, 51–56.

Semenza, G.L. (2012). Molecular mechanisms mediating metastasis of hypoxic breast cancer cells. Trends Mol. Med. *18*, 534–543.

Semenza, G.L. (2013). Hypoxia-inducible factors in physiology and dedicine. Cell *148*, 399–408.

Senger, D., Galli, S., Dvorak, A., Perruzzi, C., Harvey, V., and Dvorak, H. (1983). Tumor cells secrete a vascular permeability factor that promotes accumulation of ascites fluid. Science (80-.). *219*, 983–985.

Seo, A.N., Lee, H.J., Kim, E.J., Jang, M.H., Kim, Y.J., Kim, J.H., Kim, S.-W., Ryu, H.S., Park, I.A., Im, S., et al. (2016). Expression of breast cancer stem cell markers as predictors of prognosis and response to trastuzumab in HER2-positive breast cancer. Br. J. Cancer *114*, 1109–1116.

Shahrzad, S., Bertrand, K., Minhas, K., and Coomber, B.L. (2007). Induction of DNA hypomethylation by tumor hypoxia. Epigenetics *2*, 119–125.

Sharma, S., Kelly, T.K., and Jones, P.A. (2009). Epigenetics in cancer. Carcinogenesis *31*, 27–36.

Shi, L., Sun, L., Li, Q., Liang, J., Yu, W., Yi, X., Yang, X., Li, Y., Han, X., Zhang, Y., et al. (2011). Histone demethylase JMJD2B coordinates H3K4/H3K9 methylation and promotes hormonally responsive breast carcinogenesis. Proc. Natl. Acad. Sci. *108*, 7541–7546.

Shukla S, Robey RW, Bates SE, A.S. (2009). Sunitinib (Sutent®, SU11248), a small – molecule receptor tyrosine kinase inhibitor, blocks functions of ATP-binding cassette (ABC) transporters P-ghycoprotein (ABCB1) and ABCG2. Drug Metab. Dispos. *37*, 359–365.

Siddiq, A., Aminova, L.R., Troy, C.M., Suh, K., Messer, Z., Semenza, G.L., and Ratan, R.R. (2009). Selective inhibition of hypoxia-inducible factor (HIF) prolyl-hydroxylase 1 mediates neuroprotection against normoxic oxidative death via HIF- and CREB-independent pathways. J. Neurosci. *29*, 8828–8838.

Sin, W.C., and Lim, C.L. (2017). Breast cancer stem cells - from origins to targeted therapy. Stem Cell Investig. *4*, 96–96.

Singh, A., and Settleman, J. (2010). EMT, cancer stem cells and drug resistance: An emerging axis of evil in the war on cancer. Oncogene *29*, 4741–4751.

Singh, M., Couto, S.S., Forrest, W.F., Lima, A., Cheng, J.H., Molina, R., Long, J.E., Hamilton, P., McNutt, A., Kasman, I., et al. (2012). Anti-VEGF antibody therapy does not promote metastasis in genetically engineered mouse tumor models. J Pathol *227*, 417–430.

Sproul, D., Gilbert, N., and Bickmore, W.A. (2005). The role of chromatin structure in regulating the expression of clustered genes. Nat. Rev. Genet. *6*, 775–781.

Stichel, D., Middleton, A.M., Müller, B.F., Depner, S., Klingmüller, U., Breuhahn, K., and

Matthäus, F. (2017). An individual-based model for collective cancer cell migration explains speed dynamics and phenotype variability in response to growth factors. Syst. Biol. Appl. *3*, 5.

Stirzaker, C., Millar, D.S., Paul, C.L., Warnecke, P.M., Harrison, J., Vincent, P.C., Frommer, M., and Clark, S.J. (1997). Extensive DNA methylation spanning the Rb promoter in retinoblastoma tumors. Cancer Res. *57*, 2229–2237.

Stratmann, a, Acker, T., Burger, a M., Amann, K., Risau, W., and Plate, K.H. (2001). Differential inhibition of tumor angiogenesis by tie2 and vascular endothelial growth factor receptor-2 dominant-negative receptor mutants. Int. J. Cancer *91*, 273–282.

Strebhardt, K., and Ullrich, A. (2008). Paul Ehrlich's magic bullet concept: 100 years of progress. Nat. Rev. Cancer *8*, 473–480.

Su, H.-T., Weng, C.-C., Hsiao, P.-J., Chen, L.-H., Kuo, T.-L., Chen, Y.-W., Kuo, K.-K., and Cheng, K.-H. (2013). Stem cell marker Nestin is critical for TGF1-mediated tumor progression in pancreatic cancer. Mol. Cancer Res. *11*, 768–779.

Su, W.H., Chuang, P.C., Huang, E.Y., and Yang, K.D. (2012). Radiation-induced increase in cell migration and metastatic potential of cervical cancer cells operates via the K-ras pathway. Am. J. Pathol. *180*, 862–871.

Sudhakar, A. (2010). History of cancer, ancient and modern treatment methods. J Cancer Sci Ther. *1*, 1–4.

Sun, Y., Wang, J.W., Liu, Y.Y., Yu, Q.T., Zhang, Y.P., Li, K., Xu, L.Y., Luo, S.X., Qin, F.Z., Chen, Z.T., et al. (2013). Long-term results of a randomized, double-blind, and placebo-controlled phase III trial: Endostar (rh-endostatin) versus placebo in combination with vinorelbine and cisplatin in advanced non-small cell lung cancer. Thorac. Cancer *4*, 440–448.

Takahashi, K., Ehata, S., Koinuma, D., Morishita, Y., Soda, M., Mano, H., and Miyazono, K. (2018). Pancreatic tumor microenvironment confers highly malignant properties on pancreatic cancer cells. Oncogene *37*, 2757–2772.

Talmadge, J.E., and Fidler, I.J. (2010). The biology of cancer metastasis: Historical perspective. Cancer Res. *70*, 5649–5669.

Tan, W., Zhang, W., Strasner, A., Grivennikov, S., Cheng, J.Q., Hoffman, R.M., and Karin, M. (2011). Tumour-infiltrating regulatory T cells stimulate mammary cancer metastasis

through RANKL–RANK signalling. Nature *470*, 548–553.

Tanaka, Y., Shibata, M.A., Morimoto, J., and Otsuki, Y. (2011). Sunitinib suppresses tumor growth and metastases in a highly metastatic mouse mammary cancer model. Anticancer Res. *31*, 1225–1234.

Teicher, B.A., Herman, T.S., Holden, S.A., Wang, Y., Pfeffer, M.R., Crawford, J.W., and Frei, E. (1990). Tumor resistance to alkylating agents conferred by mechanisms operative only in vivo. Science (80-.). *247*, 1457–1461.

Tejpar, S., Prenen, H., and Mazzone, M. (2012). Overcoming resistance to antiangiogenic therapies. Oncologist *17*, 1039–1050.

Thews, O., Wolloscheck, T., Dillenburg, W., Kraus, S., Kelleher, D.K., Konerding, M.A., and Vaupel, P. (2004). Microenvironmental adaptation of experimental tumours to chronic vs acute hypoxia. Br. J. Cancer *91*, 1181–1189.

Thienpont, B., Steinbacher, J., Zhao, H., D'Anna, F., Kuchnio, A., Ploumakis, A., Ghesquière, B., Van Dyck, L., Boeckx, B., Schoonjans, L., et al. (2016b). Tumour hypoxia causes DNA hypermethylation by reducing TET activity. Nature *537*, 63–68.

Tian, Y.M., Yeoh, K.K., Lee, M.K., Eriksson, T., Kessler, B.M., Kramer, H.B., Edelmann, M.J., Willam, C., Pugh, C.W., Schofield, C.J., et al. (2011). Differential sensitivity of hypoxia inducible factor hydroxylation sites to hypoxia and hydroxylase inhibitors. J. Biol. Chem. *286*, 13041–13051.

Tirino, V., Camerlingo, R., Franco, R., Malanga, D., La Rocca, A., Viglietto, G., Rocco, G., and Pirozzi, G. (2009). The role of CD133 in the identification and characterisation of tumour-initiating cells in non-small-cell lung cancer. Eur. J. Cardio-Thoracic Surg. *36*, 446–453.

Tohme, S., Simmons, R.L., and Tsung, A. (2017). Surgery for cancer: A trigger for metastases. Cancer Res. *77*, 1548–1552.

Tsai, J.H., Donaher, J.L., Murphy, D.A., Chau, S., and Yang, J. (2012). Spatiotemporal regulation of epithelial-mesenchymal transition is essential for squamous cell carcinoma metastasis. Cancer Cell *22*, 725–736.

Uniacke, J., Holterman, C.E., Lachance, G., Franovic, A., Jacob, M.D., Fabian, M.R., Payette, J., Holcik, M., Pause, A., and Lee, S. (2012). An oxygen-regulated switch in the protein synthesis machinery. Nature *486*, 126–129.

Vaidyanathan, A., Sawers, L., Gannon, A.L., Chakravarty, P., Scott, A.L., Bray, S.E., Ferguson, M.J., and Smith, G. (2016). ABCB1 (MDR1) induction defines a common resistance mechanism in paclitaxel- and olaparib-resistant ovarian cancer cells. Br. J. Cancer *115*, 431–441.

Vandewalle, C., Comijn, J., De Craene, B., Vermassen, P., Bruyneel, E., Andersen, H., Tulchinsky, E., Van Roy, F., and Berx, G. (2005). SIP1/ZEB2 induces EMT by repressing genes of different epithelial cell-cell junctions. Nucleic Acids Res. *33*, 6566–6578.

Vartanian, A.A., Burova, O.S., Stepanova, E. V., Baryshnikov, A.Y., and Lichinitser, M.R. (2007). Melanoma vasculogenic mimicry is strongly related to reactive oxygen species level. Melanoma Res. *17*, 370–379.

Vasudev, N.S., and Reynolds, A.R. (2014). Anti-angiogenic therapy for cancer: Current progress, unresolved questions and future directions. Angiogenesis *17*, 471–494.

Verduzco, D., Lloyd, M., Xu, L., Ibrahim-Hashim, A., Balagurunathan, Y., Gatenby, R.A., and Gillies, R.J. (2015). Intermittent hypoxia selects for genotypes and phenotypes that increase survival, invasion, and therapy resistance. PLoS One *10*, 1–18.

Vermeulen, P.B., Colpaert, C., Salgado, R., Royers, R., Hellemans, H., Van Den Heuvel, E., Goovaerts, G., Dirix, L.Y., and Van Marck, E. (2001). Liver metastases from colorectal adenocarcinomas grow in three patterns with different angiogenesis and desmoplasia. J. Pathol. *195*, 336–342.

Voulgari, A., and Pintzas, A. (2009). Epithelial-mesenchymal transition in cancer metastasis: Mechanisms, markers and strategies to overcome drug resistance in the clinic. Biochim. Biophys. Acta *1796*, 75–90.

Walczak-Drzewiecka, A., Ratajewski, M., Pułaski, Ł., and Dastych, J. (2010a). DNA methylation-dependent suppression of HIF1A in an immature hematopoietic cell line HMC-1. Biochem. Biophys. Res. Commun. *391*, 1028–1032.

Wallace, E.M., Rizzi, J.P., Han, G., Wehn, P.M., Cao, Z., Du, X., Cheng, T., Czerwinski, R.M., Dixon, D.D., Goggin, B.S., et al. (2016). A small-molecule antagonist of HIF2α is efficacious in preclinical models of renal cell carcinoma. Cancer Res. *76*, 5491–5500.

Wang, J., Chen, A., Yang, C., Zeng, H., Qi, J., and Guo, F.J. (2012). A bone-seeking clone exhibits different biological properties from the ACHN parental human renal cell carcinoma in vivo and in vitro. Oncol. Rep. *27*, 1104–1110.

Wang, W., Goswami, S., Sahai, E., Wyckoff, J.B., Segall, J.E., and Condeelis, J.S. (2005). Tumor cells caught in the act of invading: Their strategy for enhanced cell motility. Trends Cell Biol. *15*, 138–145.

Wang, X., Yu, H., Linnpoila, R.I., Li, L., Li, D., Bo, B., Okano, H., Penalva, L.O.F., and Glazer, R.I. (2013). Musashi1 as a potential therapeutic target and diagnostic marker for lung cancer. Oncotarget *4*, 739–750.

Warburg, O. (1956). On the origin of cancer cells. Science. *123*, 309–314.

Weis, S.M., and Cheresh, D.A. (2011). Tumor angiogenesis: Molecular pathways and therapeutic targets. Nat. Med. *17*, 1359–1370.

Welte, Y., Adjaye, J., Lehrach, H.R., and Regenbrecht, C.R. (2010). Cancer stem cells in solid tumors: elusive or illusive? Cell Commun Signal *8*, 6.

Welti, J.C., Powles, T., Foo, S., Gourlaouen, M., Preece, N., Foster, J., Frentzas, S., Bird, D., Sharpe, K., Weverwijk, A. Van, et al. (2012). Contrasting effects of sunitinib within in vivo models of metastasis. Angiogenesis *15*, 623–641.

Wiercinska, E., Naber, H.P.H., Pardali, E., Van Der Pluijm, G., Van Dam, H., and Ten Dijke, P. (2011). The TGF-β/Smad pathway induces breast cancer cell invasion through the up-regulation of matrix metalloproteinase 2 and 9 in a spheroid invasion model system. Breast Cancer Res. Treat. *128*, 657–666.

Wigerup, C., Påhlman, S., and Bexell, D. (2016). Therapeutic targeting of hypoxia and hypoxia-inducible factors in cancer. Pharmacol. Ther. *164*, 152–169.

Wilhelm, S., Carter, C., Lynch, M., Lowinger, T., Dumas, J., Smith, R.A., Schwartz, B., Simantov, R., and Kelley, S. (2006). Discovery and development of sorafenib: A multikinase inhibitor for treating cancer. Nat. Rev. Drug Discov. *5*, 835–844.

Williams, K., Christensen, J., Pedersen, M.T., Johansen, J. V., Cloos, P.A.C., Rappsilber, J., and Helin, K. (2011). TET1 and hydroxymethylcytosine in transcription and DNA methylation fidelity. Nature *473*, 343–349.

Williamson, S.C., Metcalf, R.L., Trapani, F., Mohan, S., Antonello, J., Abbott, B., Leong, H.S., Chester, C.P.E., Simms, N., Polanski, R., et al. (2016). Vasculogenic mimicry in small cell lung cancer. Nat. Commun. *7*, 1–14.

Winkler, F., Kozin, S. V., Tong, R.T., Chae, S.S., Booth, M.F., Garkavtsev, I., Xu, L., Hicklin, D.J., Fukumura, D., Di Tomaso, E., et al. (2004). Kinetics of vascular normalization by

VEGFR2 blockade governs brain tumor response to radiation: Role of oxygenation, angiopoietin-1, and matrix metalloproteinases. Cancer Cell *6*, 553–563.

Wu, J., Wang, S.H., Potter, D., Liu, J.C., Smith, L.T., Wu, Y.Z., Huang, T.H.M., and Plass, C. (2007). Diverse histone modifications on histone 3 lysine 9 and their relation to DNA methylation in specifying gene silencing. BMC Genomics *8*, 1–9.

Wu, J., Long, Q., Xu, S., and Padhani, A.R. (2009a). Study of tumor blood perfusion and its variation due to vascular normalization by anti-angiogenic therapy based on 3D angiogenic microvasculature. J. Biomech. *42*, 712–721.

Wu, Y., Deng, J., Rychahou, P.G., Qiu, S., Evers, B.M., and Zhou, B.P. (2009b). Stabilization of Snail by NF-κB is required for inflammation-induced cell migration and invasion. Cancer Cell *15*, 416–428.

Xu, J., Lamouille, S., and Derynck, R. (2009). TGF-B-induced epithelial to mesenchymal transition. Cell Res. *19*, 156–172.

Xu, X., Wang, Y., Chen, Z., Sternlicht, M.D., Hidalgo, M., and Steffensen, B. (2005). Matrix metalloproteinase-2 contributes to cancer cell migration on collagen. Cancer Res. *65*, 130–136.

Xu, X., Tan, X., Tampe, B., Sanchez, E., Zeisberg, M., and Zeisberg, E.M. (2015). Snail Is a direct target of hypoxia-inducible factor 1α (HIF1α) in hypoxia-induced endothelial to mesenchymal transition of human coronary endothelial cells. J. Biol. Chem. *290*, 16553–16664.

Xue, W., Du, X., Wu, H., Liu, H., Xie, T., Tong, H., Chen, X., Guo, Y., and Zhang, W. (2017). Aberrant glioblastoma neovascularization patterns and their correlation with DCE-MRI-derived parameters following temozolomide and bevacizumab treatment. Sci. Rep. *7*, 1–10.

Yamamoto, K.N., Nakamura, A., and Haeno, H. (2015). The evolution of tumor metastasis during clonal expansion with alterations in metastasis driver genes. Sci. Rep. *5*, 1–14.

Yamazaki, K., Nagase, M., Tamagawa, H., Ueda, S., Tamura, T., Murata, K., Eguchi Nakajima, T., Baba, E., Tsuda, M., Moriwaki, T., et al. (2016). Randomized phase III study of bevacizumab plus FOLFIRI and bevacizumab plus mFOLFOX6 as first-line treatment for patients with metastatic colorectal cancer (WJOG4407G). Ann. Oncol. *27*, 1539–1546.

Yan, C., Grimm, W.A., Garner, W.L., Qin, L., Travis, T., Tan, N., and Han, Y.P. (2010). Epithelial to mesenchymal transition in human skin wound healing is induced by tumor

necrosis factor-α through bone morphogenic protein-2. Am. J. Pathol. *176*, 2247–2258.

Yang, W.-H., Xu, J., Mu, J.-B., and Xie, J. (2017). Revision of the concept of anti-angiogenesis and its applications in tumor treatment. Chronic Dis. Transl. Med. *3*, 33–40.

Yang, X., Han, H., DeCarvalho, D.D., Lay, F.D., Jones, P.A., and Liang, G. (2014). Gene body methylation can alter gene expression and is a therapeutic target in cancer. Cancer Cell *26*, 577–590.

Yao, D., Dai, C., and Peng, S. (2011). Mechanism of the mesenchymal-epithelial transition and its relationship with metastatic tumor formation. Mol. Cancer Res. *9*, 1608–1620.

Ye, W. (2016). The complexity of translating anti-angiogenesis therapy from basic science to the clinic. Dev. Cell *37*, 114–125.

Yoo, B.K., Gredler, R., Vozhilla, N., Su, Z. -z., Chen, D., Forcier, T., Shah, K., Saxena, U., Hansen, U., Fisher, P.B., et al. (2009). Identification of genes conferring resistance to 5-fluorouracil. Proc. Natl. Acad. Sci. *106*, 12938–12943.

You, H., Ding, W., and Rountree, C.B. (2010). Epigenetic regulation of cancer stem cell marker CD133 by transforming growth factor-β. Hepatology *51*, 1635–1644.

Yu, L., Wu, X., Cheng, Z., Lee, C. V., LeCouter, J., Campa, C., Fuh, G., Lowman, H., and Ferrara, N. (2008). Interaction between bevacizumab and murine VEGF-A: A reassessment. Investig. Ophthalmol. Vis. Sci. *49*, 522–527.

Zhang, L., Huang, G., Li, X., Zhang, Y., Jiang, Y., Shen, J., Liu, J., Wang, Q., Zhu, J., Feng, X., et al. (2013). Hypoxia induces epithelial-mesenchymal transition via activation of SNAI1 by hypoxia-inducible factor -1α in hepatocellular carcinoma. BMC Cancer *13*, 24–27.

Zhang, S., Tang, B., Fan, C., Shi, L., Zhang, X., Sun, L., and Li, Z. (2015). Effect of DNMT inhibitor on bovine parthenogenetic embryo development. Biochem. Biophys. Res. Commun. *466*, 505–511.

Zhang, Z., Neiva, K.G., Lingen, M.W., Ellis, L.M., and Nör, J.E. (2010). VEGF-dependent tumor angiogenesis requires inverse and reciprocal regulation of VEGFR1 and VEGFR2. Cell Death Differ. *17*, 499–512.

Zheng, H., and Kang, Y. (2014). Multilayer control of the EMT master regulators. Oncogene *33*, 1755–1763.

Zhu, Z.W., Chen, L., Liu, J.X., Huang, J.W., Wu, G., Zheng, Y.F., and Yao, K.T. (2018). A novel three-dimensional tumorsphere culture system for the efficient and low-cost

enrichment of cancer stem cells with natural polymers. Exp. Ther. Med. *15*, 85–92.

Zimmer, M., Doucette, D., Siddiqui, N., and Iliopoulos, O. (2004). Inhibition of hypoxia-inducible factor is sufficient for growth suppression of VHL-/- tumors. Mol. Cancer Res. *2*, 89–95.

Index of figures and tables

Figures

3. Introduction

4. Results

5. Discussion

Tables

3. Introduction

5. Discussion

6. Materials and methods

Abbreviations

µg	microgram
µm	micrometer
5-FU	5-fluorouracil
5-hMeC	5-hydroxymethylcytosine
5-MeC	5-methylcytosine
ABC	ATP-binding cassette
AKT/PKB	PKB, protein kinase B
ANGPT	angiopoietin
AP	alkaline phosphatase
APS	ammoniumpersulfate
ATCC	American type culture collection
ATP	adenosine triphosphate
AzaC	5-aza-2-deoxycytidine
BER	base excision repair
bGHpa	polyadenylation signal of the bovine growth hormone
bGHpa	bovine growth hormone polyadenylation signal
BIC	breast invasive carcinoma
BMDC	bone marrow-derived cells
BMLS	Buchmann Institute for Molecular Life Sciences
BSA	bovine serum albumin
BSA	bovine serum albumin
BVZ	bevacizumab (Avastin)
CAIX	carbonic anhydrase IX
CD133	prominin 1 glycoprotein
CD44	homing cell adhesion molecule
CDC	cluster of differentiation
CDH	cadherin
cDNA	complementary deoxyribonucleic acid
cm	centimeters
CML	chronic myelogenous leukemia
CMVp	cytomegalovirus promoter
CO	control
COX	cyclooxygenase
CpG	cytosine-guanine site
CPS	cryoprotection solution
CRISPR/Cas9	clustered regularly interspaced short palindromic repeats / caspase9
CSC	cancer stem cell
CXCR	CXC chemokine receptor
DAPI	4,6-diamidin-2-phenylindole
DB	dot blot
DEPC	diethylpyrocarbonate
dist.	distilled
DKFZ	Deutsches Krebsforschungszentrum

DLL	delta-like ligand
DMEM	Dulbecco's modified Eagle's medium
DMOG	dimethyloxalylglycine
DMSO	demethylsulfoxide
DNA	deoxyribonucleic acid
DNase	deoxyribonuclease
DNMT	DNA methyltransferase
dNTP	deoxynucleotide
DPBS / PBS	(Dulbecco's) phosphate buffered saline
EBSS	Earle's balanced salt solution
E-cadherin	epithelial cadherin
ECL	enhanced chemiluminescence
ECM	extracellular matrix
EDTA	ethylenediaminetetraacetic acid
ELISA	enzyme linked immunosorbent assay
EMA	European Medical Agency
EMT	epithelial to mesenchymal transition
EtOH	ethanol
EZH2	enhancer of zeste homolog 2
FBS	fetal bovine serum
FDA	Food and Drug Administration
FGF	fibroblast growth factor
FGFR	fibroblast growth factor receptor
FIH	factor inhibiting HIF
FLuc	firefly luciferase
For	forward
g	gram
GBM	glioblastoma multiforme
G-CSF	granulocyte colony stimulating factor
GDC	Genomics Data Commons
gDNA	genomic deoxyribonucleic acid
GIST	gastrointestinal stromal tumor
GLUT	glucose transporter
h	hour
H	histone
HAF	hypoxia associated factor
HAT	histone acetyltransferase
HBS	Hank's buffered saline
HCC	hepatocellular carcinoma
HDAC	histone deacetylase
HEPES	4-(2-hydroxyethyl)-1-piperazineethanesulfonic acid
HGF	hepatocyte growth factor
HIF	hypoxia inducible factor
hMeC	hydroxymethylcitosine
HRE	hypoxia response element

IC	inhibitory concentration
IF	immunofluorescence
IFL	irinotecan, 5-FU, leucovirin
IFN	interferon
IGF	insulin-like growth factor
IgG	immunoglobulin G
IL	interleukin
IH	intermittent hypoxia
IVIS	*in vivo* imaging system
K	lysine
KD	knockdown
kDa	kilodalton
KDM/LSD	lysine demethylase
kg	kilogram
Kit	stem cell growth factor
Km	Michaelis constant
KO	knockout
LB	Luria-Bertani
LDHA	lactate dehydrogenase A
LUAD	lung adenocarcinoma
M	molar
m.s.	median survival
mAb	monoclonal antibody
MAML3	mastermind like-3
MAPK	mitogen activated protein kinase
MDSC	myeloid-derived suppressor cells
me	methylation
MeC	methylcytosine
MEM	minimum essential medium
MET	mesenchymal to epithelial transition
mg	milligram
min	minute
ml	milliliter
MLL	mixed lineage leukemia
mM	millimolar
MMP	matrix metalloprotease
MOI	multiplicity of infection
mRNA	messenger ribonucleic acid
mTORC	mammalian target of rapamycin complex 1
MTT	3-(4,5-dimethylthiazol-2-yl)-2,5-diphenyltetrazolium bromide
n.s.	not significant
N-cadherin	neural cadherin
ng	nanogram
nm	nanometer
NRP	neuropilin

nsc	non-silencing control
NSCLC	non-small cell lung cancer
NuRD	nucleosome remodeling deacetylase
Oct4	octamer-binding transcription factor 4
OD	optical density
ODD	oxygen dependent degradation domain
OS	overall survival
P.O.R	plasmid name, from pLenti6-ODD-RLuc
PAGE	polyacrylamide gel electrophoresis
PBS	phosphate buffered saline
PCR	polymerase chain reaction
PD-1L	programmed death-ligand 1
PDGF	platelet derived growth factor
PDGFR	platelet derived growth factor receptor
PFA	paraformaldehyde
PFS	progression-free survival
PGK	phosphoglycerate kinase
pH	potential of hydrogen
PHD	prolyl hydroxylase
PI3K	phosphatidylinositol-3-kinase
PKA	protein kinase A
PlGF	placental growth factor
PNET	pancreatic neuroendocrine tumor
pSV40	simian virus 40 promoter
PVDF	polyvinylidene difluoride
pVHL	von Hippel-Lindau protein
qRT-PCR	quantitative reverse transcription polymerase chain reaction
RAC	Ras-related C3 botulinum toxin substrate
RB	retinoblastoma
RCC	renal cell carcinoma
Rev	reverse
RHO	Ras homologue
Rluc	*Renilla* luciferase
RNA	ribonucleic acid
RNase	ribonuclease
rpm	rotations per minute
RT	room temperature
RTK	receptor tyrosine kinase
S	serine
SBE	SMAD binding element
SDF	stromal cell-derived factor
SDS	sodium dodecylsulphate
SEM	standard error of the mean
sgRNA	single guide ribonucleic acid
shRNA	short hairpin ribonucleic acid

SILAC	stable isotope labeling with amino acids in cell culture
siRNA	short interfering ribonucleic acid
SMAD	human homolog of Mad and Sma
Sox2	sex determining region Y-box 2
SR	sorafenib
SU	sunitinib
SunRES	resistant to sunitinib
SV40p	SV40 virus promoter
SV40pa	polyadenylation signal of the SV40 virus
SV40pa	simian virus 40 polyadenylation signal
TAE	Tris-acetate-EDTA
TAM	tumor associated macrophage
T-cadherin	truncated cadherin
TCGA	The cancer genome atlas
TCL/LEF	T-cell factor/lymphoid enhancer factor
TE	Tris-EDTA
TEMED	tetramethylenediamine
TET	ten eleven translocation
TGFBR	transforming growth factor β receptor
tGFP / GFP	(turbo) green fluorescent protein
TGFβ	transforming growth factor β
Th	T helper
Tm	melting temperature
TNM	tumor, nodule, metastasis (classification system)
TP53	tumor protein 53
tPA	tissue plasminogen activator
Tris	2-amino-2-(hydroxymethyl)propane-1,3-diol
uPA	urokinase-type plasminogen activator
uPAR	urokinase-type plasminogen activator receptor
UTR	untranslated region
VEGF	vascular endothelial growth factor
VEGFR	vascular endothelial growth factor receptor
VIM	vimentin
VPF	vascular permeability factor
WB	Western blot
ZEB	zinc finger E-box binding homeobox 1
ZO-1	zonula occludens-1

Acknowledgments

First of all, my profound gratitude goes to **Prof. Till Acker** and **Dr. Boyan K. Garvalov** for the great opportunity to work on such an interesting project at the Giessen Institute of Neuropathology (GIN), for all the guidance, patience, and support during all the years that, taken together, immensely helped me to learn the ways of “western-style” molecular oncology.

I am grateful to **Prof. Amparo Acker-Palmer** for the opportunity and support with animal studies, which were all performed in the Department for Molecular and Cellular Neurobiology at the Goethe University Frankfurt.

My gratitude goes to **Dr. Gerrit Eichner** from the Mathematical institute at Justus Liebig University Giessen for all the guidance with statistical analysis and especially – for writing the R code used in patient data retrieval from TCGA.

I am much obliged to all former and present colleagues and friends at the Giessen Institute of Neuropathology and Buchman Institute for Molecular Life Sciences who were always helpful, supportive, and inspiring during my PhD years: **Dr. Yuanbin Xie**, **Dr. Jose H. Dopeso**, **Dr. Sarah K. Goos**, **Dr. Meng-Miao Tsai**, **Dr. Huike Jiao**, **Tao Lin**, **Adam Klajda**, **Dr. Nuray Böğürcü**, **Dr. Sascha Seidel**, **Nadja Utz**, **Dr. Sandra Baumgart**, **Dr. Attila Németh**, **Sabine Gräf**, **Carmen Selignow**, **Denis Schmelzer**, **Tarek Belefkih**, **Evelyn Rieber** and **Kristin Happich**.

A special Thank You goes to three of my dear friends and colleagues who were extraordinarily supportive both professionally and personally, kind, and extremely patient with me during all the fun and tough periods of the last 7.5 years:

Dr. Alina Filatova – for the enormous help in the very beginning of my PhD (from basic methods in the lab, to basics of life in Germany) and up till now (especially, for proofreading my thesis);

Dr. Angel Cuesta – my best “*in vivo* friend” form the Buchman Institute for Molecular Life Sciences at the Goethe University Frankfurt, for the tremendous amount of shared *in vivo*

and *in vitro* work, for proofreading my thesis, for all the unforgettable times in the animal house, fun with imaging, surgery, and above all – counting metastases;

Steffen Gretser – my first and only medical student in the Giessen Institute of Neuropathology, for the great help and excellent work on re-isolated and IH lines and the opportunity to learn how to be a better mentor.

My very special Thank You goes to my wife **Liudmyla P. Taranets**, my mother **Alla V. Trompak**, and my father **Dr. Omelyan M. Trompak** for the indescribable amount of support, unconditional love, encouragement, inspiration, belief in me and my endeavors.

This work would not have been possible without all of You, Thank You Very Much! Vielen Dank! ¡Muchas gracias! Dziękuję Bardzo! Çok teşekkür ederim! Искренне благодарю! Благодаря ти много! Щиро дякую! 非常感謝你!